BIOPROCESSING OF CRUDE OILS

Robert G. Shong
Texaco Exploration & Producing Technology Department
Houston, Texas 77042

INTRODUCTION

Research on using microorganisms to upgrade or improve crude oil properties is a high risk venture but the potential rewards of achieving such a process are significant both environmentally and economically. The main drivers for this work are: 1. tightening of environmental restrictions on total sulfur in refined oil products and lower refinery CO_2 emissions; 2. the diminishing availability of high gravity sweet crudes; 3. the rising cost of coking and hydrotreating operations; and 4. the increasing cost of meeting CO_2 and sulfur restrictions as future emission allowances are reduced.

Coking and hydrotreating operations are refinery processes to upgrade and remove sulfur from heavy crudes. Cokers use heat to remove hydrogen deficient portions of the feed as coke. The process produces a significant amount of carbon waste that must be disposed. Hydrotreating removes feed sulfur and olefins, but requires high pressure equipment, heat, hydrogen, and expensive chemical catalysts. Repeated hydrotreating to achieve very low sulfur levels becomes uneconomic. The main incentives for crude oil upgrading and desulfurization prior to refining are the economics of higher oil value, lower processing costs, and reduced air pollution that causes smog, acid rain and global warming. Refinery processing costs are projected to steadily increase as reserves of high gravity and low sulfur crude feedstocks are depleted because these feedstocks are currently used to dilute heavy oil feeds.

The use of microorganisms or their enzymes provides potential processing advantages of low pressure, low temperature, no hydrogen required, low chemical costs, and minimal equipment investment when compared to refinery operations.

RESULTS AND DISCUSSION

Potentially High Payback

Texaco has significant holdings in heavy and high sulfur crude oil reserves. The value of those reserves can be significantly increased with gravity improvement or viscosity reduction and sulfur removal. An oil field bioprocess that would reduce sulfur would significantly improve the quality and value of oil piped to a refinery. Refining a low sulfur crude would reduce refining costs and achieve lower sulfur product streams. The value of biodesulfurized oil will steadily increase as reserves of low sulfur crude oil are depleted. An estimated $295 million (Table 1) could be realized annually from four selected Texaco's fields if the sulfur content of each oil was lowered to a total sulfur percentage of 0.5% or less. These estimates do not include any savings in refining cost or environmental emission improvements.

Envisioned Advantages of Bioprocessing Crude Oil

Bioprocessing crude oil has several application advantages that make it attractive for use in the oil field prior to shipment or pipelined to a refinery. The first advantage is the potential simplicity of the process. Bioprocessing oil basically involves mixing the water soluble biocatalyst (either the microorganism or the enzyme) with air and the oil. After reaction, the formed water-oil emulsion is separated to recover the upgraded oil. The biocatalyst remains with the water potentially available for reuse. In an oil field, both water and oil are routinely coproduced at the well head as emulsions so separations of oil-water mixtures are standard procedures. The only added feature for bioprocessing is the addition of a mixing reactor prior to separation. Fit of such a bioreactor in an oil field operation are illustrated and described below.

A second advantage of bioprocessing is the selectivity of biocatalysts. Desulfurizing biocatalysts contain enzymes generated by microorganisms that need sulfur for energy and growth. Specifically, these generated enzymes catalyze oxidative cleaving of sulfur atoms from organic sulfides forming sulfate salts. The sulfate salts then migrate from the organic oil phase to the water phase. These microorganisms can be modified to remove specific sulfur structures or broader classes of sulfur compounds. Biocatalysts that can upgrade oils modify specific organic structures like cleaving or opening aromatic rings. The motivation for the organism again is to obtain chemical components for energy and growth. The advantage of this selectivity is that a process user knows what chemical changes or potential losses will occur. Unfortunately, crude

oil is a complex mixture of organic compounds and all crude oils do not have the same chemical makeup. Therefore, for crude oil applications the biocatalysts will have to be customized for each crude. The total process may involve multiple biocatalysts. Again, the oil field application is felt to be more suited to bioprocessing than at a refinery where multiple crude feeds are handled.

A third advantage is that the bioprocessed oil can be processed at a refinery using current technology at a lower cost. For sulfur, hydrotreating is very effective for removing mercaptans and straight chain sulfides, whereas biodesulfurization is more effective with organic ring sulfides like dibenzothiophene (DBT). The hydrotreating conditions are less severe (lower cost) for straight chain sulfur compounds so an economic advantage is achieved when both hydrotreating and biodesulfurization processes are used.

A fourth advantage of a bioprocessing is improvement in oil properties that affect handling the bulk oil. These property improvements could include viscosity reduction, shifts to lower molecular weight distributions, or lower asphaltene content all of, which reduce fluid piping and transportation problems and costs. Basically, a higher grade and cleaner oil (low sulfur content and high gravity) is transported and refined cheaper and lowers sulfur and CO_2 emissions.

Process Location: Refinery *vs.* Field

The bioprocess can be applied either on a crude oil in the field or later at the refinery. Five factors will be considered in comparing the advantages and disadvantages of applying biodesulfurization near the well head location or at a refinery location. The five comparison factors are greatest product value, biocatalyst solubility, reaction time, process integration, and waste stream disposal. These five points are basic, but they illustrate the envisioned application of bioprocessing a crude oil.

Processing costs will have the greatest effect on product values where the pricing margins are the smallest. In other words, one is more inclined to pay the cost of processing where the greatest product value increase can be obtained. For example, the value of a desulfurized crude oil could increase from $1 - $3/barrel assuming sulfur is reduced to less than 0.5%. In a refinery, product profit margins are squeezed by competition and environmental regulation costs. In general, refined product margins are usually much lower than $1.00/barrel. The maximum benefit of desulfurizing occurs closest to the well head based on improvement in product value.

The current envisioned biocatalysts for crude oil upgrading and desulfurization are water soluble. In an oil field operation, water is coproduced with the oil so the process of water/oil separation is a routine field process. The agitation of the oil and water mixture with biocatalyst would be the only added process step. However, prior to oil transportation to a refinery most of the water has been removed to minimize corrosion and viscosity problems. Water/oil mixing at a refinery is minimized to prevent water and emulsion carry over into the oil processing. Water/oil mixing followed by separation would be added process steps which means added capitalization and operating costs. Again, oil bioupgrading in the oil field has advantages over refinery processing.

Longer reaction times or longer biocatalyst contact with the oil results in greater oil property improvement and sulfur removal. In an oil field setting, the reaction time can range from hours to days depending on oil production rate, storage capacity, and shipment timing. Bioprocessing reaction times allowable in a refinery operation are limited to hours or less. Material holding times at a refinery are limited and most refineries maintain continuous operation and high throughput unlike a field operation where in some cases oil can be held in a tank for several days awaiting transportation.

Another major difference in chemical processing between a refinery and a field situation is the quantities of material handled. A refinery deals in volumes greater than 50,000 gallons whereas a producing field generally works with volumes less than 50,000 gallons. The size aspect with addition of process steps affects the ease of integration of bioprocessing to a refinery or a field facility. For the field case, the process integration is relatively simple. The field already has holding tank capacity and necessary oil/water separators. Added equipment is a mixing reactor. Process integration for a refinery is similar but on a much larger scale with accompanying higher cost.

A bioprocessing operation will generate a waste water stream. All sulfur removed is converted from an organic form to a sulfate salt which is soluble in the reaction water. The biocatalyst will be removed from the water and recycled but the remaining process water will contain metal, sulfur, and organic salts. The new water waste stream must be handled whether it is generated in the oil field or at the refinery. In a refinery, this new waste stream becomes an added problem.

However, in the field the water containing the formed salts can be diluted and reinjected as part of the field water flood program so waste stream has minimal effect on oil field operation. The water soluble salts may also have minimal surfactant properties which could improve the water flood sweep efficiency.

Generic Oil Field Production Facilities

A basic field production facility is illustrated in Figure 1. As the oil and water are produced accompanying gas is separated and collected for sale. The water oil mixture or emulsion is then sent to a heater treater also called a gun barrel to separate the oil and water. Any residual gas released during separation is used to blanket the rest of the separation system. The separated water and oil are transferred to separate tanks. The oil is collected for sale and transportation and the water is filtered and reinjected as part of the field water flood. A bioprocessing step can be inserted after the initial gas separation. The biocatalyst can be added to the produced water/oil emulsion and mixed. After a sufficient reaction time the oil/water emulsion would be handled as before in the field separating facility as illustrated.

Bioprocessing Results

Biodesulfurization results on a crude oil are illustrated in Figure 2. The curves are GC detector signals from a sulfur specific detector (Sievers Model 355) where the Y-axis is the detector signal and the X-axis is time in minutes. The lower curve with the single peak labeled DBT is a dibenzothiophene standard. The next two curves are the biodesulfurized oil and original oil respectively. The reaction period was 24 hours at room temperature. A reduction in sulfur content is indicated.

CONCLUSION

The potential benefits and payback justify further research on using microorganisms to upgrade crude oil. There are distinct advantages in applying a crude oil bioupgrading process in the oil producing fields rather than a refinery. Lower process temperatures, lower reaction pressures, and more environmentally friendly waste streams are a significant paradigm shift from current petroleum technology.

TABLE 1 - Estimates of the Increased $/Yr. by Reducing Sulfur in Crude Oil

A	$900,000
B	$29,200,000
C	$120,450,000
D	$146,000,000
Total	$296,550,000

Estimates based on $1 - $3 per bbl increase in price for low sulfur crude

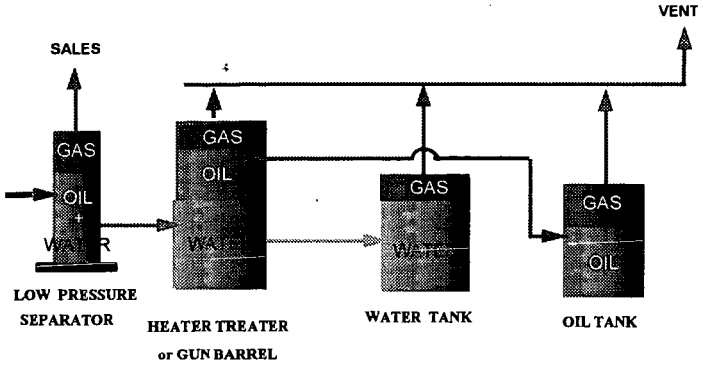

FIGURE 1 - Oil Production Facility

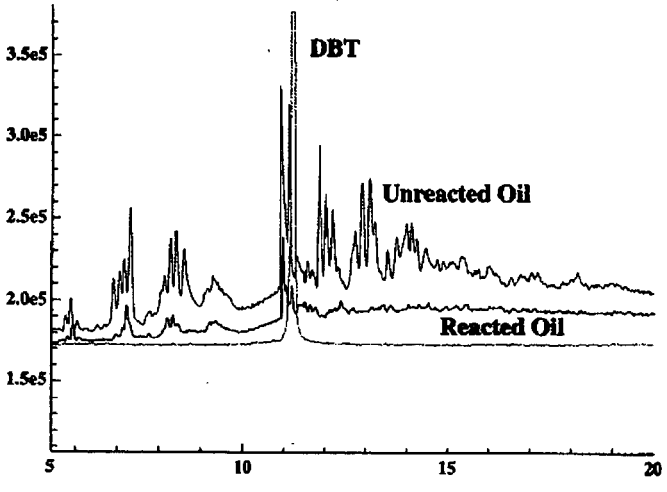

FIGURE 2 - Biodesulfurized Crude Oil Result

BIOCATALYTIC CONVERSION OF CRUDES: POSSIBLE PATHWAYS

Eugene T. Premuzic, Mow S. Lin, and Michael Bohenek
Energy Science and Technology Division, Building 318
Brookhaven National Laboratory
Upton, NY 11973-5000

Axel Johnson
BIOCAT, Inc.
100 North Country Road
Setauket, NY 11733

INTRODUCTION

Petroleum is a complex mixture of natural products which, under geological conditions (temperature, pressure, folding, migration and others), are subjected to multiple chemical, biochemical and physical reactions (1). Evolution of petroleum over geological periods of time leads to the formation of mixtures of hydrocarbons with different molecular weights and concentrations of saturates, aromatics, resins, asphaltenes and organometallics. Thus, low °API (<20) gravity oils are low in gasoline and high in residuum, i.e., as oils becomes heavier, the H/C ratios decrease, the NSO/C ratios increase and the oil becomes richer in asphaltenes and (2) Treatment of such complex mixtures with biocatalysts introduced under controlled conditions leads to bioconversion of crude oils via multiple inter- and intra-molecular chemical and biochemical processes. Some of the mechanistic aspects of such processes will be discussed.

Chemical reactions leading to the formation of different types of oils are influenced by the composition of the initial mix of natural products, their mutual interaction involving multiple reactive sites and the effects of chemical, biochemical and geological factors acting on the mixture (2,3). In spite of the chemical complexity of crude oils they can all be characterized and placed into distinct groups ranging from lights oils (°API >30) to heavy oils (°API <20). They are further distinguished by a number of chemical markers, compounds characteristic of major components of crudes which are different hydrocarbons, grouped according to their particular chemical structures: saturates, aromatics, resins and asphaltenes. Additional chemical characterization of oils distinguishes complex hydrocarbon mixtures by the relative concentration of compounds containing nitrogen, sulfur, oxygen and trace metals. The representative uniqueness of chemical markers has allowed to follow the chemical alterations in crude oils under reservoir as well as chemical and biochemical processing conditions (4-7). The latter is of particular importance in the studies dealing with biocatalytic conversion of heavy crude oils (e.g., Ref. 7). It has been shown by extensive use of chemical markers, that biochemical catalysts do not biodegrade, but rather, bioconvert heavy crudes to products with lower contents of sulfur, nitrogen and trace metals (7,8). Further, the extent and the specificity of bioconversion depends on the biocatalyst used and the chemical properties of the crude used, for example the difference between a heavy immature and a heavy biodegraded crude oil. Some aspects of the above observations will be briefly discussed in the present paper.

EXPERIMENTAL

Methods and procedures have been discussed in detail elsewhere (e.g, 7,9) and will be summarized in this section. .1. Biocatalyst and oil treatment: biocatalysts were prepared from the stock BNL collection and stirred into the reaction mixture containing the oil and nutrients and then extracted with methylene chloride; .2. gas chromatography/mass-spectrometry: the analyses were carried out with a Perkin Elmer Model 8700 gas chromatograph equipped with flame photometric detector (FPD) and a Finnigan ion trap mass spectrometer (ITD) for simultaneous analyses (GC-FPD/MS); .3. pyrolysis-gas chromatography-mass spectrometer (Py-GC-MS) utilized a Chemical Data System, Inc. (CDC) model 190 pyroprobe interfaced with GC-FPD-MS system as in .2.; .4. for nitrogen analyses appropriate nitrogen specific (nitrogen, phosphorous detector, PFPD) was used; .5. metals analyses were performed with a VG-induced-coupled-mass spectrometer (ICP-MS); .6. Saturate Aromatic, Resins and Asphaltene (SARA) analyses were carried out using a thin layer Chromatograph-Flame Ionization Detector (TLC-FID) and Chromatotron Model TH-10 of IATROSCANCO, using the rotating disc TLC-FID method (10) and .7. asphaltenes were precipitated with n-pentane from a methylene chloride solution.

RESULTS AND DISCUSSION

Experimental results to date suggest that a biocatalyst reacts at the active sites of polar molecules within the colloidal, micellar molecular solutions representative of three dimensional

structures of crudes (7-14). It is the three dimensional structure of crudes as well as the chemical composition and the molecular structures of major constituents of oil that influence the reactivities of crude oils (15, 16). It has been known for some time (14) that measurement of one gross parameter (e.g., sulfur) in analyses of catalytically converted oils, for example hydrodesulfurization and hydrodemetalization is insufficient, and may lead to erroneous conclusions. Current experience suggests that similar oil characterization scenarios apply to biocatalytically converted oils. For example, the action of a single biocatalyst, BNL-4-23 on three, chemically different oils is summarized in Table 1. Monterey 851 is a heavy, California (onshore) biodegraded oil. OSC is an immature (offshore) biodegraded oil, while MWS, Midway Sunset is a steam treated heavy crude. There is a significant variation in the effects of a single biocatalyst on eight different parameters. Similar variations have been also observed where several different biocatalysts have been used on a single oil (examples in Refs. 6,7 and others). Further, the distribution of compounds containing active sites, i.e., heteroatoms, varies in concentration throughout different types of oils, where the three dimensional structure of oils allows for formation of bridges, clathrates, inclusion complexes and clusters which, chemically represent a reaction substrate eminently suitable for multiple and simultaneous reactions. The importance of initial reactivity at active sites has led to a set of experiments described in detail elsewhere (6-9) and will be for the purpose of this discussion, summarized briefly in Figure 1. In the analyses shown in Figure 1, experimental conditions for all the samples were kept constant in each case, so that a direct comparison of spectral results is possible. These results show that significant changes also occur in the n-pentane precipitated fractions (asphaltanes) which are not detected in the analyses of the whole oil. The chemical changes which lead to reaction mixtures analyzing as shown in Figures 1c, d, g, h indicate a break down in high molecular weight fractions. The multiple parameter analysis shows lowering in total sulfur concentration and also indicates a significant re-distribution of hydrocarbons.

The usefullness and importance of multiple parameter analysis as it relates to an understanding of fundamental mechanisms by which biocatalysis occurs as well as to its effects and efficiency is further illustrated by the following examples. Table 2 lists data for several fractions of different oils with their corresponding Conradson Carbon Residue (CCR) values. When CCR values are plotted against % of resins + asphaltenes, a decrease in the concentration of resins and asphaltenes also indicates a decrease in the Conradson Carbon value, an important consideration in refining of crudes, i.e., coking processes. The effect of biocatalytic conversion of OSC and MWS follows the same trend, however, biocatalysis accomplishes this at a much lower temperature and pressure compared to conventional refining. This very important experimental observation could not have been detected without multiple parameter analyses and systematic studies of chemical/biochemical mechanisms associated with biocatalysis.

Table 1.
Characterization of Representative Biotreated Crude Oils

Oil	Monterey 851		OSC		MWS	
	%UN*	% TR** BNL-23	%UN	% TR BNL-23	%UN	% TR BNL-23
S	1.84	1.29 (-30)	4.4	2.42 (-45)	1.00	0.50 (-50)
N	0.59	0.44 (-25)	0.66	0.36 (-45)	0.79	0.63 (-20)
Ni	259 ppm	207 (-20)	80 ppm	64 (-20)	63 ppm	47 ppm (-25)
V	369 ppm	288 (-22)	22 ppm	18.5 (-16)	24 ppm	15.9 ppm (-36)
SAT %	19.2	34.4	17.3	51.6	19.2	66.3
AROM %	45.2	29.7	39.1	20.5	44.9	11.2
RESIN %	31.2	32.7	37.1	22.3	35.3	19.3
ASPH %	4.4	3.6	6.2	5.7	2.60	3.1

* UN = untreated
**TR = treated
(-) = % reduction

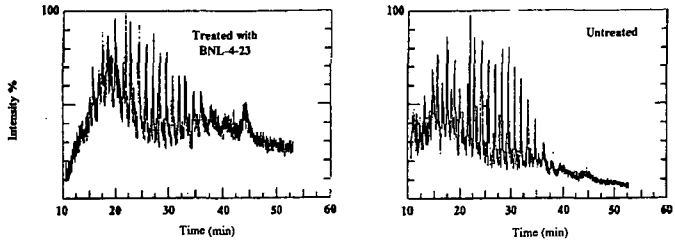

GC-MS Analysis: M/e 57 Gas Chromatogram Trace of Untreated and Treated OSC Crude.

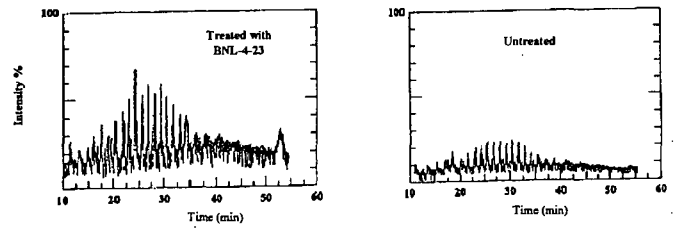

Py GC-MS: M/e 57 Gas Chromatogram Trace of Asphaltenes Derived from OSC Crude.

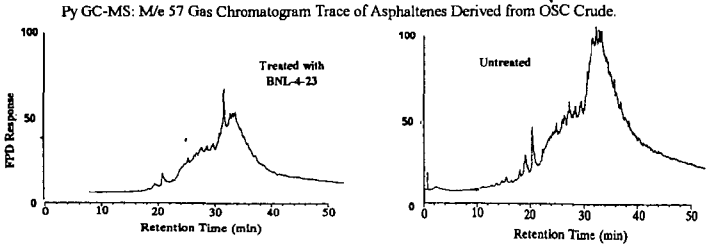

FPD (Sulfur Specific Detector) Chromatogram Trace of Untreated and Treated OSC Crude.

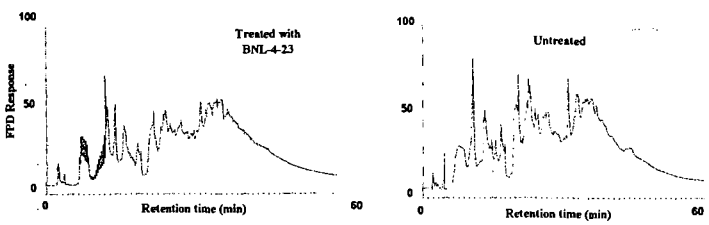

Pyrolysis-gas Chromatograph Analysis (Py-GC) FPD (Sulfur Specific Detector) Trace of Asphaltenes from OSC Crude Treated with BNL-4-23

Figure 1. *Multiple Parameter Analysis of Oils.*

Table 2.
Distribution of Fractions and Residues in Representative Oils

Reference		Asphaltenes	Resins	Res+Asph.	Carbon residue
2	Light Alberta	0.2	9.4	9.6	1.3
2	crudes	0.1	11.6	11.7	2.6
2	for comparison	0.9	12.2	13.1	2.9
2		0.3	13.0	13.3	3.0
17	Daquig	0	29.9	29.9	8.5
15	Gach Saran	6.8	28.5	35.3	8.8
2	Boscan	11.9	24.1	36.0	10.4
15	Heavy Arabian	12.6	27.5	40.1	12.6
2	Cold Lake	15.7	28.7	44.4	13.6
17	Shenghi	45.7	1.6	47.3	12.7
15	Blend	11.4	36.0	47.4	11.0
2	Bermudez Lake	35.3	14.4	49.7	13.4
2	Athabasca	16.9	34.1	51.0	18.5
15	Maya	25.2	25.9	51.1	15.3
2	Lloydminister	12.9	38.4	51.3	11.8
17	Renqiu	0	53.1	53.1	18.6
15	Hondo	13.9	40.2	54.1	10.8
2	Qayarah	20.4	36.1	56.5	15.6
2	Trinidad Lake	33.3	29.4	62.7	10.8

2-Speight
14-Dolbear, Tang and Moorhead
16-Chan and Luoyan

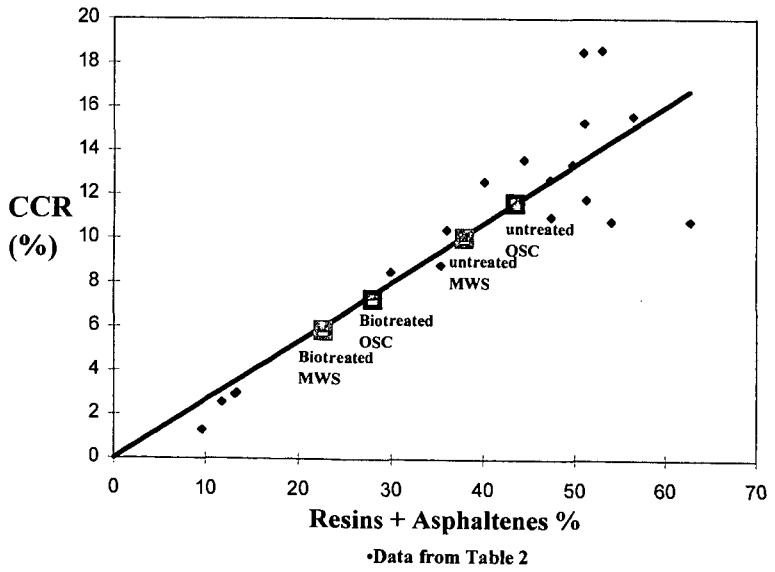

Figure 2. Conradson Carbon Residue (CCR) as a function of the Resin + Asphaltene Fraction

CONCLUSIONS

Multiple chemical changes which occur during biocatalysis of heavy crude oils are due to complex inter- and intra-molecular reactions. These reactions follow distinct trends which can be followed by a set of chemical markers associated with major heavy crude oil fractions. Experience gained with chemical catalytic conversion of crudes, shows that properties described by a single paramter only (e.g., sulfur) are not in themselves good predictors of catalytic processing. The data currently available for biocatalytic conversion of heavy crudes appear to be consistent with those of chemical catalysis and require an array of chemical markers in evaluation of biocatalytic effects.

ACKNOWLEDGMENTS

This work is supported by the U.S. Department of Energy, Division of Fossil Fuels, under Contract No. AS-405-ESTD and Contract No. DE-AC02-98CH10886 with the U.S. Department of Energy. We also wish to acknowledge B. Manowitz of BNL for valuable comments and advice.

LITERATURE CITED

(1) Hunt, J. M., Petroleum Geochemistry and Geology, W. H. Freeman and Co., San Francisco, 1979.

(2) Speight, J. G., The Chemistry and Technology of Petroleum, 2nd Edition, Marcel Dekker, New York, 1991.

(3) Tissot, B. P. and Welte, D. M., Petroleum and Occurrence, Springer-Verlag, New York, 1978.

(4) Peters, U. E. and Moldovin, J. M., The Biomarker Guide, Prentice-Hall, New York, 1993.

(5) Premuzic, E. T., Lin, M. S., Jin, J. Z., Manowitz, B., Biohydrometallurgical Technology, 401-413 (1993).

(6) Premuzic, E. T., Lin, M. S., Lian, H., Zhou, W. M., Yablon, J., Fuel Processing Technology, 52, 207-223 (1997).

(7) Premuzic, E. T., Lin, M. S., The Journal of Petroleum Science and Engineering, in press (1998).

(8) Premuzic, E. T., Lin, M. S., Bohenek, M., Zhou, W. M., Energy and Fuels, in press (1998).

(9) Lian, H., Lee, C. Z. H., Wang, Y. Y., Yen, T. F., Journal of Planar Chromatography, 5, 263-266 (1992).

(10) Yen, T. F., The Role of Trace Metals in Petroleum, Ann Arbor Science Publishers, Inc., Michigan, 1975.

(11) Yen, T. F., Encyclopedia of Polymer Science and Engineering 2nd Edition, John Wiley & Sons, New York, 1990.

(12) Strausz, O. P., Mojelsky, T. W., Lown, E. M., Fuel 71, 1355-1363 (1992).

(13) Yen, T. F., Meso-scaled Structure and Membrane Minetic Chemistry, Plenum Press, New York, 1994.

(14) Dolbear, G. E., Tang, A., Moorehead, E. L., Upgrading Studies with Californian, Mexican and Middle Eastern Heavy Oils, 14, 221-132, American Chemical Society Symposium, 1987.

(15) Speight, J. G., Asphaltene and the Structure of Petroleum, 521, Advances in Catalysis and Process for Heavy Oil Conversion, American Chemical Society Symposium, 42(2) (1997).

(16) Chen, J., Cao, H., The Structure of Carbon Residue Precusors and Their Roles in Petroleum Processing. Proceedings of the International Conference on Petroleum Refining and Petrochemical Processing, 1, 447, September 11-15, Beijing, China, 1991.

BIOCATALYTIC RING CLEAVAGE OF DIBENZOTHIOPHENE AND PHENANTHRENE IN A BIPHASIC FERMENTER SYSTEM

Q. Wu, P.M. Fedorak, M.A. Pickard, M.R. Gray, and J.M. Foght
University of Alberta, Edmonton, Alberta, Canada T6G 2E9

Keywords: Biotransformation, petroleum, fermenter

ABSTRACT

Our previous research has demonstrated the ability of *Pseudomonas fluorescens* LP6a to cleave the fused-ring aromatic hydrocarbons and heterocycles commonly present in petroleum distillates. In this study, experimental conditions for biocatalytic ring cleavage of dibenzothiophene and phenanthrene in a biphasic 3 liter fermenter system were investigated.

Compared with batch flask experiments, a fermenter system provides the advantage of large scale, easy automation and versatile control of the experimental conditions. Growth curves of the biocatalyst and the relative oxidation rate of dibenzothiophene at different growth phases were determined. Incubation of dibenzothiophene and phenanthrene in various carriers was performed in the fermenter system. Rapid complete biotransformation of dibenzothiophene in light mineral oil and improved biotransformation of phenanthrene in diesel fuel were obtained in a fermenter system compared with batch flask conditions.

INTRODUCTION

Petroleum middle distillates contain low fuel value di- and tricyclic aromatics. Currently, expensive and non-specific chemical hydrogenation processes involving high temperature and high pressure are used to reduce di- and tricyclic aromatics to alkylbenzenes to increase their fuel value. It is desirable therefore to explore other economical alternatives to conventional upgrading techniques.

Our previous research has demonstrated the ability of *Pseudomonas fluorescens* LP6a to cleave fused-ring aromatic hydrocarbons and heterocycles commonly present in petroleum distillates [Wu et al., 1998]. This provides an attractive potential alternative to conventional fuel upgrading techniques as a two-stage upgrading process: first bacteria would enzymatically cleave the fused-ring aromatics under near-ambient conditions, then mild chemical hydrogenation of the ring opening products would yield the desired alkyl aromatics.

We previously demonstrated ring cleavage of aromatics in middle distillates under batch flask conditions, typically using 200 mL of biocatalyst suspension and <1 mL of distillate [Foght et al., 1997; Wu et al. 1998]. To scale up the reaction volumes, experimental conditions for biocatalytic ring cleavage of dibenzothiophene and phenanthrene in a 3 L fermenter system were investigated in this study. A biphasic system was used, with the ring cleavage substrate dissolved in a water-immiscible carrier and the biocatalyst suspended in an aqueous buffer.

Compared with batch flask experiments, a fermenter system provides the advantage of large scale, automation and versatile control of the experimental conditions such as aeration and mixing. Growth curves of the biocatalyst and the specific rate of dibenzothiophene (DBT) ring cleavage at different growth phases were determined. Results are presented from biotransformation of the model ring cleavage substrates dibenzothiophene or phenanthrene dissolved in light mineral oil, diesel fuel or a petroleum middle.

METHODS AND MATERIALS

Preparation of biocatalyst

A transposon mutant of *P. fluorescens* LP6a was generated by conjugation with a suitable *Tn*5 donor plasmid [Foght and Westlake, 1996] and subsequent screening for desired ring cleavage products. Cultures of *P. fluorescens* LP6a mutant #21-41 were incubated to high density at 30°C with agitation for 24 h in Tryptic Soy Broth (Difco; typically 200 mL) containing kanamycin to maintain the transposon. The 200 mL seed culture was then used to inoculate a fermenter (New Brunswick, NJ) containing 3 L Tryptic Soy Broth plus kanamycin. The culture was incubated at 30° C with aeration at 4 L min^{-1} sterile air and stirring at 300 rpm.

To determine optimum biocatalyst preparation conditions, the culture optical density at 600 nm and protein concentration (BCA protein assay; Pierce, Rockford IL) were determined at intervals in the fermenter culture. As well, approximately 50 mL subsamples of the growing culture were assayed for ring cleavage activity, using crystalline dibenzothiophene (DBT) as the substrate. The

rate of DBT biotransformation was determined spectrophotometrically at 475 nm, the wavelength of maximum absorbance of the DBT ring cleavage product [Kodama et al., 1973]. Thereafter, for convenience, the fermenter cultures were grown to stationary phase overnight (ca. 18 h) under the same conditions.

Enzymatic ring cleavage activity was induced in the grown culture by adding salicylic acid [Yen and Serdar, 1988]. The induced cells were harvested with a high speed continuous centrifugation system (CEPA; New Brunswick, NJ) and resuspended in potassium phosphate buffer (pH 7) to the same density as the original grown culture. This suspension was used in the same fermenter system as the "active biocatalyst", and subsequently incubated with a model substrate dissolved in a carrier.

Model substrates and carriers

Quantitative analysis of specific changes in the composition of petroleum products is difficult due to the chemcial complexity of the substrate. Therefore, we chose to "spike" petroleum products with individual model substrates and quantify their ring cleavage against the complex background. Phenanthrene and DBT were selected as model substrates for biocatalysis, representing tricyclic and heterocyclic aromatic substrates, respectively. DBT was dissolved in 20 mL of light mineral oil while phenanthrene was dissolved in 30 mL of authentic hydrotreated middle distillate HP16 and straight run diesel and added to the suspension of induced biocatalyst. This reaction mixture was incubated with aeration and agitation for 24 h to effect biotransformation of the substrates. Parallel cell-free controls were also prepared and compared with the biocatalytic samples.

Analytical methods

The rate of biotransformation of DBT dissolved in light mineral oil was determined spectrophotometrically at intervals during biocatalysis by clarifying ca. 1 mL of reaction mixture and measuring absorption at 475 nm. Additionally, 10.0 mL samples were removed and the internal standard was added for pentane extraction of residual DBT and quantitative gas chromatography (GC) [Wu et al., 1998]. The percentage of DBT biotransformed was then calculated by difference.

Similar extraction procedures were used during biocatalysis to recover residual phenanthrene dissolved in HP16 or straight run diesel. Quantitative GC was used to estimate the percentage of phenanthrene biotransformed, using biphenyl and benzothiophene as internal standards to determine the relative residual mass of the model substrate in the pentane extracts. The biotransformation percentage was determined by comparing the relative residual mass of the model substrate recovered after incubation with the biocatalyst to that of the model compound in a parallel sterile (cell-free) control.

Routine GC analysis of fractions and distillates was performed on a Hewlett-Packard model 5890 GC system equipped with a flame ionization detector (FID) and a sulfur-selective flame photometric ionization detector (FPD). Chromatography conditions have been described previously [Foght and Westlake, 1996].

RESULTS AND DISCUSSION

Specific ring cleavage activity of the biocatalyst during culture growth

It was necessary to determine the point in the growth curve at which a growing culture should be harvested for use as a biocatalyst. We observed a short culture lag time in the inoculated fermenter, with stationary phase achieved after 6 to 8 h incubation (Figure 1). The absolute DBT ring cleavage rate of this growing culture increased during incubation (data not shown), but the specific DBT oxidation rate (i.e. the ring cleavage rate normalized to biomass protein) achieved a maximum after 6 hours (Figure 1), i.e. in stationary phase. For convenience, we chose thereafter to standardize culture growth to an overnight incubation (ca. 18 h).

Biotransformation of DBT dissolved in light mineral oil by pre-grown, induced biocatalyst

Light mineral oil was chosen as the carrier for this experiment because it approximates the aliphatic fraction of petroleum products and does not interfere with quantitative GC analysis of the residual DBT.

A rapid decrease in the residual DBT was observed in the biphasic fermenter system. By 7 hours incubation with the biocatalyst, less than 10% of the DBT remained, and within 20 hours the DBT was completely removed (Figure 2). Concomitant accumulation of the DBT ring cleavage

product, monitored spectrophotometrically at 475 nm, reached a maximum at ca. 8 h. then decreased, most likely due to side-reactions of the ring cleavage product.

Biotransformation of phenanthrene dissolved in middle distillate HP16 or straight run diesel by pre-grown, induced biocatalyst

Biotransformation of the model substrate phenanthrene incubated with biocatalyst in a biphasic fermenter system is shown in Figure 3. Middle distillate HP16 or diesel were used as carriers. Unlike DBT biocatalysis (Figure 2), complete removal of phenanthrene was not achieved within 22 h. However, significant biotransformation was observed, with similar initial rates for both carriers. The middle distillate permitted slightly better biotransformation than the diesel (ca. 80% versus ca. 60% substrate removal). The fermenter system achieved better biotransformation than typical batch flasks, which achieved 60% removal of phenanthrene dissolved in middle distillate HP16 in 24 h [Wu et al., 1998].

CONCLUSIONS

Preparation and use of the biocatalyst in fermenter system is rapid and easily controlled using aeration, agitation and temperature. In a single fermenter the biocatalyst can be grown, induced, then re-suspended in buffer (after harvesting) for incubation with the substrate. Biotransformation of model substrates in various carriers was achieved at rates surpassing those achieved in small volume batch flasks, possibly due to superior mixing in the fermenter. The biphasic fermenter system is promising and warrants further research for optimization of operating conditions and for scaling up to larger volumes.

ACKNOWLEDGMENTS

Grateful acknowledgment is made of support from Texaco Group, Inc., the National Centre for Upgrading Technology (Canada), and the Natural Sciences and Engineering Research Council of Canada (Collaborative Research & Development Program).

REFERENCES

WU, Q., FEDORAK, P., PICKARD, M., GRAY, M. and FOGHT, J. M., *216th ACS National Meetings, American Chemical Society, Boston, MA, August 23-27, 1998, Division of Fuel Chemistry, Paper 148*

FOGHT, J. M., WU, Q., FEDORAK, P., PICKARD, M. and GRAY, M., *Proceedings of BIOMINET/NCUT Symposium at the 48th Annual Technical Meeting of the Petroleum Society*, June 9, 1997

FOGHT, J. M. and D. W. S. WESTLAKE, *Biodegradation* Vol. 7, pp. 353-366, 1996.

YEN, K. M. and C. M. SERDAR, *Critical Reviews in Microbiology* Vol. 15, pp. 247-268, 1988.

KODAMA, K., UMEHARA, K., SHIMIZU, K., NAKATANI, S., MINODA, Y. AND YAMADA, K., *Agric. Biol. Chem.* Vol. 37, pp. 45-50, 1973.

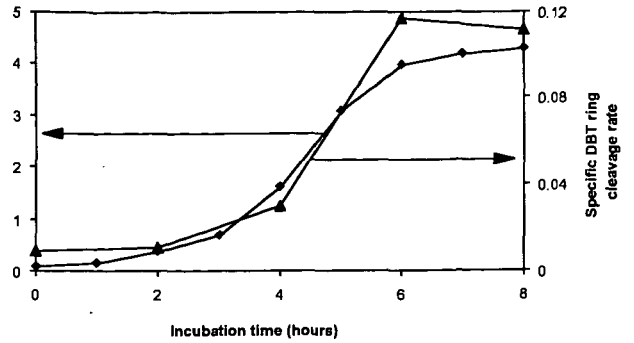

Figure 1. Correlation of culture growth and DBT ring cleavage activity. Growth curve of *P. fluorescens* #21-41 at 30°C measured as optical density at 600 nm (OD_{600}), and specific DBT ring cleavage rate (absorption units at 475nm•min^{-1}•mg biomass $protein^{-1}$) during growth.

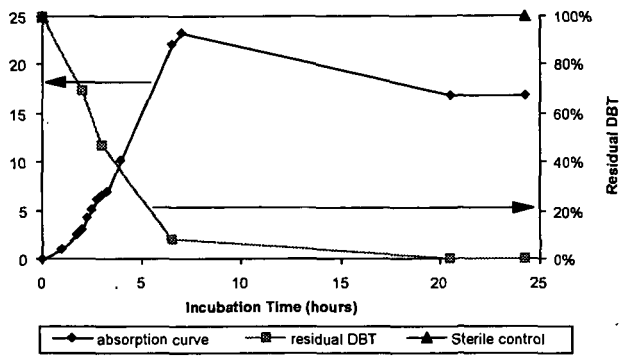

Figure 2. Biocatalysis of DBT and formation of ring cleavage product. Biotransformation of DBT dissolved in light mineral oil by *P. fluorescens* LP6a #21-41 and accumulation of its ring cleavage product, measured at 475 nm; residual DBT measured quantitatively by GC.

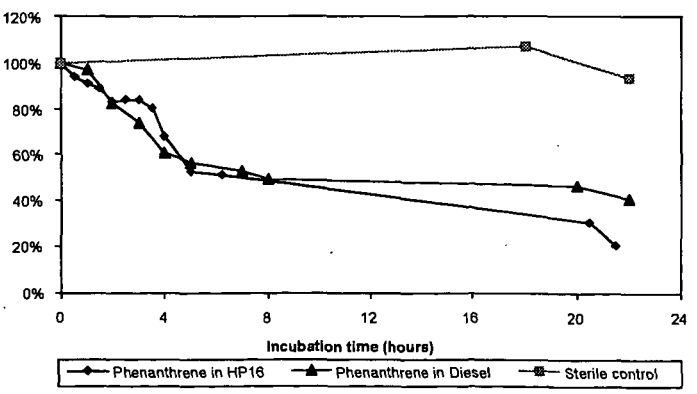

Figure 3. Biocatalysis of phenanthrene in biphasic fermenter system. Biotransformation of phenanthrene dissolved in middle distillate HP16 or diesel fuel by pre-grown, induced biocatalyst, measured by quantitative GC as removal of residual phenanthrene.

MICROBIAL DENITROGENATION OF FOSSIL FUELS

Phillip R. Gibbs[1], Robert R. Riddle[2], Michael J. Benedik[2], and Richard C. Willson[1].
1. Department of Chemical Engineering, University of Houston, Houston TX 77204-4792
2. Department of Biochemical and Biophysical Sciences, University of Houston, Houston TX 77204-5934

ABSTRACT

The microbial degradation of nitrogen compounds from fossil fuels is important because of the contribution these contaminants make to the formation of nitrogen oxides (NOx) and hence to air pollution and acid rain. They also contribute to catalyst poisoning during the refining of crude oil, thus reducing process yields. In this study carbazole was used as the model nitrogen aromatic and 1-methylnathphalene was used as the model fuel. Two-phase bioconversions were carried out with carbazole-degrading strains to investigate the feasibility of microbial upgrading of fossil fuels by the removal of nitrogen aromatic contaminants.

INTRODUCTION

Several heterocyclic aromatic nitrogen compounds are found in fossil fuels[1]. Crude oil is a heterogeneous mixture of organic molecules including all-hydrocarbon alkanes and aromatics, as well as sulfur-, oxygen-, and nitrogen-containing heteroaromatic compounds. Many applications of crude oil are hindered by the presence of sulfur-, oxygen-, and nitrogen-containing aromatic compounds. The nitrogenous compounds found in crude oils fall into two classes. The 'nonbasic' molecules include pyrroles and indoles but are predominantly mixed alkyl derivatives of carbazole, while the 'basic' molecules are largely derivatives of pyridine and quinoline (Fig. 1). The total nitrogen content of crude oils averages around 0.3% of which the nonbasic compounds comprise approximately 70-75% (Petrolite). As existing supplies of high quality, low-boiling-point crude decrease, there is a trend towards the use of lower-volatility oils with higher nitrogen contents.

The removal of aromatic nitrogen contaminants from petroleum is important for many reasons. First, their combustion leads directly to the formation of nitrogen oxides (NOx); emissions of NOx, which contributes to acid rain, are under increasingly stringent control by environmental regulations[2,3]. Second, the presence of aromatic nitrogen compounds can lead to significant poisoning of refining catalysts, resulting in a decrease in yield. Carbazole, the major nonbasic species, directly impacts the refining process in two ways: (1) it is converted during the cracking process into basic derivatives that can adsorb to the active sites of the cracking catalyst; and (2) it is unexpectedly potent as a direct inhibitor of hydrodesulfurization, which is commonly included in the refining process in order to meet sulfur content criteria[4-6]. The practical consequence of this catalyst poisoning is that the removal of carbazole and other nitrogen species can significantly increase the extent of catalytic-cracking conversion and the yield of gasoline. With a 90% reduction in nitrogen content, an increase in gasoline yields of up to 20% may be achievable (Petrolite), which would represent a major economic improvement in low-margin, high volume refining processes. Finally, the presence of nitrogen compounds promotes the corrosion of refining equipment such as storage tanks and piping, which adds to the refining costs[7].

Nitrogen heteroaromatics can be eliminated from petroleum using high pressure, high temperature hydrotreating, but such processes are expensive and hazardous, and also modify many other constituents of petroleum. Current research on microbial denitrogenation focuses on the degradation of the nonbasic nitrogen compounds and their alkyl derivatives, because they represent the majority of the total nitrogen and the basic nitrogen compounds can be readily extracted if desired. Although solvent extraction methods also exist for the nonbasic species, approximately 30% of the oil is retained in the extract phase. Such solvent treatments are thus ill-suited to the efficient removal of the nitrogen content.

We believe that microbial transformation of nitrogen heteroaromatics can be used to alleviate catalyst inhibition in several ways. Carbazole, for example, can be completely metabolized to CO_2 and biomass, or (using appropriate blocked mutant strains) converted to anthranilic acid or other intermediates. These appear likely to cause less catalyst inhibition than their parent compound, and many polar intermediates could be readily extracted from petroleum streams into water. It has been reported that carbazole enrichment cultures are capable of degrading a wide range of alkylcarbazoles present in crude oil, generally yielding water-soluble, nontoxic metabolites[8].

In this study Pseudomonad LD2 received from Prof. Phil Fedorak's at the University of Alberta was used due to its extensive metabolic characterization[9] and its high activity relative to other isolates obtained in our lab. Based on published reports of cloning of carbazole degradaing activity in the literature[10,11], the carbazole genes were cloned and mobilized to several other strains of bacteria for two-phase experiments. Many pseudomonads were selected for known solvent resistance[12]. In other model systems based on dibenzothiophene, hexadecane was used as the model fuel. However, given the low solubility of carbazole in hexadecane (~0.03 wt%), 1-methylnapthalene proved to be a better choice due to higher solubility (~0.8 wt%), low freezing point (-22°C), and ease of emulsion separation in the two-phase system. While 1-methylnapthalene proved to be a superior solvent, the toxicity of the oil phase to the microorganisms was problematic compared to hexadecane. Thus several organisms were tested in the model system to find a strain compatible with the 1-methylnapthalene two-phase system.

MATERIALS AND METHODS

Microorganisms and media

A pure culture of Pseudomonas sp. LD2 was obtained from Phil Fedorak's lab at the University of Alberta. Other Pseudomonas strains were obtained from Dr. Jurtshuk at the University of Houston. The growth medium for the culturing of the microorganisms had the following composition (g/L) Tryptone 10, Yeast Extract 10, K_2HPO_4 5, and glycerol 10. Trace metals solution was added at 5 ml to 1 L and had the following composition (g/L) $MgSO_4$ 4.0, NaCl 0.2, $FeSO_4*7H_2O$ 0.2, $MnSO_4*4H_2O$ 0.2, D.I. H_2O 100ml. Solid media were prepared by adding 15 g/L agar to LB medium. LB medium had the following composition (g/L) Tryptone 10, Yeast Extract 5, NaCl 10.

Growth conditions

Seed cultures were started by inoculating 5 ml of media with a sterile loop dipped in -80°C frozen seed cultures with 25% glycerol. The seed cultures were incubated at 30°C in a water bath shaker for 6-8 hours or until approximately 1-2 OD was reached. One ml of this seed culture was added to 1L of media in a 2.8L Fernbach baffled shake flask and incubated at 30°C and 250rpm. After 12-16 hours of growth, the cells were harvested by centrifugation at 4,000 rpm in a Beckman J6B. The supernatant was discarded, and the cells were resuspended in 500 ml of LB for use in two-phase experiments.

Two-phase model system

Thirty ml of cell slurry was added to a 300 ml baffled shake flask. To this flask, 10 ml of 1-methylnapthalene with 0.8 wt% carbazole was added. In hexadecane experiments, 10 ml of carbazole-saturated hexadecane were added. These flasks were incubated at 30 °C and 250 rpm. Time samples were taken by removing a flask and emptying the contents into a 40 ml polypropylene centrifuge tube. The sample was then centrifuged at 15,000 rpm for 30 minutes. After centrifugation a disposable pipette was used to remove approximately 2 ml of the 1-methylnapthalene layer. The 1-methylnapthalene phase was added to an amber 1.5 ml GC sample vial for analysis.

GC analysis

The 1-methylnapthalene phase was analyzed on a HP 6890 gas chromatograph. One µl of sample was injected on a HP-5 column at an initial column temperature of 160°C. The method held the column at the initial temperature for 2 minutes then increased the temperature at a rate of 8°C/min until 250°C was attained. This final temperature was held for 2 minutes. The detector was a NPD, which is specific for nitrogen.

Results and Discussion

Several strains were tested, and the results are summarized in Table 1. All strains tested in the hexadecane model systems showed removal of a low level (~0.03 wt%) of soluble carbazole. However, only one strain showed any ability to remove carbazole in the 1-methylnapthalene two-phase system. None of the tested strains were observed to grow on 1-methylnapthalene as the sole source of carbon. Thus, the 1-methylnapthalene did not supply a co-metabolic substrate for carbazole degradation. In the systems containing *P. fraggi*, the total observed removal of carbazole was 4.7% after 3 hours, 11.3% after 18 hours, and 13.3% after 28 hours relative to the stock solution. An additional flask at 45 hours did not show any further decrease in carbazole concentration relative to the stock solution. In the hexadecane experiments, no carbazole was detected after 2 hours of incubation. No intermediates of carbazole metabolism were detected in

the GC analysis in either of the model system runs. However, control samples analyzed by GC were able to detect anthranilic acid, which is a known intermediate in carbazole degradation[13]. The control flask not containing microorganism did not show any change in carbazole concentration relative to the stock solution. A specific activity was not calculated since growth occurred during the reaction, and the 1-methylnapthalene prevented measurement of optical density or dry cell weight.

CONCLUSIONS

The investigation of biodenitrogenation of fossil fuels requires the selection of a model fuel for use in two-phase experiments. While systems utilizing hexadecane have been used for similar studies in desulfurization, the low solubility of carbazole in hexadecane eliminates this solvent from serious consideration. 1-methylnaphalene is a good solvent for carbazole, is easily purchased, and forms an emulsion during testing that was easily broken by centrifugation. However, the observed toxicity of the solvent to many normally solvent-resistant strains of bacteria necessitated the search for a compatible biocatalyst for the model system. This initial screening indicates that at least one strain, *P. fraggi*, is capable of removing carbazole with 1-methylnapthalene as the model fuel. This strain may also prove more resistant to the toxicity of petroleum refining streams

REFERENCES

1. Gibson, D. T., Zylstra, G. J. and Chauhan, K. (1991) in Psuedomonas Biotransformations, Pathogenesis, and Evolving Biotechnology (Silver, S., Chakrbarty, A. M., Iglewski, B. and Kaplan, S., eds), pp 121-132 American Society for Microbiology.

2. Campbell, I. M. (1992) Coal Biodenitrogenation: Microbial Processing of Nitrogen-containing Coal Model Compounds, DOE Pittsburgh Energy Technology Center Report D91-65, PA, USA.

3. Cooney, C. M. (1997) Environ. Sci. Technol. 31, 554-555.

4. Girgis, M. J. and Gates, B. C. (1991) Ind. Eng. Chem. Res. 30, 2021-2058

5. La Vopa, V. and Satterfield, C. N. (1988) J. Catal. 110, 375-387

6. Nagai, M. and Kabe, T. (1983) J. Catal. 81, 440-449

7. Kobayashi, T., Kurane, R., Nakajima, K., Nakamura, Y., Kirimura, K. and Usami, S. (1995) Biosci. Biotechnol. Biochem. 59, 932-933

8. Fedorak, P. M. and Westlake, D. W. S. (1984) Appl. Environ. Microbiol. 47, 858-862

9. Gieg, L. M., Otter, A. and Fedorak, P. M. (1996) Appl. Sci. Technol. 30, 575-585

10. Sato, S., Nam, J., Kasuga, K., Nojiri, H., Yamane, H. and Omori, T. (1997). J. Bacteriol. 179, 4850-4858

11. Sato, S., Ouchiyama, N., Kimura, T., Nojiri, H., Yamane, H. and Omori, T. (1997). J. Bacteriol. 179, 4841-4849

12. Inque, A., Horikoshi, K., (1991) J. of Ferm. Bioeng. 71, 3, 194-196

13. Ouchiyama, N., Zhang, Y., Omori, T. and Kodama, T. (1993) Biosci. Biotechnol. Biochem. 57, 455-460

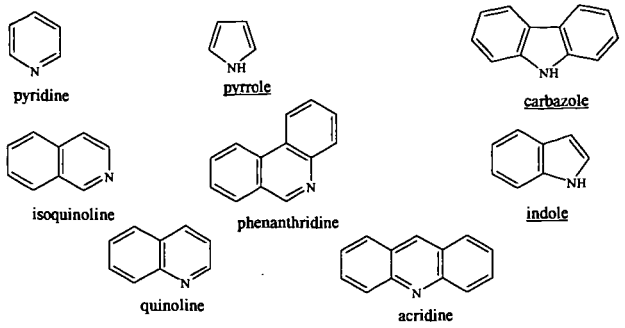

Figure 1: Examples of common nitrogen aromatic compounds found in fossil fuels. The nonbasic species are underlined.

Strain	Hexadecane system	1-methylnapthalene system
E. coli	+	-
P. sp. LD2	+	-
P. fraggi	+	+
P. mendicino	+	-
P. idaho	+	-
P. putida	+	-

Table 1. Tested strains harboring the carbazole degradation genes. Removal of carbazole from the model oil phase is denoted with a +.

BIOCATALYTIC UPGRADING OF PETROLEUM

Lisa J. Nash and Stephen R. Palmer
Energy BioSystems Corporation
4200 Research Forest Drive
The Woodlands, TX 77381

INTRODUCTION

Sulfur, nitrogen, metals and high viscosity in petroleum cause expensive processing problems in the refinery. Conventional technology does not exist to economically remove these contaminants from crude oil, so the problem is left for the refiners to handle downstream at a high cost.

Sulfur is the major concern for producers and refiners and has long been a key determinant of the value of crude oils for several reasons. First, sulfur presents a processing problem for refiners. Desulfurization offers refiners the opportunity to reduce the sulfur of their crude feedstocks before they ever enter the refinery system, minimizing downstream desulfurization costs. Secondly, the amount of sulfur in many finished products (i.e. diesel, gasoline) is limited by law. The regulations restricting allowable levels of sulfur in end products continues to become increasingly stringent. This creates an ever more challenging technical and economical situation for refiners as the sulfur levels in available crude oils continue to rise and creates a market disadvantage for producers of high-sulfur crudes. Lower-sulfur crudes continue to command a premium price in the market, while higher sulfur crude oils sell at a discount. Desulfurization would offer producers the opportunity to economically upgrade their resources.

Metals in petroleum lead to two major problems for the industry. Combustion of these fuels leads to the formation of ash with high concentrations of the metal oxides, leading to undesirable waste disposal issues. Also, when crude oil is refined, the metals are concentrated in the residual fraction. The residual fraction is often subjected to catalytic cracking where metals from the oil deposit on the cracking catalysts, resulting in the poisoning of the catalysts and decreasing their selectivity and activity. Like metals, nitrogen in oil also leads to the poisoning of the refinery catalysts and also results in increased nitrogen oxide emissions upon combustion in car engines.

High viscosity significantly hampers the pumping, transportation, refining and handling of petroleum. Common methods used to overcome problems associated with high viscosity include heating, dilution and chemical additives. All are expensive and require specialized equipment and/or safety procedures. Industry has long recognized the need for a safe, economical and effective method for reducing viscosity.

Biocatalytic processes for addressing these problems offers the petroleum industry potentially great rewards. Studies by Energy Biosystems Corporation (EBC) have focused on the removal of sulfur from crude oil and refinery streams by a microbial process, termed biocatalytic desulfurization (BDS). Furthermore, preliminary work has also been performed (and patented) on biocatalytic approaches to viscosity reduction and the removal of metals and nitrogen as additional approaches to fuel upgrading. Here, results of work performed on the biocatalytic desulfurization of crude oil will be presented.

MATERIAL AND METHODS

Materials and Equipment. 40 mL shake flasks and 500 mL batch stirred reactors (BSRs) were used to contact cells and crude oil. The reactor vessels are maintained at a constant temperature of 30°C by placing them in an incubator (shake flasks) or temperature controlled water jackets (BSRs).

Cells. Derivatives of the *Rhodococcus erythropolis* strain IGTS8 (ATCC 52986) used in these experiments are known for their ability to use organically-bound sulfur as the sole sulfur source. These cells catalyze the transformation of dibenzothiophene (DBT) to 2-hydroxybiphenyl (2HBP) and sulfate [1-3].

Oil. The crude oils used in the experiments were supplied by Texaco Exploration and Production Technology. Figure 1 shows chromatograms resulting from the sulfur chemiluminescence detector (SCD, sulfur-specific) of several crude oils. The sulfur contents range from 0.8 to 3.7 wt%. As a control, a model oil consisting of hexadecane (HD) and DBT dissolved to ~2600 ppm was utilized.

Procedures. A cell concentration of 12 to 50 g wet cell paste (WCP) per liter of total liquid volume contained in the reactor was utilized. Frozen cells were first added to sodium phosphate buffer (pH 7.5 at 0.156 mM) with 3% glucose. The cell slurry was placed in the reactor, agitated at 1000 rpm and sparged with 0.2 vvm air. The oil was added in the ratio of 1 part oil to 3 parts buffer. Shake flasks were taken down at specified times and BSRs were sampled at regular intervals to monitor sulfur concentrations. Samples were centrifuged at 39,000 x g for 10 minutes in order to separate the mixture of oil, water and cells. To ensure that any observed change was strictly cell-dependent, parallel experiments were performed without cells.

Analytical Methods. An HP 6890 gas chromatograph with electronic pressure control and detection by flame ionization detector (FID) and a Sievers model 350 flameless SCD was employed for crude oil analysis. The column was a Restek RTX-5, 15 meter, 0.25 mm ID with a 0.25 µm film thickness. The injection port was held at 340°C. The oven temperature program began at 50°C and was held for 2 minutes. The temperature was then increased by 15°C/minute to 320°C and was held for 10 minutes. A typical SCD chromatogram consists of a group of resolved peaks above a broad envelope of sulfur compounds (Figure 1).

A GC/MS SIM method for the quantitation of Cx-DBTs and Cx-benzonaphthothiophenes (Cx-BNTs) in crude oil was performed using a HP 5890 Series II plus gas chromatograph with electronic pressure control and mass spectrometric detection performed with an HP 5972 MSD. The column was a Restek RTX-1, 30 meter, 0.25 mm ID with a 0.5 µm film thickness. The injection port was held at 290°C. The oven temperature program began at 100°C, increased at a rate of 4°C/min to 315°C and held for 20 minutes.

Total sulfur quantitation of crude oils was performed with either a Horiba SLFA-1800H x-ray fluorescence analyzer or a Leco SC-444 Sulfur and Carbon Combustion Analyzer with infrared detection.

Sulfur XANES analyses were obtained at beam-line X-19A of the National Synchrotron Light source (NSLS), Brookhaven National Laboratory. Work was performed under contract with the University of Kentucky.

RESULTS AND DISCUSSION

Biocatalyst Development

The development of BDS for crude oil is complicated by the fact that the oil has a very wide boiling point range and that relatively little is known about the number and types of sulfur compounds and their concentrations present in crude oils. The state of EBC's analytical capabilities has greatly advanced to characterize crude oil including sulfur content, sulfur speciation and quantification, and physical properties. Many specialized techniques have been developed that have allowed us to gain valuable insight into the substrate specificity of the catalyst.

We have shown that the enzyme system in the *R. erythropolis* IGTS8 is extremely effective in transforming DBT, BNT, benzothiophene (BT) and their alkylated congeners in crude oil. Sulfur specific chromatograms of crude oil BDS samples reveal that the majority of these substrates have been removed (Figure 2). These results have been confirmed by GC/MS analysis developed to quantify the levels of the DBTs and BNTs in the crude oil (Figure 3). These methods have also revealed that the concentrations of these molecules were low in the crude oils tested and directly correlated to the amount of sulfur removed.

Attempts were made to characterize the sulfur species remaining after BDS (referred to as "Dsz recalcitrant material" or DRM). It was determined by XANES analysis that the majority of the sulfur in the DRM of this material is thiophenic (Figure 4) and, therefore, good targets for the IGTS8 catalyst.

A method to isolate and identify sulfur compounds from various oils and their DRMs was developed. The sulfur-containing species were selectively oxidized and converted to their corresponding sulfones. The sulfones were then separated from the hydrocarbon matrix by solid phase extraction (SPE). This powerful technique has allowed for the identification of the types of sulfur compounds remaining in the treated crude.

Other biocatalytic processes are under investigation that will result in crude upgrading. "Biocracking" has been investigated as a means to break down larger sulfur molecules so they will be small enough to enter the cell and to reduce the viscosity. Attempts were made to isolate organisms able to degrade compounds in the high molecular weight range. Proof-of-concept experiments were performed and validated with methylenebis-DBT (MBD). The goal was to isolate strains that could cleave the bond between the two DBTs. Soil samples were prepared and incubated with MBD. These enrichments were serially transferred, then plated to purify colonies. Individual isolates were obtained for further study.

In addition, if the sulfur bearing heterocycles contribute significantly to the viscosity of the oil, biocatalytic oxidative cleavage of at least one carbon-sulfur bond adjacent to the sulfur heteroatom(s) would result in the opening of the heterocyclic rings and sites of free rotation in the molecules formed effectively lowering the overall viscosity [4].

It has been shown that metals can be removed from crude by contacting the oil with an enzyme that degrades the metalloporphyrin molecules under conditions suitable for the removal and subsequent separation of the metals from the oil. The metals that were removed by the method [5] include nickel, vanadium, cobalt, copper, iron, magnesium and zinc.

Removal of nitrogen is also being investigated as an additional approach to fuel upgrading. This work is being performed at the University of Houston [6] and has been subsidized by EBC. Work has focused on the carbazole-degrading Pseudomonad LD2. Approaches in progress include isolation and characterization of the carbazole degradation enzymes, as well as the characterization and cloning of the genes encoding these enzymes.

The goal is to put all these catalytic activities together either in a single biocatalyst or a consortia to upgrade the petroleum by removing the sulfur, nitrogen, metals and reducing the viscosity in a single process step.

Process Development
Shake flask and BSR experiments were performed to address process concerns, such as reaction characteristics, separation characteristics, and catalyst stability and effectiveness. The effect of these parameters were determined in a series of assays designed to compare initial rates of desulfurization under a variety of process conditions. The assay results determined the optimum process conditions for BDS. The key parameters evaluated were water to oil ratio (WOR), catalyst to oil ratio (COR), mixing effects, oxygen demand, and temperature and pH optimum.

A process concept for the biodesulfurization of crude oil was developed based on the knowledge generated, a bench scale unit was constructed and proof-of-concept experiments were performed to develop a design basis specifying performance criteria, unit operations and process parameters for the biodesulfurization of crude oil. As part of the process flow diagram (PFD) development, a general description of the expected site conditions and product stream attributes was compiled. In addition, the process assumptions and equipment issues were delineated that were crucial to the design.

At this time, we envision a simple system capable of running with minimum operator intervention in the oilfield. The base case scenario for a field process is a batch reaction utilizing a pump and inductor for mixing and aeration. Separations will be performed with standard oilfield equipment, with desulfurized oil returning to storage and process water reinjected into a disposal well in the field. The spent catalyst will be inactivated and landfilled. The stored product oil would be tested for sulfur and other oil quality specifications prior to transport. Based on this process concept, the identified process parameters and assumptions, the attached PFD (Figure 5) was developed.

CONCLUSIONS

Significant progress has been made toward the commercialization of crude oil biodesulfurization. This progress includes the characterization of crude oil candidates for the BDS process; improved biocatalyst performance that directly relates to crude oil biodesulfurization; development of analytical methodology, which led to breakthroughs in the characterization of DRM; development of a process concept for crude oil BDS; and construction and testing of a prototype bench unit.

Technical hurdles still need to be overcome to achieve commercialization. The major obstacles to the economical biodesulfurization of crude oil include catalyst specificity and rate. Work continues to modify the catalyst to increase its effectiveness and to screen other organisms for additional desulfurization capabilities. In addition, mass transfer and separations hurdles must be overcome in crude oils with increased oil viscosity and density.

ACKNOWLEDGEMENTS

The authors would like to acknowledge the National Institute of Standards and Technology (NIST) for support received through an Advanced Technology Program (ATP) grant for crude oil BDS, Phil Gibbs and Richard Willson of the University of Houston for their work on denitrogenation, Texaco Exploration and Production Technology for providing the crude oils and the many dedicated people at Energy BioSystems Corporation.

REFERENCES

[1] Kilbane, J. J. and K. Jackowski. 1992. Biodesulfurization of water-soluble coal derived material by *Rhodococcus erythropolis* IGTS8. Biotechnol. Bioeng. **40**:1107-1114.

[2] Monticello, D. J. 1993. Biocatalytic desulfurization of petroleum and middle distillates. Environmental Progress. **12**:1-4.

[3] Gray, Kevin A., O. Pogrebinsky, G. Mrachko, L. Xi, D. J. Monticello and C. Squires. 1996. Molecular mechnanisms of biocatalytic desulfurization of fossil fuels. Nature Biotechnology. **14**:1705-1709.

[4] Monticello, D. J. and W. M. Haney. 1996. Biocatalytic process for reduction of petroleum viscosity. U. S. Patent #5,529,930.

[5] Xu, G., K. Mitchell and D. J. Monticello. 1997. Process for demetalizing a fossil fuel. U. S. Patent #5,624,844.

[6] Gibbs, P. R., R. R. Riddle, M. J. Benedik and R. C. Willson. Biochemistry of carbozole degradation. ACS Biotechnology Secretariat Symposium on Environmentally Benign Synthesis and Biocatalysis in Remediation. Boston, MA, USA, August 23-27, 1998.

Figure 1. Example SCD Chromatograms of Selected Crude Oils

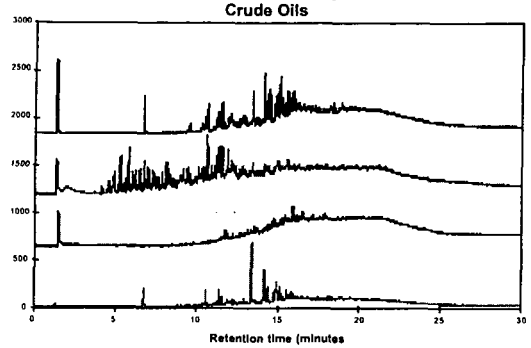

Figure 2. BDS of a Target Crude Oil

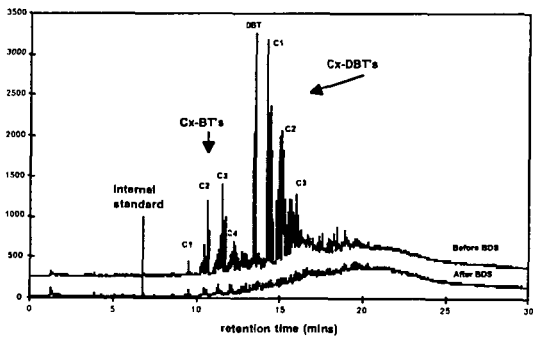

Figure 3. DBT Concentrations Before and After BDS for a Typical Crude Oil

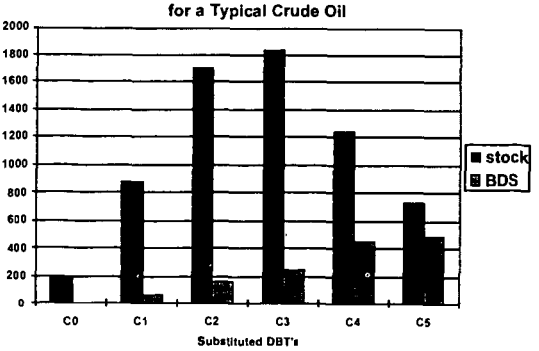

Figure 4. XANES Data for Various Petroleums

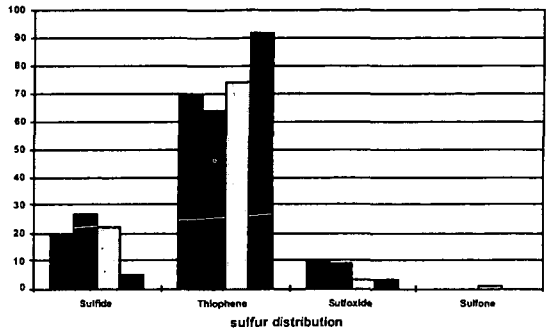

Figure 5: Proposed Process Flow Diagram for Crude Oil Biodesulfurization

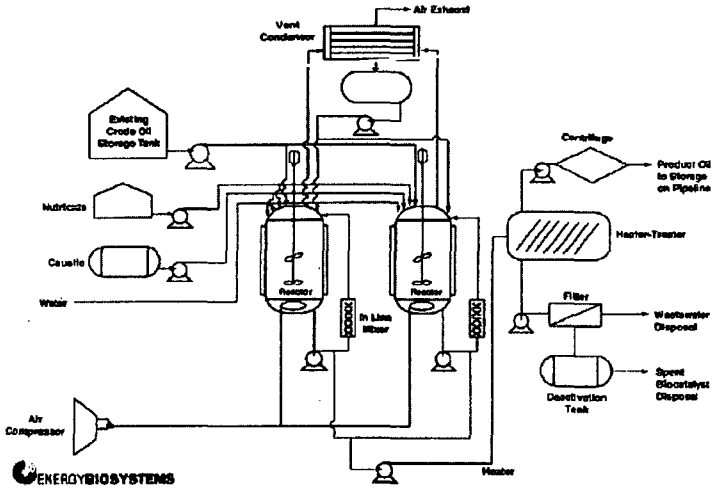

PROCESS CONSIDERATIONS IN CRUDE OIL BIODESULFURIZATION

Abhijeet P. Borole and Eric N. Kaufman
Bioprocessing Research and Development Center
Chemical Technology Division
Oak Ridge National Laboratory
Oak Ridge, Tennessee, USA 37831-6226

ABSTRACT

Biodesulfurization offers an attractive alternative to conventional hydrodesulfurization due to the mild operating conditions and reaction specificity afforded by the biocatalyst. The enzymatic pathway existing in *Rhodococcus* has been demonstrated to oxidatively desulfurize the organic sulfur occurring in dibenzothiophene while leaving the hydrocarbon intact. In order for biodesulfurization to realize commercial success, a variety of process considerations must be addressed including reaction rate, emulsion formation and breakage, biocatalyst recovery, and both gas and liquid mass transport. This study compares batch stirred to electro-spray bioreactors in the biodesulfurization of both model organics and actual crudes using a *Rhodococcus* IGTS8 biocatalyst in terms of their operating costs, ability to make and break emulsions, ability to effect efficient reaction rates and enhance mass transport. Additionally, sulfur speciation in crude oil is assessed with respect to sulfur specificity of currently available biocatalysts.

KEY WORDS: crude oil desulfurization, *Rhodococcus*, electrostatic spraying, dibenzothiophene, biodesulfurization

INTRODUCTION

Biological processing of fossil fuel feedstocks offers an attractive alternative to conventional thermochemical treatment due to the mild operating conditions and greater reaction specificity afforded by the nature of biocatalysis. Efforts in microbial screening and development have identified microorganisms capable of petroleum desulfurization (see for example, [1-3]), denitrification [4], demetalization [4], cracking [5] and dewaxing. Biological desulfurization of petroleum may occur either oxidatively or reductively. In the oxidative approach, organic sulfur is converted to sulfate and may be removed in process water. This route is attractive due to the fact that it would not require further processing of the sulfur and may be amenable for use at the well head where process water may then be reinjected. In the reductive desulfurization scheme, organic sulfur is converted into hydrogen sulfide, which may then be catalytically converted into elemental sulfur, an approach of utility at the refinery. Regardless of the mode of biodesulfurization, key factors affecting the economic viability of such processes are biocatalyst activity and cost, differential in product selling price, sale or disposal of co-products or wastes from the treatment process, and the capital and operating costs of unit operations in the treatment scheme.

In all fossil fuel bioprocessing schemes, there is a need to contact a biocatalyst containing aqueous phase with an immiscible or partially miscible organic substrate. Factors such as liquid / liquid and gas / liquid mass transport, amenability for continuous operation and high throughput, capital and operating costs, as well as ability for biocatalyst recovery and emulsion breaking are significant issues in the selection of a reactor for aqueous / organic contacting. Traditionally, impeller-based stirred reactors are utilized for such mixing due to their ease of operation and wide acceptance in the chemical and biological processing industries. Such mechanically stirred reactors contact the aqueous and organic phases by imparting energy to the entire bulk solution, i.e. the impeller must move the contents of the reactor.

Recent advances in the area of contactors for solvent extraction have lead to the development of electrically driven emulsion phase contactors (EPC™) for efficient contact of immiscible phases [6]. In this concept, the differing electrical conductivity between the aqueous and organic phases causes electrical forces to be focused at the liquid / liquid interface, creating tremendous shear force. This shear causes the conductive phase to be dispersed (5 □m droplet size) into the non-conductive phase, but does so with decreased energy requirements relative to mechanical agitators due to the fact that energy is imparted only at the liquid / liquid interface and not the entire bulk solution. In a configuration of the EPC™ developed at the Oak Ridge National Laboratory, the contactor serves to disperse aqueous phase containing biocatalyst into an organic

phase. The EPC™ creates droplets of water containing biocatalyst ~5 □m in diameter within an organic phase.

Here, we compare the performance of the EPC™ to that of a batch stirred reactor (BSR), investigate the required level of biocatalyst activity before the surface area afforded by the EPC™ becomes a factor in reactor performance, and characterize the emulsion formed by both reactors in the presence of bacteria. We have investigated the emulsion quality formed in the EPC, evaluated the power requirements and analyzed the mass transfer issues in comparison to stirred reactors. Results on biodesulfurization of actual crude oil by wild type *Rhodococcus* IGTS8 are also included. Finally, we assess the sulfur specificity of available biocatalysts with respect to sulfur compounds present in crude oils.

MATERIALS AND METHODS

The experimental procedures used for studying biodesulfurization in model systems have been discussed in detail in previous publications [7-9]. A detailed description of oil experiments is provided here.

Biodesulfurization of Van Texas Crude oil

Biodesulfurization of Van Texas crude oil was studied in batch stirred reactors to evaluate the substrate specificity of the biocatalyst. The experiment was conducted over a treatment period of 6 days. The crude had an API specific gravity of 31°, and a sulfur content of 0.96 wt.%. The crude oil did not contain volatiles due to production at elevated temperature (~99°C). Experiments were performed in batch stirred reactors utilizing 50 g of frozen *Rhodococcus sp.* wild type strain IGTS8 (ATCC 53968) cell paste which were brought up to 750 mL with 0.156M (pH 7.5) phosphate buffer. The cells were suspended in the phosphate buffer prior to addition to the reactor. The reactor vessel used was a 1-L VirTis Omni-Culture fermentor (model 178657, Gardiner, NY), utilizing a 6-bladed Rushton-type impeller with 2 baffles. The reactor was kept at 30^{o}C, agitated at 800 RPM, and aerated with room air at a rate of 0.2 standard liters per minute (SLPM). A water condenser was used on each reactor to capture volatiles which were expected to be minimal or non-existent considering the fact that the operating temperature was much less than that of the oil reservoir. The experiment was conducted with 250 mL of crude oil, treated with 750 mL of the aqueous phase. Samples (30 mL from the top of the organic phase) taken during the course of biological treatment were collected after ceasing the agitation and aeration for 5 min to allow the aqueous and organic phases to separate. The reactor contents were emptied at the end of the run and centrifuged at 6000 rpm in a Beckman Model TJ-6 centrifuge to obtain a sample of treated crude oil. Closed samples were boiled in a closed container for 30 min to halt biological activity.

Analytical

Model system experiments

In the experiments reported here, DBT and 2-HBP concentrations in the aqueous phase were below our levels of detection. DBT and 2-hydroxybiphenyl (2-HBP) concentrations in n-hexadecane were measured by gas chromatography using a Hewlett Packard 5890 gas chromatograph equipped with a flame ionization detector.

Crude oil

A GC-SCD method was used to determine the sulfur content of the aromatic fraction of the oil. To allow facilitated observation of sulfur in the treated oil, whole oil samples were fractionated according to ASTM method D2007. An extended ASTM D2887 procedure was used for chromatographic separation of the aromatic fraction of the crude oil. Sulfur analysis was performed by modifying the ASTM D2887 procedure by adding a Sievers Chemiluminesence sulfur specific detector after the flame ionization detector.

RESULTS AND DISCUSSION

Rate of biodesulfurization

The specific rate of DBT desulfurization by *Rhodococcus sp.* was typically between 1 and 5 mg 2-HBP produced per dry g of biocatalyst per hour. Specific rates of 2-HBP production in the batch stirred reactor and the EPC™ reactor systems were within experimental variance and no

appreciable difference in desulfurization rates were seen between the two reactors. Due to the high surface area reported in the EPC™ [7], higher rates were expected in the EPC™, however, similar performance was observed in both reactors. The reaction rate obtained was without any supplemental carbon or energy source. Note that the only available carbon and energy source for the biocatalyst other than what may be carried over in the frozen cell paste, was hexadecane and DBT. However, DBT was not used as the carbon source by the biocatalyst, since the end product of DBT conversion was 2-HBP (thus preserving the carbon number and fuel value). Other studies (outlined in [7]) have utilized additional external carbon and energy sources and have reported higher activities with *Rhodococcus sp.* A commercial scale biodesulfurization process may require a higher cell density to achieve maximum conversion in a minimum time, provided it does not affect yield with respect to biocatalyst usage. In order to study effect of cell density, experiments were conducted in the BSR at different cell loadings. This experiment also lead to determination of the cell density at which point the BSR becomes mass transfer limited. A following experiment in the EPC™ at this cell density was conducted to evaluate the benefits of high surface area afforded by the EPC™.

Mass transport issues

The rate of desulfurization, when normalized with respect to cell mass, was found to decrease with increasing cell density indicating that mass transfer resistance was the controlling process in desulfurization. A statistical analysis of the data indicated mass transfer limitation between 5X and 10X cell density in the BSR. The mass transfer limitation may be due to gas-liquid or liquid-liquid mass transport resistance.

The results of experiments conducted in the BSR at 10X cell density indicated no gas-liquid mass transfer limitation. Increasing the rate of air supply or increasing the oxygen tension in the reactor through the use of pure oxygen rather than air did not seem to affect HBP production. This suggests that the system may be limited by liquid-liquid mass transfer. Since the EPC™ reportedly provides larger liquid-liquid interfacial area, the BSR was compared with the EPC™ for desulfurization activity at the high cell density.

Comparison of the EPC™ and BSR performance at 10X cell density showed no difference in the desulfurization rates between the two reactors. Thus, either the system is not truly mass transport limited or the EPC™ did not provide a larger surface area for reaction under the present conditions. A detailed characterization of the emulsions formed in the BSR and EPC™ in the presence and absence of biocatalyst was conducted and is reported below.

Emulsion quality in BSR and EPC™

A detailed drop size analysis of the two-phase emulsion formed in the BSR has been reported previously [7]. Characterization of the emulsion quality in BSR in the absence of biocatalyst has revealed 100-200 micron droplets under the conditions of experiments conducted here. The droplets formed in the EPC; however, are in the 1-10 micron range. The ability to form fine emulsions in the EPC™ without increasing energy utilization (see energy utilization section below) could have tremendous impact upon processing costs assuming that the biocatalyst utilized is active enough to be mass transport limited.

Emulsion quality in the presence of biocatalyst

Due to the opaqueness rendered by presence of biocatalyst, observations could not be made *in situ* during reactor operation. To determine the emulsion quality formed in the EPC™ and BSR, and to determine whether the EPC™ offers larger surface area than BSR, samples were collected from the reactors and observed under a microscope using a 100x oil emersion objective. Microscopic examination of samples showed formation of a very fine emulsion in both reactors with droplet sizes ranging from 1 to 10 □m. Formation of such an emulsion in the BSR may be presumed due to production of biosurfactants by the biocatalyst IGTS8. Average droplet size for EPC™ and BSR samples were 2.54 ± 2.40 □m and 3.08 ± 1.78 □m, respectively (n>300). Further, a significant amount of the biocatalyst was extracted and existed in the organic phase. Thus, a very fine emulsion is formed in the EPC™ as well as the BSR, and it appears that it is for this reason that an augmentation in desulfurization rate is not seen in the EPC™ relative to the BSR. A couple of process issues warrant consideration here. Firstly, due to the formation of a fine stable emulsion, downstream separation of the multiphase mixture to obtain clean organic fuel may require additional separation processes. Secondly, the *Rhodococcus* biocatalyst used in these experiments was extracted into the organic phase. If biocatalyst recovery and reuse is desired, separation of the biocatalyst from aqueous as well as organic phases will be required.

Energy utilization by EPC™

Typically, stirred reactors or impeller based reactors are capable of achieving water or oil droplet sizes of 100 -300 □m in diameter under the conditions used in this study when surfactants are not present. Tin order to create such droplet size distribution, the energy required is on the order of 1-6 W/L (based upon empirical correlation's [10]). It is estimated that if impeller based systems were capable of producing 5 □m droplets, it would require ~25 kW/L [11] if surfactants are not present. The EPC™ creates droplets of water containing biocatalyst ~5 □m in diameter within an organic phase, and does so with a power requirement of 3 W/L [7]. Thus, if a high activity biocatalyst is available, which is actually limited by mass transport, the EPC™ could result in tremendous savings over the batch stirred reactor. For instance, on a 1 L basis, a BSR using a 3:1 water to oil ratio and producing oil droplets of 150 mm in diameter creates 1×10^5 cm^2 of interfacial surface area. On the same volume basis, an EPC™ creating 5 □m diameter aqueous droplets and having a 5% aqueous hold-up creates 6×10^5 of interfacial area at $1/15^{th}$ the aqueous volume to do so. In a mass transport system, the rate of desulfurization would thus be expected to be six times as large using 93% less biocatalyst. An additional important point which needs to be noted here is that the fine emulsion formed in the EPC™ is an unstable emulsion i.e., the emulsion breaks easily upon removal of the electric fields giving easy separation of the organic and aqueous streams.

Crude oil biodesulfurization

Oil samples collected from the BSR were analyzed by GC-SCD to obtain the distribution of organosulfur compounds in the crude oil. Analysis was done on the aromatic fraction of the oil and not the whole oil, since the baseline did not return to its initial value in case of the whole oil. This fraction of the Van Texas oil accounted for 22% of the oil's original volume. As shown in Figure 1, the total sulfur content of this aromatic fraction was reduced from 3.8 to 3.2% in 6 days of treatment with IGTS8.

The results indicate removal of comparatively low molecular aromatic sulfur compounds; however, a large portion of the organosulfur fraction does not seem to be affected by the biodesulfurization process. Additional analysis by GC-MS (not shown here) has revealed up to 90% sulfur removal from DBT and substituted DBT compounds. While it appears that this biocatalyst is capable of desulfurizing the majority of sulfur species present in diesel (DBT and substituted DBT compounds) and that only improvements in the rate of desulfurization are needed for the commercialization of this process, a great deal of research is needed for oil biodesulfurization to be realized. The sulfur specific oxidation of DBT by *Rhodococcus* resulted from over 15 years of research using DBT as the model organic sulfur compound in coal and oil. Detailed sulfur speciation studies and biocatalyst development is needed to achieve desulfurization of the broad spectrum of organic sulfur species present in crude oil and to realize the promises of petroleum biodesulfurization.

CONCLUSIONS

A variety of process considerations in the biodesulfurization of petroleum feedstocks were addressed in this study including reaction rate, emulsion formation and breakage, biocatalyst recovery, and both gas and liquid mass transport. Comparison of batch stirred reactor to EPC™ revealed formation of high surface area in the EPC™ in the absence of surface-active agents. Presence of biocatalysts capable of producing biosurfactants results in fine emulsions in both reactors; however, poses a potentially more difficult problem with downstream multiphase separation. The use of EPC™ as a biodesulfurization reactor can result in up to several orders of magnitude energy savings over BSR in the absence of surfactants. Gas-liquid mass transfer was not a limiting factor in biodesulfurization studies with model systems. Further, biodesulfurization experiments with actual crude oil showed that presently available biocatalysts such as *Rhodococcus* sp. IGTS8 are capable of removing DBT and substituted DBT type compounds but do not affect the remaining portion of the organosulfur compounds. Thus, there is a need for further development in biocatalysts capable of desulfurization of higher molecular weight non-DBT type sulfur compounds present in crude oil.

ACKNOWLEDGMENTS

This work was supported by the Office of Oil & Gas Processing, U.S. Department of Energy under contract DE-AC05-96OR22464 with Lockheed Martin Energy Research Corp. The authors wish to thank Dr. Robert Shong of Texaco for GC-SCD analysis of Van Texas crude oil. The authors acknowledge the material contributions of Energy BioSystems Corp.

REFERENCES

1. Lee, M.K., J.D. Senius, and M.J. Grossman, *Sulfur-specific microbial desulfurization of sterically hindered analogs of dibenzothiophene.* Applied and Environmental Microbiology, 1995. **61**(12): p. 4362-4366.
2. Monticello, D.J., *Biocatalytic desulfurization.* Hydrocarbon Processing, 1994. **February 1994**: p. 39-45.
3. Shennan, J.L., *Microbial attack on sulfur-containing hydrocarbons: Implications for the desulfurization of oils and coals.* J. Chem. Tech. Biotechnol., 1996. **67**: p. 109-123.
4. Lin, M.S., *et al., Biochemical processing of heavy oils and residuum.* Applied Biochemistry and Biotechnology, 1996. **57/58**: p. 659-664.
5. Premuzic, E.T., *et al., Biochemical Alteration of Crude Oils in Microbial Enhanced Oil Recovery,* in *Biohydrometallurgical Technologies,* A.E. Torma, M.L. Apel, and C.L. Briarley, Editors. 1993, The Minerals, Metals, and Materials Society. p. 401-413.
6. Scott, T.C., D.W. DePaoli, and W.G. Sisson, *Further development of the electrically driven emulsion phase contactor.* Ind. Eng. Chem. Res., 1994. **33**: p. 1237-1244.
7. Kaufman, E.N., *et al., Development of an electro-spray bioreactor for crude oil processing.* Fuel Processing Technology, 1997. **52**: p. 127-144.
8. Kaufman, E.N., *et al. Biodesulfurization of dibenzothiophene and crude oil using electrospray reactors.* in *3rd International Petroleum Environmental Conference.* 1996. Albuquerque, NM.
9. Kaufman, E.N., J.B. Harkins, and A.P. Borole. *Biodesulfurization of Dibenzothiophene and Crude Oils Using Batch Stirred and Electro-spray Reactors.* in *International Petroleum Environmental Conference.* 1997. San Antonio, TX.
10. Perry, R.H., D.W. Green, and J.O. Maloney, eds. *Perry's Chemical Engineering Handbook.* 6 ed. . 1984, McGraw-Hill: New York. 2336.
11. Scott, T.C. and W.G. Sisson, *Droplet size characteristics and energy input requirements of emulsions formed using high intensity pulsed electric fields.* Separation Science and Technology, 1988. **23**: p. 1541-1550.

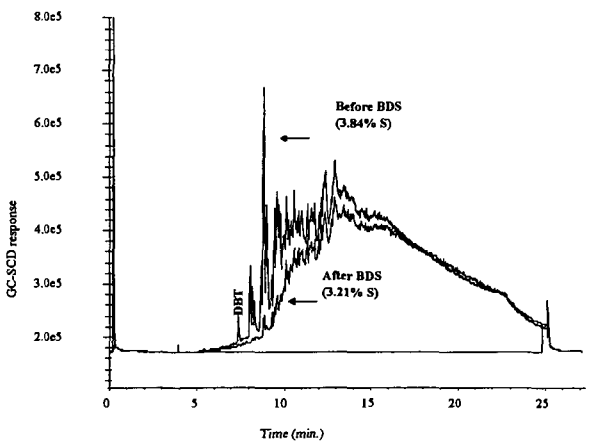

Figure 1. Analysis of the aromatic fraction of Van Texas crude oil by GC-SCD. The biotreatment results in removal of low molecular weight DBT-type compounds; however, the higher molecular weight compounds are not affected.

BACTERIAL DESULFURIZATION STUDIES OF ORGANOSULFUR-ENRICHED MAYAN CRUDE OIL EXTRACTS USING LIQUID CHROMATOGRAPHY/ATMOSPHERIC PRESSURE CHEMICAL IONIZATION/ MASS SPECTROMETRY

Walter E. Rudzinski, Rene Rodriguez, Steve Sassman,
Matthew Sheedy, Todd Smith, and Linette M. Watkins
Department of Chemistry
Southwest Texas State University
San Marcos TX 78666

INTRODUCTION

The sulfur content in coal and petroleum products ranges from 0.025 to 11%, thus creating a potential problem through the production of sulfur dioxide which is a major component in acid rain.[1] As fossil fuel consumption increases, governments are forced to implement stricter controls on sulfur dioxide emissions in order to reduce the occurrence of acid rain. A regulatory burden will necessitate the development of methods which can be used to lower the sulfur content of fuels, both before and after processing. Inorganic sulfur can be successfully removed by a variety of physical separation methods. However, sulfur removal from organosulfur compounds is more difficult to achieve. The current methodology, hydrodesulfurization, involves the use of inorganic catalysts at high temperature and pressure to generate desulfurized hydrocarbon. The approach is expensive, produces hydrogen sulfide, and is ineffective for many classes of organosulfur compounds. Another approach , which has been well established by the work of Kilbane, involves bacterial systems, including *Rhodococcus* IGTS8, for the bacterial desulfurization of coal and petroleum[2-7]. These systems offer many advantages over hydrodesulfurization including the use of much milder conditions, and the generation of water-soluble sulfite or sulfate products as well as desulfurized hydrocarbon. Most importantly, bacteria are able to remove sulfur from a much broader range of organosulfur compounds.

In order to assess the efficacy of bacteria for the desulfurization of crude oil, we have developed a protocol which involves the isolation of organosulfur compounds from a Mayan crude oil, followed by the analysis of the extract using liquid chromatography/ atmospheric pressure chemical ionization/ mass spectrometry (LC/APCI/MS). Concurrently, the organosulfur isolate is used as a food source for the bacterium, *Rhodococcus* sp. IGTS8. By analyzing the mass spectrum before and after bacterial inoculation, we hope to delineate the specificity of the bacteria toward the range of organosulfur compounds that are found in petroleum products.

EXPERIMENTAL

The Maya crude oil (density = 0.91 g/mL) was provided by Mobil Oil Corporation from their Beaumont, TX refinery. The Maya crude was characterized by a series of distillations and was found to contain: 38% light distillate (the fraction that distills below 200^{0}C under 1 atm pressure), 22% middle distillate (the remaining fraction that distills below 180^{0}C under 20 torr external pressure) and 22% residue (the fraction that remains). The corresponding densities were 0.804 g/mL for the light distillate, 0.917 g/mL for the middle distillate and 1.013 g/mL for the residue.

A standard mixture of polyaromatic hydrocarbons (PAH: 7.51 mM flourene, 6.78 mM fluoranthene, 6.57 mM phenanthrene, 4.94 mM pyrene, 5.39 mM chrysene, 4.28 mM benzo[k] fluoranthene) and 10. 37 mM dibenzothiophene (DBT) was prepared in dichloromethane.The mix of PAH and DBT would be used in the evaluation of the ligand exchange protocol.

Alumina (Brockman Activity I, 80-200 mesh, Fisher, Fairlawn, N.J.) was dried at 200^{0}C overnight. CuCl/silica was prepared by mixing approximately 100 g of silica gel (100-200 mesh, Fisher) with 5 g of cupric chloride (Aldrich) in distilled water, drying the mixture to a wet powder with a rotary evaporator, and then drying at 200^{0}C in an oven for 24 h prior to use.[9] PdCl/silica was prepared by mixing approximately 100 g of silica gel (100-200 mesh, Fisher) with 5 g of palladium (II) chloride (Aldrich) suspended in an aqueous solution, drying in an oven at 95^{0}C overnight, then holding at 200^{0}C for more than 24 h prior to use. [10]
Approximately 0.2-0.5 g of the Maya crude oil was dissolved in 5 mL of methylene chloride then adsorbed onto 3 g of neutral alumina. The solvent was removed from the alumina by vigorously stirring the mixture under a gentle stream of dry nitrogen gas. The alumina with the adsorbed sample was then packed on top of 6 g of neutral alumina in an 11 x 300 mm. The sample was eluted with the following chromatographic grade solvents: 20 mL of hexane which removes aliphatic hydrocarbons (designated as fraction A-1) ; 50 mL of benzene which removes poly aromatic hydrocarbons (designated as fraction A-2) Figure 1. illustrates the entire fractionation and isolation scheme for the sulfur compounds.[11]

Fraction A-1 was adsorbed onto 0.5 g of the CuCl /silica gel then packed on top of 5 g of CuCl /silica gel in an 11 x 300 mm column. 50 mL of n-hexane were added in order to elute the aliphatic hydrocarbons (designated as fraction C-1) [9]. One hundred mL of chloroform/diethyl ether (9:1 , v: v) were then used to elute the aliphatic sulfur hydrocarbons (designated as fraction C-2). See Figure 1.[9]

Fraction A-2 was adsorbed onto 0.5 g of the PdCl/silica gel then packed on top of 5 g PdCl/silica gel in an 11 x 300 mm column. Thirty mL of chloroform/n-hexane (1:1) were used to elute the polyaromatic hydrocarbons (PAH, designated as fraction P-1). A further fifty mL of the same eluent , chloroform/n-hexane (1:1), were used to elute the polyaromatic sulfur heterocycles (PASH, designated as fraction P-2). One hundred mL of chloroform/diethyl ether (9:1) were used to elute other sulfur polyaromatic compounds (S-PAC, designated as fraction P-3). Fractions P-2 and P-3 were reduced in volume to approximately 1 mL by rotary evaporation, after which 50 µL of diethylamine were added ,in order to break up the Pd complexes. Fraction P-3 was further cleaned by passing it through neutral alumina with 50 mL of benzene.[12] Fractions P-1, P-2, and P-3 were evaporated to dryness and redissolved in 5 mL of methylene chloride. See Figure 1.

The PAH and DBT mixture was analyzed using a Beckman 110 B solvent delivery system, an Altex 210A injection valve, and a Beckman Model 160 absorbance detector set at 254 nm. The HPLC system attached to the Finnegan LCQ included a Model P4000 pump and a Model AS3000 autosampler (Thermo Separation Products Inc., San Jose, CA.). The analytical column employed for both HPLC systems was a LiChrosorb Amino (4.6 x 150 mm, dp = 5 um) column (Phase Separations, Franklin, MA). The mobile phase employed for the separation of the standard mixture was 100% hexane while the mobile phase employed for the LC/APCI/MS analysis consisted of n-hexane and methylene chloride on a gradient from 100% n-hexane to (60:40) n-hexane/methylene chloride over a period of 6 minutes. For both HPLC systems, the flow rate was constant at 1.0 mL/minute, the column temperature was ambient, and the sample volume was 20 uL.

Atmospheric pressure chemical ionization (APCI/MS)was performed on an LCQ ion-trap mass spectrometer equipped with an APCI source (Finnigan MAT, San Jose, CA). The APCI source parameters were as follows: discharge voltage, 5 kV; vaporizer temperature, 450 C; nitrogen sheath gas, 80 psi; nitrogen auxiliary gas,10 psi; heated capillary, 150 C; capillary voltage, 5 V; and tube lens voltage, 5 V. NAVIGATOR Version 1.2 software (Finnigan MAT, San Jose, CA). was used for sample acquisition and data reduction.

The bacterial strain *Rhodococcus erythropolis* sp. IGTS8 was obtained from ATCC (ATCC 53968). Two different media were used for the growth of *Rhodococcus* IGTS8: a Difco nutrient media and a sulfur-free minimal media designated BSM2.[8] *Rhodococcus* was grown to saturation in overnight tubes containing nutrient media. The cells were then concentrated by centrifugation and washed twice with BSM2 media, before suspension in 100 mL of BSM2 media. The sulfur source necessary for growth was excluded in the negative control, was 200 µM dibenzothiophene (DBT) in the positive control, or was an aliquot of the sulfur-containing extract from crude oil. Growth was monitored by optical density measurements at 600 nm using a Beckman Model 7500 ultraviolet-visible spectrophotometer.

RESULTS AND DISCUSSION

The standard mixture of the PAH and DBT was fractionated according to the ligand exchange chromatography scheme illustrated in Figure 1. Fraction P-1 exhibited the PAH compounds as well as some of the DBT as previously noted.[13]

Fractions P-2 and P-3 did not exhibit any PAH compounds, thus validating the efficacy of the protocol for the isolation of sulfur compounds.

Both the Maya crude oil and the residue were also fractionated using ligand exchange chromatography. Fractions P-2 and P-3 from the residue were then added to *Rhodococcus erythropolis* sp. IGTS8. No bacterial growth was observed. Most of the polyaromatic sulfur heterocycles (PASH) and other sulfur polyaromatic (S-PAC) compounds are in the light and middle distillates and so this result was expected. The implication however is that *Rhodococcus erythropolis* sp. IGTS8 may not be very effective in the biodesulfurization of Maya crude oil residue.

Fractions P-2 and P-3 from the crude oil were investigated using LC/APCI/MS. Each fraction gave a single broad peak under the chromatographic conditions employed. Any attempt to use a

weaker mobile phase (e.g., 100% hexane) in order to better resolve the multi-component mixture results in the precipitation of some of the components from the mixture. A mass/charge (m/z) scan of the chromatographic peak for each fraction results in a broad mass spectral envelope. Fraction P-2 shows significant intensity extending from about 400 to 1600 m/z (the mass spectrum (MS) is shown in Figure 2). The first statistical moment of the distribution lies around 1000 m/z with local maxima at about 850, 1100 and 1220 m/z. The distribution can be regarded as a fingerprint for the polyaromatic sulfur heterocycles (PASH) in the Maya crude. The mass spectrum (MS) of fraction P-3 shows significant intensity extending from about 400 to 2000 m/z. The distribution features a maximum around 900 m/z. This distribution can be regarded as a fingerprint for the other sulfur polyaromatic compounds (S-PAC) in the Maya crude. Both m/z scans contain multiple peaks, possible fragments, and possible long-lived adducts from the nebulization and chemical ionization process; however, with further method developments in the fractionation of sulfur compounds, the selection of other sorbents and mobile phase eluents for optimal liquid chromatographic resolution, coupled with mass spectral optimization of the nebulization and ionization process, as well as the implementation of MS^n acquisitions, we hope to further delineate the distribution and composition of the P-2 and P-3 fractions.

Fractions P-2 and P-3 from the crude oil will also be added to the *Rhodococcus erythropolis* sp. IGTS8. Bacterial growth will be monitored for up to 30 days. An internal standard will be added to the aliquots and the loss of intensity at individual m/z values will be monitored. Those signals which exhibit a significant loss of intensity will be further explored via MS^n experiments in order to assess the chemical structure.

ACKNOWLEDGEMENTS

WER would like to thank the Environmental Protection Agency (Grant No.R825503) for the acquisition of the Finnegan LCQ mass spectrometer as well as for support of this project. WER would also like to thank the Institute for Industrial and Environmental Chemistry of Southwest Texas State University for assistance in the management of this project.
LMW acknowledges the donors of the Petroleum Research Fund, administered by the American Chemical Society , for partial support of this research .

REFERENCES

1) Monticello, D. J.; Finnerty, W. R. *Ann. Rev. Microbiol.* **1985**, *39*, 371-389.
2) Kilbane II, J. J. *Mutant Microorganisms Useful for Cleavage of Organic C-S Bonds*; Kilbane II, J. J., Ed.; Institute of Gas Technology: USA, 1992.
3) Kilbane II, J. J. *Enzyme from Rhodococcus Rhodochrous ATCC 53968, Bacillus Sphaericus ATCC 53969 or a Mutant Thereof for the Cleavage of Organic C-S bonds*; Kilbane II, J. J., Ed.; Institute of Gas Technology: USA, 1996.
4) Kilbane, J. J. *Appl. Biochem. Biotechnol.* **1995**, *54*, 209-221.
5) Kilbane, J. J.; Jackowski, K. *Biotechnol. Bioeng.* **1992**, *40*, 1107-1114.
6) Kilbane, J. J.; Bielaga, B. A. *ChemTech* **1990**, 747-751.
7) Kayser, K. J.; Bielaga-Jones, B. A.; Jackowski, K.; Odusan, O.; Kilbane II, J. J. *J. Gen. Microbiol.* **1993**, *139*, 3123-3129.
8) Li, M. Z.; Squires, C. H.; Monticello, D. J.; Childs, J. D. *J. Bacter.* **1996**, *178*, 6409-6418.
9) Nishioka,M.; Tomich,R.S. *Fuel* **1993,** *72,* 1007- 1010.
10) Nishioka,M.; Campbell, R.M.; Lee, M. L.; Castle, R.N. *Fuel* **1986,** *65,* 270 - 273.
11) Later,D.W.; Lee,M.L.; Barlte,K.D.; Kong, R.C.; Vassilaros,D.L. *Anal. Chem.* **1981,** *53,* 1612.
12) Nishioka,M. *Energy & Fuels* **1988,** *2,* 214 - 219.
13) Andersson, J.T. *Anal. Chem.* **1987,***59,* 2207-2209.

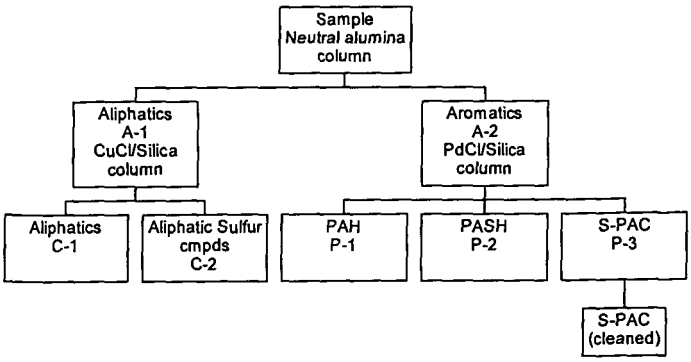

Figure 1. Fractionation and Isolation Scheme for Sulfur Compounds

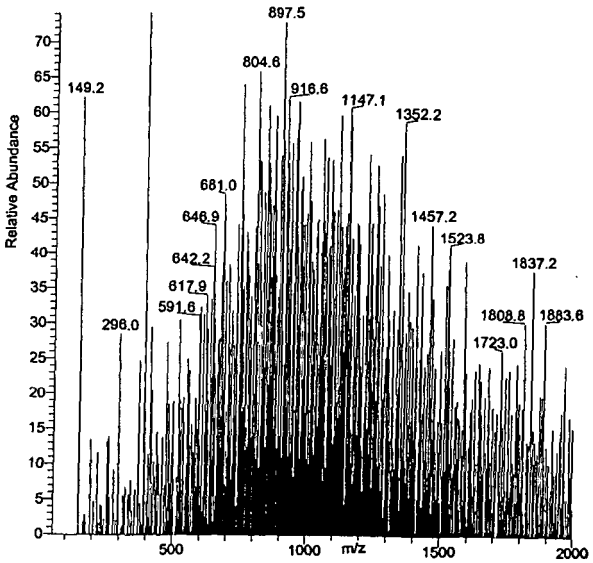

Figure 2. Mass Spectrum of the P-2 Crude Oil Fraction.

BIODESULFURIZATION GENE EXPRESSION BY PROMOTER REPLACEMENT IN *RHODOCOCCUS*

Peter C.K. Lau, Claude Denis-Larose,
Tanya MacPherson, Charles W. Greer, Jalal Hawari
Biotechnology Research Institute
National Research Council Canada
Montreal, Quebec, Canada H4P 2R2

Matthew J. Grossman
Corporate Research
Exxon Research and Engineering Company
Annandale, New Jersey, 08801

Bruce M. Sankey
Imperial Oil Resources Ltd, Calgary, Alberta, Canada T2L 2K8

INTRODUCTION

Biodesulfurization is a pathway-driven and enzymatic process, best known in select strains of *Rhodococcus*, that removes sulfur specifically from sulfur heterocycles such as dibenzothiophene (DBT) present in fossil fuels (*1-6*). The ability of several rhodococcal strains to desulfurize is thus far a plasmid-encoded phenotype involving three genes (*soxABC* [also known as *dszABC*]) and at least a chromosomal gene product which provides the reduced flavin and oxidized NADH required for the two initial oxygenase activities (Fig. 1). The end products of this sulfur-specific removal scheme are liberation of inorganic sulfur as sulfate or sulfite and production of 2-hydroxybiphenyl (2-HBP) without disruption of the original aromatic rings. The practical advantages of this biodesulfurization process include unnecessary loss of calorific values of the fuel upon combustion and a reduced emission of harmful sulfur dioxide into the atmosphere (*1, 4, 5, 11-13*).

We are interested in developing an efficient desulfurization biocatalyst based on a native *Rhodococcus* strain. This strategy, while not compromising the possible advantages offered by the *Rhodococcus* background, necessitates a resolution of the repression problem faced by the sulfur oxidation genes when the native cells are grown in the presence of sulfur-containing compounds (*1, 3, 7, 14, 15*). Here we report a promoter replacement strategy and the results of a preliminary study showing the feasibility of *sox* gene expression in a rich and sulfate-proficient background.

EXPERIMENTAL AND DISCUSSION

Bacterial strains and shuttle expression vector

The rhodococcal host used in this study is a plasmid-free derivative of the desulfurizing strain *Rhodococcus* sp. X309 (ATCC 55309), designated *Rhodococcus* sp. strain X309-10-2 (henceforth strain 10-2; ref. *3*). The *sox* phenotype was scored by growth on DBT as a sole sulfur source and the fluorescence formed around patches of bacteria on a DBT plate spray assay (*3, 7*). Bacterial growth media including minimal salt medium (MSM) and general recombinant DNA techniques were as previously described (*3, 15, 16*).

Plasmid pKSΔ6-1 (Fig. 2) is capable of replication in both *Escherichia coli* and *Rhodococcus* by virtue of the origin of replication from the *E. coli* pBluescript II KS- vector and the replication region of the pSOX desulfurization plasmid from strain X309 (*16*). For selection the gene markers are ampicillin (Ap; 50 μg/ml) resistance and chloramphenicol (Cm; 30 μg/ml) resistance, respectively. The pBluescript KS vector component also provides the blue-white color selection when the cells are plated on indicator plates containing IPTG and X-gal. Previously, we found that the levansucrase-encoding gene (*sacB*) from *Bacillus subtilus* (*17*) could be expressed in *Rhodococcus* and served as a counterselectable marker in the shuttle expression plasmid designated pKSΔ6-1*sac* (*16*). Importantly, the *sacB* promoter is not known to be repressed by sulfate, a feature that is explored in the following construct.

Promoter replacement for expression of soxABC genes in *Rhodococcus*

The concept is to replace the sulfate-repressed *sox* promoter (*14*) by that of *sacB* to drive the expression of *soxABC* genes. Knowledge of the precise sequence of these DNAs was used to design primers for PCR (polymerase chain reaction) amplification and cloning of the specific DNA fragments in the core shuttle plasmid pKSΔ6-1 by a step-wise procedure. i). The *sacB* promoter fragment was amplified by the following primers using pUM24 plasmid as template (*18*). Primers SacBpro5' (5'-CGCAGGGCCCATCACATATACCTGC) and SacBpro3' (5'-

GCTGACTAGTCATCGTTCATGTCTCCTT) were designed to contain the *Apa*I and *Spe*I restriction sites (boldfaced), respectively. The underlined bases correspond to nucleotides 13-30 and 467-448 of the *sacB* noncoding sequence, respectively (*17*). Both primers have a calculated melting temperature of 54 ^{0}C. The CAT sequence adjacent to the *Spe*I site specifies the complementary sequence of the initiator codon of *sacB*. ii). The 3.7-kb DNA fragment of strain X309 pSOX plasmid containing the *soxABC* genes was amplified based on the sequence derived from the *Rhodococcus* sp. IGTS8 strain (*7*). The forward oligomer contains the sequence 5'-CCTGACTAGTCAACAACGACAAATGCATCT (*Spe*I site underlined), and the sequence of the reverse oligomer is 5'-GTCTCTAGATCAGGAGGTGAAGCCGGG (*Xba*I site underlined). The sequence 3' to the *Spe*I site represents the third to eight codons of the *soxA* sequence. In the reverse oligomer the TCA triplet represents the complement of the *soxC* stop codon.

Digestion of the purified *sacB* promoter-containing fragment by *Apa*I and *Spe*I endonucleases allowed specific and directional cloning at the MCS of the pKSΔ6-1 vector (Fig. 2). After plasmid isolation the *soxABC*-containing fragment was cloned at the *Spe*I and *Xba*I sites of the MCS after generation of the compatible restriction ends (Fig. 2).

As a result of transformation in *E. coli* strain DH10B, recombinant plasmids were isolated and checked for authenticity of the clones. A straightforward double digestion by *Spe*I and *Xba*I would verify the correct size of the insert. But it was necessary to first transform the plasmid in an *E. coli dam*-minus strain since in our primer design we had inadvertantly introduced an adenine methylation sequence adjacent to the *Xba*I cleavage site (TCTAGATCA; methylated base underlined). The orientation of the clone was verified by *Not*I restriction, an unique site within the *soxB* gene (Fig. 2). Using SacBpro5'as primer the DNA sequence encompassing the cloned junction was also verified.

Expression of soxABC genes in *Rhodococcus* and metabolite analysis

Two independent clones of *soxABC* genes (clone #4B and #7) of the above constructs were transformed into rhodococcal strain 10-2 by electroporation using the conditions and Bio-Rad Gene Pulser apparatus as previously described (*16*). The recombinants were selected on MSM media plates containing DBT (0.52 mM; Aldrich Chemical Co., Wilwaukee, WI) and Cm (30 μg/ml). The *sox* phenotype was first examined under UV for fluorescence around patches of bacteria on a DBT spray plate assay. Neither the plate nor the liquid culture imparted fluorescence. This could be due to low level of expression or no expression at all. To check for these possibilities, metabolites of DBT transformation were analyzed by the solid phase microextraction (SPME) technique coupled to GC-MS (*19*). The solventless SPME technique is known for its speed and sensitivity, detection in the microgram per liter range. Sample preparation and analysis of metabolites were carried out as previously described (19). As a result, although the peaks are minor (not shown), both 2-HPB (m/z 170) and DBT-sulfone (m/z 216) were detected as metabolites besides the starting material DBT (m/z 184). Extracts of cells grown in the rich Luria Bertani (LB) broth were also analyzed. Similar pattern was observed for the recombinant strain but not the native X309 strain which is known to be repressed by the presence of sulfates. As a positive control, the plasmid-free 10-2 mutant strain did not yield any of the characteristic products.

CONCLUSIONS

This preliminary study showed the feasibility of expression of sulfur oxidation genes in *Rhodococcus* by a heterologous promoter that is not repressed by the presence of sulfate. Undoubtedly, the shuttle expression system provides a good base for further improvement and optimization. Recently, recombinant *Pseudomonas* strains have been constructed to carry out an improved level of biodesulfurization (*20*).

ACKNOWLEDGMENTS

Funding from Imperial Oil Resources Ltd. is gratefully acknowledged. We thank H. Bergeron for the computer graphics.

REFERENCES

(1) Kilbane, J. J. *Trends Biotech.* 1989, *7*, 97-101.
(2) Finnerty, W. R. *Annu. Rev. Microbiol.* 1992, *46*, 193-218.
(3) Denome, S. A.; Olson, E. S.; Young, K. D. *Appl. Environ. Microbiol.* 1993, *59*, 2837-2843.
(4) Monticello, D. J. *Environ. Progress.* 1993, *12*, 1-4.
(5) Ohshiro, T.; Suzuki, K.; Izumi, Y. *J. Ferm. Bioeng.* 1996, *81*, 121-124.

(6) Denis-Larose, C.; Labbé, D.; Bergeron, H.; Jones, A. M.; Greer, C. W.; Hawari, J.; Grossman, M.J.; Sankey, B. M.; Lau, P. C. K. *Appl. Environ. Microbiol.* 1997, *63*, 2915-2919.
(7) Denome, S. A.; Oldfield, C.; Nash, L. J.; Young, K. D. *J. Bacteriol.* 1994, *176*, 6707- 6717.
(8) Piddington, C. S.; Kovacevich, B. R.; Rambosek, J. *Appl. Environ. Microbiol.* 1995, *61*, 468-475.
(9) Lei, B.; Tu, S. *J. Bacteriol.* 1996, *178*, 5699-5705.
(10) Xi, L.; Squires, C. H.; Monticello, D. J.; Childs, J. D. *Biochem. Biophys. Res. Comm.* 1997, *230*, 73-75.
(11) Gray, K. A.; Pogrebinsky, O. S.; Mrachko, G. T.; Xi, L.; Monticello, D. J.; Squires, C. H. *Nat. Biotech.* 1996, *14*, 1705-1709.
(12) Finnerty, W. R. *Curr. Opinion Biotech.* 1992, *3*, 277-282.
(13) Monticello, D. J. *CHEMTECH* 1998, *28*, 38-45.
(14) Li, M. Z.; Squires, C. H.; Monticello, D. J.; Childs, J. D. *J. Bacteriol.* 1996, *178*, 6409-6418.
(15) Sambrook, J.; Fritsch, E. F.; Maniatis, T. Molecular cloning: A laboratory manual, 2nd edition. 1989. Cold Spring Harbor Laboratory Press, Cold Spring Harbor, NY.
(16) Denis-Larose, C.; Bergeron, H.; Labbé, D.; Greer, C. W.; Hawari, J.; Grossman, M. J.; Sankey, B. M.; Lau, P. C. K. *Appl. Environ. Microbiol.* 1998, *64*, 4363-4367.
(17) Steinmetz, M.; Le Coq, D.; Aymerich, S.; Gonzy-Treboul, G.; Gay, P. *Mol. Gen. Genet.* 1985, *200*, 220-228.
(18) Reid, J. L; Collmer, A. *Gene*, 1987, *57*, 239-246.
(19) MacPherson, T.; Greer, C. W.; Zhou, E.; Jones, A. M.; Wisse, G.; Lau, P. C. K.; Sankey, B.; Grossman, M. J.; Hawari, J. *Environ. Sci. Technol.* 1998, *32*, 421-426.
(20) Gallardo, M. E.; Ferrandez, A.; de Lorenzo, V.; Garcia, J. L.; Diaz, E. *J. Bacteriol.* 1997, *179*, 7156-7160.

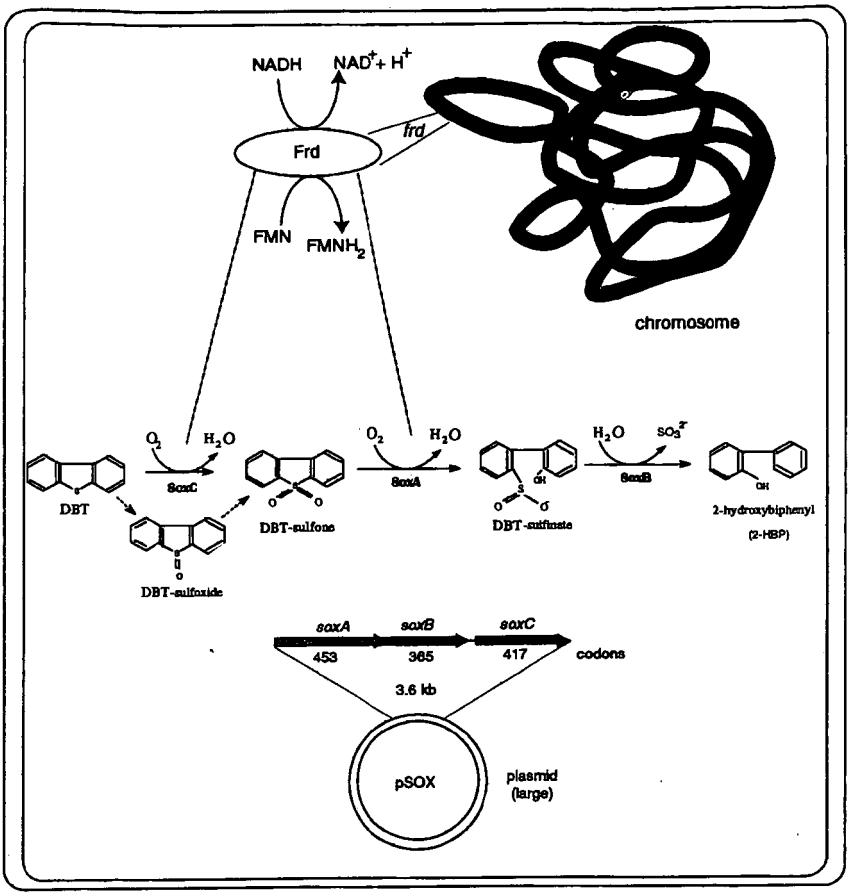

Fig. 1 The sulfur oxidation (*sox*)/desulfurization pathway of dibenzothiophene (DBT) and its genes in *Rhodococcus* spp. SoxA, DBT sulfone monooxygenase; SoxB, 2-(2-hydroxybiphenyl)-benzenesulfinate; SoxC, sulfite/sulfoxide monooxygenase; Frd, flavin reductase (FMN-NADH oxidoreductase). Compiled from references *6-11*.

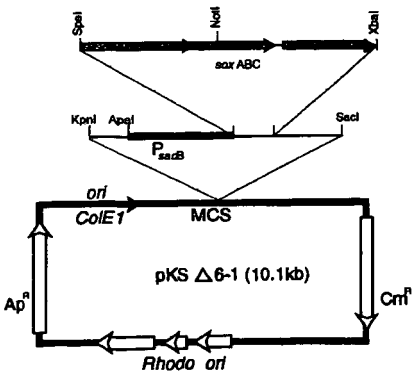

Fig. 2 Step-wise construction of the *sox*-gene expression plasmid under the control of the *Bacillus subtilis sac*B promotor element (P*sac*B). MCS is the multiple-cloning site of the *Rhodococcus-Escherichia coli* shuttle plasmid pKSΔ6-1 as previously described (16). Cm^R, chloramphenicol resistance gene; Ap^R, ampicillin resistance gene. *Rhodo ori* and *ColE1 ori*, origins of replication of *Rhodococcus* sp. strain X309 and *E. coli*, respectively.

INCREASE IN FOSSIL FUEL UTILIZATION IN THE TWENTY-FIRST CENTURY: ENVIRONMENTAL IMPACT AND LOWER CARBON ALTERNATIVES

Hal Gluskoter
MS 956 National Center
U.S. Geological Survey
Reston, VA 20192

Keywords: fossil fuel, environment, economic growth

INTRODUCTION

Interest in the utilization of fossil fuels has greatly increased during the past few years; not because of the benefits to be derived from the energy produced, but rather because of the concerns related to the continued increase of emissions of greenhouse gases and their potential relationship to global climate change. It is generally recognized that there are trade-offs between the benefits to society that accrue from economic development and the possible ecological and environmental degradation brought about by that development. Within the next half century, the world's population will increase and, in order to serve the needs of growth and economic development, energy production will necessarily increase by a significant amount. The means by which the world will simultaneously resolve the dilemma posed by increased population, demand for energy, and concern for the environment will greatly impact the quality of life for most of the people on Earth.

POPULATION

The most recent biennial revision of population estimates and projections of the United Nations Population Division (1998) shows the rate of increase in the world population to be slowing. The current world population is 5.9 billion persons and the medium fertility projection, which the U.N. authors consider most likely, is for the world population to reach 8.9 billion in 2050. That is somewhat lower than previous projections. This slowing of the rate of population increase is the result of two factors; one of which most people would consider positive and the other negative. The global fertility rates have decreased in the past 50 years from five births per woman to the current level of 2.7 births. Although, the decline in fertility is worldwide, it is most pronounced in the developed countries, many of which have birth rates below that necessary to maintain a stable population.

The second factor affecting the rate of population growth is the devastation brought about by the epidemic of HIV/AIDS in much of the world, especially Africa. According to the United Nations Population Division report (1998), the 29 hardest hit African countries have average life expectancies that are seven years less than they would have been in the absence of AIDS.

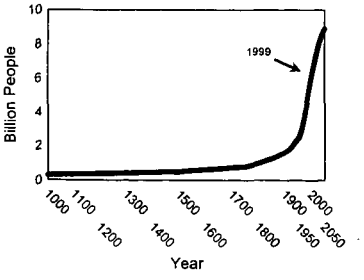

Figure 1. World population, 1000 - 2050, United Nations 1998 Revision of the World Population Estimates and Projections.

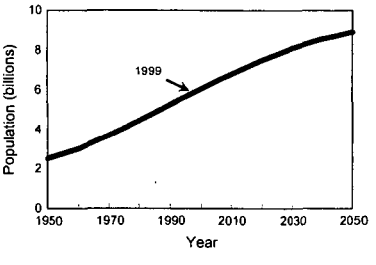

Figure 2. World Population, 1950 - 2050, United Nations 1998 Revision of the World Population Estimates and Projections.

The pattern of growth in the world population from the year 1000 AD projected to 2050 (figure 1)

is what one might expect from a living organism, and the population total is increased by an additional billion people every 12 to 13 years. The future does not appear as desperate if only one segment of that curve, from 1950 to 2050, is considered (figure 2). The world population will increase 50 percent over the next 50 years, primarily in Africa and Asia, accompanied, in these regions, by a significant trend to increased urbanization. The underdeveloped countries have a rate of urbanization that is 3.5 times that in developed regions (World Resources Institute, 1996, p. 1).

POPULATION AND ENERGY CONSUMPTION

Historically, a growth in world population has been accompanied by an increase in demand for energy. From 1970 to 1990 the total world commercial energy consumption increased 59 percent while the world population was increasing 43 percent (figure 3). Commercial energy includes energy

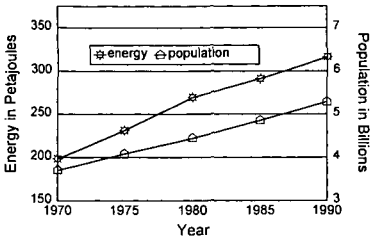

Figure 3. Growth in world population and world energy consumption, 1970 - 1990. Data from World Resources Institute, 1996, World Resources 1996-97, files HD 16101 and 21201.

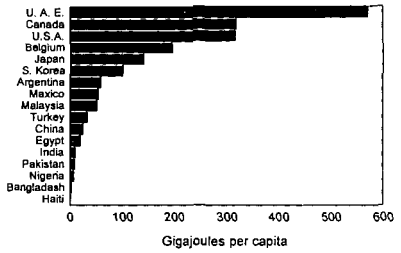

Figure 4. Commercial energy consumption, per capita, for selected countries. In gigajoules per capita. Source: World Resources Institute, 1996.

from solid, liquid, and gaseous fuels and primary electricity (hydroelectricity, nuclear, solar, wind, etc.), but does not include traditional fuels such as wood, charcoal, and animal wastes.

Population, alone, is not an accurate predictor of energy consumption. That is because there is a wide range in energy consumption per capita between the developed, developing, and undeveloped countries (figure 4). On a worldwide basis, the mean annual per capita energy consumption is 59 gigajoules (1 gigajoule = 947,800 Btu). However, the median per capita value is much lower than 59 gigajoules because the developed nations consume energy at a rate that is one or two orders of magnitude greater than that of the developing countries. For example, Mexico, Malaysia, and Argentina have per capita energy consumption near the mean value (59, 52 and 60 gigajoules, respectively) and the per capita consumption in the United States and Canada is 317-319 gigajoules. At the lower end of the scale are Nigeria (7 gigajoules), Bangladesh (3 gigajoules), and Haiti (1 gigajoule)(World Resources Institute, 1996 data table 12.2).

If we were to project energy consumption in the year 2050 based upon population alone it would increase 50 percent, the same amount as the population increase. However, the population growth will be mainly in countries in which the energy use is below the mean for the world. The 10 countries projected to have the largest national populations in 2050 are, in descending order, India, China, United States, Pakistan, Indonesia, Brazil, Nigeria, Bangladesh, Ethiopia, and the Democratic Republic of the Congo (United Nations, 1998). If they were to keep their per capita energy consumption constant during the next 50 years, they would only utilize 140 percent of their current energy in 2050. If the United States were to continue using energy at the current rate and the other nine countries were to increase their rate to that of Spain (85 gigajoules per capita), then the ten largest countries in 2050 would increase their energy consumption to 395 percent of that used today. Spain was chosen because it is at the lower end of energy consumption per capita of the countries in Europe.

India is projected to have the largest national population in 2050 with more than 1.5 billion people and China will be nearly as large (United Nations, 1998). These two countries currently utilize coal as the primary source of commercial energy. India uses five times as much energy from coal as from liquid fuels and China four times as much (World Resources Institute, 1996, data table 12.1). It is reasonable to assume that these two countries will continue using their indigenous coal resources as their primary fuel for electricity generation as their populations increase and, hopefully, their economies grow.

The Gross Domestic Product (GDP) is an economic indicator that correlates with many parameters considered to be associated with standard of living or quality of life. Darmstadter and Lile (1997) analyzed data from 114 countries in the world and found that there was a good positive correlation with adult literacy rate, life expectancy, and percentage of the population with access to sanitation. They concluded that GDP is a useful tool for evaluating key contributors to standard of living. Economists have adopted a form of GDP that allows for comparison of a currency's purchasing power within its own country. This is GDP based on "Purchasing Power Parity" or PPP and it represents the amount of a common "market basket" of goods each currency can purchase locally. It is that form of GDP (per capita) used in this paper.

Examples of parallel growth of GDP and energy consumption in two countries experiencing rapid

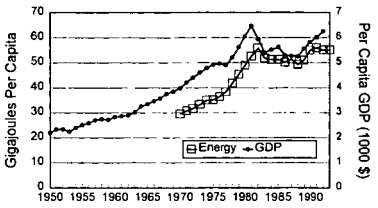

Figure 5. Per capita GDP and energy consumption per capita in Mexico, 1950 - 1993. Data from World Resources Institute, 1996, World Resources 1996-97, data files EI 15124 and EM 21202

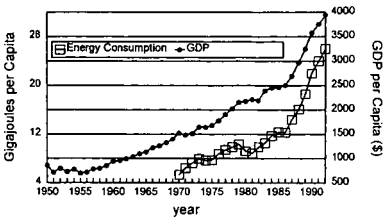

Figure 6. Per capita GDP and energy consumption per capita in Thailand, 1950 - 1993. Data from World Resources Institute, 1996, World Resources 1996-97, data files EI 15124 and EM 21202

economic development are shown in figure 5 and figure 6. From 1970 to 1992, the per capita energy consumption in Mexico increased 86 percent and the GDP increased 57 percent. During the same time period, a per capita increase in GDP in Thailand of 160 percent was accompanied by an increase in energy consumption of 387 percent. Because of the correlation between economic development, expressed as GDP, and energy consumption, it is reasonable to use GDP as a proxy for energy usage. There have been a few cases in which the rate of increase in GDP in a country has been greater than the rate of increase in energy consumption and therefore the proxy would not be valid. That has occurred only in highly developed countries with high GDP. One example is the response of the United States economy to increased energy prices of the 1970's (figure 7) and the continuing conservation efforts in what had been a profligate energy consuming economy.

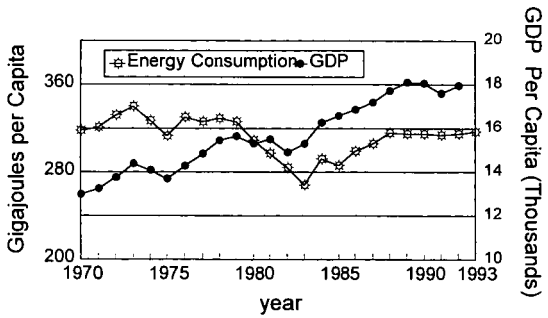

Figure 7. Per capita GDP and energy consumption per capita in the United States, 1970 - 1993. Data from World Resources Institute, 1996, World Resources 1996-97, data files EI 15124 and EM 21202

ECONOMIC GROWTH AND THE ENVIRONMENT - KUZNETS CURVES

The environmental Kuznets curve, named for Nobel laureate economist, Simon S. Kuznets, plots the relationships between environmental quality factors and per capita income. Seldon and Song (1994) looked at sulfur dioxide, suspended particulate matter, carbon monoxide and nitrogen oxides in a multi-national study. Grossman (1995) plotted Kuznets curves for sulfur dioxide and suspended particulate matter on a multi-national basis, and also analyzed suspended particulate matter, airborne

lead, sulfur dioxide, carbon monoxide, and nitrogen dioxide on a county basis for the United States. Shafik (1994) developed curves for the following ten environmental parameters: lack of safe water, lack of urban sanitation, annual deforestation, total deforestation, dissolved oxygen in rivers, fecal coliform in rivers, suspended particulate matter, ambient sulfur dioxide, municipal solid waste per capita, and carbon emission per capita.

Environmental Kuznets curves commonly exhibit one of three shapes. The first represents an environmental benefit that increases continually with increasing per capita income, an example of which is lack of safe water (figure 8). In this case, Shafik (1994, p. 761) explains that the benefits to individuals are high (survival is at stake) and the costs of provision are fairly low. Figure 9 exhibits the second shape, showing a continuous increase with rising incomes. This example, carbon emissions per capita represents current practice and only reinforces the concerns as to fossil fuel

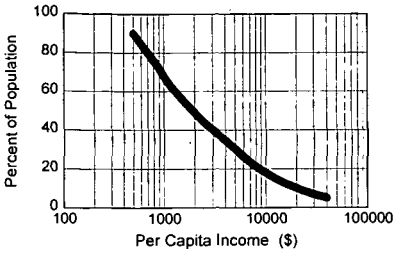

Figure 8. Lack of safe water and per capita income (per capita GDP). After Shafik, 1994, p.764.

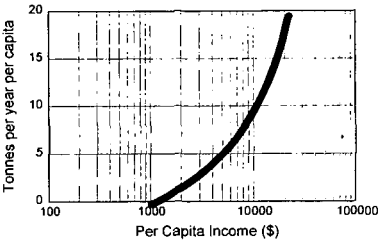

Figure 9. Carbon emissions per capita and per capita income (per capita GDP). After Shafik, 1994, p.764.

combustion.

The Kuznets curve that has received the most interest and has elicited the most discussion has an inverted 'U' shape and it has been used to predict air quality as related to economic development (figure 10). The inverted 'U' shape indicates that outdoor air pollution, including sulfur dioxide and suspended particulate matter, increases in the early stages of a nation's development, eventually reaches a maximum, and then declines as per capita income continues to increase. Similar shape curves have been reported for these two air pollution factors by three sets of researchers, although they reported different levels of income for the 'turning points'. Grossman (1995) calculated that the turning point for both factors was approximately $5000 (1985 US); Shafik (1994) placed the top of the curves between $3000 and $4000; and Selden and Song (1994) calculated much higher values, $8700 for sulfur dioxide and $10300 for suspended particulate matter.

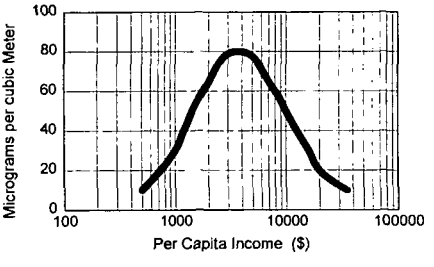

Figure 10. Ambient sulfur dioxide and per capita income (per capita GDP). After Shafik, 1994, p. 764.

The inverted 'U' shaped Kuznets curve could be interpreted to suggest that some environmental impacts of economic development are not serious because they will decline over time. Environmental degradation can be offset at a cost - scrubbers on power plants, for example - and increased per capita income gives nations the wealth with which to afford the cost. Technological developments and increase in the rate of technology transfer from the developed to the developing countries could accelerate the rate of improvement of environmental quality and allow for improvements in air quality to take place at lower per capita income levels than predicted from the historical data.

Not all economists are as sanguine about the concept of the Kuznets curves as the preceding paragraph might suggest. Stern and others (1996) summarized the current literature and critically

reviewed the concept of the environmental Kuznets curve . Among the points they and others (Arrow and others, 1995) make is that the data are analyzed by country and do not take into consideration international trade and the possibility that wealthier countries are "exporting " their environmental problems to less developed countries. Criticism of the Kuznets curves is in how they are interpreted; their usefulness as a descriptive tool is generally accepted. Most recently, the entire May 1998 edition of "Ecological Economics", the journal of the International Society for Ecological economics, edited by Rothman and de Bruyn , was devoted to the environmental Kuznets curve. Six articles explored the structural factors (in economic terms) that might relate to the empirically observed relationships between income levels and measures of environmental impact. The authors of these articles generally conclude, from quite varied analyses, that the interpretation of the environmental Kuznets curve is more complicated than the simple observation that economic growth is good for the environment. Most of the previous researchers had also stated similar positions.

ALTERNATIVE ENERGY SOURCES

In an essay entitled "The Liberation of the Environment", Ausubel (1996) observed that there are two central tendencies that define the evolution of the energy system. One is rising efficiency and the other is that the system is freeing itself from carbon (see also Nakicenovic, 1996). For the past two hundred years the world has progressively undergone decarbonization as the most desirable fuels for energy generation evolved from wood to coal to oil and then to gas. The truly desirable element in these fuels is not the carbon they contain, but rather their hydrogen. The global rate of decarbonization, as measured by the amount of carbon per unit of primary energy produced, has decreased by 40 percent in the past century. Ausubel (1996) suggests that "...over the next century the human economy will squeeze most of the carbon out of its system and move, via natural gas, to a hydrogen economy." The displacement of carbon will be a huge environmental and economic challenge. Globally, the per capita use of carbon is 1000 kilograms per year (Ausubel. 1996).

More than two thirds of the primary fuels currently consumed in the world is used to produce electricity, twice the share of 50 years ago. But, there are still two billion people in the world - one third of the population - without access to electricity (Ausubel, 1998). The installed electricity capacity of the world is predominantly thermal (coal, gas, and oil) with hydroelectric and nuclear power contributing significant amounts. Geothermal, wind, solar, biomass, photovoltaic and other "renewable" sources make up less than one percent (figure 11). The United States leads the world in the use of renewables for generating electricity, comprising 80 percent of the world's total. Proponents of renewables for generating electricity take some encouragement from the double-digit

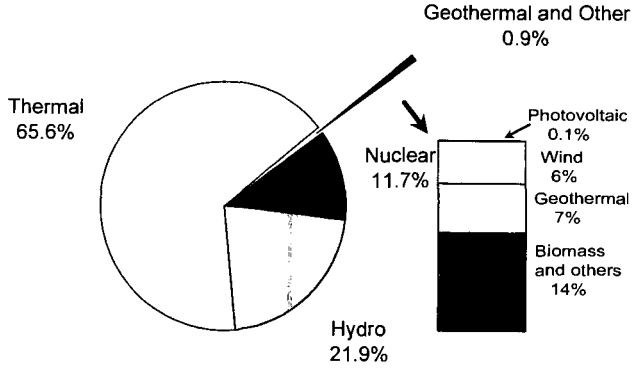

Figure 11. World electricity installed capacity and renwable energy sources used for generating electricity - 1996. From EIA, International Energy Annual, 1998, and Brown, and others, 1997

growth in global shipments of photovoltaic cells (O'Meara,1997) and in a similar growth rate in global wind power generating capacity (Flavin, 1997). However, there will necessarily have to be much larger absolute increases in generating capacity from wind and solar before they have a significant impact on the world's totals. Currently, photovoltaics produce 0.003 percent of the world's electricity and wind produces 0.2 percent.

CONCLUSION

The challenge is great and may not be met. However, technological changes can transform society in a matter of decades. Ausubel (1996) uses the example of the electric lamp, which was invented a little more than 100 years ago. The modern version of that lamp is 90 times as efficient as the original. Nuclear energy as a source of generating electricity did not exist half a century ago and now represents 12 percent of the world's installed capacity and accounts for 77 percent of the electricity produced in France. Looking ahead 50 years to the future is much more challenging than reviewing the past. But it is certainly not out of the realm of the plausible to imagine an energy regime that has not only evolved beyond fossil fuels but has done so before the current coal, oil, and gas resources are exhausted.

REFERENCES

Arrow, K., Bolin, B., Constanza, R., Dasgupta, P., Folke, C., Holling, C. S., Jansson, B., Levin, S., Maler, K., Perrings, C., and Pimental, D., 1995, Economic Growth, Carrying Capacity, and the Environment: Science, v. 268, p. 520-521.

Ausubel, J. H., 1996, The liberation of the environment: Daedalus, v. 125, no.3, p.1-17.

Ausubel, J. H., 1998, Resources and environment in the twenty-first century: Seeing past the phantoms: World Energy Council Journal, July 1998, p. 8-16.

Brown, L. R., Renner, Michael, and Flavin, Christopher, 1997, Vital Signs 1997: Worldwatch Institute, 165p. Data tables also available on "Database Disk - January, 1998".

Darmstadter, Joel and Lile, Ron, 1997, GDP: Does It Matter: Resources, published by Resources For The Future, issue 127, p. 6.

Energy Information Agency, 1998, International Energy Annual, 1996: DOE/EIA-0219(96), 244p.

Flavin, Christopher, 1997, Wind power growth continues: *in* Brown, L.R., Renner, M., and Flavin, C., eds, Vital Signs, 1997, Worldwatch Institute, p. 52-53.

Grossman, G. M., 1995, Pollution and growth: What do we know?: *in* The Economics of Sustainable Development, Goldin, I. and Winters, L.A., eds., Cambridge University Press, p. 19-50.

Nakicenovic, Nebojsa, 1996, Freeing energy from carbon: Daedalus, v. 125, no. 3.

O'Meara, Molly, 1997, Cell shipments keep rising: *in* Brown, L.R., Renner, M., and Flavin, C., eds, Vital Signs, 1997, Worldwatch Institute, p. 54-55.

Rothman, Dale and de Bruyn, Sander, 1998, eds, Special Issue, The Environmental Kuznets Curve, Ecological Economics, v. 25, 229p.

Selden, T. M. and Song, D., 1994, Environmental Quality and Development: Is There a Kuznets Curve for Air Pollution Emissions?: Journal of Environmental Economics and Environmental Management, v. 27, p. 147-162.

Shafik, N., 1994, Economic Development and Environmental Quality: An Econometric Analysis: Oxford Economic Papers, v. 46, p. 757-773.

Stern, D. I., Common, M. S., and Barbier, E. B., 1996, Economic Growth and Economic Degradation: The Environmental Kuznets Curve and Sustainable Developrnent: World Development, v. 24, no. 7, p. 1151-1160.

United Nations Population Division, 1998, 1998 Revision of the World Population Estimates and Projections: available online and to be published as *World Population Prospects: The 1998 Revision* and as a wall chart *World Population 1998.*

World Resources Institute, 1996, (jointly with United Nations Environment Program, United Nations Development Program, and the World Bank), World Resources 1996-97: Oxford University Press, 365 p. Data tables are also available as "World Resources 1996-97 Database Diskette",

WORLD ENERGY PROJECTIONS FROM THE INTERNATIONAL ENERGY OUTLOOK 1998

Linda E. Doman
Energy Information Administration
Washington, DC 20585

KEYWORDS: regional energy demand, forecasts, carbon emissions

The Energy Information Administration publishes the report, *International Energy Outlook* (*IEO*), on an annual basis [1]. The report presents an assessment of world energy markets through 2020. The *Outlook* provides projections of total primary energy consumption, as well as projections of energy consumption by primary energy type (oil, natural gas, coal, nuclear, and hydroelectric and other renewable resources); and projections of net electricity consumption. By fuel projections of energy consumed for electricity generation and energy consumed at the transportation sector are also included. Carbon emissions resulting from fossil fuel use are derived from the energy consumption projections. All projections are computed in 5-year intervals through 2020.

In the 1998 edition of the *IEO*, we projected that by 2020, the world will consume three times the amount of energy it consumed in 1970 (Figure 1). Despite the economic crisis in Southeast Asia which began in the spring of 1997 and continued throughout 1998, we expect that almost half of the world's projected energy increment will occur in developing Asia. Indeed in our *International Energy Outlook 1998*, the reference case projections for Asia assumed the crisis in this part of the world would not be protracted and that the region will experience a return to the strong economic growth the region exhibited before the economic crisis. Energy demand levels should, therefore, return to the levels expected before the recession in the long run. By 2010, energy use in developing Asia (including China and India, but excluding Japan, Australia, and New Zealand) surpasses consumption in all of North America (comprised of the United States, Canada, and Japan) in our reference case. By 2020, developing Asia's consumption levels exceed that of North America by 36 percent (50 quadrillion British thermal units—Btu).

Figure 1. World Energy Consumption, 1970-2020

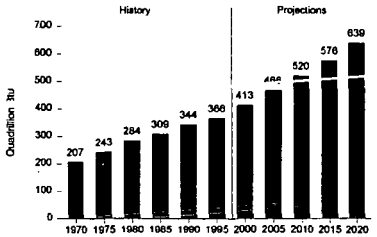

Source: EIA, International Energy Outlook 1998

In the 1998 reference case forecast, world energy consumption reaches 639 quadrillion Btu, growing by 2.3 percent annually between 1995 and 2020. All sources of energy, except for nuclear power, grow over the projection period. Renewable energy sources do not grow as quickly in the forecast period as they have in the past 25 years (Figure 2). By 2020, the total increment in world energy consumption from the 1995 level is projected to be about 274 quadrillion Btu, representing a 75-percent increase in total energy consumption.

Figure 2. World Energy Consumption by Fuel, 1970-2020

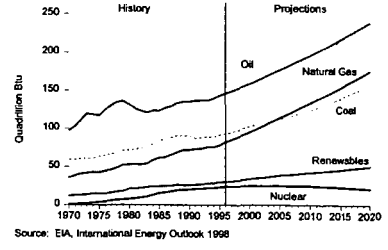

Source: EIA, International Energy Outlook 1998

Much of the growth in energy consumption occurs outside the industrialized world—which today consumes about 86 quadrillion Btu more than the developing world. In fact, by 2005, nonindustrialized countries (that is, the developing countries plus countries of Eastern Europe and the former Soviet Union) are expected to consume as much energy as the industrialized countries. But by the end of the forecast, energy consumption in the developing countries (developing Asia, the Middle East, Africa, and Central and South America) exceeds that of the industrialized world by 16 quadrillion Btu. Such large increases will have an enormous impact on the energy markets of the future. The projections assume substantial levels of new investment in all phases of energy production and distribution. To achieve such investment in many areas of the world, government policies must evolve, favoring private incentives for saving, trade, and development.

Reference Case Trends

World energy consumption is expected to reach 639 quadrillion Btu by 2020 according to our reference case projections. Much of the growth stems from increased fossil fuel use. Natural gas use is expected to have the fastest growth rate among the primary energy sources, at 3.3 percent per year between 1995 and 2020. However, the use of all fossil fuels is expected to grow faster over the next twenty-five years than it has in the past twenty-five years.

By 2020, oil consumption is expected to reach 116 million barrels per day, a 66 percent increase over the 1995 level. Oil has been the dominant energy source historically and is expected to remain so over the forecast period. However, oil demand is expected to grow more slowly than total energy consumption in the forecast, as it has for the past twenty-five years. In the industrialized countries, oil use continues to grow in the transportation sector where petroleum fuels have limited competition from other energy sources. In the rest of the world, oil demand is expected to grow in all economic sectors.

The worldwide growth in oil demand is expected to result in some increases in oil prices over the projection period. In the *IEO98* projections, prices rise from $18 per barrel (U.S. 1996 dollars) in 1995 to over $22 per barrel in 2020. The year-end 1996 price of oil was $24 a barrel. General perceptions are that near-term price risks are more heavily weighted on the downside, rather than the upside; in 1998, many analysts lowered their near-term projections by $1.00 or more per barrel for at least the next year or so, a sharp reversal of the views held early in 1997. In the *IEO98* forecast, prices were expected to recover from the lows experienced in early 1998. However, the recently released price path for our sister publication, the *Annual Energy Outlook 1999* suggest prices that do not recover until after 2005. Indeed, in the year 2000, world oil prices are more than $5 per barrel lower in this year's *Annual Energy Outlook* than they were in last year's report (Figure 3) [2].

Figure 3. Comparison of 1998 and 1999 World Oil Price Paths

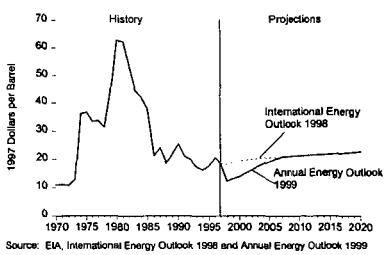

Source: EIA, International Energy Outlook 1998 and Annual Energy Outlook 1999

We expect oil prices to generally stay low because non-OPEC nations will be able to continue to expand oil production in the short-term. Improvements in technology associated with oil exploration, development, and production will allow the non-OPEC production to achieve these expectations. The use of three-dimensional seismic imaging, horizontal drilling, and subsea well completion technologies has helped to extend the productive life of mature oil fields and to reduce development and production costs at new fields. While the Middle East may possess the largest portion of reserves that can be developed most economically, the reserves and production potential of other areas of the world have been substantially broadened. Nevertheless, OPEC producers are projected to gain share in the world oil production market, providing about 52 percent of the world's oil supply in 2020, compared to 39 percent in 1996.

Among all primary energy sources, natural gas is expected to grow the most rapidly, by 3.3 percent annually over the next 25 years. Natural gas resources are fairly widespread and burn more cleanly than other fossil fuels. This is particularly true in electric power generation where much of the future growth in gas demand is expected to occur. Moreover, combined-cycle gas-fired generators require shorter construction periods and are often more efficient than other fossil fuel generators or nuclear power plants. In the *IEO98* reference case projections, gas use surpasses coal by 2005, and by 2020 it exceeds coal demand by almost 18 quadrillion Btu (today, gas demand is about 13 quadrillion Btu less than coal).

There is much activity designed to expand the natural gas infrastructure worldwide. According to *Oil and Gas Journal*, in February 1997, 11,000 miles of gas pipeline were under construction and expected to be completed by the end of 1997, and over 34,000 miles of gas pipeline were planned for years beyond 1997 [3]. Natural gas demand is expected to grow most quickly in the developing world. In developing Asia, gas grows by 7 percent annually between 1995 and 2020. In Brazil alone, gas use increases by 14 percent annually in the reference case. There is robust activity in developing Central and South America's gas infrastructure needed to bring natural gas to industrial customers and electric generators. Construction began on several major pipelines in 1997, including work on the $2 billion Bolivia-to-Brazil pipeline, the first portion of which is scheduled to be completed by the end of 1998, and the entire 1,973-mile line should be finished by the end of 1999

[4].

Worldwide coal consumption in the *IEO98* grows 1.7 times above the 1995 levels, reaching 8.6 billion short tons by 2020. The strongest growth in coal use occurs in Asia in the reference case projections. Indeed, nearly 90 percent of the increment in coal use is attributed to countries of developing Asia. What's more, 95 percent of the developing Asia increase is attributed to only two countries: China and India. In these two countries, coal continues to be the major primary fuel source. Outside of China, almost all of the increase in coal use will be for electricity generation.

Coal's role in energy use worldwide has shifted substantially over the past twenty-five years, from a fuel used extensively in all end-use sectors to one that is now primarily used for primary electricity generation, and in a few key industrial sector uses such as steel, cement, and chemicals. The coal share of total energy consumption decreases only slightly over the projection period, from 25 percent in 1995 to 24 percent in 2020, mostly because of the large increases projected in developing Asia. Coal use is shrinking in Eastern Europe and the former Soviet Union and this trend is expected to continue. Slow growth is projected in the industrialized countries where decreases in coal used in Western Europe offset gains in Japan and North America. Of course, the relatively stable outlook portrayed for coal in the *IEO98* could change dramatically as a result of the reductions in carbon emissions targeted in the Kyoto Climate Change Protocol. If the proposed reductions occur, the coal industry could face a rapidly declining market for its product in the years to come.

Nuclear power declines over the forecast horizon, and the source loses share of total energy consumption, falling from 6 percent in 1995 to 3 percent by 2020. At the end of the projection period, electricity generation from nuclear energy falls below the 2,203 billion kilowatthours consumed in 1995. Use of nuclear energy peaks worldwide in 2005 at 2,368 billion kilowatthours, after which the United States and other countries with mature nuclear programs are expected to phase out the nuclear generation and retire nuclear capacity without replacing it. A substantial reduction in nuclear capacity is also expected in the former Soviet Union after 2010. Nevertheless, some countries—particularly Japan and some of the countries of developing Asia—have plans to increase their reliance on nuclear power for electricity generation.

Nuclear power provided 17 percent of total electricity generation in 1996. In nine countries it provided more than 40 percent of electricity generation. Nevertheless, market competition from natural gas, public concerns about the safety of nuclear reactor operations, and problems associated with the disposal of nuclear waste products are constraining the expansion of nuclear power programs in many countries. The widespread trend towards privatization and deregulation of the electric utility sector has also undermined the viability of the nuclear option, because of the high costs associated with constructing and operating nuclear facilities. It is possible, however, that ratification of the Kyoto Protocol could change the outlook for nuclear power. Industrialized countries could conceivably extend the lives of their nuclear power plants in an effort to constrain the growth of greenhouse gas emissions.

Hydroelectricity and other renewable energy resources are expected to retain their 8-percent share of the world energy markets throughout the forecast period. Low fossil fuel prices make it difficult for renewables to compete for market share—despite the progress that has been made to reduce the per kilowatthour costs associated with generating electricity with renewables, particularly wind. In the reference case, renewables grow by 67 percent worldwide, with strongest growth projections in the developing world. There are some efforts in the industrialized world to increase the penetration of renewable energy sources to help mitigate the growth of greenhouse gases. In particular, the European Union announced a stimulus package for encouraging renewables, and plans to invest about $11 billion in wind plants in hopes of installing 10 gigawatts of wind capacity by 2010 [5].

In the *IEO98* reference case, world carbon emissions are expected to reach 8.3 billion metric tons by 2010 and 10.4 billion metric tons by 2020. According to this projection, world carbon emissions would exceed 1990 levels by 81 percent at the end of the forecast period. By 2010, emissions in the developing world are projected to be almost equal to those of the industrialized nations with 78 percent of the world's increment in emissions between 1990 and 2010 attributed to the developing countries. If the Annex I countries[1] that are parties to the Kyoto Protocol were able to achieve the proposed target reductions, the forecast for their emissions would be altered; but emissions levels

[1]The Annex I countries are defined as: Australia, Austria, Belarus, Belgium, Bulgaria, Canada, Croatia, Czech Republic, Denmark, European Economic Commission, Estonia, Finland, France, Germany, Greece, Hungary, Iceland, Ireland, Italy, Japan, Latvia, Lithuania, Luxembourg, the Netherlands, New Zealand, Norway, Poland, Portugal, Romania, Russia, Slovakia, Slovenia, Spain, Sweden, Switzerland, the Ukraine, the United Kingdom, and the United States.

Figure 4. Carbon Emissions in 1990, 2010, and 2020 in Two Cases: Annex I vs. Non-Annex I

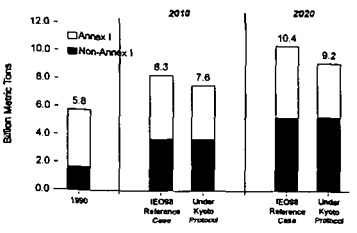

Source: EIA, International Energy Outlook 1998

worldwide would continue to increase (Figure 4). Meeting the requirements of the Protocol exactly would mean a reduction of more than 700 million metric tons of carbon relative to the reference case forecast for 2010.

Uncertainty in the Forecast

At present, there are several areas which may be considered volatile in terms of trying to determine the future trends in energy demand. Asia is one, particularly given the recession that has remained in several key economies in the region—the largest being Japan, but also in the region's developing markets. The Asian crisis did lead to some short-term reductions in the expectations for energy use in this region in the 1998 *Outlook*. If the crisis does not soon show some signs of abating in Southeast Asia, it could have a deepening affect on the growth in energy use in developing Asia. Thailand, Indonesia, Malaysia, and South Korea currently account for just less than 20 percent of the energy use in developing Asia. The recession has already caused energy projects to be either delayed in those countries, and a quick economic recovery is key to support their completion.

Another development which could have a dramatic affect on the growth in energy consumption worldwide is the Kyoto Climate Change Protocol. No adjustments were made to the projections of energy demand based upon the effects of the Kyoto Protocol because the *IEO98* was developed based on current laws and regulations in place. While some 60 countries have signed the Protocol (including the United States, although this occurred many months after the *IEO98* was published in November 1998 [6]), only Fiji and Antigua and Barbuda have ratified the treaty. None of the participating countries had ratified the treaty at the time our report was published. The Protocol will only become legally binding when at least 55 countries, including Annex I countries accounting for at least 55 percent of these countries' 1990 carbon dioxide emissions have signed and then ratified it.

The Kyoto Protocol could substantially affect energy use in the industrialized countries. For the emissions targets specified by the Protocol to be achieved solely through a reduction in fossil fuel use, projected energy demand in 2020 would have to be scaled by between 40 and 60 quadrillion Btu—equivalent to between 20 and 30 million barrels of oil per day. Of course, the reality is that fuel-switching opportunities, emissions trading permits, and other offsets allowed under the Protocol, such as reforestation will make a more modest reduction in fossil fuel use necessary.

Figure 5. Energy Consumption in the Former Soviet Union, 1990-2020

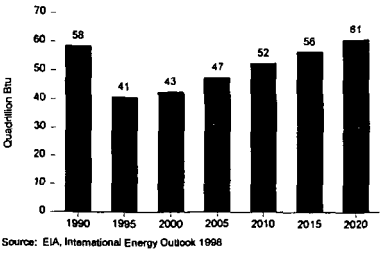

Source: EIA, International Energy Outlook 1998

Russia and the other countries of the former Soviet Union (FSU) pose a third challenge in terms of volatility in the forecast of energy demand. In the *IEO98*, energy consumption in the FSU only overtakes the 1990 level at the end of the projection period (Figure 5). This projection was published in April 1998, before the recent devaluation of the Russian rouble. Indications are that the economy has worsened in this region enough that the forecast may well need to be scaled back even further in our next report. Moreover, the *IEO98* projected that oil production in the FSU would increase to 12.6 million barrels per day by 2020, compared to an oil consumption of 7.5 million barrels per day in that same year. However, Russian First Deputy Prime Minister Yury Maslyukov warned that unless serious actions were taken to "change the situation of the oil industry," Russia could become a net oil importer in as little as two years as the country's oil output has been in decline for the past ten years [7].

Future Considerations

As we prepare our next edition of the *International Energy Outlook*, we must address the levels of uncertainty we have about development of the world's energy markets given the events outlined above. Evaluating the long-term impact of the Southeast Asian economic recession, the length of

time it will take the former Soviet Union—especially Russia—to recover from the collapse of their centrally planned economies, and the affects of the Kyoto Protocol on industrialized countries is a difficult task. Because regional gross domestic product (GDP) growth rates are one of two major assumptions we use to derive energy consumption projections (the other is an energy elasticity measure of the change in GDP divided by the change in energy consumption), adjusting economic growth will have a substantial impact on the growth in energy use. Growth expectations for GDP in Japan, the former Soviet Union, and countries in developing Asia will be somewhat reduced compared to last year's forecast. No doubt this will result in some reduction in the energy consumption forecast for these regions. In the *Annual Energy Outlook 1999*, the world oil demand projections showed a slight downward adjustment of 1.4 million barrels per day by 2020 from last year's *IEO*.

As of November 1998, none of the Annex I countries had ratified the Kyoto Protocol treaty so it is unlikely that this year's *IEO* reference case projections would be altered to incorporate the treaty. However, we expect to continue to address the potential effects the Protocol might have on various energy markets worldwide.

References

1. Projections that appear in this paper are taken from the Energy Information Administration, *International Energy Outlook 1998*, DOE/EIA-0484(98) (Washington, DC, April 1998).

2. Energy Information Administration, *Annual Energy Outlook 1999*, DOE/EIA-0383(99) (Washington, DC, December 1998).

3. W.R. True, "World Pipeline Construction Looks to Remain Robust to Century's Turn," *Oil and Gas Journal* (February 10, 1997), pp. 36 and 37.

4. Brazil in Action web site (http://www.brazil-in-action.gov.br), "Bolivia-Brazil Gas Pipeline: Investment Opportunities," (July 22, 1998).

5. "European Union Maps Plans for Major Renewables Expansion," *Wind Energy Weekly*, Vol. 16, No. 776, (December 8, 1997), pp. 1-2.

6. United Nations Framework Convention on Climate Change Press Release, "Climate Change Meeting Adopts Buenos Aires Plan of Action," (November 17, 1998).

7. Itar-Tass via NewsEdge Corporation release (http://www.newspage.com), "Russia's Oil Output Mishandled - Maslyukov," (November 23, 1998).

COAL QUALITY AND COAL UTILIZATION IN THE TWENTY-FIRST CENTURY

R.B. Finkelman and H. Gluskoter
U.S. Geological Survey, MS 956, National Center, Reston, VA 20192

KEYWORDS: Coal quality, domestic databases, international databases

Abstract

Worldwide coal utilization in the 21st Century will be influenced by concerns about the effects of coal combustion on the local, regional, and global environment and on human health. Reliable coal quality data can help decision makers to better assess the risks and limit the possible environmental degradation and impact on health. Although millions of coal analyses have been performed worldwide, existing national coal quality databases are generally of limited use because much of the data are not readily accessible; geographic coverages are not comprehensive; analytical data may not be accurate; and samples may not be representative, or current. The U.S. Geological Survey is collaborating with agencies from other coal producing countries to create an integrated, electronic, worldwide coal quality database. The database, on coals currently being burned, includes results of proximate and ultimate analyses; sulfur form data; concentrations of major, minor, and trace elements; semi-quantitative analyses of minerals; and modes of occurrence of environmentally important elements.

Introduction

When the U.S. Congress passed the 1990 Clean Air Act amendments (1) worldwide attention was focused on the potential environmental and human health problems that could be caused by the emissions of hazardous air pollutants from coal-burning power plants. Among the potential pollutants were about a dozen trace elements including the elements, or compounds of, antimony, arsenic, beryllium, cadmium, chlorine, chromium, cobalt, fluorine, manganese, mercury, nickel, lead, selenium, and radionuclides (e.g. uranium and thorium) as well as scores of organic compounds. The U.S. Environmental Protection Agency, therefore, sought reliable, comprehensive coal quality information to help assess the potential environmental and human heath impacts of these substances that might arise from coal use. These concerns may be with us well into the 21st Century as we learn more about the effects of long-term, low-level exposure to toxins.

Concerns about the environmental and health impacts of coal use are not constrained to the United States. Environmental and human health problems attributed to coal use have been documented from Czechoslovakia (2), China (3, 4), India (5), Ukraine (6), Russia, and elsewhere. The social cost of these problems is enormous and will continue to grow, especially in developing countries that tend to use poor quality coal in boilers with little or no pollution control systems or use coal for domestic cooking and heating.

The World Resources Institute (7) estimates that as many as 3.5 billion people rely on traditional fuels for cooking and heating. The World Bank (8) estimates that between 400 million and 700 million woman and children are exposed to severe air pollution, generally from cooking fires, a substantial proportion of these people rely on coal. The particulates, metals, gases (such as SO_x), and organic compounds (such as polycyclic aromatic compounds: PAC) can cause serious respiratory problems and toxic reactions.

While many of the environmental and health problems caused by coal use are local, some of the volatile pollutants (CO_2, SO_x, NO_x, Hg, Se, Cl, F) may have regional and even global environmental and human health impacts. Clearly these environmental and health problems create complex economic and social ills that will require carefully considered, multidisciplinary, 21st Century solutions. Reliable, comprehensive and readily available coal quality data can help decision makers to better assess the risks and limit the possible environmental degradation and impact on health.

Domestic Databases

Domestic databases of quality of coals in the United States, while incomplete, are available. The U.S.Geological Survey (USGS) maintains the largest publicly available coal quality database. The database contains information on almost 14,000 coal samples from every major coal basin in the U.S. Approximately 136 parameters are recorded for each sample. These parameters include geographical, geologic, and stratigraphic information, quantitative information on about 60 elements,

proximate and ultimate data, sulfur-form information, ash fusion temperatures, etc. Recently, much of this information has been made available on CD-ROM (9) and on the World Wide Web at URL http://energy.er.usgs.gov/products/databases/coalqual/intro.htm.

The Illinois State Geological Survey, the New Mexico Bureau of Mines and Minerals Resources, the University of North Dakota's Energy and Environmental Research Center (EERC), and the Pennsylvania State University also maintain high-quality, publicly available coal quality databases containing several hundred to more than 1,000 analyses.

A weakness of all the publicly available coal quality databases is that the samples represent coal that has been mined. For example, approximately 75 percent of the information contained in the USGS database was obtained prior to 1985. Twenty-first Century decisions will require information that reflects the characteristics of the coal that is currently being mined and burned and of the coal that will be mined in the near future. Moreover, current environmental concerns require new types of information to be included in these databases. For example, semi-quantitative analyses of minerals and modes of occurrence of environmentally important elements are necessary for the development of computer models to predict the behavior of these elements during coal cleaning and combustion. Petrographic characterization of coal may provide useful insights into the types and amounts of PAC's generated during domestic coal combustion (10).

To address these concerns, the USGS is teaming with other organizations to create a new coal quality database. This new database, known as the National Coal Quality Inventory (NaCQI) is supported by a partnership forged among federal and state governmental agencies, the utility and mining industries, and universities (11).

The project participants will collect suites of samples (core/channel, run-of-mine, raw/clean, power plant feed, etc.) from the major coal producing regions in the U.S. that will provide coal in the 21st Century. The samples will be characterized by traditional methods (12) for proximate and ultimate analysis, sulfur form data, major, minor and trace elements. The scope of this database will be broadened to include modes of occurrence information and semi-quantitative mineralogy on selected samples.

International Coal Quality Databases

Most of the growth in energy consumption in the 21st Century will be seen in developing countries such as China, India, and Indonesia, all of which have large indigenous coal resources (13). Increasing populations and rapid industrialization is placing enormous pressures on these countries to produce energy through increased coal use. With this rapid expansion of coal use comes the potential for serious environmental and human health problems. Unfortunately, many of these countries lack the reliable, comprehensive, electronic coal quality database needed to help minimize these problems.

Although millions of coal analyses have been performed worldwide, most existing national coal quality databases are generally of limited use because:

- Much of the data are in obscure publications, are in the native languages, or the data reside in paper files that are not readily accessible;
- Geographic coverages are not comprehensive;
- Analytical data may not be accurate or may be incompatible with analytical schemes used in other countries;
- The analyzed coal samples may not be representative of the full deposit, or the samples may have been collected and analyzed many years, often several decades, ago.
- Information is lacking on trace element concentrations, mineralogy, and modes of occurrence of the elements of environmental concern.

To help develop an integrated, electronic worldwide coal quality database, the USGS has initiated a unique compilation of coal quality information from all the coal-producing countries in the world. The database (World Coal Quality Inventory: WoCQI), will focus on information from coals currently being burned and will include results of proximate and ultimate analyses, sulfur form data, concentrations of major, minor, and trace elements, semi-quantitative analyses of minerals, and modes of occurrence of environmentally important elements on selected samples. The information in the database will be made available on the World Wide Web (WWW) and through a searchable CD-ROM.

The sources of coal quality information that will be incorporated into the database include capturing existing computerized databases and salvaging information from publications and hardcopy files. However, the highest priority will be given to developing cooperative agreements with representatives of coal-producing countries. In most agreements the host country will be responsible for the collection of the sample using appropriate sample collection protocols and the USGS would be responsible for sample characterization, database development, and information dissemination.

The information in the WoCQI database could be used to evaluate:

- National and regional energy resources
- Export/import potential
- Potential environmental and health impacts
- Technological behavior
- Technology transfer potential
- International Policy decisions
- Byproduct potential

WoCQI currently contains approximately 2,000 analyses from about 20 countries (exclusive of the U.S.). We intend to expand the scope of coal quality characteristics to include information on mineralogy, petrography, washability, modes of occurrence, etc.

We should strive to develop coal quality databases that anticipate the potential future uses of the coal quality data. This would require that 21st Century coal quality databases contain a broader range of coal quality parameters including quantitative information on modes of occurrence of the elements, semi-quantitative mineral composition, and information on the behavior of the elements during coal cleaning, leaching, and combustion.

In addition to addressing environmental and health problems, coal quality data can also be used to better anticipate technological problems such as boiler fouling, slagging, corrosion, erosion, and agglomeration. This, in turn, could lead to coal-blending or additives that would minimize these costly problems. Information on the textural relations (mineral-mineral and mineral-maceral intergrowths) should be useful in anticipating the removability of trace elements during physical, chemical, and biological coal cleaning. Anticipating the removability of certain elements from coal might create opportunities for economic byproduct recovery.

Coal quality data could play an important international role by providing useful information on potential foreign investment prospects. This information may also help to identify markets for coal industry goods and services.

Quantitative coal quality data, comprehensive databases containing a broader array of quantitative coal quality parameters, and multi-disciplinary, multi-organizational, and multi-national cooperation should help to ensure the efficient and environmentally compatible use of our global coal resources in the 21st Century.

References

1. U.S. Statutes at Large (1990) Public Law 101-549, Provisions for attainment and maintenance of national ambient air quality standards, 101st Congress, 2nd Session, 104, Part 4, 2353-3358.

2. Bencko, V. and Symon, K., 1977, Health aspects of burning coal with a high arsenic content. II. Hearing aspects of burning coal with a high arsenic content. Environmental Research, Vol. 13, p. 386-395.

3. Belkin, H E, Zheng, B, Zhou, D, and Finkelman, R B, 1997, Preliminary results on the geochemistry and mineralogy of arsenic in mineralized coals from endemic arsenosis areas in Guizhou, Province, P. R. China. Proceedings of the Fourteenth Annual International Pittsburgh Coal Conference and Workshop. (CD-ROM).

4. Finkelman, R. B. in press, Health impacts of domestic coal use in China, National Academy of Sciences colloquium on "Geology, Mineralogy, and Human Welfare.

5. Singh-Mahendra, P., Singh, R.M., Chandra, D., 1985, Environmental and health problems due to geochemical alterations associated with trace elements in coals, Ghugus Coalfield, Wardha Valley,

Maharashtra. Quarterly Journal of the Geological, Mining and Metallurgical Society of India. Vol. 57, no. 2, p. 99-103.

6. Panov, B.S., Shevchenko, O.A., Matlak, E.S., and Dudik, A. M., in press, On pollution of the biosphere in industrial areas: the example of the Donets Coal Basin. International Journal of Coal Geology.

7. World Resources Institute, 1998, World Resources 1998-1999. The World Resources Institute, New York. 369 p.

8. World Bank, 1992, The World Bank Development Report 1992: Development and the Environment, Washington, D.C., p. 53.

9. Bragg, L. J., Oman, J. K., Tewalt, S. J., Oman, C. L., Rega, N. H., Washington, P. M., and Finkelman, R. B., 1997, U.S. Geological Survey Coal Quality (COALQUAL) Database: Version 2.0, U.S. Geological Survey Open-File Report 97-134.

10. Crowley, S.S., Orem, W.H., Roth, M.J., Finkelman, R.B., Scroggs, E.A., Willett, J.C., 1998, Possible Relation Between Esophageal Cancer and Coal Combustion in China: A Preliminary Study: Abstracts of the 15th Annual Meeting of the Society for Organic Petrology, Vol. 15, p. 96-98.

11. Finkelman, R.B., 1996, The national coal quality inventory: An example of industry, federal and state cooperation: 13th Annual International Pittsburgh Coal Conference, vol. 1, p. 403.

12. ASTM (American Society for Testing and Materials), 1997, Annual Book of ASTM Standards. Volume 05.05 Gaseous Fuels; Coal and Coke, ASTM, Philadelphia, PA.

13. World Energy Council, 1993, Energy for Tomorrow's World. St. Martins Press, 320 p.

CURRENT AND FUTURE ISSUES FACING HIGH-SULFUR MIDWESTERN COALS

Subhash B. Bhagwat
Illinois State Geological Survey, 615 E. Peabody Drive, Champaign, IL 61820

INTRODUCTION

Coal markets have been dramatically affected by the Clean Air Act (CAA) and its many amendments, and by price competition among fuels and between coals of different quality. Regulations regarding electricity generation, distribution and pricing now being eliminated. International concerns about global climate change will affect coal markets in the future. This paper presents an analysis of how these and other factors have affected high-sulfur coals in the past and how they will affect them in the future.

DEMAND-SIDE ISSUES

Coal demand in the U.S. increased from 523 million tons in 1970 to 1007 million tons in 1997. Electric utilities accounted for 61% of domestic total in 1970, and 90 % in 1997. Coal-fired power plants generated 46 % of the electricity for the utilities in 1970 and over 57 % in 1997 [1]. Nuclear electricity generation increased from 1.4 % of the total in 1970 to 22.5 % in 1995, but fell to 20.1% in 1997 due to plant safety and maintenance problems. The oil and natural gas price shocks in 1974 and 1979-81 resulted in significant fuel switching by electric utilities. By 1997, oil and natural gas-based electricity generation had fallen to 2.5% and 9.1% of the total respectively, well below their 1970 levels of 11% and 24%. Electricity generated by non-utility producers contributed an additional 3 to 12 percent to total electricity generated by utilities **(Figure 1)**. Available data indicate that natural gas is the preferred fuel of non-utility producers, thus increasing gas-based generation of electricity in 1997 to 14.5% of U.S. total. Growth in U.S. demand for electricity averaged about 4% per year in 1970, but declined to about 2% by 1997 **(Figure 2)**. However, increased post 1990 non-utility generation resulted in slowing down growth in utility generation to 1% in 1997 **(Figure 3).**

In 1991, the U.S. Department of Energy and four other institutions forecasted U.S. electricity demand to grow at 1.4 to 2.4% per year from 1990 through 2010 [2]. Subsequently published DOE Annual Energy Outlooks revised the forecast to 1.26% per year between 1995 and 2010 [3] [4], 1% per year for utilities and 3% for non-utility producers. These estimates indicate the continuation of the trends depicted in figures 2 and 3. Based on these forecasts, U.S. coal production in year 2010 is estimated to be about 1,225 million tons. Thermal conversion efficiency is a critical factor. A 1 percent increase in it can reduce coal demand by 2.5% or 30 million tons. Such a change is conceivable as less efficient, older plants are retired or their usage reduced.

REGULATORY ISSUES

Two sets of regulations affect coal markets: the Clean Air Act amendments (CAAA) of 1990 and the deregulation of the electricity generating industry. The potential for future regulation of "greenhouse gases" may already be affecting fuel choice decisions by utilities. The 1990 CAAA were the result of Congressional desire to create economic incentives and freer markets for pollution control. Accordingly, the mandatory 90% emission reduction was eliminated but a reduction in nation-wide SO_2 emissions of 5 million tons by January 1995 (Phase I) and another 5 million tons by January 2000 (Phase II) together with an overall cap on emissions at the year 2000 level were mandated. The mechanism to do this is the "pollution credit," which allows plants that reduce emissions below the legal limits to achieve a credit that they can sell to plants that are over the limit. Utilities in need of emission reduction can reduce emissions or purchase pollution credits in the market. The decision is to be made by individual companies on an economic basis. In the first phase of the 1990 CAAA that ended in 1995, a majority of plants opted for low-sulfur Wyoming coal or natural gas and created a large stock of pollution credits with few buyers. Consequently, the price of pollution credits fell from the originally predicted $1,500 per unit (1 Unit = 1 ton of SO_2 per year) to $65 to $70 per unit [5] by March 1996. In October 1998, they were trading at $160 to $180 per unit [6].

To comply with the second phase of the 1990 CAAA, utilities have been switching to lower sulfur fuels for the past three years and an acceleration of the trend is likely in 1999. For example: Illinois Power, the largest consumer of high-sulfur coal in Illinois, has decided to

switch to Wyoming coal in the next twelve months. Because the delivered prices of low- and high-sulfur coals are comparable in most states, demand for western coal is expected to rise through the year 2000 and possibly through 2010. After 2000, sulfur-free fuels such as natural gas will be preferred by users who must comply with the SO_2 emission "cap". Available technologies like Flue Gas Desulfurization (FGD) and Fluidized Bed Combustion (FBC), and emerging ones like Integrated Gasification Combined Cycle (IGCC) would permit coal-burning with little or no SO_2 emission. Decisions to use them, however, will depend on their total generating cost compared with the total cost of using sulfur-free fuels.

Emissions of nitrogen oxides (NO_x) are also regulated under the Clean Air Act. Some NO_x rules apply only to plants that are affected by CAA SO_2 regulations. Each affected unit must hold NO_x emissions below 0.45 or 0.5 lbs per million Btu, depending upon the boiler type. Stricter limits apply to ozone non-attainment areas. States must determine what approach is reasonable to achieve this goal.

The 1990 amendments also propose to control emissions of Hazardous Air Pollutants (HAPs). When regulations are established, they may affect coal use because up to 16 HAPs are known to be released by combustion. Of these, mercury is likely to be one of the first to be regulated. Resource Data International (RDI) recently estimated the cost of curbing mercury emissions to range between $0.5 billion and $7.8 billion annually and add up to 0.2 cents to the cost per kWh of electricity [7]. Mercury-free fuels would thus have an advantage over other fuels in the future.

Utilities have been "regulated monopolies." Customers within a utility's service area could only purchase electricity from that utility. A state commission determined the utility's rate of return on investment, and approved all expenses the company charged to consumers. Electric utilities are now being deregulated under the 1992 National Comprehensive Energy Policy Act. "Independent" unregulated power companies are now permitted. These independents are free to produce and sell electricity to anyone anywhere. Utilities are also now permitted to merge. Wholesalers who buy electricity for resale are free to purchase it anywhere, and utilities are required to provide transmission for a fair market charge. Retail customers, however, are still required to purchase electricity from the same utilities as before until state laws are amended.

Deregulation will likely intensify price competition among producers of electricity and force cost-cutting measures in the industry. Some of the consequences of the increased competition are as follows:
*Old low-efficiency and high-cost generating units will be retired earlier than planned.
*Lower-cost units will increase their capacity utilization (load factor).
*Independent producers will not have price or sales guarantees.
*Independent electricity distribution networks, including intra-city, may emerge.
*Gas-fired combined-cycle electricity generation may assume a greater role in production.
*Nuclear power plants may face economic hardships because of unrecovered investments, called the "stranded costs".
*Rural electric power supply companies facing loan servicing problems may require federal assistance worth billions of dollars to avoid bankruptcies [8].

INTER FUELS COMPETITION

Coal availability in the United States is not a problem. According to DOE, recoverable coal reserves in the U.S. total about 265 billion tons. About 61 billion tons of the U.S. recoverable coal reserves are in the Interior Region and about 80% of that is in the Illinois Basin, which includes parts of Illinois, Indiana and western Kentucky. Thus, nearly 49 billion tons of recoverable coal reserves, or 18.5% of the national total, are in the Illinois Basin [9]. However, the low-sulfur (<1.2 lbs SO_2 per million Btu) recoverable reserves in the U.S. are about 100 billion tons, very little of which is in the Interior Region. Little or no Illinois Basin coal can comply with the maximum allowable SO_2 limit through the year 2000 without additional cleaning or other forms of emission controls **(Figure 4)**. About 87% of the nation's low-sulfur coal reserves are in the western states, while 61% of high-sulfur (>3.36 lbs SO_2 per million Btu) recoverable coal reserves are in the Interior Region, mostly in the Illinois Basin.

Fuel cost is the main determinant of generating plants' operating cost but fuel choice is determined not only by its price but also by the cost of equipment needed to burn it cleanly and to safely dispose of waste. In the short run, the additional equipment costs

disadvantage high-sulfur coal. In the long run, however, the deciding factor will be the cost of coal. To understand high-sulfur coal's current and near term disadvantage in comparison to other fuels, the cost of these fuels and the comparative costs of various pollution abatement strategies must be understood.

Pollution control and waste disposal costs of fossil fuels have been included in the price of coal-generated electricity, but the nuclear industry's costs of development and waste disposal have not been fully internalized, and insufficient money is being set aside to pay for the decommissioning of nuclear plants [10]. These un-internalized costs helped nuclear energy grow at exceedingly high annual rates in the past 25 years. Despite their low operating costs, nuclear plants are economically troubled by their stranded costs that must be recovered through higher rates, or borne by investors.

Gas-based generation increased at 2.4% per year during 1989 to 1995, after a sustained 16 year decline. Although gas based non-utility generation increased in 1996 and 1997, utilities used less gas than in 1995 with the result that total gas based generation remained unchanged. Delivered prices of natural gas to utilities increased 40 % in 1996-97. Gas fired power plants have important economic advantages because of their high thermal efficiency (60%) compared with coal-fired plants (40%). Gas-fired plants take only 1 to 3 years to build and cost at least 40% less than coal-fired plants [11]. Unlike in the 1980s, gas is no longer perceived as a commodity in short supply. DOE estimates proven U.S. gas reserves to be about 165 trillion cubic feet (Tcf), the equivalent of ten years of supply at the current rate of production. Seven times more than that can be found and produced at current prices and with currently available technology [12]. Planned capacity additions by electric utilities indicate that of the 32,000 MW to be added between 1993 and the year 2000, about 60% will be gas-based and only 20% coal-based [13].

According to the 1996 DOE annual energy outlook, the growth in coal-based electricity generation between 1995 and 2010 will come from an increase in capacity utilization from 62% to about 75%. No net addition to coal-based generating capacity is expected. Coal mined in the western states enjoys a price advantage over Midwestern coal primarily because mine productivity is high, mining costs are extremely low **(Table 1)**, and because average nationwide rail transportation rates declined 17% between 1986 and 1993 as a result of the transportation industry deregulation in the late 1970s [14]. As a result of increased use of Wyoming coal, the federal EPA reports a 2.3 million unit (1 Unit = 1 ton SO_2) over-compliance in January 1995. With this, almost half of the reductions targeted in the 1995-2000 period have already been achieved. A further increase in the use of low-sulfur coal through the year 2000 is likely.

THE KYOTO AGREEMENT

In December 1997, over 140 nations met in Kyoto, Japan, to discuss the possible effects of carbon dioxide emissions on global climate. The agreement reached at that meeting requires industrialized nations to reduce carbon emissions to an average of 7 percent below the 1990 carbon emission level by the year 2010. Most developing countries are exempt from these requirements because their current contributions to carbon emissions are low. The effectiveness of the Kyoto agreement is questionable for two reasons: 1) Economic growth rates in developing countries are two to three times those in developed countries. Thus, in twenty years most carbon emissions would be coming from those countries. 2) A reduction of carbon emissions to pre-1990 levels in industrialized countries would require a drastic reduction in energy consumption starting immediately. Such reductions would disrupt the entire world economy and threaten the livelihood of billions, including those in the developing countries that depend on exports to industrialized countries. The combined effects of the factors discussed above on the future demand for various fuels are summarized in the following chart: (An upward arrow indicating higher, a downward arrow lower demand)

	1990 CAAA	Deregulation	Kyoto agreement
Coal			
Low Cost	↑	↑	↓
High Cost	↓	↓	↓
Natural Gas	↑	↑	↑
Nuclear	↓	↓	↓ (?)

FUTURE OF HIGH-SULFUR COAL

The coal mining industry in the high-sulfur coal states has been hit hard by the dynamics of the coal market. High-sulfur coal production began to decline after the passage of the 1990 CAAA. Coal production in Illinois, Indiana, western Kentucky and Ohio declined by about 19 percent, from 176.5 million tons in 1990 to 143.3 million tons in 1997. Illinois coal production fell about 30%. Dozens of Illinois coal mines closed and over half the jobs were lost. Long-term sales contracts are declining rapidly. The future demand for high-sulfur coal will depend upon its price. The delivered prices of high-sulfur coals in most areas are higher than the prices of low-sulfur western coals. The conditions for high-sulfur coals in the first decade of the next century remain unchanged: slow growth in electricity demand, an even slower growth in coal-based electricity generation, and a higher price in comparison with low-sulfur western coal. Unfortunately, mine productivity in the high-sulfur coal states has not grown sufficiently to narrow the price gap. More power producers are opting for lower sulfur coals and natural gas. Under continuing prospects for lower coal production, the expected year 2010 production from Illinois, Indiana, western Kentucky and Ohio may be in the range of 100 to 105 million tons.

REFERENCES:

(1)Monthly Energy Review, Jun.1998, Energy Information Administration, U.S. Department of Energy, Washington, DC, DOE/EIA-0035(98/06), page 95.
(2)Annual Energy Outlook 1991 With Projections to 2010, March 1991, Energy Information Administration, U.S. Department of Energy, Washington, DC, DOE/EIA-0383(91), page 38.
(3)Annual Energy Outlook 1993 With Projections to 2010, January 1993, Energy Information Administration, U.S. Department of Energy, Washington, DC, DOE/EIA-0383(93), page 49.
(4)Annual Energy Outlook 1996 With Projections to 2015, Energy Information Administration, U.S. Department of Energy, Washington, DC, DOE/EIA-0383(96), pages 94 and 95.
(5)EPA Credit Auction Shows mid-$60 Prices; Announces Massive 1995 Over-compliance, Coal Week, April 1,1996, pages 1 and 2.
(6)Power Marketers Splash into Allowance market, Todd A. Myers, Coal Age, October, 1998,
(7)National Mining Association, November 9, 1998,
(8) U.S.Giving Electric Co-ops Relief on Loans, The Wall Street Journal, October 3,1996, p.A3-A4.
(9)Coal Data: A Reference, February 1995, Energy Information Administration, U.S. Department of Energy, Washington, DC, DOE/EIA-0064(93), page 47.
(10)Heinze Fry, Gene R. The Cost of Decommissioning U.S. Reactors: Estimates and Experience. The Energy Journal, International Association for Energy Economics, Special Nuclear Decommissioning Issue, Volume 12, 1991, pages 87- 104.
(11)Proceedings: 1986 Fuel Supply Seminar, Electric Power Research Institute, Palo Alto, CA., EPRI Project 2369-10, Sept. 1987, pages 5-10.
(12)Natural Gas 1994 - Issues and Trends, Energy Information Administration, U.S. Department of Energy, Washington, DC, DOE/EIA-0560(94), pages 8-9.
(13)Inventory of Power Plants in the United States 1992, Energy Information Administration, U.S. Department of Energy, Washington, DC, DOE/EIA-0095(92).
(14)Philo, Gary R.; Keefe, Daniel, E; South, David W. and Bailey, Koby A.: Outlook for the Illinois Coal Industry, Dec. 1995, Illinois Coal Development Board, Illinois Department of Commerce and Community Affairs and Argonne National Laboratory, Table 2, page 11.

Table 1: Coal Prices at Mine and Productivity

	Mine price ($/t)	Productivity in 1995 (t/person/day)	Annual productivity change 1985-95 (%)
Illinois	23.05	3.87	5.6
Indiana	21.71	4.68	3.7
Kentucky			
East	26.00	3.47	4.6
West	20.75	3.97	3.4
Colorado	19.26	6.14	5.3
Montana	9.62	21.06	2.0
Wyoming	6.58	30.06	7.5

Source: DOE/EIA-0584(95) Coal Industry Annual 1995, Oct.1996, Table 48, Page 74 and Table 80, Page 154.

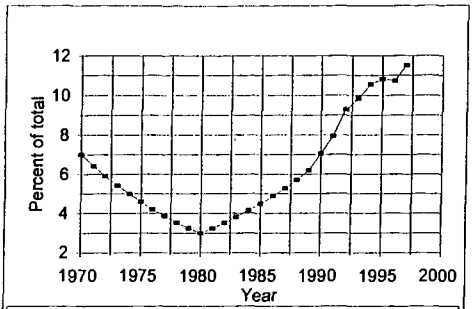

Figure 1: Share of non-utility generation of electricity in the U.S.

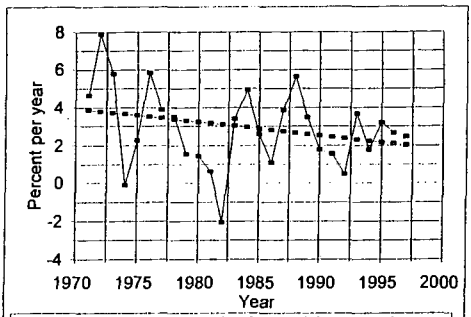

Figure 2: Growth rates in total U.S. electricity generation

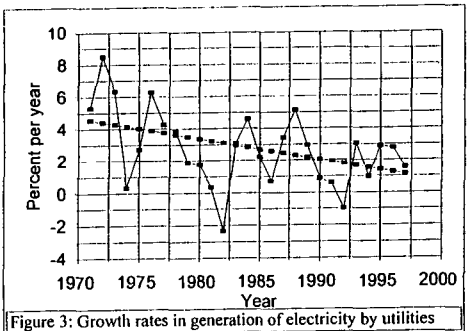

Figure 3: Growth rates in generation of electricity by utilities

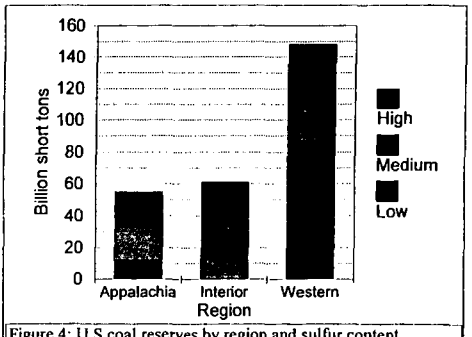

Figure 4: U.S.coal reserves by region and sulfur content

COALBED AND COAL MINE METHANE IN THE ILLINOIS BASIN: OCCURRENCE, COMPOSITION, ORIGIN, AND CURRENT ACTIVITIES

Heinz H. Damberger and Ilham Demir
Illinois State Geological Survey, 615 E. Peabody Drive, Champaign, IL 61820

Keywords: coalbed methane, coal mine gas, Illinois basin

BACKGROUND

Coalbed methane generally refers to methane and other gaseous hydrocarbons associated with coal, methane being the dominant one. Other gases, in particular carbon dioxide and nitrogen, are commonly associated with the hydrocarbons in variable proportions. The gases, which are by-products of the maturation process of coal, as it became buried and exposed to elevated temperatures during geologic time[1], are stored primarily in the form of a mono-molecular layer adsorbed to the very large internal surface area of the coal. During the early stages of coal maturation, in the sub-bituminous and high volatile bituminous coal stages, water and carbon dioxide are the main by-products, with methane gradually becoming more important. In medium volatile bituminous and higher rank coals, methane becomes the dominant by-product of coal maturation.

During mining, coalbed methane is released as coal is broken up into small particles, dramatically shortening pathways to the surface, and as ambient gas pressure is reduced to about 1 atm. Also, each cut during mining exposes new coal at the face and enhances degassing. Since mixtures of 5-15% methane in air are explosive, mining regulations have long required the dilution of methane with sufficient fresh ventilation air (generally to <1% methane content) to prevent the formation of explosive mixtures. The venting of large quantities of methane into the atmosphere during and after mining has recently become a major concern because methane is a potent greenhouse gas (each gram of methane is equivalent to the impact of 21 grams of carbon dioxide, over a 100 year period[2]). US EPA estimates that each year active coal mines in the U.S. vent about $5 \cdot 10^9$ m^3 methane into the air[2].

Efforts by the coal mining industry to recover at least a portion of this coalbed methane have resulted in the sale of about $1 \cdot 10^9$ m^3 methane by 1995[2], in states with gas-rich coals such as Alabama, Colorado, Pennsylvania, Virginia, and West Virginia. No significant recovery of coalbed methane during mining has taken place yet in the Illinois basin, primarily because of the relatively low methane concentrations in the basin's coal beds.

METHANE IN ILLINOIS BASIN COALS

Even though the methane content of coals in the Illinois basin is small in comparison to such gas-rich coal fields as the Black Warrior in Alabama, or the San Juan in New Mexico and Colorado, the total methane resources in the basin are huge ($>600 \cdot 10^9$ m^3)[3], because of the huge coal resources. Several factors cause a rather uneven distribution of coalbed methane concentration within the basin. Coal rank increases systematically from lowest rank high volatile C bituminous in the northwest part of the basin to highest rank high volatile A bituminous in the southeast[4]. Everything else being equal, coalbed methane contents in lower rank coals are much smaller than in higher rank ones. Another important factor is depth. The coalbed methane content of coal tends to increase with depth, due primarily to increasing gas pressure which increases the amount of gas adsorbed to coal. The simultaneous increase in temperatures with depth tends to work somewhat against this trend. Because regional dips of coal beds in the basin are commonly only around two meters per kilometer, large portions of the major coal seams lie at shallow depths (about half at depths <160 meters), and even in the deepest part of the basin only small parts of the major coals occur at depths in excess of 400 meters. In other coal basins, the greatest methane contents generally are associated with coals that lie at depths >700 meters[5].

Table 1 lists all published methane content results as determined by desorption tests of coal samples taken from drill holes. The average methane content of 1.9 ± 0.8 (std.dev.) cm^3/g probably understates the methane content of in-situ Illinois basin coals. Likely reasons for the underestimate (see also footnote of Table 1) are: (1) the amount of gas lost before the coal sample could be sealed in a gas-tight container to make observations on gas desorption was underestimated; (2) the gas contents were not standardized to clean coal because the petrologic composition of the coal was not determined; (3) the gas contents were not standardized to in-situ p-T conditions; (4) the sample set is biased towards coals that tend to have smaller than average methane content because of either low rank or shallow depth, or both. In the past few years several operators have been testing coals in the southern portion of the basin for coalbed methane. They claim to have found significantly greater methane contents than have been reported in the literature; however, so far their specific data have been kept confidential. Because of their relatively low rank and shallow depth, the in-situ methane content of Illinois basin coals probably is generally well below 5-6 cm^3/g; more data are needed to

properly account for the factors listed above.

Relatively little information is available on the chemical and isotopic composition of gas associated with in-situ coal in the Illinois basin. Tables 2 and 3 summarize available published and some unpublished data. The chemical data were not all reported on the same basis; for instance some probably include air trapped in the desorption canister when the coal sample was sealed in the container, as suggested by the presence of O_2 and N_2. Generally, methane represents the bulk of hydrocarbons. The amount of other gases varies significantly depending perhaps primarily on local geologic conditions and the sampling method. The few carbon isotopic analyses of methane associated with Illinois coals that have been published show δC^{13} values between -52 and -63‰, surprisingly light, certainly for thermogenic methane (Table 3). The possibility of fractionation due to migration from other sources, and also an at least partial biogenic origin must be contemplated.

COAL MINE METHANE IN ILLINOIS

It has long been known that the large voids left behind after room-and-pillar mining are an ideal place for methane to accumulate. In Illinois methane has been extracted from abandoned coal mines for many years, primarily in the southern portion of the basin, both by coal companies and by operators specializing in this technology. In recent years interest in recovering this gas has increased greatly. The amount of gas that can be extracted from abandoned mine workings is limited, though; its pressure is only about 1 atm, and the quality of the gas is variable, primarily because mine workings tend to be connected to the surface through drill holes and shafts that are not tightly sealed. When a shaft is sealed at the time of mine abandonment regulations require that vents be installed in the seal to prevent potentially dangerous buildup of gas pressure and to permit the mine to "breathe", as high and low pressure weather systems move through the area. When a high pressure system passes through, air is pushed into the mine through such vents, and any other openings, causing dilution by air of the mine gas (mostly methane). When a low pressure system follows, gas is then emitted through the vents. Coal mine methane has been used in the Illinois basin for such local applications as heating water for wash houses at mines, heating buildings and green houses, and running motors that drive electric generators, or other equipment. The chemical composition of gas samples taken from mine vents (Table 4) indicates variable admixtures of air to the usually large methane content of gas released by coal.

Active underground mines release considerable amounts of methane into the air[2]. Most is diluted in the ventilation air that is circulated through the mine to provide fresh air to the workers and to dilute any methane liberated from mined coal, from the coal left in pillars and around the perimeter of the mine, and from other coals and oil and gas pools below the mine. Values between 3,000 and 252,000 m^3 CH_4/day have been reported for mines in the Illinois basin (Table 5); the average is $50{,}000 \pm 56{,}000$ m^3 (std. dev.) CH_4/day. The specific emission values range between <1 and 35 m^3 CH_4 per metric ton of produced coal, and the average is 8 ± 7 m^3/ton Since these values are significantly above the methane content of in-situ coal, considerable amounts of methane apparently come from sources other than from the mined coal, anywhere from a few to over ninety percent, depending on the local geologic conditions.

ACKNOWLEDGEMENTS

Most the gas samples from abandoned coal mines were collected by Wayne Meents of the ISGS Oil and Gas Section between 1954 and 1982 and analyzed by chemists in the ISGS Analytical Chemistry Laboratory. Dennis Coleman was in charge of the ISGS Isotope Geochemistry Laboratory when most of the carbon isotope analyses on coalbed and coal mine methane samples were performed.

REFERENCES

1. Clayton J. L. (1998) Geochemistry of coalbed gas - A review. International Journal of Coal Geology, vol. 35, p. 159-173.
2. US EPA Atmospheric Pollution Prevention Division (1997) Identifying Opportunities for Methane Recovery at U.S. Coal Mines: Draft Profiles of Selected Gassy Underground Coal Mines. United States Environmental Protection Agency, EPA 430-R-97-020
3. Archer P. L. and Kirr J. N. (1984) Pennsylvanian geology, coal, and coalbed methane resources of the Illinois –Illinois, Indiana, and Kentucky. In Rightmire, C. T., Eddy, G.E. and Kirr, J. N., Coalbed Methane Resources of the United States. AAPG Studies in Geology #17, p.105-134.
4. Damberger, H. H. (1971) Coalification pattern of the Illinois Basin. Econ. Geol., v.66, p. 488-494.
5. Scott A. R. (1997) Exploration Strategies Based on a Coalbed Methane Producibility Model. Manual for Unconventional Gas Workshop sponsored by Petroleum Technology Transfer Council, December 5, 1997, Grayville, Illinois, 238 p.
6. Harper D. (1991) Coalbed Methane in Indiana. Indiana Geological Survey Occasional Paper 56, 18 p.

7. Popp J. T., Coleman D. D., and Keogh R. A. (1979) Investigation of the Gas Content of Coal Seams in the Vicinity of Charleston, Illinois. Illinois Institute of Natural Resources Doc. No. 79/38 and Illinois State Geological Survey Open File Series 1979-2, 36 p.
8. Meents W. F. (1981) Analyses of Natural Gas in Illinois. Illinois State Geological Survey Illinois Petroleum 122, 64 p.

Table 1. Coalbed methane content of coals in the Illinois Basin, as determined by desorption tests[6,7]

State	County	Drill hole	Analyzed or reported by	Coal seam	Depth (m)	Coal thickness (m)	Lost gas (cm^3/g)	Desorbed gas (cm^3/g)	Residual gas (cm^3/g)	Total gas (cm^3/g)
IL	Clay	n. a.	TRW	Briar Hill	328	n. a.	n. a.	n. a.	n. a.	1.00
IL	Clay	n. a.	TRW	Danville	303	n. a.	n. a.	n. a.	n. a.	1.00
IL	Clay	n. a.	TRW	Herrin	316	n. a.	n. a.	n. a.	n. a.	1.00
IL	Clay	n. a.	TRW	Seelyville	412	n. a.	n. a.	n. a.	n. a.	1.00
IL	Clay	n. a.	TRW	Springfield	332	n. a.	n. a.	n. a.	n. a.	1.00
IL	Coles	Charleston	IL Geol. Surv.	Danville	294	0.8	0.03	1.98	0.70	2.71
IL	Coles	Charleston	IL Geol. Surv.	Herrin	325	0.8	0.05	0.94	0.52	1.47
IL	Coles	Charleston	IL Geol. Surv.	Shelbyville	154	0.6	0.02	0.12	0.09	0.25
IL	Coles	Charleston	IL Geol. Surv.	Springfield	333	0.4	0.00	0.33	1.10	1.43
IL	Coles	Charleston	IL Geol. Surv.	Springfield	333	1.0	0.05	1.36	0.83	2.22
IL	Franklin	n. a.	USSteel	Herrin	183	n. a.	n. a.	n. a.	n. a.	1.95
IL	Franklin	n. a.	USSteel	Springfield	204	n. a.	n. a.	n. a.	n. a.	1.67
IL	Jefferson	n. a.	USBM	Herrin	223	n. a.	n. a.	n. a.	n. a.	1.90
IL	Jefferson	n. a.	USBM	Springfield	242	n. a.	n. a.	n. a.	n. a.	1.00
IL	Peoria	n. a.	Northern IL Gas	Colchester	40	n. a.	n. a.	n. a.	n. a.	1.02
IL	Wayne	n. a.	USBM	Herrin	275	n. a.	n. a.	n. a.	n. a.	1.90
IL	Wayne	n. a.	USBM	Herrin	296	n. a.	n. a.	n. a.	n. a.	3.40
IL	Wayne	n. a.	USBM	Springfield	308	n. a.	n. a.	n. a.	n. a.	3.10
IL	Wayne	n. a.	USBM	Springfield	326	n. a.	n. a.	n. a.	n. a.	2.70
IN	Gibson	BP 64	IN Geol. Surv.	Springfield	182	1.9	0.09	2.28	0.16	2.53
IN	Gibson	BP 59	IN Geol. Surv.	Springfield	191	1.9	0.05	2.00	0.31	2.38
IN	Knox	SDH 267	IN Geol. Surv.	Bucktown	159	0.6	0.13	1.72	n.a.	1.84[1]
IN	Knox	SDH 266	IN Geol. Surv.	Coal in Staunton Fm.	230	1.1	0.00	0.22	n.a.	0.22[1]
IN	Knox	SDH 259	IN Geol. Surv.	Danville	103	1.1	0.09	1.59	n.a.	1.69[1]
IN	Knox	SDH 267	IN Geol. Surv.	Danville	126	1.1	0.13	2.06	n.a.	2.19[1]
IN	Knox	SDH 285	IN Geol. Surv.	Danville	156	1.1	0.06	1.88	n.a.	1.94[1]
IN	Knox	SDH 259	IN Geol. Surv.	Hymera	110	0.5	0.16	2.88	n.a.	3.03[1]
IN	Knox	SDH 267	IN Geol. Surv.	Hymera	134	1.6	0.16	2.00	n.a.	2.16[1]
IN	Knox	SDH 266	IN Geol. Surv.	Seelyville	200	1.1	0.03	0.38	n.a.	0.41[1]
IN	Knox	SDH 267	IN Geol. Surv.	Seelyville	233	0.9	0.06	1.16	n.a.	1.22[1]
IN	Knox	SDH 267	IN Geol. Surv.	Springfield	163	1.1	0.16	2.34	n.a.	2.50[1]
IN	Knox	SDH 267	IN Geol. Surv.	Survant	211	0.8	0.25	2.56	n.a.	2.81[1]
IN	Posey	SDH 300	IN Geol. Surv.	Coal in Dugger Fm.	73	0.8	0.00	1.78	0.31	2.09
IN	Posey	SDH 300	IN Geol. Surv.	Danville	44	0.9	0.00	0.72	0.19	0.91
IN	Posey	SDH 301	IN Geol. Surv.	Danville	142	0.7	0.03	1.00	0.09	1.13
IN	Posey	SDH 343	IN Geol. Surv.	Danville	143	0.9	0.00	1.38	0.13	1.50
IN	Posey	SDH 302	IN Geol. Surv.	Danville	154	0.9	0.06	1.91	0.19	2.16[1]
IN	Posey	SDH 343	IN Geol. Surv.	Herrin	155	0.9	0.06	1.16	0.00	1.19
IN	Posey	SDH 301	IN Geol. Surv.	Herrin	158	1.1	0.00	0.03	0.50	0.53[1]
IN	Posey	SDH 302	IN Geol. Surv.	Herrin	171	1.5	0.06	2.41	0.19	2.66
IN	Posey	SDH 285	IN Geol. Surv.	Herrin	176	1.4	0.13	1.63	0.00	1.75[1]
IN	Posey	SDH 301	IN Geol. Surv.	Houchin Creek	222	0.5	0.03	1.38	0.41	1.81
IN	Posey	SDH 302	IN Geol. Surv.	Houchin Creek	235	0.7	0.03	1.75	0.50	2.28
IN	Posey	SDH 300	IN Geol. Surv.	Hymera	54	1.0	0.00	1.09	0.19	1.28
IN	Posey	SDH 300	IN Geol. Surv.	Seelyville	131	1.0	0.00	2.19	0.31	2.50
IN	Posey	SDH 301	IN Geol. Surv.	Seelyville	268	0.5	0.00	0.31	0.50	0.81[1]
IN	Posey	SDH 301	IN Geol. Surv.	Seelyville	272	1.5	0.13	2.13	0.41	2.66
IN	Posey	SDH 302	IN Geol. Surv.	Seelyville	284	3.5	0.09	2.69	0.50	3.28
IN	Posey	SDH 302	IN Geol. Surv.	Seelyville	285	3.5	0.16	3.38	0.91	4.44
IN	Posey	SDH 285	IN Geol. Surv.	Seelyville	287	1.8	0.13	1.22	n.a.	1.34[1]
IN	Posey	SDH 300	IN Geol. Surv.	Springfield	80	1.5	0.00	2.09	0.31	2.41
IN	Posey	SDH 301	IN Geol. Surv.	Springfield	188	1.1	0.06	0.31	0.41	0.78[1]
IN	Posey	SDH 285	IN Geol. Surv.	Springfield	202	1.2	0.16	2.53	n.a.	2.69[1]
IN	Posey	SDH 302	IN Geol. Surv.	Springfield	203	1.2	0.00	1.06	0.31	1.38[1]
IN	Posey	SDH 303	IN Geol. Surv.	Springfield	203	1.3	0.13	2.09	0.41	2.63
IN	Posey	SDH 303	IN Geol. Surv.	Springfield	204	1.3	0.16	2.00	0.19	2.38
IN	Posey	SDH 343	IN Geol. Surv.	Survant	184	1.1	0.06	1.75	0.50	2.31
IN	Posey	SDH 301	IN Geol. Surv.	Survant	240	0.4	0.06	1.44	0.50	2.00[1]
IN	Posey	SDH 302	IN Geol. Surv.	Survant	252	0.8	0.09	2.72	0.41	3.22[1]
IN	Sullivan	SDH 344	IN Geol. Surv.	Houchin Creek	177	0.7	0.06	1.44	0.13	1.63
IN	Sullivan	SDH 344	IN Geol. Surv.	Seelyville	227	1.2	0.03	2.31	0.25	2.59
IN	Sullivan	SDH 344	IN Geol. Surv.	Seelyville	230	1.1	0.03	2.06	0.34	2.44
IN	Sullivan	SDH 266	IN Geol. Surv.	Springfield	128	1.1	0.06	2.69	n.a.	2.75[1]
IN	Sullivan	SDH 344	IN Geol. Surv.	Survant	189	0.5	0.13	1.03	0.44	1.59

[1] Value may be low because of leakage from canister, and/or because measurement of lost gas or residual gas were not made.
n. a. = not available or not analyzed.

Table 2. Chemical composition of gas associated with in-situ coal in the Illinois Basin (Popp et al.[7] and ISGS database). Illinois samples are from Charleston drill hole and Indiana samples are from SDH302 drill hole.

State	County	Coal seam	Depth (m)	Thick-ness (m)	Typeof gas	%CO_2	%O_2	%N_2	%CH_4	%C_2H_6	%C_3H_8	%C_4H_{10}	Btu/ft^3 (gross)
IL	Coles	Shelbyville	154	0.58	Released gas	17.0	-	25.0	54.0	3.0	1.0	0.0	930
IL	Coles	Danville	294	0.79	Released gas	1.9	-	15.1	80.2	2.2	0.5	0.1	867
IL	Coles	Danville	294	0.79	Residual gas	3.1	-	13.9	73.5	6.6	2.5	0.4	940
IL	Coles	Danville	294	0.79	Total gas	2.2	-	14.8	78.5	3.3	1.0	0.2	886
IL	Coles	Herrin	325	0.76	Released gas	3.7	-	0.0	88.9	4.6	2.4	0.4	1061
IL	Coles	Herrin	325	0.76	Residual gas	5.5	-	16.6	48.8	15.9	11.1	2.1	1440
IL	Coles	Herrin	325	0.76	Total gas	4.5	-	7.7	70.4	9.8	6.4	1.2	1240
IL	Coles	U.Springfield	333	0.37	Released gas	6.1	-	35.7	53.9	2.6	1.3	0.4	640
IL	Coles	U.Springfield	333	0.37	Residual gas	3.2	-	15.3	66.3	8.9	5.4	0.9	1001
IL	Coles	U.Springfield	333	0.37	Total gas	3.9	-	20.0	63.4	7.4	4.5	0.8	918
IL	Coles	L.Springfield	333	0.98	Released gas	1.4	-	21.1	70.4	4.5	2.2	0.4	862
IL	Coles	L.Springfield	333	0.98	Residual gas	2.5	-	16.2	63.2	10.7	6.1	1.3	1032
IL	Coles	L.Springfield	333	0.98	Total gas	1.8	-	19.3	67.8	6.8	3.6	0.7	926
IN	Posey	Seelyville	284	3.51	Released gas	1.3	3.7	37.0	58.0	0.02	2ppm	0.0	527
IN	Posey	Seelyville	284	3.51	Released gas	1.1	1.7	33.0	65.0	0.02	2ppm	0.0	588

Table 3. *Carbon isotopic composition of coalbed methane in some Illinois coals* (Popp et al[7] and ISGS database) and of coal mine methane from abandoned coal mines in Illinois (ISGS data base)

Lab No.	County	Drill hole or Coal Co.	Mine name and Mine Index #	Coal seam	Depth (m)	Coal thick-ness (m)	Type of gas	Number of samples analyzed	δC^{13} CH_4 (‰)
-	Coles	Charleston drill hole	-	Danville	294	0.8	released	9	-62.9 to -61.4
-	Coles	Charleston drill hole	-	Danville	294	0.8	residual	1	-59.8
-	Coles	Charleston drill hole	-	Herrin	325	0.8	released	4	-57.4 to -56.1
-	Coles	Charleston drill hole	-	Herrin	325	0.8	residual	1	-52.1
-	Coles	Charleston drill hole	-	U.Springfield	333	0.4	released	3	-57.1 to -56.5
-	Coles	Charleston drill hole	-	U.Springfield	333	0.4	residual	1	-55.4
-	Coles	Charleston drill hole	-	L.Springfield	333	1.0	released	7	-57.3 to -56.6
-	Coles	Charleston drill hole	-	L.Springfield	333	1.0	residual	1	-54.5
3549	Christian	Joe Simkins #1 Kincaid	Peabody # 7 Mine MI# 2040	Herrin	106		mine gas	1	-67.7
3540	Clinton	Pessina #1 Kampwerth	Breese-Trenton Buxton Mine 3, MI# 85	Herrin	132	2.4	mine gas	1	-65.1
3801	Gallatin	Peabody CC	Eagle Mine #2, MI# 898	Springfield	76	1.7	seapage at fault	1	-61.6
3888	Montgomery	Gerald Stieren	Crown Mine #1, MI# 707	Herrin	108	2.1	mine gas	1	-69.1
3933	Montgomery	Gerald Stieren	Crown Mine #1, MI# 707	Herrin	108	2.1	mine gas	1	-69.4
3583	Montgomery	Freeman United MC	Crown Mine #1, MI# 707	Herrin	108	2.1	mine gas	1	-69.6
3578	Saline	Albert Farris	Dering Mine #2, MI# 125	Springfield	139	1.8	mine gas	1	-62.7
3831	Saline	Albert Farris	Dering Mine #2, MI# 125	Springfield	139	1.8	mine gas	1	-60.0
3835	Saline	Albert Farris	Dering Mine #2, MI# 125	Springfield	139	1.8	mine gas	1	-62.2
3594	Saline	Wasson Mine shaft	Wasson Mine #1, MI# 45	Springfield	99	1.6	mine gas	1	-62.3
3923	Saline	M. L. Devillez #3	Wasson Mine #1, MI# 45	Springfield	110	1.6	mine gas	1	-62.2
3216	Saline	Cahaba #1 Willis	Peabody Eldorado Mine #20, MI# 46	Springfield	127	1.8	mine gas	1	-60.7
3791	Saline	Cahaba #1 Willis	Peabody Eldorado Mine #20, MI# 46	Springfield	127	1.8	mine gas	1	-61.6
3796	Saline	Cahaba #1 Willis	Peabody Eldorado Mine #20, MI# 46	Springfield	127	1.8	mine gas	1	-61.8
3797	Saline	Cahaba #1 Willis	Peabody Eldorado Mine #20, MI# 46	Springfield	127	1.8	mine gas	1	-61.8
3832	Saline	Cahaba #1 Willis	Peabody Eldorado Mine #20, MI# 46	Springfield	127	1.8	mine gas	1	-61.5
3311	Saline	Phillip Barrett, Schlafly #1 Morris	Dering Mine #2, MI# 125	Springfield	139	1.8	mine gas	1	-63.6
3215	Saline	Jade Oil & Gas	Dering Mine #2, MI# 125	Springfield	139	1.8	mine gas	1	62.2
3830	Saline	Dan January	O'Gara 10 Mine, MI# 799	Springfield	121	1.7	mine gas	1	-61.9
3614	Saline	Wilson, Sutton #1P	O'Gara 8 Mine, MI# 800	Springfield	123	1.7	mine gas	1	-60.9
3750	Saline	Wilson, Sutton #1P	O'Gara 8 Mine, MI# 800	Springfield	123	1.4	mine gas	1	-61.5
3834	Saline	Wilson, Sutton #1P	O'Gara 8 Mine, MI# 800	Springfield	123	1.4	mine gas	1	-60.5

Table 4. Chemical composition of gas collected from abandoned coal mines (Meents[8] and ISGS database)

Lab No.	State	County	Mine/drill hole	%CO_2	%O_2	%N_2	%CH_4	%C_2H_6	C_3H_8	Btu/ft^3
3539	IL	Christian	Joe Simkins #1	16.3	1.1	63.1	19.0	0.45	0.09	202
3549	IL	Christian	Joe Simkins #1	22.0	1.0	58.7	11.8	0.40	0.10	189
2213	IL	Clinton	8reese-Trenton	11.8	0.4	27.1	60.3	0.20	0.10	620
3540	IL	Clinton	Pessina #1	10.2	0.3	20.7	68.8	0.00	0.00	696
2372	IL	Franklin	Zeigler	5.9	0.6	28.8	64.7	tr	0.00	655
3742	IL	Franklin	Peabody #18	0.1	14.7	60.0	25.2	0.02	0.00	255
3694	IL	Gallatin	8 & W Coal	0.1	20.7	79.2	0.0	0.00	0.00	0
3887	IL	Montgomery	Gerald Stieren	4.4	0.5	30.8	64.0	0.22	0.02	652
3888	IL	Montgomery	Gerald Stieren	5.0	0.4	30.0	64.3	0.22	0.01	655
3933	IL	Montgomery	Gerald Stieren	3.4	1.2	32.3	62.9	0.16	0.00	639
3583	IL	Montgomery	Freeman United	5.9	0.8	47.5	45.4	0.39	0.02	467
3689	IL	Perry	Frank Hepp	19.0	0.8	56.8	23.4	0.00	0.00	236
3817	IL	Randolph	Moffat Coal #2	3.3	11.6	85.1	0.0	0.00	0.00	0
2371	IL	St. Clair	Peabody Coal test	0.3	tr	10.5	89.2	0.00	0.00	903
1409	IL	Saline	A. Farris, Dering Mine	6.7	1.0	14.4	77.9	0.00	0.00	788
1774	IL	Saline	A. Farris, Dering Mine	6.8	0.8	9.0	83.4	0.00	0.00	845
1918	IL	Saline	A. Farris, Dering Mine	6.6	0.2	4.9	88.3	0.00	0.00	894
1488	IL	Saline	Charter Oil #1A	0.0	0.6	12.8	75.9	9.50	0.00	960
2803	IL	Saline	A. Farris, Dering Mine	4.0	0.5	5.2	90.3	0.00	0.00	914
3577	IL	Saline	A. Farris, Dering Mine	5.0	0.3	3.7	91.1	0.00	0.00	921
3578	IL	Saline	A. Farris, Dering Mine	5.5	0.1	3.4	90.9	0.00	0.00	920
3831	IL	Saline	A. Farris, Dering Mine	5.6	0.2	2.5	91.7	0.02	0.00	928
3835	IL	Saline	A. Farris, Dering Mine	5.8	0.2	3.5	90.6	0.02	0.00	916
1408	IL	Saline	Wasson Mine shaft	7.2	0.3	48.9	43.6	0.00	0.00	441
1446	IL	Saline	Wasson Mine shaft	7.0	0.1	45.9	45.5	1.40	0.00	486
1910	IL	Saline	Wasson Mine shaft	6.2	0.6	40.7	51.0	1.50	0.00	543
3594	IL	Saline	Wasson Mine shaft	9.4	0.5	17.3	72.7	0.00	0.00	736
3923	IL	Saline	Devillez	3.3	4.1	50.8	41.8	0.01	0.00	423
3312	IL	Saline	Phillip 8arret	2.7	tr	4.1	93.2	0.00	0.00	943
951	IL	Saline	W Duncan #1	5.7	0.3	7.3	85.7	0.00	0.00	870
1507	IL	Saline	Adams Unit Mine	6.2	0.2	2.2	90.2	0.00	0.00	917
1879	IL	Saline	Adams Unit Mine	5.1	0.6	4.6	89.7	0.00	0.00	908
2802	IL	Saline	Cahaba #1/Adams	6.6	1.9	9.2	82.3	0.00	0.00	833
3216	IL	Saline	Adams, Cahaba M.	5.9	0.1	2.7	91.3	0.00	0.00	924
3791	IL	Saline	Cahaba #1 Willis	6.3	0.7	4.3	88.7	0.00	0.00	897
3796	IL	Saline	Cahaba #1 Willis	6.2	0.2/	2.9	90.6	0.07	0.00	917
3797	IL	Saline	Cahaba #1 Willis	6.3	0.2	2.8	90.7	0.06	0.00	918
3832	IL	Saline	Adams Mine	5.9	0.1	2.9	91.1	0.05	0.00	921
3833	IL	Saline	Adams Mine	6.3	0.1	2.8	90.8	0.02	0.00	919
3133	IL	Saline	Phillip 8arret	3.3	0.4	4.1	92.2	0.00	0.00	933
3311	IL	Saline	Phillip 8arret	5.9	tr	2.6	91.5	0.00	0.00	926
1559	IL	Saline	Jade Oil, Dering Mine	7.7	1.4	5.3	84.3	0.30	0.00	862
1944	IL	Saline	Jade Oil, Dering Mine	6.7	0.2	5.7	87.4	0.00	0.00	884
3215	IL	Saline	Jade Oil, Dering Mine	6.2	1.5	8.9	83.4	tr	0.00	844
1656	IL	Saline	Sahara #10 Mine	3.9	14.2	71.7	10.2	0.00	0.00	103
1924	IL	Saline	Sahara #10 Mine	8.7	3.5	64.8	23.0	0.00	0.00	233
3830	IL	Saline	Dan January	3.1	0.7	9.8	86.3	0.02	0.00	874
3770	IL	Saline	Ogara #8 Mine	8.0	4.0	22.2	65.8	0.00	0.00	666
3774	IL	Saline	Ogara #8 Mine	10.1	0.7	11.5	77.7	0.00	0.00	785
3613	IL	Saline	John Wilson	6.7	0.1	3.3	89.9	0.00	0.00	909
3614	IL	Saline	John Wilson	7.6	0.0	2.1	90.3	0.00	0.00	913
3750	IL	Saline	John Wilson #1P Sutton	6.1	0.2	3.1	90.6	0.00	0.00	917
3782	IL	Saline	John Wilson #1P	6.4	0.0	2.9	90.6	0.00	0.00	917
3834	IL	Saline	Wilson #1P Sutton	5.9	0.1	2.7	91.3	0.04	0.00	924
1518	IL	Saline	Frank Genet, Mine	8.6	0.8	0.0	90.1	0.00	0.00	913
1973	IL	Saline	Frank Genet, Mine	9.1	0.1	2.1	88.7	0.00	0.00	898
1608	IL	Saline	Sahara #1 Mine	1.4	14.6	79.4	3.8	0.00	0.00	41
1909	IL	Saline	Sahara #1 Mine	7.0	3.7	72.7	16.6	0.00	0.00	168
3091	IL	Vermilion	Bunsenville Mine	6.5	14.4	79.1	0.0	0.00	0.00	0
3134	IN	Sullivan	Old coal test hole	0.6	0.1	7.0	92.3	tr	0.00	934

Table 5. Amount of methane liberated by some coal mines in the Illinois basin (US EPA[2])

State	County	Mine	Years averaged	Coal seam	Coal thickness (m)	Mine depth (m)	Total annual emissions, average ± s.d. (thousand m^3/d)	Annual coal production, average ± s.d. (million tons)	Specific emissions, average ± s.d. (m^3/ton)
IL	Clinton	Monterey #2	1993/96	Herrin	2.3	101	10 ± 3.7	2.0 ± 0.9	2.0 ± 0.7
IL	Franklin	Old 8en 24	1993/96	Herrin	2.1	198	35 ± 6	1.3 ± 0.8	14.0 ± 9.5
IL	Franklin	Old 8en 25	1993/94	Herrin	2.1	183	34 ± 8	1.4 ± 0.1	8.8 ± 1.5
IL	Franklin	Old 8en 26	1993/96	Herrin	2.6	198	52 ± 7	2.4 ± 0.7	8.6 ± 3.8
IL	Jefferson	Orient 6	1993/96	Herrin	1.8	244	21 ± 2	1.2 ± 0.1	6.6 ± 0.8
IL	Jefferson	Rend Lake	1993/96	Herrin	2.4	183	48 ± 16	2.4 ± 0.8	7.6 ± 1.9
IL	Logan	Elkhart	1993/96	Springfield	1.7	85	11 ± 2	1.6 ± 0.2	2.7 ± 0.7
IL	Macoupin	Crown II	1993/96	Herrin	2.4	101	17 ± 2.3	1.5 ± 0.1	3.1 ± 2.1
IL	Macoupin	Monterey #1	1993/96	Herrin	2.0	91	20 ± 5	1.9 ± 0.3	3.9 ± 1.1
IL	Saline	8rushy Creek	1993/96	Herrin	1.8	76	21 ± 6	0.8 ± 0.4	10.4 ± 4.2
IL	Saline	Galatia	1993/96	Springfield	2.1	213	206 ± 56	4.6 ± 1.1	16.5 ± 3.5
IL	Wabash	Wabash	1993/96	Springfield	2.1	183	127 ± 34	2.7 ± 0.3	17.9 ± 6.7
IL	White	Pattiki	1993/96	Herrin	1.7	307	46 ± 12	1.7 ± 0.1	9.9 ± 3.1
IN	Sullivan	8uck Creek	1993/55	Springfield	1.5	91	12 ± 2	0.5 ± 0.2	10.7 ± 4.7
KY	Union	Camp No. 11	1993/96	Springfield	1.6	418	22 ± 5	2.1 ± 0.6	3.9 ± 0.6
KY	Webster	8aker	1993/96	Baker (KY 13)	2.0	274	35 ± 15	3.6 ± 1.3	3.5 ± 0.3
KY	Webster	Dotiki	1993/96	Springfield	1.8	152	18 ± 1	2.4 ± 0.4	2.6 ± 0.2
KY	Webster	Wheatcroft 9	1993/96	Springfield	2.0	274	72 ± 46	1.7 ± 1.5	15.0 ± 15

WYOMING FOSSIL FUELS FOR THE 21ST CENTURY

Robert M. Lyman and Rodney H. De Bruin
Wyoming State Geological Survey
P.O. Box 3008
Laramie, WY 82071

KEYWORDS: Oil, Natural Gas, and Coal.

ABSTRACT

Wyoming's petroleum industry produced 1.2 trillion cubic feet of natural gas and 63.2 million barrels of oil in 1998. Over the last 10 years Wyoming's proved reserves of natural gas have risen from 10.3 to 13.6 trillion cubic feet despite production of 10.1 trillion cubic feet over the same period. Production of natural gas, including coalbed methane, is projected to reach 1.4 trillion cubic feet by 2005. Additionally, Production of natural gas liquids is projected to reach 40 million barrels and production of crude oil will be about 42 million barrels in 2005.

The Wyoming coal industry produced over 300 million short tons of coal in 1998, and production is projected to reach 365 million short tons per year by 2005. Today, 97% of Wyoming coal is used to feed coal-fired power plants in 29 states, Canada, and Spain. Future constraints on Wyoming coals, such as environmental-political policy changes and transportation availability, will provide more opportunities for coal-derived liquid fuels (LFC) and solid fuels from coal (SFC) processes.

INTRODUCTION

Wyoming is well positioned to supply fossil fuels for the United States' energy needs into the 21st century. By the year 2005, Wyoming's coal production should reach 365 million short tons (mt) (Figure 1), natural gas production should almost reach 1.4 trillion cubic feet (tcf)(Figure 2), natural gas liquids production should reach 40.0 million barrels (mmbbl) (Figure 3), and crude oil production will decline to about 42.0 mmbbl (Figure 4). For comparison, Wyoming's coal production in 1998 was 300 Mt, natural gas production was 1.2 tcf, natural gas liquids production was 36.0 mmbbl, and crude oil production was 63.2 mmbbl. Among all of the states, Wyoming is first in reserves of coal, third in reserves of natural gas, fifth in reserves of natural gas liquids, and sixth in reserves of crude oil (Table 1).

OIL, NATURAL GAS, AND NATURAL GAS LIQUIDS

The first commercial oil well in Wyoming was completed in 1884 near an oil seep. Over 1,600 oil and gas fields have been discovered in Wyoming since that time, and those fields have produced 6.5 billion bbl of oil, 23.6 tcf of gas, and over 500 mmbbl of natural gas liquids.

In Wyoming, oil and gas are produced from reservoirs of Tertiary, Cretaceous, Jurassic, Triassic, Permian, Pennsylvanian, Mississippian, Devonian, Ordovician, and Cambrian age. Commercial oil and gas production comes from every major basin and the Overthrust Belt of western Wyoming (De Bruin, 1996).

Over 75 % of Wyoming's present oil production comes from the Powder River, Bighorn, and Wind River basins (Figure 5) and is concentrated in reservoirs that are Cretaceous, Jurassic, Permian, and Pennsylvanian in age (De Bruin, 1993). The main oil reservoirs are the Cretaceous Shannon Sandstone, Sussex Sandstone, Frontier Formation, Muddy Sandstone, and Dakota Sandstone; the Jurassic/Triassic Nugget Sandstone; the Permian Phosphoria Formation; the Permian and Pennsylvanian Minnelusa Formation; and the Pennsylvanian Tensleep Sandstone (De Bruin, 1996).

Over 85 % of Wyoming's present natural gas liquids and natural gas production comes from the Overthrust Belt, Green River Basin, Great Divide Basin, and Washakie Basin (Figure 5), and is concentrated in reservoirs that are Tertiary, Cretaceous, Jurassic, and Mississippian in age (De Bruin, 1993). The main natural gas liquids and natural gas reservoirs are the Tertiary Fort Union Formation; the Cretaceous Lance Formation, Frontier Formation, Almond Formation, Muddy Sandstone, and Dakota Sandstone; the Jurassic/Triassic Nugget Sandstone; and the Mississippian Madison Limestone (De Bruin, 1996).

Wyoming's proved reserves of crude oil declined from 0.928 billion bbl in 1980 to 0.627 billion bbl in 1997. Production of crude oil during that period was 1.6 billion bbl. Proved reserves of natural gas increased from 9.100 tcf in 1980 to 13.562 tcf in 1997 despite production of 15.1 tcf over the

same period. Proved reserves of natural gas liquids increased from 0.239 billion bbl in 1980 to 0.600 billion bbl in 1997, but fluctuated more than proved reserves of crude oil or natural gas (Table 2). Production of natural gas liquids since 1980 was 431 million barrels.

Wyoming has remaining discovered and undiscovered resources of approximately 5.7 billion barrels of oil, 4.5 billion barrels of natural gas liquids, and 176.3 trillion cubic feet of natural gas (U.S. Geological Survey National Oil and Gas Resource Team, 1995). These resources are technically recoverable, but not all are economically recoverable at the present time. The oil, natural gas liquids, and natural gas resources include proved reserves, reserve growth in conventional fields, undiscovered conventional resources, and continuous-type accumulations in sandstones, shales, chalks, and coal beds. Among the states, Wyoming has 5.1 % of the remaining oil, 15.4 % of the remaining natural gas liquids, and 16.4 % of the remaining natural gas. Almost 60 % of the oil resources are located or will be discovered in the Powder River Basin. Most of the rest of the oil is located or will be found in the Bighorn and Wind River basins (Figure 5). About 96 % of Wyoming's natural gas liquids and natural gas resources are located in or will be discovered in the Overthrust Belt, the Green River Basin, the Great Divide Basin, and the Washakie Basin (Figure 5).

COAL

Wyoming's recorded coal production started in the 1860s, but until the 1970 Clean Air Act (CAA), the state's coal production remained stagnant at under 5-million short ton/year (mty). In 1969 the total production of Wyoming's coal mines was only 4.606 mt. The 1970 CAA limit on SO_2 emissions stimulated an explosion of mine development in Wyoming's Powder River Coal Field, starting in 1972 when the state's coal miners broke the 10 mty barrier. Today Wyoming mines have crossed the 300 mty milestone and are projected to reach the 365 mty mark by 2005 (Figure 1).

In 1997, 92.3% or 259.8 mt of coal produced in Wyoming came from the Wyodak coal zone (Paleocene Fort Union Formation) in the eastern Powder River Coal Field. While the mined portions of the zone consist of one to three beds of coal with an aggregate thickness between 50 and 110 feet (ft), the thickest expression is 200 ft. The delivered coal from this zone averages 0.33% sulfur, 5.12% ash, and 8,590 Btu/lb. (Glass, and Lyman, 1998).

In the Powder River Basin, coal beds occur in rock sequences deposited during either the Late Cretaceous Epoch (81 to 66.4 million years ago) or during the Paleocene or Eocene Epochs (66.4 to 36.6-million years ago) of the younger Tertiary Period. These Wyoming coals are young when compared to the 266-320 million-year-old coals that occur in the Pennsylvanian Period in the midcontinent and eastern coalfields of the U.S.

The Cretaceous peat deposits (precursors to the coal) were most often located in deltaic, coastal plain, or other nearshore settings along a Cretaceous epeiric seaway. The Tertiary coals accumulated as fresh-water peats at a time when crustal downwarping formed the basin and regional uplift caused the epeiric seaway to withdraw from the Powder River Basin area of Wyoming. Tertiary peat swamps were associated with fluvial and fluvio-lacustrine depositional systems rather than with any marine influences (Glass, 1977; Moore and Shearer, 1993).

Due to the contrasting tectonic and sedimentary settings under which Cretaceous and Tertiary coal beds formed, the Cretaceous coals are generally more laterally extensive, thinner, and higher in sulfur (> 1%) than the Tertiary coals (Glass, 1977; Moore and Shearer, 1993). These latter two differences partially explain why the Cretaceous coals are not currently mined in the Powder River Coal Field.

The remaining demonstrated strippable reserve base of the Wyodak coal bed is the largest for any single coal bed in Wyoming and perhaps for any coal bed in the U.S. This remaining reserve base is an estimated 16.5 billion short tons (bt), of which 12.7 bt is compliant coal (modified from Jones and Glass, 1992). For comparison, the strippable reserve base for the Wyodak coal bed is almost 74% of the remaining strippable reserve base in the Powder River Coal Field and 65% of the remaining strippable reserve base for Wyoming. Production and mining losses from the Wyodak coal zone through 1997 have totaled more than 3.1 bt and most of that production has occurred since 1972. Production from this coal bed was 259.8 mt in 1997.

Wyoming's remaining discovered and undiscovered resources of coal are an estimated 1,458 bt. Wood and Bour (1988) estimated that Wyoming's Powder River Coal Field contained 1.03 trillion short tons of original in-place coal resources. Of this resource, the remaining demonstrated strippable reserve base in the coalfield is an estimated 22.3 bt (modified from Jones and Glass, 1992). Of that, an estimated 13.2 bt is compliant coal, i.e., containing 0.6 or less pounds of sulfur

per million Btu. The estimate of the remaining strippable reserve base in the Powder River Basin is very conservative because it is based on an overburden cut-off of only 200-ft. The remaining strippable reserve base is likely more than double the current estimate.

LIQUIDS FROM COAL AND SOLID FUELS FROM COAL

Into the 21st century, two currently developed processes will aid in the economic utilization of Wyoming's coal resources. KFx's process to form upgraded coal (K-Fuel) from Powder River Basin coals involves a decarboxylation process. The resultant fuel is a clean, stable fuel that is essentially anhydrous. The K-Fuel has upward of 40% more heating value per pound than its feedstock coal. The LFC process, being introduced by ENCOAL, is a process which produces hotter and cleaner burning coal, oil, and gas, from low grade coal feedstock (mine waste coal). The process causes thermal fraction of coal by mild pyrolysis, and uses a controlled temperature regimen adjusted to the feed coal's properties. Reduced ash, 1/3 less NO_x and 1/2 the SO_2 emissions will help these sorts of emerging technologies come of age.

COALBED METHANE

Production of coalbed methane, derived from the Wyodak coal zone, is currently occurring just west and downdip from the coal mines on the outcrop and is increasing each year. Coalbed methane was first recognized and used in the Powder River Basin in 1916, when a rancher began using gas coming out of his water well. That well, located on a ranch near the Montana state line, apparently produced desorbed coalbed methane from a sandstone reservoir (Olive, 1957).

The first commercial venture in Wyoming that produced methane directly from a coal bed was development of the Rawhide Butte field. The wells were completed in the Wyodak coal at a depth of 400 to 500 ft. The coal bed is up to 140 ft. thick (Jones and DeBruin, 1990). The discovery of this field was directly related to surface seepage of methane gas into a housing development. Rawhide Village subdivision, located about nine miles north of Gillette and only a few miles from the Rawhide coal mine, was evacuated when methane was discovered in residents' backyards and basements as well as in the streets (Jones and others, 1987; Jones and Taucher, 1989).

In 1998, production of coalbed methane from the Wyodak coal zone in the Powder River Basin was about 56.2 million cubic feet per day or 20.5 billion cubic feet for the year (Figure 6). Production could more than triple by 2005, when the number of online wells will increase and additional pipeline capacity will be available. In regard to reserves, it is conservatively estimated that the Powder River Basin of Wyoming and Montana contains 30 tcf of recoverable coalbed methane (Ayers and Kelso, 1989).

REFERENCES CITED

Ayers, W.B., Jr., and Kelso, B.S., 1989, Knowledge of methane potential for coalbed resources grows, but needs more study: Oil and Gas Journal, v. 87, no. 43, p. 64-67.

De Bruin, R.H., 1996, Oil and gas map of Wyoming: Wyoming State Geological Survey Map Series 48, scale 1:500,000.

De Bruin, R.H., 1993, Overview of oil and gas geology of Wyoming, *in* Snoke, A.W., Steidtmann, J. R., and Roberts, S. M., editors, Geology of Wyoming: Geological Survey of Wyoming Memoir No. 5,v.2, p.#836-873.

Glass, G.B., 1977, Wyoming coal deposits *in* Geology of Rocky Mountain coal, a symposium: Colorado Geological Survey Resource Series 1, p. 73-84.

Glass, G. B., and Lyman, R.M., 1998, Geology of Wyoming's Powder River Basin coalfield: Mining Engineering, v. 50, no. 7, p. 33-39.

Jones, R.W., and De Bruin, R.H., 1990, Coalbed methane in Wyoming: Geological Survey of Wyoming Public Information Circular 30, 15 p.

Jones, R.W., De Bruin, R.H., and Glass, G.B., 1987, Investigation of venting methane and hydrogen sulfide gas at Rawhide Village, Campbell County, Wyoming, *in* Rawhide II Project Report, Appendix I. Geology: Wyoming Department of Environmental Quality, Cheyenne, Wyoming (unpublished), 23 p., 12 plates.

Jones, R.W., and Glass, G.B., 1992, Demonstrated reserve base of coal in Wyoming as of January 1, 1991: Geological Survey of Wyoming Open File Report 92-4, 26 p.

Jones, R.W., and Taucher, P.J., 1989, Coal geology, geophysical logs, and lithologic descriptions from a drilling program at the Rawhide Village subdivision, Campbell County, Wyoming: Geological Survey of Wyoming Open File Report 89-2, 59 p.

Moore, T.A., and Shearer, J.C., 1993, Processes and possible analogues in the formation of Wyoming's coal deposits: Geological Survey of Wyoming Memoir 5, v. 2, p. 874-896.

Olive, W.W., 1957, The Spotted Horse coalfield, Sheridan and Campbell Counties, Wyoming: U.S. Geological Survey Bulletin 1050, 89 p.

U. S. Department of Energy, 1998, U.S. crude oil, natural gas, and natural gas liquids reserves: Advance Summary, 1997 Annual Report: Washington, D. C., 12 p.

U.S. Geological Survey National Oil and Gas Resource Team, 1995, 1995 National Assessment of United States oil and gas resources: U. S. Geological Survey Circular 1118, 20 p.

Wood, G.H., Jr., and Bour, W.V., III, 1988, Coal map of North America: U.S. Geological Survey Special Geologic Map, scale 1:5,000,000 [includes a 44 p. pamphlet].

Figure 1. Annual coal production from Wyoming (1985-1998) with forecasts to 2005 (millions of tons). Source: Wyoming State Geological Survey Coal Section.

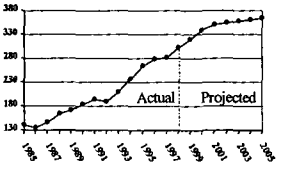

Figure 2. Annual production of Wyoming natural gas from 1980 to 1998 with forecasts to 2005 (billions of cubic feet). Source: Wyoming Oil and Gas Conservation Commission.

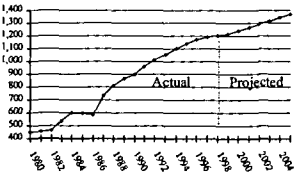

Figure 3. Annual production of Wyoming natural gas liquids from 1980 to 1998 with forecasts to 2005 (millions of barrels). Source: Wyoming Oil and Gas Conservation Commission.

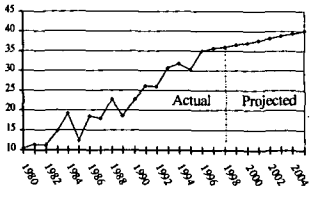

Figure 4. Annual production of Wyoming crude oil from 1980 to 1998, with forecasts to 2005 (millions of barrels). Source: Wyoming Oil and Gas Conservation Commission.

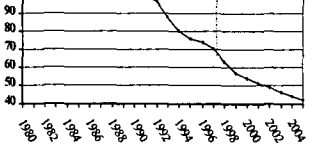

Figure 6. Annual production of Wyoming coalbed methane from 1987 to 1998, with forecasts to 2005 (billions of cubic feet). Source: Wyoming Oil & Gas Conservation Commission.

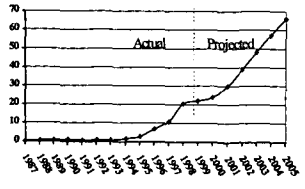

Figure 5. Index map of Wyoming basins and ranges.

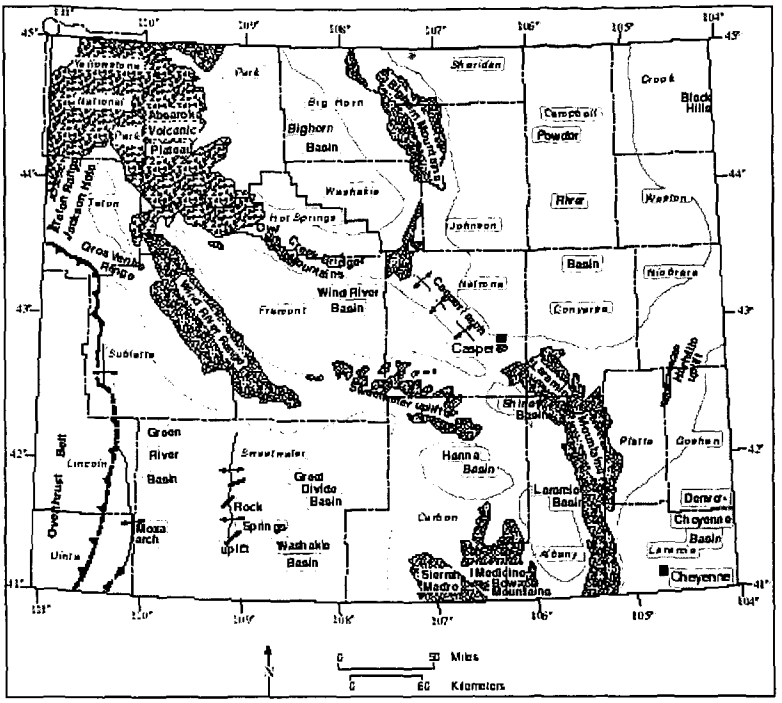

Table 1. Wyoming's ranking in proved reserves of crude oil (billions of barrels), dry natural gas (trillions of cubic feet), and natural gas liquids (billions of barrels) at the beginning of 1998.
Source: U.S. Department of Energy, 1998

State	Crude Oil	State	Dry Natural Gas	State	Natural Gas Liquids
Texas	5.687	Texas	37.761	Texas	2.687
Alaska	5.161	New Mexico	15.514	New Mexico	0.869
California	3.750	Wyoming	13.562	Oklahoma	0.685
New Mexico	0.735	Oklahoma	13.439	Alaska	0.631
Louisiana	0.714	Alaska	10.562	Wyoming	0.600
Wyoming	0.627	Louisiana	9.673	Louisiana	0.437
Oklahoma	0.605	Kansas	8.989	Kansas	0.271
North Dakota	0.279	Colorado	8.828	Colorado	0.264
Kansas	0.238	Alabama	4.968	Utah	0.181
Utah	0.234	West Virginia	2.846	California	0.095

Table 2. Comparison of Wyoming's proved reserves of crude oil (billions of barrels), dry natural gas (trillions of cubic feet), and natural gas liquids (billions of barrels) for the years 1980 through 1997.
Source: U.S. Department of Energy, 1998

Year	Crude Oil	Dry Natural Gas	Natural Gas Liquids[1]
1980	0.928	9.100	0.239
1981	0.840	9.307	0.269
1982	0.856	9.758	0.477
1983	0.957	10.227	0.552
1984	0.954	10.482	0.602
1985	0.951	10.617	0.684
1986	0.849	9.756	0.565
1987	0.854	10.023	0.647
1988	0.625	10.308	0.808
1989	0.815	10.744	0.627
1990	0.794	9.944	0.568
1991	0.757	9.941	0.524
1992	0.689	10.826	0.462
1993	0.624	10.933	0.420
1994	0.565	10.789	0.395
1995	0.605	12.166	0.415
1996	0.603	12.320	0.505
1997	0.627	13.562	0.600

[1] Estimated from U.S. Department of Energy figures

NATURAL GAS IS KEY TO FOSSIL FUEL CO_2 GLOBAL WARMING MITIGATION

Meyer Steinberg
Brookhaven National Laboratory
Upton, NY 11973

Key words - CO_2 mitigation, natural gas, efficient technologies

INTRODUCTION

Fossil Fuel energy is being blamed for the impending global warming problem. The emission of the radiative gas CO_2 from a particular country is intimately connected with the size of its population, its efficiency of utilization of fossil energy and the carbon content of the fuel.[1] This paper deals with CO_2 mitigation technologies including the reuse of emitted CO_2 and indicates a direction for CO_2 emissions reduction for the U.S. economy.[2]

The average CO_2 emissions for the three fossil fuels are as follows: Coal - 215 LbsCO_2/MMBTU (HHV = 11,000 BTU/Lb and C content of 76%); Oil - 160 Lbs CO_2/MMBTU (HHV = 6 MMBTU/Bbl) and Gas = 115 Lb CO_2/MMBTU (HHV = 1 M BTU/cu. ft.). Table 1 shows the U.S. fossil energy consumption and CO_2 emission, the total world consumption and emission and the principal energy supply service. In the U.S., most of the coal is used for generation of electrical power, in large central power stations. Oil is mainly used for production of transportation fuel (gasoline and diesel) with some limited electrical power production and gas is mainly used for industrial and domestic heating. However, there is also lately a growing consumption of natural gas for electrical power production.

Substituting Natural Gas for Coal for Electrical Power Production

If all the current electrical power production in the U.S. is generated by natural gas in combined cycle power plants, two benefits of CO_2 emission are achieved. First, the efficiency of electrical power production is increased from the current average coal-fired plant efficiency of 34% to over 55% for a modern natural gas fired turbine combined cycle plant and secondly the CO_2 emission per unit of energy from the fuel is reduced by 47% compared to the coal-fired plant. Applying this to the U.S. consumption,[3] and assuming that natural gas usage remains the same a 22% reduction in the total CO_2 emission can be realized.

Substituting Natural Gas for Oil for Automotive Transportation

Compressed natural gas (CNG) vehicles are already on the market and if natural gas is substituted for oil in the transportation sector a 13% reduction in CO_2 emissions can be realized in the U.S. Thus, the substitution of natural gas for Coal and Oil in the electrical power and transportation sectors adds up to a 35% overall reduction in CO_2 emissions.

The Carnol System for Preserving the Coal Industry for Electrical Power Production and Reducing Oil Consumption by Substituting Methanol in the Transportation Sector

The Carnol System consists of generating hydrogen by the thermal decomposition of methane and reacting the hydrogen produced with CO_2 recovered from coal-fired central power stations to produce methanol as a liquid transportation fuel.[4,5,7,10] Figure 1 illustrates the Carnol System which has the following advantages: 1. The Carnol System preserves the coal industry for electrical power production. 2. The Carnol System produces a liquid fuel for the transportation sector which fits in well with the current liquid fuel infrastructure. 3. The Carnol System reduces consumption of the dwindling domestic supplies of fuel oil in the U.S.

In the Carnol System, the carbon from the coal is used twice, once for production of electricity and a second time for production of liquid fuel for fueling the transportation sector, in automobile vehicles. The reduction in CO_2 emissions results from two aspects. The elemental carbon produced from the thermal decomposition of the methane is not used as fuel. It is either sequestered or sold as a materials commodity. In this respect, thermal decomposition of methane (TDM) has an advantage over the conventional steam reforming of methane (SRM) for hydrogen production reduced. In the TDM process, carbon is produced as a solid which is much easier to sequester than CO_2 as a gas. Furthermore, the energy in the carbon sequestered is still available for possible future retrieval and use. The carbon can also be used as a materials commodity, for example, as a soil

conditioner. Table 2 gives the estimate of CO_2 emissions using the Carnol System applied to the U.S. 1995 consumption and indicates a 45% overall CO_2 emissions reduction. The methanol in this case is used in conventional internal combustion engines (IC) which is 30% more efficient than gasoline driven IC engines.[6] The natural gas requirement would have to increase to 62 Quad which is three times the current consumption of natural gas for heating purposes. The rise in natural gas requirement is because only about 58% of the natural gas energy is used for hydrogen for methanol production. The carbon produced is sequestered unburned to the extent of 0.58 GT. This can be considerably reduced by adopting to fuel cell vehicles.

Carnol System with Methanol Fuel Cells for the Transportation Sector and Substituting Natural Gas with Combined Cycle Power for Coal Fired Central Station Power

In the not too distant future, fuel cells will be developed for automotive vehicles. This will improve the efficiency of automotive engines by at least 2.5 times compared to current gasoline driven internal combustion engines.[8] Direct liquid methanol fuel cells are under development.[11] If we use coal or oil for central power stations, there will be too much CO_2 generated for liquid fuel methanol by the Carnol Process for use in the transportation sector with fuel cells. Therefore, it is much more energy balanced if we use natural gas for power because it generates the least amount of CO_2 per unit of energy. In this scenario, the natural gas in a combined cycle plant displaces coal for power production and displaces oil for methanol by the Carnol Process for transportation. The results are shown in Table 3. Thus, by applying natural gas for electrical power production, liquid fuels production for fuel cell driven automotive engines and for heating purposes an overall CO_2 emissions reductions of over 60% can be achieved. This degree of CO_2 emission reduction could stabilize the CO_2 concentration and prevent the doubling of the CO_2 in the atmosphere expected by the middle of the next century if business is conducted as usual. The 0.32 GT of carbon required to be sequestered is about 3 times less than the amount of coal mined in the U.S. currently. If a market can be found for this elemental carbon, such as a soil conditioner, the cost of methanol production can be significantly decreased.

Natural Gas Supply and Utilization

The all natural gas energy system of Table 3 requires a three-fold annual consumption in natural gas. Recent reports indicate that the current estimated reserve of conventional natural gas is of the same order of magnitude as the current estimated oil reserves which might last only for another 80 years or so. However, unconventional resources, especially methane hydrates[9] and coal bedded methane indicate an enormous resource which is estimated to be more than twice as large as all the fossil fuel resources currently estimated in the earth. If this is so, then we can begin to think of utilizing natural gas for reducing CO_2 emissions in all sectors of the economy. It appears that even today, deep mined coal in several parts of the world, especially in England, Germany, and the U.S., has become too expensive; and, as a result, many of these mines have been closed. Most economical coal used today comes from surface mined coal. Furthermore, the contaminants in coal, sulfur, nitrogen and ash in addition to the high CO_2 emission mitigate against its use. Rail transportation of coal also becomes a problem compared to pipeline delivery of natural gas. When natural gas becomes available, even at a somewhat higher cost, it can displace coal and even oil for power production and transportation. Long term supply of economical natural gas is the main concern for increased utilization of natural gas.

Economics of Natural Gas Displacing Coal and Oil

The current unit cost for fossil fuel in the U.S. is roughly for coal $1.00/MMBTU, oil $3.00/MMBTU and for gas $2.00/MMBTU. For the total consumption of 76 Quad in 1995, the primary fossil fuel energy bill was $167 billion. Applying this to the all natural gas scenario of Table 3, we come up with a natural gas fuel bill for the required 49 quads of $98 billion. So there is a resulting 41% savings in the current fossil fuel bill. The cost of natural gas could go up to $3.50/MMBTU without the fuel bill exceeding the current fuel bill. In order to achieve these results, capital investment for the replacement of new technologies must be made. Only incremental replacement cost need be considered, since capital investment will be needed, in any case, to replace old equipment under business as usual conditions. Table 4 indicates the incremental capital replacement cost to achieve the all natural gas economy based on the following data.

a) Replacement of coal fired plants including scrubbers, etc., runs about $2000/kw(€); for the more efficient natural gas combined cycle plants runs about $1000/KW(€); thus, there is a $1000/Kw(€) capital cost savings and when applied to an installed capacity of 400,000 MW(€), the savings amounts to $400 billion.

b) For replacing oil refineries with new Carnol methanol plants which require CO_2 removal and recovery from the natural gas power plants, it is estimated that the current unit cost is $100,000 per daily ton of methanol. The total incremental cost to supply the total 14 quads of methanol for fuel cell vehicles is then $220 Billion. No credit was taken for the replacement of oil refineries, over time, so that this incremental capital cost is probably high.

c) New pipelines and LNG tanks will have to be built to transport the natural gas and new methods of extracting natural gas eventually from deep sea wells containing methane hydrates. Assuming $1 million per mile for these new gas supply facilities and a rough estimate of 200,000 miles needed gives a capital cost of roughly $200 billion. It is also assumed that the liquid methanol pipeline and tanker distribution will be about equal to the current liquid gasoline distribution for the transportation sector.

d) In terms of replacing the current existing more than 100 million gasoline driven IC engine vehicles with fuel cell vehicles, it eventually should not cost much more than the present average cost of $15,000 to $20,000 per vehicle. And, so the incremental cost should be negligible and may even show a savings because of the more efficient fuel cell vehicle than the IC engine vehicle.

Table 4 indicates that the incremental savings due to the new technologies in the one electrical power sector just about balances the incremental cost in the other three sectors. Thus, the new total incremental capital replacement cost, over the long run, is negligible compared to the capital cost requirement for continuing with the current business as usual current power technology structures.

Conclusions

The ability of achieving a 60% reduction in the U.S. CO_2 emissions by natural gas fuel substitution with improved technologies is based on the following assumptions and developments:

1. that there are vast reserves of natural gas that can be recovered from both conventional and non-conventional natural gas resources especially from methane hydrates and coal bedded methane at costs which are not more than about double current gas productions cost.
2. that an efficient Carnol process for methanol production based on thermal decomposition of methane can be developed.
3. that an efficient direct methanol fuel cell vehicle can be developed.

The benefits in terms of mitigating global warming provides a strong incentive for working on and achieving the required development goals. The all natural gas economy with efficient technologies for CO_2 global warming mitigation avoids alternatives of (1) sequestering CO_2 in the ocean or underground, (2) switching to nuclear power, and (3) relying solely on solar and biomass energy.

References

1. Kaya, Y., et al., "A Ground Strategy for Global Warming," paper presented at Tokyo Conference on Global Environment (September 1989).

2. Steinberg, M., "Natural Gas and Efficient Technologies: A Response to Global Warming." BNL 65451, Brookhaven National Laboratory, Upton, N.Y. 11973 (February 1998).

3. Carson, M.C., "Natural Gas Central to World's Future Energy Mix," Oil and Gas Journal, pp. 34-37 (August 11, 1997).

4. Steinberg, M., "Production of Hydrogen and Methanol from Natural Gas with Reduced CO_2 Emission," Proceedings of the 11th World Hydrogen Energy Conference (WHEC), Vol. 1, pp. 499-510, Stuttgart, Germany, (June 23-28, 1996).

5. Steinberg, M., "Methanol as an Agent for CO_2 mitigation," Energy Conversion 38 Supplement, pp. S423-S430 (1997).

6. U.S. Environmental Protection Agency, "Analyses of the Economic and Environmental Effects of Methanol as an Automotive Fuel," Research Report 0.730 (NTIS PB90-225806), Office of Mobile Sources, Ann Arbor, MI (1989).

7. Steinberg, M., "Natural Gas Decarbonization Technology for Mitigating Global Warming," BNL Report 65452, Brookhaven National Laboratory, Upton, NY (January 1998).

8. World Car Conference 1996, Bourns College of Engineering Center for Environmental Research and Technology, University of California, Riverside, CA (January 21-24, 1996).

9. Paul, C., "Atlantic Gas Hydrates Target of Ocean Drilling Program, Target of Ocean Drilling Program Leg," Oil and Gas Journal, pp. 116-118 (October 16, 1995).

10. Steinberg, M., "CO_2 Mitigation and Fuel Production," BNL Report 65454, Brookhaven National Laboratory, Upton, NY (October 1997).

11. Halput, G., et al., "Direct Methanol Liquid Fuel Cell," JPL Report, Jet Propulsion Laboratory, Pasadena, CA (May 1997).

FIG. 1

INTEGRATED SYSTEM FOR CO_2 EMISSION REDUCTION

CARNOL PROCESS

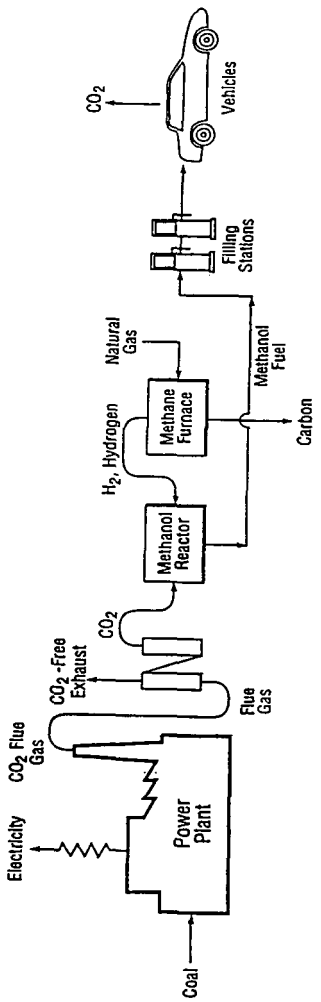

Table 1
Total Fossil Fuel Energy Consumption and CO_2 Emission for the U.S. in 1995[1]

Fuel Type	Quantity	Energy Consumption Quads 10^{15} Q BTU	Principal Energy Service	CO_2 Emission	
				$GT(CO_2)$	%
Coal	0.9×10^9 tons	20	electricity	2.15	35%
Oil	5.8×10^9 bbls	35	Auto transport	2.80	45%
Gas	21.0 TCF	21	heating	1.21	20%
U.S. Total World Total		76 330		6.16 (1.68 GT(C)) 22.7 (6.2 GT(C))	

TCF = Trillion (10^{12}) cubic feet
GT = Giga (10^9) tons
Q = Quads (10^{15}) BTU

Table 2
Carnol Methanol Substitution for Oil in the Conventional Auto Transportation Sector Produced from Natural Gas and CO_2 from Coal-fired Power Plants

Fuel Type	Natural Gas Consumed Quads	Energy Consumed Quads	Energy Service	CO_2 Emissions $GT(CO_2)$
Coal[a]	--	20	Electricity	0.22
Methanol[b] substitutes for gasoline	41	24	Auto Transport	1.96
Gas	21	21	Heating	1.21
Total	62	65		3.39
Reduction from current CO_2 emission				2.77
% CO_2 Emission Reduction from 1995 level				45.0%
Elemental carbon sequestered				0.58 GT (C)

Table 3
Natural Gas substituted for Coal Fired Power Production, Carnol Process for Methanol Production, Substituting for Oil in Fuel Cell Vehicles for the Transportation Sector

Fuel Type	Natural Gas Consumption Quads	Energy Consumption Quads	Energy Service	CO_2 Emission $GT(CO_2)$
Natural gas for coal[a]	14	14	Electricity	0.08
Methanol for oil	24	14	Auto Transport Fuel Cells	1.12
Gas	21	21	Heating	1.21
Total	59	49		2.41
Reduction from Current CO_2 Emissions				3.75
% CO_2 Emission Reduction from 1995 level				61%
Elemental carbon sequestered				0.34 GT (C)

a) Natural gas for combined cycle power plant is 55% efficient and 90% of CO_2 emissions is recovered for Carnol plant.

Table 4
Capital Investment Required to Replace Present Power Structure

Present Power Structure (and capacity)	Replacement Structure (and capacity)	Incremental Unit Capital Cost	Incremental Replacement Capital Cost $10^9 ($ Billions)
Coal fired electrical [a] power 400,000 MWe	Natural gas fired combined cycle electrical power	- $1000/kw (savings)[a]	- $400
Oil refineries[b] 35 Quads	Carnol methanol plants 14 Quads	$10^3/T/D$ Methanol[b]	+ $200
Wells and pipelines [c]	additional pipeline and new methane hydrate wells	$10^6/mile[c] 200,000 miles of gas lines	+ $200
Automotive IC vehicles 100×10^6	Fuel cell vehicles	0 [d]	- 0
Net total incremental replacement cost			- 0

THE ROLE OF NUCLEAR POWER IN U.S. ENERGY SUPPLY

Robert T. Eynon
U. S. Department of Energy
1000 Independence Ave SW
Washington, DC 20585

KEYWORDS: nuclear power, Kyoto protocol, energy forecasts

ABSTRACT

Commercial nuclear reactors provide almost one-fifth of U. S. electricity supply. This paper describes the costs and performance of these plants and provides projections of their contribution through 2020. The economics and engineering issues that determine if plants will retire before their operating licenses expire or if plants will seek license renewal are presented. Environmental considerations that could alter outcomes are also addressed including impacts on fossil fuel consumption and carbon emissions. The projections are drawn from the Energy Information Administration reports *Annual Energy Outlook 1999* and *Impacts of the Kyoto Protocol on U.S. Energy Markets and Economic Activity.*

BACKGROUND

Nuclear power plants provided 18 percent of the electricity generated in the United States in 1997. It is the second largest contributor behind coal which provides about 53 percent. Oil and natural-gas fired plants contribute about 17 percent and renewable sources (including hydroelectric) make up the balance. However, the role of nuclear power is expected to diminish in the future as plants begin to retire and no new capacity is built. This is likely to occur even though the plants currently operating have shown remarkable improvement in operating performance over the last several years. Since 1985 the performance of nuclear plants as measured by the capacity factor[1] has improved from 58 percent to 77.4 percent in 1995 before dropping back to 70.8 percent in 1997.[2] These improvements reflect a coordinated industry wide effort[3] to reduce incidents where plants are taken out of service (forced outages) and to increase periods between refueling outages. At the same time efforts have been made to reduce operating costs of plants to make them competitive with other generator types in response to the opening of markets for generation services to competition.

Nuclear plants have operating licenses that expire after 40 years. However, to this date no plants have actually achieved this period of service. Several plants have retired early (after operating 17 to 35 years) because of combinations of high operating costs, performance problems, and needs for significant capital investment to replace components such as steam generators.

In order to determine what role nuclear power will have in the future it is necessary to consider the remaining lives for the balance of plants currently in service[4]. To that end, it has been assumed that if it is economic to continue to operate a nuclear plant an age related investment of about $150 per kilowatt (about $150 million for a typical unit) will be required after 30 years of operation for plants with older designs (about one half of the existing capacity) in order to permit them to continue generating for 10 additional years.[5] Units with newer designs are estimated to require somewhat

---

[1]Capacity factor is the ratio of the actual electricity produced by a plant divided by the electricity that could have been produced at continuous full-power operation over the entire year.

[2]Energy Information Administration, *Annual Energy Review 1997,* DOE/EIA-0384(97) (Washington, DC, July1998).

[3]The nuclear industry formed a collaborative organization called the Institute for Nuclear Power Operations to address comprehensive improvements in the operation of nuclear generators.

[4]The Energy Information Administration produces projections of U.S. energy markets published in the *Annual Energy Outlook 1999.* The report has projections for nuclear power through 2020. See Energy Information Administration, *Annual Energy Outlook 1999,* DOE/EIA-0383(99) (Washington, DC, December 1998).

[5]Plants that have already incurred capital expenditures for steam system replacements are assumed to operate for 40 years with no additional investment.

lower costs. This expenditure is intended to be equivalent to the cost that would be associated with any of several needs such as a one time investment to replace aging equipment (steam generators), a series of investments to fix age related degradation, increases in operating costs, or costs associated with decreased performance. This investment is compared with the cost of building and operating the lowest cost new plant (typically a natural gas-fired combined-cycle unit) over the same 10 year period. If the cost of the investment for the nuclear plant is less than the alternative, it is assumed to remain in service. If the alternative is less expensive, then the nuclear plant is retired after 30 years of operation. Using these assumptions results in projections of almost 24 gigawatts of nuclear capacity being retired prematurely. This is in addition to the almost 7 gigawatts of capacity that has already been retired. A substantial portion of this capacity is located in the Northeastern United States and is expected to retire between 2000 and 2006. The retired capacity in the Northeast is almost 11 percent of total capacity available in that region.

A similar method is used to determine if it is economic to apply for license renewal and operate plants for an additional 20 years. Nuclear plants are estimated to face an investment of $250 per kilowatt (about $250 million for a typical one gigawatt unit) after 40 years of operation to refurbish aging components. This investment is compared with the lowest cost new plant alternative evaluated over the same 20 years that the nuclear plant would operate. If the nuclear plant is the lowest cost option, it is projected to continue to operate. EIA projects that it would be economic to extend the operating licenses for six gigawatts of capacity[6].

PROJECTIONS

Given the retirements (determined by the economic test at 30 years and by the expiration of operating licenses[7]) and license renewals discussed previously, nuclear generation is projected to decline over time. Nuclear generation is projected to drop from 629 to 359 billion kilowatt hours from 1997 to 2020 in the reference case[8]. Most of this decrease is expected to occur after 2010 when plants installed in the 1970's which don't pass the license renewal test begin to retire at the end of their operating licenses. As a result of lower output, the share of nuclear generation is expected to decline from 18 percent in 1997 to 7 percent in 2020. By 2020, renewable sources (including hydroelectric generation) account for more generation than nuclear plants. Nuclear generation drops from the second largest provider in 1997 to fourth in 2020 behind coal, natural gas, and renewable sources.

Because there is considerable uncertainty related to the investments required to allow plants to operate for 40 years, two alternative cases with higher and lower cost assumptions were analyzed. In the higher cost case the $150 per kilowatt investment to allow a plant to continue operations after 30 years was assumed for all reactors including the newer design units. This assumption captures the possibility of plant degradation and fuel storage costs beyond those assumed in the reference case. In this case an additional 16 gigawatts are retired by 2020. The retired nuclear capacity is replaced with new coal-fired steam units (30 percent) and new natural gas-fired combined cycle units (28 percent) and combustion turbines (42 percent). The consumption of coal and natural gas are higher in 2020 by about 0.4 quadrillion Btu for each fuel or 2 and 5 percent, respectively. Because more fossil fuels are consumed, the emissions of carbon are 17 million metric tons higher than the 745.5 million metric tons in the reference case in 2020.

In the more optimistic case it was assumed that plants could operate beyond 40 years without incurring a major capital expenditure at either 30 years or 40 years. This assumption is made to determine the impacts under the most optimistic outcome. These assumptions result in higher nuclear generation which causes fossil-fired additions to decline by 28 gigawatts and renewable sources to decrease by almost 1 gigawatt compared with the reference case in 2020. Carbon emissions are 30 million metric tons less than in the reference case in 2020. This reduction represents about 15 percent of the growth in carbon emissions from electricity production between 1997 and 2020. This means that 15 percent of the increase in carbon emissions could be offset if nuclear plants continued to operate beyond 40 years.

---

[6] In 1998 Baltimore Gas and Electric, owner of Calvert Cliffs, and Duke Power, owner of Oconee, applied to the Nuclear Regulatory Commission to renew the licenses for those plants.

[7] There are currently no announcements for early retirement of plants beyond those that have already been shutdown.

[8] Energy Information Administration, *Annual Energy Outlook 1999,* DOE/EIA-0383(99) (Washington, DC, December 1998). The report is available at http://www.eia.doe.gov.

The availability of a permanent storage site for high level waste is an issue important to the future of nuclear power. The lack of a permanent storage site is a major factor in the decision to build nuclear capacity. The requirements for spent fuel disposal vary slightly for the cases described above. In addition to the 35 thousand metric tons of spent fuel already accumulated, an additional 39 to 43 thousand metric tons would be generated by 2020 for the cases analyzed, more than doubling current inventories.

Beyond the waste storage problem there are also high investment requirements for new nuclear plants that make them non-competitive with new coal-fired steam plants and natural gas-fired combined cycle units through 2020. Table 1 provides the cost information for a coal-fired steam plant, a natural gas combined-cycle unit, and a nuclear unit. The nuclear cost assumes that plants can be built at guaranteed prices[9]. The table shows that the capital portion of the cost of the nuclear plant is higher than the other technologies. Even though nuclear plants have a very low fuel cost compared with the other types, the difference is not sufficient to overcome the differences in capital costs. As a result the total cost of producing electricity from a new nuclear unit is higher than for the other generating types.

Although there are significant impediments to construction, it is useful to examine the impacts that existing nuclear power plants could have on achieving reductions in carbon emissions required in the Kyoto Protocol.[10] There are a number of cases considered in this analysis that vary assumptions regarding trading of carbon permits, carbon sinks, and carbon offsets. These assumptions result in different levels of the carbon fee and cause the costs of providing electricity from fossil-fired plants to vary. As a result the economic test used to determine the operating lives of existing nuclear plants results in different levels of retirements of nuclear capacity. Figure 1 show the levels of nuclear capacity that result. Nuclear capacity ranges from 48 to 86 gigawatts in 2020 for the reference case and three percent below 1990 case, respectively. This range is the result of the different carbon fees only as all other assumptions regarding nuclear power are unchanged.

In order to determine if new nuclear capacity could also help reduce carbon emissions, two sensitivity cases were analyzed[11]. In one case it was assumed that carbon emission limits could be set at 9 percent above 1990 levels in 2010 if international activities including trading of carbon permits and offsets from other greenhouse gases and forestation projects are allowed. Although this case raises the costs of generating power from fossil-fired units by incorporation of a carbon fee ($163 per ton by 2010) to the delivered price of fuel, the increases are not sufficient to overcome the difference in costs between new nuclear capacity and fossil-fueled technologies. As a result, there are no new nuclear plants built through the year 2020 in this case.

In the second sensitivity case, a more stringent target of 3 percent below 1990 levels was set for carbon emissions eliminating the carbon permits in international markets but allowing credit for sinks and offsets. For this sensitivity test it was assumed that the initial nuclear units could be constructed without the cost premium typically associated with new designs. The basis for this assumption is that vendors would be willing to build plants at a fixed price in order to be competitive with other providers and to gain a market share.

Under these assumptions, about 40 gigawatts of nuclear power are constructed, mostly between 2015 and 2020. The use of fossil fuels declines compared with a case where the same emissions

---

[9]It is assumed that there is no uncertainty in costs quoted before a new design is built and, if costs exceed the original estimate, they are not passed on to the plant owner. The costs used under this assumption are those that would be expected for the fifth unit constructed under reference case assumptions. The cost of the fifth unit is assumed to be that of a mature technology where uncertainties in cost estimates have been eliminated.

[10] For a description of the protocol and analysis see Energy Information Administration, *Impacts of the Kyoto Protocol on U.S. Energy Markets and Economic Activity,* SR/OIAF/98-03 (Washington, DC, October 1998).

[11]These sensitivity cases are compared with the reference case used in the Kyoto analysis. The Kyoto reference case, although similar, is not the same as the reference case used in the *Annual Energy Outlook 1999* because of differences in assumptions regarding technological improvements and costs. The differences are discussed in Energy Information Administration, *Impacts of the Kyoto Protocol on U. S. Energy Markets and Economic Activity* , SR/OIAF/98-03 (Washington, DC, October 1998), Appendix A. The assumptions regarding the operating lives of nuclear plants are the same as those used in the *Annual Energy Outlook 1999.*

targets are assumed but without the option for new nuclear generators. Total fossil fuel consumption declines by 1 quadrillion Btu or 6 percent when new nuclear plants are built. In addition, even though consumers are projected to increase their use of electricity by one percent above the case where new nuclear power is excluded, there is a drop in the price of electricity. Average electricity prices to consumers decline by 4 mills per kilowatt hour (4 percent) compared with the case without new nuclear power. The addition of new nuclear power plants results in reductions in the cost of a carbon allowance. The price for an allowance would decline from $245 to $203 per metric ton of carbon (1996 dollars) in 2020[12]. It is also interesting to note that slightly less existing nuclear capacity would be economic to operate in 2020 (about 2 gigawatts) because the lower cost of the carbon permit causes fossil-fired plants to be more competitive with nuclear plants.

These results indicate the potential for nuclear power in a carbon constrained environment. However, the case does not address the impacts of developing the supporting infrastructure for nuclear power that would be required to permit the rapid expansion that these results suggest. If costs associated with new infrastructure are required, then there could be less penetration of new nuclear capacity than projected in this case.

CONCLUSIONS

Nuclear power which currently provides 18 percent of electricity supply is expected to drop to 7 percent by 2020 as existing plants retire and no new plants are built. Some existing plants will retire before the end of their operating licenses due to performance problems and age related investment requirements. New plants are not expected to be built because high capital costs make them non-competitive with other technologies and because permanent storage for waste is not available. The reduced contribution of nuclear power in the future increases consumption of fossil fuels and increases carbon emissions. If aging and performance problems do not cause plants to be shutdown early, then the growth in carbon emissions between 1997 and 2020 could be reduced by 15 percent. If there are mandates to reduce carbon emissions to 3 percent below 1990 levels by 2010 and thereafter, then nuclear power plants would be economic to build starting about 2015, given that vendors offer firm prices for construction.

ACKNOWLEDGEMENTS

The author expresses appreciation for technical assistance and comments provided by Laura Church, James Hewlett, Mary Hutzler, David Schoeberlein, and Scott Sitzer.

Table1 Cost of Producing Electricity from New Plants

	Pulverized Coal		Advanced Combined-Cycle		Advanced Nuclear	
1996mills/kWh	2010	2020	2010	2020	2010	2020
Capital	24.21	24.95	6.24	6.32	33.81	35.05
Fixed O&M	3.18	3.18	1.97	1.97	7.79	7.79
Fuel	10.09	9.55	22.13	23.54	3.74	3.86
Total	37.48	37.67	30.34	31.83	45.34	46.70

Note: Costs calculated on 80 percent capacity factor; Variable O&M included in fuel component. The cost for the advanced nuclear unit is for a mature technology which is assumed to occur when the fifth unit is constructed.

[12]Although it is assumed that carbon reduction targets must be met by 2010, there are no nuclear units constructed by then and there is no change in the carbon permit price.

Figure 1 Projections of Nuclear Capacity, 2000-2020

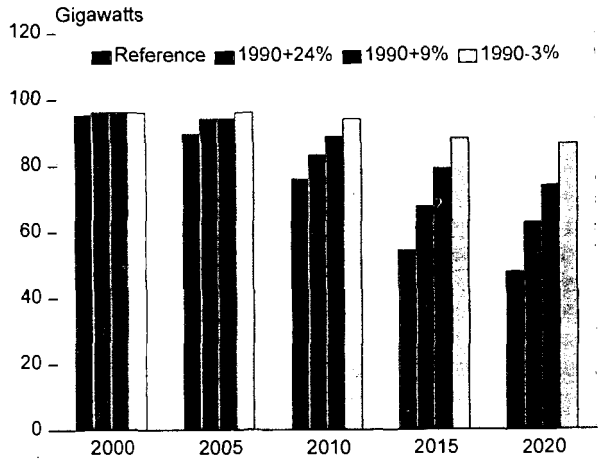

Future Sources of Heavy Crude and their Production and Upgrading Technology

Teh Fu Yen
School of Engineering
University of Southern California
Los Angeles, CA 90089-2531

KEY WORDS: nanotechnology, asphaltene, bitumen

ABSTRACT

Worldwide premium-quality lighter crude has been depleting during the last two decades. Future demands for petroleum is centercd on the use of heavy and extra-heavy oil, which is difficult to produce, transport and refine. An assessment is made on the types and sources of heavy crude as feedstocks for the conventional upgrading tcchnology, including the requirements for stringent environmental regulations. A strategy for future production (the up-stream) and upgrading (the down-stream) will be presented. Horizontal drilling, the use of microorganisms and a number of physical methods, such as ultrasound, median microwave, cold plasma, electrokinetic and monocrystallinc intermetallics, etc., will be discussed for the first time.

INTRODUCTION

U.S. DOE[1] has assessed that for the world crude oil supply from 1900 to 2100, extra heavy crude and bitumen will be used as a significant portion of the total consumption (40 Mbbl/ day), near the year 2060. At present, engineers have developed a myriad of processes to convert fossil fuel residues to lighter liquids. For example, both thermal cracking and hydrotreating (hydrocracking) have been commercialized worldwide. Certain designs of a given process usually depend on the properties of the feed. In order to adopt a given unit for a variety of other feed streams, the particular process must be modified from the original tailor-made system developed and intended for a given source or type. Without exception, all existing and frequently used processes, e.g., the H-oil and LC fining, suffer from this shortcoming.

Typical heavy oils produced at different geographical locations are quite different in properties. In this analysis, the common heavy oil sources used by the traditional processes are listed. After most of these sources are depleted, other massive sources of heavy oil or bitumens will be explored for commercial uses. Also, future potential sources of extra-heavy oil and bitumens are evaluated. The current technology of the refining process is based on the following principles: carbon fragmentation, carbon rejection, hydrogen addition and carbon rearrangement.

In this manner, asphaltene becomes pivotal, for example, in the processes of deasphaltene, asphaltene cracking, asphaltic interconversion, hydrogenation, hydrogenolysis of the aromatics and heterocyclics[2]. Usually, the mass distribution of the four asphaltic fractions—asphaltene, resin, aromatics and saturates (SARA)—is the primary factor that determines the characteristics of a given heavy oil. For heavy oil or bitumens from tar sands, the asphaltic fractions (nonvolatile) are the major constituents. For naturally occurring asphalt and solid bitumens, the asphaltene content of both may reach 90%+. There is a vital need for an alternative, due to the present refining technology, and it is much preferred if this technology is mild (without the application of high temperature and pressure), to minimize pollutant formation, and is flexible in process design (modular, with no restriction of capacity). For the first time, a summary report of the new technologies, such as the chemical-assisted ultrasound and the nanotechnology-aided refining, has been evaluated.

ANALYSIS OF FUTURE SOURCES

Conventional heavy oil sources up to the present are as follows: bottom or residua from delayed coking or vacuum distillation (paving asphalt); fractions after hydrotreatment; native bitumens (native asphaltenes and native asphaltites); native asphaltoids (e.g., wuzterlite, ingramite, etc.); oil sand bitumens; pyrolized kerogen product mixed with bitumen (oil shale); residue field oil after thermal or fire flooding; mined green oil after well closure (after tertiary recovery process); coal derived liquid, either from stagewise pyrolysis or hydrogenation[3].

Due to the geochemical nature of oils from the same geological regions, oils that have been exposed to the same paleogeological environments should be similar. From these aspects, crudes from

different sources are different in composition. Some of the massive reserves of heavy oils have been exploited for commercial use: the Venezuelan bitumen of the Orinoco basin and the heavy oil of Alberta and Saskachewan, for example, Cold Lake and Lloydminister; continental type of heavy oil from Liaohe and Karamay in China; residua of Maya and Isthumas from Mexico; and immature coastal deposits from California.

As the world turns around the corner of 2000, further potential resources become increasingly important, especially in many localities of the world, which can be extra heavy oil or bitumen: Eocene oil sand at Canbay basin in India; Volga-Urals' natural bitumens in Katakstan and Turkmenistan; Campos basin biodegraded oil in Brazil; Coastal bitumen type of Benin basin in Nigeria; Aswari limestone reservoir deposit in Iran; Duri field heavy oil in Sumatra of Indonesia; Zagros fold belt heavy oil in the Middle East; Narrows graben organic-rich oil shale in Queensland, Australia; Giant Green River oil shale in the U.S. For this study, the worldwide resources of coals, which can liquefy into liquids, are not included.

PRESENT TECHNOLOGY

At present, major, matured, commercial refining and upgrading processes can be summarized as: Foster Wheeler's delayed coking; Exxon's fluid coking and flexicoking (fluid coke gasified with air and steam); HRI-Cities Service's H-oil of ebullating-bed (now Texaco); Amoco's LC-Fining of demetallization and desulfurization (now Lummus Crest); Verba oil's VCC (Verba Combi Cracking) for liquid phase hydrogenation; and catalytic hydrofining; Shell's HYCON for HDM and HDS in series; Petro-Canada's CANMET using ferric sulfate as catalyst; Asahi-Chiyoda-Nippon Mining's SOC (super oil cracking) in slurry phase reactor; IFP-ELF-TOTAL's HYVAHL process.

Even for this short list, thermal cracking is still the major process. The success of a given process is dependent on the marketplace, but one can safely conclude that the combination of more than one is of advantage. A simple example is the combination of thermal cracking and hydrotreatment. Three different modes of hydrocracking are mentioned, which are fixed bed, ebullating bed and moving bed. The addition of a fixed-bed hydrotreater to the existing hydrocracking unit is very effective for the high-quality liquid. In this way often an integrated multi-stage unit is superior when compared to a single-stage unit.

HORIZONTAL DRILLING

Horizontal well steam stimulation has been adopted by a number of companies for pilot tests. For the thermal recovery of heavy oil, the conventional steam stimulation (CSS) and single-well steam circulation (CWSC) for drilling the horizontal length can reach one mile (usually somewhat below 2600 feet in order to avoid drainage of the existing vertical wells). Therein, extension and enlargement of zones can be used for chemicals, physical methods, instruments and microorganisms equally well. If completion work is done in a horizontal well, the layers in the horizontal well serve as both spaces and as individual reactors for further conversion of the oil.

CHEMICAL ASSISTED ULTRASOUND

Since asphaltene and related asphaltics (resin, gas oil, etc. the non-volatiles in petroleum, etc.) in residual oil are very complex in their intermolecular forces among individual species, such as association, assemblage, aggregation, interaction, etc., thermal energy by high temperature heating is not selective and may result in damage. For example, good (premiere) molecules may undergo polymerization and become coke. The effects caused by ultrasound can be attributed to three phenomena. First, there is a rapid movement of fluids caused by a variation of sonic pressure, which subjects the solvent to compression and rarefaction. The second phenomenon, and by far the most important, is cavitation. It is generally accepted that the formation and collapse of microbubbles is responsible for most of the significant chemical effects that are observed. The instantaneous pressure at the center of a collapsing bubble has been estimated from theoretical considerations to be about 75,000 psi. The temperature has been similarly estimated to reach values as high as 5200K. Actually, this technique can be operated at one atmosphere and room temperature. This process is called cold cracking. This violent implosion of the microbubbles also gives rise to luminescence. Thirdly, there is microstreaming, where a large amount of vibrational energy is put into small volumes with little heating. The application of ultrasound frequency for radiation can maintain the range from 25 to 40 kHz at an energy density of 20-600 W/cm^2. Under the cavitation conditions, two events may occur simultaneously, thermal scission of bonds of heavy oil according to Rice mechanism of cracking, and the generation of hydrogen atoms. These are essential for the upgrading of heavy molecules in residual oil and other residua. Fossil fuels, so far, that have been studied include Athabascar tar sand, Kentucky tar sand, paving asphalt, Monterey crude, coal liquids, Stuart

and Maoming oil shales and the improvement of the quality of reducing the asphaltene content has been found. Furthermore, the ultrasound can be applied in situ for generations of oil by reduction of viscosity using a drilling wanted with a number of transducers.

COLD PLASMA

The often-used control technology for hydrogen sulfide is the Claus method and the process stream after hydrodesulfurization from reformer, which has to purify this sour gas through Claus/SCOT unit. All these will lose the value of hydrogen since both processes require oxidation. The microwave method of utilizing the plasma dissociation process has also been developed. The plasma dissociation will save 0.24×10^{12} BTU/y for every 156 ton/d of Claus/SCOT plant.[5]

INTERMETALLIC FILTERS

Most recently, an intermetallic filter specifically for the removal of sulfur and improvement of the quality of feed has been in development.[6] The surface of Sn-Sb intermetallic has been shown to react with the sulfur species through the adsorption destruction by nanoscale technology. The preliminary results are very encouraging for high sulfur-containing crude oil; in general, a few pass through a fixed bed; the sulfur content has decreased by 50% and the asphaltene has also been reduced by 20%. As indicated in standard textbooks,[7] a filter can be a biofilter where the microorganisms are applied or an electrokinetic filter (potential difference, applied or induced), where the intermetallics are used. The device is very versatile, which can be attached or connected to any configurations in series or in parallel.

MICROBIAL ENHANCED OIL RECOVERY (MEOR)

Contrary to the Public's understanding, the MEOR method is more efficient for the recovery of heavy oil rather than light oil.[8] In a horizontally-drilled well, microorganisms can be introduced at certain levels of the pay zone. Very recently, one case has been found that all the recovery methods failed; MEOR is the only successful one.[9] The advantage of using special thermophilics for fermentation at the bottom of the hole has been described for the future ultimate oil recovery (UOR), as described earlier.[10]

CONCLUSION

A challenge is made to produce, transport, and refine the extraordinary crude and bitumens. A recommendation is therefore made for the future of the refining and upgrading industry for applying different, newly developed devices to enhance their efforts.

The use of a successive, multi-step unit (including the pre- and post-treatment unit to the maintrain) is to selectively eliminate the small amounts of bad molecules (molecules containing S, N, X and M), by targeting the destructive power on bad molecules, using a specific frequency of the irradiation (e.g., ultrasound, microwave, cold plasma, electrokinetic, induced field, magnetic force). Conventional refining technology, based on the premise that both good (major) molecules, and bad (minor) molecules, are treated with much excessive power in order to crack the very small amount of bad molecules, is not energy-saving. To achieve success in future refining and upgrading of heavy oil, research should not be centered on catalysts and reactor design alone, but also on the overall interdisciplinary knowledge of the nature of asphaltene pertaining to the geochemical transformation and formation. The recent concept,[11] that asphaltene and its related substances are continuous in transformation, is of paramount importance for the conversion.

REFERENCES

1. U.S.DOE, 1990, "Energy Outlook to the Year 2000, An Overview", Washington, D.C.

2. Yen, T.F., 1990, "Asphalt Materials" in *Encyclopedia of Polymer Science and Engineering*, Supplementary Volume, John Wiley, New York, pp. 1-10.

3. Yen, T.F., 1998, "Correlation between Heavy Crude Sources and Types and their Refining and Upgrading Methods," *Proceeding of the 7th UNITAR International Conference on Heavy Crude and Tar Sands*, Beijing, Vol. 2, pp. 2137-2144.

4. Yen, T.F., 1997, "Upgrading Through Cavitation and Surfactant," *Proceedings of the 15th World Petroleum Congress*, Forum 17, John Wiley, London.

5. Goyski, A.J., Daniels, E.J., and Harkness, J.B.L., 1990, *Treatment of Hydrogen Sulfide Waste Gas*, Argonne National Lab., ANL/ESD/TM-14.

6. Duffield, R., German, R., Iacocca, R., and Yen, T.F., 1998, Treatment of Fluids, Irish patent applied by Klinair Environmental Technology Ltd., Dublin, Ireland.

7. Yen, T.F., 1998, Chapter 31, "Filtration," in *Environmental Chemistry: Chemical Principles for Environmental Processes*, Vol. 4B, Prentice Hall, Upper Saddle River, NJ, pp. 1405-1439.

8. Yen, T.F., 1990, *Microbial Enhanced Oil Recovery: Principle and Practice*, CRC Press, Boca Raton, FL.

9. Mei, B.W., et al., 1998, Unpublished Results Jianghan Petroleum University, Jin-Zhou, China.

10. Yen, T.F., 1995, "Asphaltenes and Improved Oil Recovery," *Proceedings of the 6th UNITAR International Conference on Heavy Crude and Tar Sands*, DOE, Battlesville, OK, pp.231-236.

11. Yen, T.F., 1999, Chapter 2, "The Realms and Definitions of Asphaltenes," in *Asphaltenes and Asphalts* (T.F.Yen and G.V. Chilingar, eds.) Vol. 2, Elsevier Science, Amsterdam, the Netherlands.

COMPARISON OF FUEL PROPERTIES OF PETROLEUM COKES AND COALS USED IN POWER GENERATION

Jun M. Lee, James J. Baker, Jeffrey G. Rolle, Robert Llerena,
A. J. Edmond Co.
1530 West 16th Street, Long Beach, CA 90813

Keywords: petroleum coke, coal, fuel properties

INTRODUCTION

U.S. petroleum coke production is projected to continue to increase, reaching 90,000 st/cd (short tons per calendar day) by the year 2002, primarily due to refining heavier and higher sulfur content crudes [1]. In 1996 the coke production was 86,805 st/cd and 65.7% of the annual production was exports. Green (raw) petroleum cokes are mostly used as utility fuels (about 73% for fuel grade) combining with coal to make fuel in processing industries. Petroleum cokes are produced at refineries using three different types of coking processes: delayed, fluid, and flexicoking. The delayed coker is mostly used at forty-eight refineries. The other fluid coker (4 units) and flexicoker (2 units) are less utilized. Coke products from a delayed coker are classified as shot, sponge or needle coke depending on their chemical and physical characteristics.

Utility companies used 3,852 st/cd of petroleum coke (less than 5% of annual production) as a power plant supplemental fuel blending with coal in 1996, because petroleum coke has advantages of low price (36% lower at $/st or 46% lower at $/MMBtu), high heating value, and low ash content [1]. The disadvantages of petroleum coke as a fuel are expense of a dual solid fuel handling and crushing system, high sulfur, high nickel and vanadium content. Normally cokes are blended with coals at 10-20% before burning in boilers because of their low volatile matter and high sulfur content. Average quality of coke burned is: on as-received basis, 13,930-14,820 Btu/lb, 5.5% sulfur, and 0.5-3.8% ash.

Some refineries consume a portion or all of the coke they produce as a solid fuel to generate steam, and more recently, as fuel for cogeneration facilities. An average of 1,767 st/cd of petroleum coke was used within refineries in 1996. Texaco cogeneration power plant at El Dorado refinery, Kansas gasifies a delayed coke to produce syn-gas for a combustion turbine fuel [2]. Typical composition of the delayed coke is: on dry basis, 90% carbon, 4% hydrogen, 4% sulfur, 1.5% nitrogen, 0.5% oxygen, and 0.5% ash. Other coke-fueled cogeneration plants burn 100% delayed coke [3] or 100% fluid coke [1] in a circulating fluidized bed (CFB) steam generator. Delayed coke fines sized to 0.25 in. (6 mm) is fed to the CFB furnace along with crushed limestone. Typical composition of the delayed coke feed is: on dry basis, 89.2% carbon, 3.7% hydrogen, 5% sulfur, 1.8% nitrogen, 0.3% ash, and 15,050 Btu/lb of high heating value (HHV). The coke contains approximately 10.6% moisture.

Cement industry consumes a large portion of fuel-grade petroleum coke (35.5% of world demand) to combust in kilns [1]. The addition of cokes can constitute up to 50% of the fuel mixture and is carefully controlled conducting test burn due to detrimental effects of high sulfur and vanadium content to concrete quality. Sulfur contamination can cause cement cracking and preheater plugging-fouling due to combination with alkalies, and high vanadium content above 500 ppm can cause cement to lose strength. The cement kilns operate as scrubbers, absorbing sulfur and other contaminants into finished cement.

U.S. utility companies consume about 80% of annual coal production (approximately 1,000 million short tons in 1995) burning in boilers to generate electricity [4]. The coal production consists of 60% bituminous, 30% subbituminous, 8% lignite and small percentage of anthracite. U.S. exports annually about 90-110 millions tons (9-11% of total production).

Coal gasification process technologies have been extensively tested in conjunction with integrated gasification combined cycle (IGCC) systems to improve efficiency, environmental performance, and overall cost effectiveness in electric power generation [5]. Several successful demonstration projects are: British Gas/Lurgi gasifier, Texaco Cool Water gasification plant, Shell Coal Gasification Process, Dow Coal Gasification Process (Destec), etc. Full-scale projects are now proceeding in The Netherlands, Germany, Spain and Italy on a commercial basis. Utah (SUFCO) coal, an export western bituminous coal, was the predominate coal gasified at the Texaco Cool Water plant [6] and also tested in the Shell demo-plant [5]. Typical coal properties are: 0.4% sulfur, 8.8% ash, 12,360 Btu/lb (HHV), and 2,200 deg F of ash fusion temperature. The SUFCO Utah coal has low sulfur, low iron and high sodium content. Shell demo-plant tested a delayed coke which has low ash, high sulfur, low oxygen, low calcium, high vanadium, and high nickel

content. Feed properties of the delayed coke are: on dry basis, 10.6% volatile matter, 0.5% ash, 5.2% sulfur, 89.3% carbon, 3.6% hydrogen, 1.35% nitrogen, 0.03% chlorine, 0.1% oxygen, 15,350 Btu/lb (HHV), and 61 hardgrove grindability index (HGI). The coke contains 9.3% moisture and ash mineral analysis shows 0.8% lime, 1.2% sodium oxide, 71.8% vanadium pentoxide, and 7.4% nickel oxide. Texaco and Kellogg (KRW) gasification processes also extensively tested petroleum cokes as raw material to gasifier [7,8].

Coal ash is classified into two categories: lignitic ash is defined as having more (CaO+MgO) than ferric oxide; and bituminous ash is defined as having more ferric oxide than the sum of CaO and MgO. The Utah coal is classified a western high volatile bituminous coal, but has lignitic ash. Ash characterization methods such as slagging and fouling indices are different in calculation depending upon bituminous or lignitic ash [9]. Chemical composition of coal ash affects slag viscosity, which is an important criterion for determining the suitability of a coal ash for use in a slag-tap cyclone furnace. Slag flow readily at or below a viscosity of 250 poise. The temperature at which this viscosity of ash occurs is called T_{250} temperature. The preferred maximum T_{250} for wet-bottom applications is 2,450 deg F.

The alkali metals, sodium and potassium, have long been associated with the fouling tendencies of coal ash. Correlations in fouling index have been developed using various parameters such as strength of sintered fly ash and total alkali content for bituminous ash, and sodium content alone for lignitic ash. All bituminous coals contain enough sulfur and alkali metals to produce corrosive ash deposits on superheaters and reheaters, and those containing more than 3.5% sulfur and 0.25% chlorine may be particularly troublesome. The elements in coal ash corrosion are sodium, potassium, aluminum, sulfur and iron, which are derived from the mineral matter in coal. Fouling observed in a CFBC boiler firing coal and petroleum coke was attributed to agglomeration of sulfate and carbonate, not due to high concentration of nickel and vanadium present in petroleum coke (306 and 870 ppm, respectively) [10].

The objective of this study is to evaluate and compare various fuel properties of petroleum cokes and bituminous coals used in power generation, comparing different cokes produced from several refineries in U.S. and export western coals sampled at the Los Angeles Export Terminal (LAXT). Four fluid cokes, fourteen delayed cokes and five export coals are included for evaluation based on recent analysis data accumulated for the past two years (1997-1998).

SAMPLING, PREPARATION AND ANALYTICAL METHODS

Representative samples of petroleum cokes and coals have been obtained from various refineries located in California, Texas, Louisiana, Kansas, Illinois and other states, and storage facilities at numerous national ports. Laboratory samples are prepared for fuel properties analysis following the procedures and principles in handling listed in the ASTM Methods D 346, D 2013 and D 2234. Laboratory test methods using various advanced analytical instruments are described in the Quality Assurance Manual of A. J. Edmond Company [11].

RESULTS AND DISCUSSION

Important fuel properties of three significantly different types, delayed coke, fluid coke and export western coal are presented for comparison in Tables 1-3. Petroleum cokes evaluated for this study are produced in various U.S. refineries located in west coast (WC), Gulf coast (GC), mid west (MW), and south east (SE), which are primarily consumed in export to foreign countries (65.7%) and in smaller extent (less than 10%) used in domestic power generation and cement kiln fuel mix. Export western coals sampled at the LAXT are high volatile bituminous coals with low sulfur and iron content. They are primarily produced in Utah and Colorado for power generation. The throughput capacity of LAXT is 10 million metric tons per year, which is correspondent to about 10% of current coal export to foreign countries.

Based on data presented in Tables 1-3, five different arbitrary groups of concentration or value of several primary fuel properties are used as indicators of different levels of properties as follows:

Fuel Property	Very Low	Low	Medium	High	Very High
Sulfur, wt%		1-2	2-4	4-6	
Ash, wt%	0.5	1-2		9-10	
Volatile Matter, wt%		2.5-6.1	9.5-13	40.2-41.1	
Btu/lb		12600-13400	14200-14600	15200-15600	
Nitrogen, wt%		1.2-2.2		2.8-3.2	
Vanadium, ppm		270-400	500-800	900-1400	2300-2900
Nickel, ppm		25-200	400-500	700+	

Fluid Coke Fuel for Cogeneration Plants

Table 1 summarizes analysis results of fuel properties of petroleum cokes used in power generation. Three fluid cokes (WC-1, WC-2 and WC-3), one bed coke (WC-4) and six delayed cokes (WC-5, SW/MW-1, SW/MW-2, SE, SE/GC, E/MW) are included for comparison. Fluid and bed cokes (WC-1 to WC-4) have been extensively used in circulating fluidized bed combustors at cogeneration power plants. WC-2 and WC-3 fluid cokes also represent export quality to foreign countries.

Fluid coke generated from a fluidized bed reactor is a solid, spherical particulate normally smaller than 8 mesh (98% for WC-2 and WC-3, and 74% for WC-4, as shown in Table 1). The coke is very hard and abrasive, suitable for direct use in a circulating fluidized bed combustor, and generally have lower HGI than delayed coke and coal. Typical moisture content is very low in the range of 0.3 to 1.2% except for export cokes having 7-11.5% which increased to control dust during transportation. Sulfur content for fluid cokes, WC-1, WC-3 and WC-4, is low in the range of 1.0 to 2.1%; and WC-2 coke has medium sulfur with 3.3%, somewhat lower than other delayed cokes listed in Table 1 (4-6%). Ash content of WC-1 and WC-2 cokes is very low in the range of 0.35 to 0.46%, and WC-1 and WC-2 cokes have a little higher ash from 1.1 to 1.5%. These ash values are significantly lower compared to coals (9.2-10%), which is normally claimed as an advantage as fuel.

Calorific value for all fluid cokes studied is medium in the range of 14,200-14,400 Btu/lb (dry basis), relatively high compared to coals (12,600-13,400 Btu/lb dry basis). Volatile matter content is low in the range of 2.5 to 6.1% for all fluid cokes, compared to delayed cokes (9.5-13%) and coals (40.2-41.1%). Power plant startup is easier with fuels having higher volatile matter. However, serious operational problems in burning petroleum cokes as 100% or 10-20% blend mix have not been reported. Fluid cokes, WC-2, WC-3 and WC-4, have relatively low nitrogen content in the range of 1.4 to 2.2%, while WC-1 has a higher nitrogen of 3%, similarly observed with some delayed cokes (2.8-3.2%). Coals evaluated for this study have a low nitrogen of 1.2 to 1.5%.

Vanadium content for WC-1 and WC-2 is medium in the range of 650 to 850 ppm, near concentration used in the cement kiln fuel mix (530-760 ppm for SW/MW-1 and SW/MW-2), but higher than that for good anode-grade cokes (270-400 ppm). WC-3 and WC-4 cokes show the highest V content in the range of 2300 to 2900 ppm among petroleum cokes and coals evaluated for this study. Detrimental affects with this high V content (as much as 10,000 ppm) have not been reported in the operation of steam generating combustors [12]. Sodium content for WC-1 and WC-2 cokes is low in the range of 80 to 180 ppm, which is similarly observed in good anode-grade sponge cokes (25-200 ppm). WC-3 and WC-4 cokes have a higher Na content of 480 to 500 ppm compared to WC-1 and WC-2. Most of delayed cokes studied have a low Na content (50-160 ppm) except for WC-5 and WC-E4 (380-450 ppm).

Delayed Coke Fuel for Utility and Cement Plants

Six delayed cokes in Table 1 (WC-5, SW/MW-1, SW/MW-2, SE, SE/GC, E/MW) have been used as fuel blend mix in pulverized coal combustors for steam generation and cement kilns. These cokes are fuel grade, green (raw) cokes with high ash, high sulfur and high metal content ranging sponge to shot coke. Typical ash content is in the range of 0.25 to 0.65%; sulfur content in the range of 3.1 to 6%; vanadium from 530 to 1700 ppm; nickel from 190 to 600 ppm; and sodium from 80 to 380 ppm. Calorific value is high in the range of 15,000 to 15,580 Btu/lb (HHV, dry basis), producing more heat during combustion than fluid cokes and coals. Size distribution covers wide range of particle size from -6 mm to +40 mm depending on fines, lump or ROC (run of coker) delivered from refineries. Typical HGI is in the range of 35 to 60, mostly higher than coal HGI (45), with shot content varying from 0 to 80%. Typical moisture content is in the range of 5 to 9%, and volatile matter varies from 9.5 to 13%.

Two delayed cokes, SW/MW-1 and SW/MW-2 have been frequently used in cement kiln operation, as fuel mix (up to 50%). Typical sulfur and vanadium content (controlled quality parameters for cement application) of these cokes vary in the range of 3.1 to 3.8% and 530 to 760 ppm, respectively. Sulfur and vanadium content are higher than those required for good anode-grade sponge coke (3% and 400 ppm, respectively).

Quality of Export Petroleum Cokes

Table 2 presents analysis results from eight export delayed cokes. These cokes have been mostly used as utility fuels combining with coal to make fuel in processing industries. Fuel property data in the table update export quality analysis of petroleum cokes previously reported [11]. Export quality criteria of green (raw), fuel-grade cokes are dependent upon buyer's requirements of coke specifications. As shown in the following for west coast cokes, primary criteria frequently used

are: size distribution, moisture, sulfur, ash, volatile matter, fixed carbon content and calorific value; and secondary criteria are: nitrogen, vanadium and sodium content. In addition, complete ash mineral analysis is sometimes required to report.

Fuel Property	Criteria Specified
Size, mm	0x6, 0x10 or lump -2 & +25
Moisture, wt% (dry basis)	8-12, 9-12 or 9 max
Sulfur, wt%	1 max, 2 max or 3 max
Ash, wt%	0.5 max, 1 max or 1.5 max
Volatile Matter, wt%	9-13, 11-12.5 or 14 max
Fixed Carbon, wt%	88-90 or 87 min
HGI	45-50 or 50 min
Btu/lb	15,000 min
Nitrogen, wt%	2, 2.5-3.5 or 2.9 max
Vanadium, ppm	500-800 or 700 max
Sodium, ppm	200-300 or 700 max

Eight delayed cokes in Table 2 (WC-E1 to WC-E8) are produced in refineries located in west coast. These cokes are good quality, fuel-grade green (raw) cokes, which generally have lower ash, sulfur and metal content than six delayed cokes in Table 1 used in domestic power generation. Typical ash content is in the range of 0.18 to 0.45%; sulfur content in the range of 0.8 to 4%; vanadium from 270 to 1150 ppm; nickel from 180 to 550 ppm; and sodium from 50 to 450 ppm. Calorific value is high in the range of 15,300 to 15,520 Btu/lb (HHV, dry basis), as similarly observed with delayed cokes in Table 1. Size distribution covers wide range of particle size from -6 mm (30-99%) with fines, to +40 mm (3-47%) with lump or ROC (run of coker) depending on delivery from refineries. Typical HGI is in the range of 35 to 80, mostly higher than coal HGI (45), with shot content varying from 0 to 60%. Typical moisture content is in the range of 7 to 12%, and volatile matter varies from 10 to 12.5%.

Quality of Export Western Coals

Table 3 summarizes analysis results from five export western coals (type I to V). These coals sampled at the LAXT are high volatile bituminous coals with low sulfur and iron content. They are primarily produced in Utah and Colorado and used as utility fuels for power generation. Coal quality specifications for export were previously reported [11]. Primary fuel properties of coal are: proximate, ultimate, calorific value, HGI, size distribution, ash mineral analysis and ash fusion temperatures.

Typical ash content of export western coals is high in the range of 9.2 to 10%; sulfur content is very low in the range of 0.45 to 0.6%. These coals are classified as western high volatile bituminous coal, but have lignitic ash having more (CaO+MgO) than ferric oxide [9]. Primary constituents of coal ash are silica (52.3-58.6%), alumina (11.6-21%) and lime (5-13.1%). Ferric oxide content in ash is low from 4.4 to 5.9% compared to eastern bituminous coal (20-30%); sodium oxide content is high from 1.8 to 4.2%. Calorific value is low in the range of 12,640 to 13,360 Btu/lb (HHV, dry basis), compared to fluid cokes and delayed cokes in Tables 1 and 2. Size distribution shows top size of 2 inches having 92-100% 50 mm x 0 mm and 11.6-33% 2 mm x 0 mm. Typical HGI is in the range of 43 to 46. Typical moisture content is in the range of 7.7 to 10.3%, and volatile matter varies from 40.2 to 41.1%.

Data for coal ash characteristics used for selection of feed coal and boiler design criteria are also presented in Table 3. Ash and slag viscosity plot parameters are: silica ratio, base-to-acid (B/A) ratio, T_{250}, and slagging index. Fouling plot parameters are: alkalies as sodium oxide and fouling index [9]. Typical silica ratio is in the range of 0.712 to 0.828; B/A ratio from 0.2 to 0.386; T_{250} from 2,420 to 2,760 deg F; and slagging index is medium to high in the range of 2,114 to 2,263. Typical alkalies as sodium oxide is high in the range of 2.5 to 4.5; and fouling index is high from 1.8 to 4.2. Very low sulfur content with theses coals may lower corrosive ash deposits caused by reacting with sodium, potassium, aluminum and iron, but addition of high sulfur petroleum cokes as fuel mix may increase corrosion reactions with alkali metals. Coal type III and V with high B/A ratio of 0.386 and 0.372 have low T_{250} (2,420 and 2,450 deg F, respectively) meeting requirement for operation of slag-tap cyclone furnace.

SUMMARY

Various fuel properties of four fluid cokes, fourteen delayed cokes and five export western coals were analyzed and are compared for use in power generation. Important fuel quality parameters (typical and range) are tabulated for comparison, using recent analysis data accumulated for the

past two years (1997-1998). Primary properties evaluated are: heating value, sulfur, nitrogen, ash, moisture, volatile matter content, hardgrove grindability index, size distribution, and mineral analysis. In addition, coal ash characteristics such as silica ratio, base-to-acid ratio, ash fusibility, alkalies, T_{250}, slagging index, fouling index, etc. are discussed.

Petroleum cokes as 100% fuel or 10-20% fuel mix with coal have been used in power generation without serious operational problems reported, even burning with some cokes of high vanadium content (1,000-3,200 ppm). Some cokes have high sulfur content up to 7%, high nitrogen content up to 3.5%, and low HGI down to 25 (for delayed coke). Typical sulfur content of most cokes studied varies in the range of 0.8 to 4.1%; nitrogen varies in the range of 1.3 to 3.2%; and HGI varies from 40 to 80 (for delayed coke), mostly higher than coal HGI (45).

Petroleum cokes as fuel mix (up to 50%) have been used in cement kiln operation. Typical sulfur and vanadium content (controlled quality parameters for cement application) of delayed cokes mixed in kiln vary in the range of 3.1 to 3.8% and 530 to 760 ppm, respectively.

Export delayed cokes are good quality, fuel-grade green (raw) cokes, which generally have lower ash, sulfur and metal content than delayed cokes used in domestic power generation. Typical ash content is in the range of 0.18 to 0.45%; sulfur content from 0.8 to 4%; vanadium from 270 to 1,150 ppm; nickel from 180 to 550 ppm; and sodium from 50 to 450 ppm. Calorific value is high in the range of 15,300 to 15,520 Btu/lb (HHV, dry basis).

Price of fuel grade petroleum coke is normally below 5 $/ton at refinery, however, transportation cost significantly increases the price at power plant (21 $/ton, 1996 annual average delivered). Demand and supply of petroleum coke are dictated by three important factors such as refinery cost, coke quality and transportation cost. Location of refinery and power plant seems an important factor to be considered.

Export western coals are high volatile bituminous coals with low sulfur and iron content, and are used as utility fuels for power generation. Typical ash content is high in the range of 9.2 to 10%; sulfur content is very low in the range of 0.45 to 0.6%. Ash from these coals are defined as lignitic ash having more (CaO+MgO) than ferric oxide. Ferric oxide content in ash is low from 4.4 to 5.9% compared to eastern bituminous coal (20-30%); sodium oxide content is high from 1.8 to 4.2%. Calorific value is low in the range of 12,640 to 13,360 Btu/lb (HHV, dry basis), compared to petroleum cokes. Coal ash characteristics used for selection of feed coal and boiler design criteria are discussed relating to slag viscosity, fouling, and corrosion. Coal type III and V have low T_{250}, meeting requirement for operation of slag-tap cyclone furnace.

The SUFCO Utah coal, one of five export western bituminous coals evaluated for this study, was extensively tested at several gasification demonstration plants for IGCC systems in addition to variety of petroleum cokes as feed material to gasifiers.

REFERENCES

1. E. J. Swain, Oil & Gas Journal, Nov. 10, 1997, 79-82; May 20, 1991, 49-52.
2. A. K. Rhodes, Oil & Gas Journal, Aug. 5, 1996, 31-35.
3. K. W. Richardson and F. D. Taibi, Oil & Gas Journal, Apr. 5, 1993, 38-42.
4. R. Graham, ASTM Standardization News, Mar. 1998, 36-43.
5. Kerk-Othmer Encyclopedia of Chemical Technology, Volume 6, 4th Ed., Gasification, 541-568 (1993).
6. D. H. Watts, Sixth Annual International Pittsburgh Coal Conference, Sep. 25-29, 1989, 569-581.
7. A. M. Robin, et. al., Sixth Annual International Pittsburgh Coal Conference, Sep. 25-29, 1989, 244-254.
8. F. M. Floyd and R. K. Agrawal, Sixth Annual International Pittsburgh Coal Conference, Sep. 25-29, 1989, 559-568.
9. Babcock & Wilcox Company, "Steam - Its Generation and Use: Steam 40", Chap. 20, Fuel Ash Effects on Boiler Design and Operation (1992).
10. E. J. Anthony, et. al., 215th ACS National Meeting, Dallas, Preprints of Symposia, Division of Fuel Chemistry, Vol. 43, No. 1, 163-166 (1998).
11. J. M. Lee, J. J. Baker, R. Llerena, J. G. Rolle, 214th ACS National Meeting, Las Vegas, Preprints of Symposia, Division of Fuel Chemistry, Vol. 42, No. 3, 844-853 (1997).
12. R. W. Bryers, ACS National Meeting, Preprints of Symposia, Division of Fuel Chemistry, Vol. 38, No. 4, 1237-1244 (1993).

Table 1. FUEL PROPERTIES OF FLUID AND DELAYED COKES USED IN POWER GENERATION

Industry Location	WC-1		WC-2		WC-3		WC-4		WC-5	
Process	Cogeneration		Cogeneration/Export		Cogeneration/Export		Cogeneration		PCC	
	CFBC		CFBC		CFBC		CFBC		Cement Kiln	
Coke Type	Fluid		Fluid		Fluid		Bed		Delayed (Blend)	
Properties	*Typical*	*Range*	*Typical*	*Range*	*Typical*	*Range*	*Typical*	*Range*	*Typical*	*Range*
(as-received)										
Moisture, wt%	0.5	0.2-1.4	0.3	0.02-0.8	11.5	10-15	1.2	0.2-2.5	9	4-13
(dry-basis)			(Export: 6-8%)							
Proximate, wt%										
VCM	6.1	5-7	5.3	4-7	4.6	2.9-7.5	2.5	1.6-3.1	13	11-15
Ash	0.46	0.3-0.6	0.35	0.25-0.5	1.1	0.7-1.2	1.5	1.2-1.9	0.65	0.3-0.7
FC (by diff.)	93.4	93-94.5	94.3	93.4-95.2	94.3	91.5-96.5	95.6	-	86.5	85-88
Ultimate, wt%										
Sulfur	2.1	1.5-2.5	3.3	3.0-3.6	1.2	0.8-2.5	1.0	-	4.6	3.8-5.5
Carbon	92.2	91.6-93	91.7	91-92.5	94.8	-	94.6	-	86.5	-
Hydrogen	1.7	1.3-2.2	2.0	1.8-2.2	1.0	-	0.8	-	3.8	-
Nitrogen	3.0	2.7-3.4	2.2	1.8-2.4	1.4	-	1.7	-	2.9	2.8-3.1
Oxygen (by diff.)	0.54	-	0.45	-	0.5	-	0.4	-	1.55	-
Chlorine (ppm)	-	-	160	70-260	-	-	-	-	265	-
Metals, ppm										
Silicon	150	80-200	150	60-230	350	100-570	400	230-530	150	100-210
Iron	380	230-500	150	110-240	1600	1080-2060	1600	1120-2060	170	80-290
Vanadium	650	430-860	850	700-1130	2300	1940-2750	2900	2670-3200	1700	1400-2100
Nickel	620	480-700	450	400-540	2200	2050-2840	2350	2050-2630	600	490-730
Aluminum	45	10-95	80	40-200	90	50-180	100	30-160	70	20-170
Calcium	210	160-290	120	40-210	800	420-1140	800	500-1030	200	140-360
Sodium	180	90-250	80	40-170	480	340-740	500	290-740	380	200-510
Calorific Value										
Btu/lb	14540	14280 -14700	14550	14300 -14750	14330	14200 -14460	14200	- -	15000	14900 -15150
HGI	-	-	-	-	-	-	-	-	60	50-67
Shot, %	-	-	-	-	-	-	-	-	0	0-5
Size, wt%										
-6 mm	-	-	98.6	-	97.7	-	-	-	-	-
+4 mesh	-	-	-	-	-	0	-	-	-	-
+8 mesh	-	-	-	1.5	-	2	-	-	-	-
-50 mesh	-	-	-	94	-	-	-	74	-	-
-100 mesh	-	-	-	52	-	38	-	24	-	-
-200 mesh	-	-	-	4	-	7	-	7	-	-
Fuel Ratio	15.3	-	17.8	-	20.5	-	38.2	-	6.7	-

Table 1. FUEL PROPERTIES OF FLUID AND DELAYED COKES USED IN POWER GENERATION *(Continued)*

Industry Location	SW/MW-1		SW/MW-2		SE		SE/GC		E/MW	
Process	PCC		PCC		PCC		PCC		PCC	
	Cement Kiln		Cement Kiln		Cement Kiln		Cement Kiln		Cement Kiln	
Coke Type	Delayed (Blend)		Delayed (Blend)		Delayed (Blend)		Delayed (Blend)		Delayed (Blend)	
Properties	*Typical*	*Range*	*Typical*	*Range*	*Typical*	*Range*	*Typical*	*Range*	*Typical*	*Range*
(as-received)										
Moisture, wt%	5	2-10	5	1-10	7	1-24	8	5-14	8	7-13
(dry-basis)										
Proximate, wt%										
VCM	10.5	9.8-11.1	11	9-14	11	7-13	10.5	9-12	9.5	8.6-10.5
Ash	0.25	0.21-0.32	0.28	0.2-0.4	0.45	0.3-0.6	0.52	0.35-0.65	0.32	0.2-0.53
FC (by diff.)	89.2	88.7-90	88.6	87-90	88.5	87-92	89.0	87-91	90.2	89.3-91.2
Ultimate, wt%										
Sulfur	3.1	2.8-3.6	3.8	2.9-4.9	5	3.5-6.5	6.0	5-7	4.1	3.3-5.8
Carbon	-	-	89.8	-	-	-	86.8	85-89	89.9	89-91
Hydrogen	-	-	3.9	-	-	-	3.8	3.6-4.0	3.6	3.4-3.9
Nitrogen	-	-	1.3	-	1.8	1.4-2.2	1.7	1.5-1.8	1.5	1.1-2.2
Oxygen (by diff.)	-	-	0.92	-	-	-	1.2	-	0.58	-
Chlorine (ppm)	-	-	130	50-200	-	-	200	100-300	270	-
Metals, ppm										
Silicon	60	-	85	-	150	50-310	140	50-300	80	-
Iron	300	-	650	-	200	50-550	200	100-400	230	-
Vanadium	530	450-610	760	540-860	1400	1100-1900	1100	530-1650	730	600-890
Nickel	190	-	240	220-280	350	260-450	300	250-350	350	210-550
Aluminum	10	-	30	-	70	-	100	50-200	40	-
Calcium	80	-	90	-	-	-	150	50-300	160	-
Sodium	130	-	100	-	100	-	80	50-150	130	-
Calorific Value										
Btu/lb	15580	15360	15500	15350	15350	15170	15240	15050	15450	15350
		-15710		-15750		-15480		-15400		-15600
HGI	50	41-56	50	40-70	50	30-80	48	35-70	35	26-51
Shot, %	80	40-100	50	0-100	60	0-100	75	40-100	60	5-90
Size, wt%							(ROC)			
+40 mm	-	-	-	-	-	-	+30 mm	7-11	-	-
40x30 mm	-	-	-	-	-	-	30x15	7-82	-	-
20x12 mm	-	-	-	-	-	-	-15	10-85	-	-
12x6 mm	-	-	-	-	-	-	-	-	-	-
-6 mm	-	-	-	-	-	-	-	-	-	-
-200 mesh	-	-	-	-	-	-	-	-	-	-
Fuel Ratio	8.5	-	8.1	-	8.1	-	8.5	-	9.5	-

Table 2. FUEL PROPERTIES OF EXPORT DELAYED COKES USED IN POWER GENERATION

Industry Location	WC-E1		WC-E2		WC-E3		WC-E4		WC-E5	
Process	Export		Export		Export		Export		Export	
	PCC, etc.		PCC, etc.		PCC, etc.		PCC, etc.		PCC, etc.	
Coke Type	Delayed (Blend)		Delayed (Blend)		Delayed (Blend)		Delayed (Blend)		Delayed (Blend)	
Properties	*Typical*	*Range*	*Typical*	*Range*	*Typical*	*Range*	*Typical*	*Range*	*Typical*	*Range*
(as-received)										
Moisture, wt%	9	5-13	7	5-11	10	8-14	10	6-14	10	7-14
(dry-basis)										
Proximate, wt%										
VCM	11.5	10-13	10	9-11.5	11.5	10-13	11.5	10-13.5	10	9-12
Ash	0.2	0.1-0.4	0.4	0.3-0.5	0.35	0.3-0.6	0.45	0.3-0.6	0.35	0.25-0.45
FC (by diff.)	88.3	-	89.6	-	88.1	-	88.0	-	89.6	-
Ultimate, wt%										
Sulfur	0.8	0.7-1.1	1.2	0.9-1.4	1.3	1-1.8	2.7	2.5-3.1	2.9	2.3-3.4
Carbon	90.5	89.5-91.6	90.5	89.8-91.7	90.2	89-91	89.0	88.8-89.3	89.4	88.5-89.9
Hydrogen	4.1	3.9-4.3	3.9	3.8-4	4.0	3.8-4.2	3.9	3.8-4.1	3.9	3.7-4.1
Nitrogen	3.2	3-3.5	3.1	2.7-3.3	3.2	2.7-3.4	2.8	2.7-3.0	2.8	2.5-3.2
Oxygen (by diff.)	1.20	-	0.9	-	0.95	-	1.15	-	0.65	-
Chlorine (ppm)	150	90-280	180	110-320	-	-	-	-	200	90-270
Metals, ppm										
Silicon	80	20-240	110	60-260	150	50-360	100	30-200	70	40-220
Iron	230	120-380	340	290-430	270	180-400	300	170-500	350	160-640
Vanadium	270	230-330	600	450-720	550	470-720	900	690-1200	900	780-1060
Nickel	540	480-640	550	490-720	500	440-610	500	430-560	520	400-650
Aluminum	40	10-100	100	40-210	120	40-220	50	20-150	40	10-110
Calcium	50	20-110	190	170-220	230	90-400	150	90-300	100	50-210
Sodium	70	40-140	110	80-160	160	80-210	450	360-670	140	90-220
Calorific Value										
Btu/lb	15450	15300	15450	15350	15500	15400	15350	15200	15350	15200
		-15650		-15650		-15650		-15500		-15450
HGI	60	50-70	40	30-52	50	40-65	55	45-75	35	25-40
Shot, %	40	5-80	60	20-100	20	5-60	30	0-80	60	10-90
Size, wt%	(Fines)	(ROC)	(Fines)	(ROC)	(ROC)	(Lump)	(Fines)	(Lump)	(Fines)	(Lump)
+40 mm	-	-	-	2-6	-	-	-	13-47	-	3-17
40x30 mm	-	-	-	0-9	0-28	21-54	4-19	13-45	0	5-25
20x12 mm	-	-	0-1	9-26	0-15	10-36	7-32	10-34	3	11-89
12x6 mm	-	-	1-4	2-9	3-22	1-19	22-55	1-23	6	5-26
-6mm	-	-	96-99	65-98	39-88	1-49	30-61	1-39	91	11-55
-200 mesh	9	-	-	-	8	-	9	-	9	-
Fuel Ratio	7.7	-	9.0	-	7.7	-	7.7	-	9.0	-

Table 2. FUEL PROPERTIES OF EXPORT DELAYED COKES USED IN POWER GENERATION (Continued)

Industry Location	WC-E6		WC-E7		WC-E8					
Process	Export PCC, etc.		Export PCC, etc.		Export PCC, etc.					
Coke Type	Delayed (Blend)		Delayed (Blend)		Delayed (Blend)					
Properties	*Typical*	*Range*	*Typical*	*Range*	*Typical*	*Range*				
(as-received)										
Moisture, wt%	11.5	9-15	8	5-13	12	8-20				
(dry-basis)										
Proximate, wt%										
VCM	11.5	10-13	10	8-11	12.5	11.4-14.4				
Ash	0.2	0.18-0.33	0.18	0.08-0.41	0.31	0.26-0.44				
FC (by diff.)	88.3	87.2-89.8	89.8	88.4-91.3	87.2	86.2-88.3				
Ultimate, wt%										
Sulfur	3.5	2.4-5	2.9	2.6-3.2	4	2.7-5.2				
Carbon	89.7	88.5-90.8	90.7	89.8-91.4	89.5	88.5-90.5				
Hydrogen	3.9	3.7-4.1	3.8	3.7-3.9	3.8	3.6-3.9				
Nitrogen	2.0	1.7-2.4	1.6	1.4-1.8	2.1	1.7-2.4				
Oxygen (by diff.)	0.7	-	0.82	-	0.29	-				
Chlorine (ppm)	-	-	220	-	-	-				
Metals, ppm										
Silicon	70	20-230	60	20-190	70	40-130				
Iron	220	110-320	70	30-180	130	100-180				
Vanadium	370	300-560	370	300-440	1150	960-1280				
Nickel	310	250-400	180	130-230	460	430-600				
Aluminum	45	20-100	30	30-90	20	10-40				
Calcium	80	30-200	40	20-100	80	40-140				
Sodium	80	40-160	50	30-90	110	100-130				
Calorific Value										
Btu/lb	15520	15350 -15620	15500	15400 -15630	15400	15330 -15460				
HGI	80	60-96	55	35-75	70	54-83				
Shot, %	0	0-5	30	0-70	20	0-60				
Size, wt%	(Fines)	(ROC)	(Fines)	(Lump)	(Fines)	(Lump)				
+40 mm	8-18	3-15	0	13-30	-	-				
40X30mm	4-9	2-42	0	7-58	-	5-16				
20x12mm	9-13	3-20	1-4	4-30	-	15-25				
12x6mm	6-15	1-20	7-92	6-23	-	16-35				
-6mm	31-47	2-55	4-92	1-41	-	3-32				
-200 mesh	11	-	5	-	9	-				
Fuel Ratio	7.7	-	9.0	-	7.3	-				

Table 3. FUEL PROPERTIES OF EXPORT WESTERN COALS USED IN POWER GENERATION

Coal Source	I		II	III		IV	V
Process	Export PCC, etc.		Export PCC, etc.	Export PCC, etc.		Export PCC, etc.	Export PCC, etc.
Coal Type	Bituminous		Bitumin.	Bituminous		Bitumin.	Bitumin.
Properties	*Typical*	*Range*	*Typical*	*Typical*	*Range*	*Typical*	*Typical*
(as-received)							
Moisture, wt%	9.4	8.4-10.4	10.1	10.3	9.2-11.2	7.7	9.8
(dry-basis)							
Proximate, wt%							
VCM	41.1	39.5-42.7	40.8	40.3	39.8-41.2	41	40.2
Ash	10	8.6-10.9	9.8	9.7	8.6-10.8	9.2	9.9
FC (by diff.)	48.9	-	49.4	50		49.8	49.9
Ultimate, wt%							
Sulfur	0.53	0.43-0.62	0.52	0.42	0.36-0.52	0.5	0.6
Carbon	72.2	71.2-72.3	72.1	72.1	71.1-73.7	73.3	72.3
Hydrogen	5.4	5-5.5	5.3	5.0	4.7-5.2	5.5	5.2
Nitrogen	1.33	1.15-1.54	1.47	1.17	1.02-1.22	1.28	1.3
Oxygen (by diff.)	10.54	10.4-12	10.81	11.61	11.4-12.4	10.22	10.75
Chlorine (ppm)	150	100-300	100	100	-	150	120
Mineral of Ash, wt%							
Silica	58.6	52.5-61.7	56.7	52.3	50.4-54.1	58.6	56.1
Alumina	14.5	12-16.5	21	13.7	11.9-14.7	14.7	11.6
Ferric Oxide	5	2.9-7	4.9	5.9	5.3-6.2	4.4	5.7
Lime	10	7.7-14	5	13.1	10.7-15.3	8.9	13.1
Magnesia	1.8	1.6-2.1	1.9	2.2	2-2.5	2.4	2.4
Sodium Oxide	1.8	0.8-3	2.9	4.2	3.5-4.9	1.8	3.6
Potassium Oxide	1.2	0.5-1.5	1	0.4	0.2-0.8	1.1	0.7
Titania	0.7	0.5-0.9	0.8	0.9	0.8-0.9	0.7	0.8
Manganese Oxide	0.04	0.01-0.05	0.03	0.04	0.03-0.05	0.03	0.09
Calorific Value							
Btu/lb	12870	12750 -12990	12870	12640	12580 -12700	13360	12800
HGI	44	-	46	43	-	44	46
Size, wt%							
50 mm x 0 mm	100	-	100	100	-	96	92
2 mm x 0 mm	30.3	-	-	11.6	-	33	32.6
Fuel Ratio	1.2	-	1.2	1.2	-	1.2	1.2
Silica Ratio	0.777	-	0.828	0.712	0.68-0.75	0.789	0.726
B/A Ratio	0.268	0.18-0.4	0.2	0.386	0.34-0.45	0.251	0.372
Alkalies (Na2O), wt%	2.6	-	3.6	4.5	3.5-5.1	2.5	4.1
T250, deg F	2600	-	2760	2420	2400-2475	2700	2450
Ash Fusion T, deg F (Reduction/Oxidation)							
IDT	2192/2228		2221	2117/2149		2160	-
ST	2237/2291		2320	2128/2174		2250	-
HT	2300/2354		2383	2179/2220		2310	-
FT	2390/2444		2421	2294/2340		2410	-
Slagging Index	2147	2114-2224	2263	2114	2098-2180	2200	-
Fouling Index	1.8	0.8-3	2.9	4.2	3.5-4.9	1.8	3.6

ENVIRONMENTAL ASPECTS OF PRODUCING ELECTRICITY FROM A COAL-FIRED POWER GENERATION SYSTEM - A LIFE CYCLE ASSESSMENT

Pamela L. Spath
Maraget K. Mann
National Renewable Energy Laboratory
1617 Cole Blvd.
Golden, CO 80401

A life cycle assessment (LCA) of different coal-fired boiler systems was performed at the National Renewable Energy Laboratory in collaboration with the Federal Energy Technology Center. Three designs were examined to evaluate the environmental aspects of current and future coal systems. The boundaries of the analysis include all material and energy streams from the following three subsystems: coal mining, transportation, and electricity generation. Upstream processes required for the operation of these three subsystems were included as well as any necessary waste disposal and recycling opportunities. Both surface and underground mining were examined with the coal being transported from the mine to the power plant via rail, a combination of rail and barge, or truck. Additionally, a sensitivity analysis was conducted to determine the parameters that had the largest effects on the conclusions. This paper discusses the results of the life cycle assessment including resource consumption, air and water emissions, wastes, and energy requirements.

INTRODUCTION

Life cycle assessment is a systematic method to identify, evaluate, and help minimize the environmental impacts of a specific process or competing processes. Material and energy balances are used to quantify the resource depletion, emissions, and energy consumption of all processes between transformation of raw materials into useful products and the final disposal of all products and by-products. Three cases were examined for this coal-to-electricity LCA: 1) a plant that represents the average emissions and efficiency of currently operating coal-fired power plants in the U.S. (this tells us about the status quo), 2) a new coal-fired power plant that meets the New Source Performance Standards (NSPS), and 3) a highly advanced coal-fired power plant utilizing a low emission boiler system (LEBS). The overall system consists of coal mining, transportation, and electricity generation. Upstream processes required for the operation of these three subsystems were also included in this study. All three coal systems are fueled with the same type of coal, Illinois No. 6, which will be excavated from mines located in central Illinois. The coal is either surface mined via strip mining or mined by the underground technique of longwall mining. The coal is transported via rail, a combination of rail and barge, or truck. Four different transportation cases were evaluated for this assessment: average user by land, average user by river, farthest user, and mine mouth. Other materials such as chemicals and wastes are transported via truck and rail. The information about the methodology and the results contained in this paper are taken from a larger, more detailed report (Spath and Mann, 1998).

AVERAGE PLANT

The average coal power plant consists of the following main equipment/process steps: pulverized coal boiler, baghouse filter, conventional limestone flue gas clean-up (FGC) system, heat recovery steam generator (HRSG), and steam turbine. The emissions for this case represent the average emissions from all U.S. coal-fired power plants in 1995. These were calculated by dividing the total coal-generated U.S. emissions of a particular pollutant on a weight basis (kg) by the total electricity generated (kWh) from coal in the U.S. To maintain a mass balance around the power plant, a specific plant with emissions similar to the calculated averages and which is feeding the designated type of coal for this LCA was identified. The actual resource requirements, final emissions, and energy consumption from this specific plant were used to represent the average power plant in this study.

NSPS PLANT

Emissions for this case are calculated based on flue gas clean-up removal efficiencies such that the power plant meets the New Source Performance Standards (NSPS). The following are the standards of performance in g/GJ heat input on a higher heating value basis, with lb/MMBtu in parenthesis, for new electric utility steam generating units using bituminous coal: NOx = 260 (0.60), SOx = 258 (0.60), and particulates = 13 (0.03). These values were taken from the Code of Federal Regulations, 40 CFR 60.42a, 60.43a, and 60.44a; new plants built after 1978 are required to meet these standards. Except for higher pollutant removal efficiencies achieved through boiler modifications and more advanced clean-up technologies, the process configuration for this case is the same as that for the average plant.

LEBS PLANT

Emissions for this case are those forecasted from a future plant utilizing a Low Emission Boiler System (LEBS). LEBS is projected to have significantly higher thermal efficiency, better performance, and a lower cost of electricity than current coal-fired power plants. The technology being considered in this assessment is by the developer DB Riley Inc., and is being researched under the Department of Energy's sponsorship. The objective of the LEBS program is to produce technologies that result in lower emissions such that the NOx and SOx emissions are 1/6 of the NSPS and the particulate emissions are 1/3 of the NSPS. The DB Riley technology uses a low-NOx system with advanced burners, air staging, and a wet ash slagging system. The copper oxide flue gas clean-up process utilizes a regenerable sorbent, removing both SO_2 and NOx from the flue gas and producing sulfuric acid or sulfur as a by-product instead of producing a solid waste. The sorbent is regenerated using natural gas as the reducing agent.

COAL MINING

For this study, both strip mining and underground longwall mining were examined. The resources, emissions, and energy use associated with the excavation of the coal were included in this LCA. The processes studied include raw material extraction, equipment manufacture, coal mining, coal preparation/cleaning, all necessary transportation of chemicals, etc., and all necessary upstream processes. The resources, energy, and emissions associated with the mining equipment are based on the types of machinery used for each coal excavation process, the fuel requirements, and the lifetime of the machinery. Additionally, the process steps involved in land reclamation are included in the surface mining option. Overall, the environmental impacts from surface versus underground mining are not significantly different in any of the three power plant cases examined (average, NSPS, and LEBS). The main difference between these two mining techniques is that the surface mining subsystem results in a higher amount of airborne ammonia emissions due to the production of ammonium nitrate explosives which are used at the mine. Another important difference is that underground mining requires limestone which emits a large amount of particulates during its production. Therefore, results in this paper are presented for the surface mining cases only.

COAL TRANSPORTATION CASES

The inventory assessment for the transportation subsystem includes the energy required and emissions generated for the transportation of coal by barge, train, or truck between the boundaries of the coal mining and power generation subsystems. The resources, energy, and emissions related to extracting crude oil, distilling it, producing a usable transportation fuel, and distributing it to refueling stations plus the emissions produced during combustion of the fuel were included in the total inventory. The material requirements for each of the various modes of transportation were used in determining the resources, energy, and emissions associated with vehicle production and decommissioning.

The following four transportation cases were examined for this study: (1) average user by land: railcar = 483 km, (2) average user by river: railcar = 48 km plus barge = 435 km, (3) farthest user: railcar = 1,538 km plus barge = 504 km, and (4) mine mouth: minimal truck transport = 2 km. The average user by land was determined based on the fact that most of the utilities serviced from the Perry County region fall within the distance of 483 km, which is the rail distance from E. St. Louis to Chicago. This distance also includes at least parts of the states of Illinois, Wisconsin, Iowa, Indiana, Kentucky, Alabama, Mississippi, and Missouri. When considering barge transport, the coal must first be hauled 48 km by rail to the Mississippi River before being loaded onto a coal barge. The barge distance of 435 km listed above for the average user by river case reaches up the Mississippi River to Iowa or down the river to the state of Mississippi and could include traffic up the Ohio River. The farthest user consists of rail transport to the Mississippi River (48 km) then river transport to Memphis, Tennessee (504 km) and finally rail transport to central Florida (1,490 km). The transferring of coal between rail and barge was not included but should be minimal compared to the actual transportation of the coal.

RESULTS: RESOURCE REQUIREMENTS

Fossil fuels, metals, and minerals are used in all of the processes steps required to convert coal to electricity. In terms of resource depletion, coal is used at the highest rate. For the average and NSPS cases, limestone and oil account for the majority of the remaining resources consumed compared to the LEBS case, where the bulk of the remaining resource consumption is natural gas and oil. Table 1 shows the majority of the resources used for each coal case studied.

Table 1: Resource Consumption

Resource	Average		NSPS		LEBS	
	% by	g/kWh	*% by*	g/kWh	*% by*	g/kWh
Coal	*80.4*	474.44	*78.0*	433.84	*97.3*	352.49
Limestone	*17.4*	102.84	*19.7*	109.49	*0.0*	0.04
Oil	*1.9*	11.48	*2.0*	11.32	*1.3*	4.88
Natural gas	*0.2*	1.25	*0.2*	1.26	*1.3*	4.53

(a) Numbers are reported for the surface mining case. However, the underground mining numbers are similar to those listed above.
(b) Transportation = average user by river.
(c) Percent of total resource consumption. Not all resources consumed by the system are shown; therefore the numbers do not add up to 100%.
(d) Resource consumption per kWh of net electricity produced averaged over the life of the system.

RESULTS: AIR EMISSIONS

In terms of total air emissions, CO_2 is emitted in the greatest quantity accounting for 98-99 wt% of the total air emissions for all cases examined. The following are the total CO_2 emissions for the average, NSPS, and LEBS case: 1,022 g/kWh, 941 g/kWh, and 741 g/kWh of net electricity produced. The majority of the CO_2, greater than 95%, is emitted from the power plant subsystem during operation of the coal-fired plant. As shown in Table 2, the next highest air emissions include particulates, SOx, NOx, CH_4, CO, and NMHCs. In all three coal cases the power plant produces most of the SO_x, NO_x, and CO while the methane comes primarily from the coal mine. For the average and NSPS case, the majority of the particulates come from the production of limestone. For the LEBS case, the majority of the particulates are emitted by the power plant during normal operation and the second major source of particulates is copper oxide production. For all three cases, the NMHC emissions are evenly distributed among the mining, transportation, and power plant subsystems. However, for the LEBS case it should be noted that a significant amount of the total NMHC emissions are emitted during natural gas production.

Table 2: Air Emissions (Excluding CO2)

Air	Average		NSPS		LEBS	
	% by	g/kWh	*% by*	g/kWh	*% by*	g/kWh
Particulates	*44.3*	9.21	*61.0*	9.78	*4.4*	0.11
SOx	*32.2*	6.70	*15.7*	2.53	*28.0*	0.72
NOx	*16.1*	3.35	*14.6*	2.34	*21.3*	0.54
CH_4	*4.4*	0.91	*5.2*	0.84	*27.9*	0.75
CO	*1.3*	0.27	*1.5*	0.25	*7.5*	0.19
NMHCs (e)	*1.0*	0.21	*1.3*	0.20	*7.5*	0.19

(a) Numbers are reported for the surface mining case. However, the underground mining numbers are similar to those listed above.
(b) Transportation = average user by river.
(c) Percent of total air emissions *excluding* CO_2 emissions. Not all resources consumed by the system are shown; therefore the numbers do not add up to 100%.
(d) Air emissions per kWh of net electricity produced averaged over the life of the system.
(e) NMHCs = non-methane hydrocarbons including volatile organic compounds (VOCs).

RESULS: WATER EMISSIONS AND WASTES

For all three coal cases, the majority of the water emissions from the system occurred in the mining and power plant subsystems. The water emissions were evenly distributed between these two subsystems. In general, though, the total amount of water pollutants was found to be small compared to other emissions.

A large amount of the solid waste in the average and NSPS cases comes from the power plant in the form of flue gas clean-up waste and ash that must be landfilled, 58-61% and 20-23% of the total waste, respectively. For these two cases, non-hazardous solid waste accounts for the balance of the total waste and the majority of this waste is generated during limestone production. The flue gas clean-up process for the LEBS case utilizes a regenerable sorbent, therefore, the bulk of the waste

from this system is ash which accounts for 87-93% of the total waste. The remaining waste for the LEBS case is non-hazardous solid waste which primarily comes from the mining operations.

RESULTS: ENERGY

The energy use within the system was tracked so that the net energy production could be assessed. Several types of efficiencies can be defined to study the energy budget of the coal system. The first being the power plant efficiency defined in the traditional sense as the energy delivered to the grid divided by the energy in the feedstock to the power plant (coal and natural gas in the LEBS case). Four other types of efficiencies can be defined as follows:

Table 3: Energy Efficiency and Ratio Definitions

Life cycle efficiency (%) (a)	External energy efficiency (%) (b)	Net energy ratio (c)	External energy ratio (d)
$=\frac{Eg-Eu-Ec-En}{Ec+En}$	$=\frac{Eg-Eu}{Ec+En}$	$=\frac{Eg}{Eff}$	$=\frac{Eg}{Eff-Ec-En}$

where:
Eg = electric energy delivered to the utility grid
Eu = energy consumed by all upstream processes required to operate power plant
Ec = energy contained in the coal fed to the power plant
En = energy contained in the natural gas fed to the power plant (LEBS case only)
Eff = fossil fuel energy consumed within the system (e)

(a) Includes the energy consumed by all of the processes.
(b) Excludes the heating value of the coal and natural gas feedstock from the life cycle efficiency formula.
(c) Illustrates how much energy is produced for each unit of fossil fuel energy consumed.
(d) Excludes the energy of the coal and natural gas to the power plant.
(e) Includes the coal and natural gas fed to the power plant since these resources are consumed within the boundaries of the system.

The net energy ratio is a more significant measure of the net energy yield from the system than the external energy ratio because it accounts for all of the fossil energy inputs. The following table contains the resulting efficiencies and energy ratios for each coal case.

Table 4: Efficiencies and Energy Ratio Results

Case (1*, 2*)	Power plant efficiency (%) (3*)	Life cycle efficiency (%) (3*)	External energy efficiency (%) (3*)	Net energy ratio	External energy ratio
Average	32	-76	24	0.29	5.0
NSPS	35	-73	27	0.31	5.1
LEBS	42	-66	34	0.38	6.7

(a) Coal LCA numbers are reported for the surface mining case. However, the underground mining numbers are similar to those listed above.
(b) Transportation = average user by river
(c) Efficiencies are on a higher heating value basis.

One of the most surprising results of this study was that upstream processes consumed such great quantities of energy. Intuitively obvious is the fact that because the power plant efficiency is less than one, the net energy ratio, which includes the energy in the coal consumed by the power plant, will be a fractional value. However, in subtracting out the energy of the coal feed in the external energy ratio, one would expect the results to be much higher than they are. However, in the average and NSPS cases, limestone production was found to require a significant amount of energy; in the LEBS case, excluding the coal feed, the majority of the total energy is used in natural gas production. Limestone production accounts for 25% and 28% of the total system energy consumption for the average and NSPS cases, respectively, and for the LEBS case natural gas production accounts for 37% of the total system energy consumption.

For all three cases examined (average, NSPS, and LEBS), a large amount of energy was also consumed by the transportation subsystem (except for the mine mouth case), primarily from the energy required to extract crude oil, distill it, produce a usable transportation fuel, and distribute it to refueling stations. The following percentages are for surface mining and transportation via the average user by river case. For all three power plant cases the energy consumption for the fuel required to transport the coal by a combination of train and barge accounts for 30-33% of the total system energy consumption.

SENSITIVITY ANALYSIS

A sensitivity analysis was conducted to determine the parameters that had the largest effects on the results and to determine the impact of estimated data as well as variations in data on the conclusions. The following variables had the largest effect on resource consumption, emissions, and energy usage: reducing the power plant construction materials, changing the power plant operating capacity factor, and increasing or decreasing the transportation distance. Varying the amount of mining methane emissions had a large impact on the overall methane emissions from the system, however, this variable will be site-specific and ultimately should be examined on a case by case basis. Changing the power plant efficiency or changing the coal transport distance are the only variables that had a noticeable effect on the efficiency and energy ratio results. In all sensitivity cases tested, however, the net energy ratio varied by only small amounts, mostly due to the energy in the coal feed, the energy consumed in limestone and natural gas production, and the energy used in transportation. For the average, NSPS, and LEBS cases, the net energy ratios range from 0.24 - 0.33, 0.27 - 0.36, and 0.33 - 0.42, respectively.

CONCLUSIONS

Overall, the environmental impacts from surface versus underground mining are not significantly different in any of the three power plant cases examined (average, NSPS, and LEBS). As expected, the majority of the overall methane emissions come from the mine itself. However, as stated above these emissions are site-specific and ultimately should be evaluated on a case by case basis. Additionally, about half of the system's water emissions come from the mining subsystem.

For the average and NSPS cases a large amount of the total energy requirement for the power generation subsystem comes from limestone production whereas for the LEBS case the majority of the total energy is required for natural gas production. Therefore, even with increased power plant efficiency, the overall system energy balance of coal-fired power plants will not increase significantly unless technologies can be developed to reduce upstream energy consumption.

Of the three subsystems examined (coal mining, transportation, and electricity generation), transportation required the least amount of resources and had the lowest air, water, and solid waste emissions even when considering the farthest user case. However, the energy consumption for this subsystem was significant (excluding the mine mouth case). As anticipated, for mine mouth operation, all resource consumption, emissions, and energy usage are a small percentage of the total over the life of the system. For the other three transportation cases (average user by river, average user by land, and farthest user) oil consumption as well as a few air and water emissions are high. It was found that the transportation distance has a significant effect on the oil consumption, a few of the system's emissions, and the energy consumption whereas the mode of transportation has virtually no effect on the results.

In all three coal cases the power plant produces the majority of the SO_x, NO_x, and CO. Also, half of the water emissions occurred in the power plant subsystem. Most of the solid waste in the average and NSPS cases comes from the power plant in the form of flue gas clean-up waste that must be landfilled. For these two cases there is also a high percentage of ash which is landfilled and limestone production produces a considerable amount of non-hazardous solid waste. The flue gas clean-up process for the LEBS case utilizes a regenerable sorbent, therefore, the primary waste from this system is ash. As expected, the LEBS plant requires fewer resources and energy and produces fewer emissions and waste per unit of energy delivered to the utility grid than the average or NSPS cases. The life cycle efficiency, external energy efficiency, net energy ratio, and external energy ratio are similar for the average and NSPS plant. The energy efficiency and ratio numbers are all somewhat higher for the LEBS.

FUTURE WORK

The primary goal of this life cycle assessment was to assess the environmental aspects of producing electricity from a coal-fired power system. The focus of this initial work was on an inventory of all resources, environmental emissions, and energy flows of the system, studied in a cradle-to-grave manner. Therefore, a comparative analysis was not performed at this time. Ultimately, the resulting emissions, resource consumption, and energy requirements of this system will be compared to a previously completed LCA of electricity production from a biomass gasification combined-cycle (BIGCC) power plant (Mann and Spath, 1997) and a study currently being conducted which involves co-firing biomass in a coal-fired boiler.

REFERENCES

1. P.L. Spath and M.K. Mann. (1998) "Life Cycle Assessment of Coal-fired Power Production," National Renewable Energy Laboratory, Golden, CO. TP-570-25119.

2. Office of the Federal Register National Archives and Records Administration. (1996) *Code of Federal Regulations. Protection of Environment.* Title 40. Part 60, July.

3. M.K. Mann and P.L. Spath. (1997) "Life Cycle Assessment of a Biomass Gasification Combined-Cycle Power System," National Renewable Energy Laboratory, Golden, CO. TP-430-23076.

ECONOMIC PLANT PRODUCING TRANSPORTATION FUELS & FEED FOR CARBON PRODUCTS FROM COAL

Theodore B. Simpson
U.S. Dept. Of Energy, Fossil Energy Division, Office of Coal Fuels and Industrial Systems
Washington, D.C. 20585

INTRODUCTION

The U.S. needs a stable supply of environmentally clean, affordable fuels. After the oil embargo and gasolene shortage of the early 1970's when oil reached a price of $35/bbl, the U.S. Dept of Energy (DOE) intensified its work on making transportation fuels by the direct liquefaction of coal, which is the most abundant energy source in the U.S. Continuing improvement in this technology has resulted in confidence in the advanced technology developed on a small scale (to 3TPD.) This evolutionary development ran from bench scale and the Cresap, PA, donor solvent pilot plant in the '70's to the Ft. Lewis, WA, Solvent Refined Coal pilot plant and the Wilsonville, AL, 3TPD process demonstration unit (PDU) in the late 1970's to the demonstration plant program (approximately 200 TPD) in the early 1980's. Thereafter, Exxon offered commercial licenses without any takers, and the program slowed down to further bench-scale and PDU tests at Wilsonville and its successor, Hydrocarbon Technologies, Inc (NJ.)

Further scale-up remains needed, however, to establish commercial readiness. But, partly as a result of improved techniques for exploration for petroleum, world reserves have expanded, mostly in developing nations whose economic needs have pushed marketing and driven oil prices down to about $14/bbl. Nonetheless, Table 1[a] shows that projections are that not only will oil prices increase, but also supply will start to decline starting at about the year 2020 while demand will steadily increase. This would lead in the absence of new factors to an inevitable rapid increase in price. If a partial solution is found in the conversion of coal, Table 1 shows that an expected decline in the cost of coal should be a mitigating factor.

APPROACH

The present price of about $14/bbl is a much more difficult target for liquids from coal. This has led DOE to look for profitable co-products to improve the economics of the liquefaction process. A particularly attractive one of these is a heavy, clean hydrocarbon pitch suitable as feed to make carbon products. In addition to such million-tons/yr markets for carbon products as anode coke for the aluminum industry and graphite anodes, there is the rapidly growing need for feed for manufacturing Carbon Fibers for use in composite materials. These carbon fibers and composites thereof have an unusual combination of superior strength and light weight. As a consequence this is likely to lead to their becoming commodity materials used for structural members and bodies for high mileage cars. This in turn could result in a dramatic reduction in emissions from vehicles as well as a significant decrease in the cost of their fabrication. Another desirable outcome is that the carbon products produced tie up carbon for an extended period and reduce the emissions of the Greenhouse Gas, CO2, that would result if the product were fuel.

This paper describes a proposed giant step in process development/demonstration based on data developed in the 1980's by DOE with the 3 TPD Wilsonville, AL, coal liquefaction PDU (b.) Liquefying coal requires its dissolution, liquefaction at ~ 825F and 2000 psi hydrogen pressure, plus deashing either by filtration or critical solvent deashing, and further selective hydrotreating to produce light hydrocarbons without over cracking them. With the carbon-product pitch as a valuable co-product obtained as a bottom of the barrel product of the first of the two stages, further selective hydrocracking of this co-product is no longer required so that the complexity of the process and its severity and hydrogen requirement are significantly decreased. Figure 1 compares the two process variants. Instead of two expensive slurry bed catalytic stages and ash separation as presently specified to produce an all distillate product, a thermal reaction stage, ash separation and a fixed catalytic stage suffice. Fixed bed catalysis has been estimated to cost one-fifth of the cost of ebullated bed catalytic reactors. With removal of the first stage heavy fraction as a source of the Carbon Product feed, the cost of the second stage fixed bed catalytic reactor will be smaller and cheaper. As a result the process economics are estimated to be significantly improved.

DATA

Table 2 compares the conditions selected for the 1982 one product configuration vs. the proposed co-product plant. As stated the primary source of cost reduction is reduction in the amount and hence cost of hydrogen. In the present one product, "all distillate" plant, the hydrogen cost has been estimated to be one-half of the total cost of the conversion of coal to distillate hydrocarbon fuels or

$15/bbl of product. Table 3 lists the ways in which hydrogen requirement is reduced. The lower severity (temperature, pressure, residence time) results in a drop in C1-C4 gaseous hydrocarbons which require much hydrogen but have little more than fuel value. The decrease is estimated to be from 7% to 3% on feed coal with an average composition of CH3 giving a 1.65% drop in total H2 needed. Moreover, for a process requiring a total residence time of one hour or more, its reduction to reduce severity would help. This should work since the PDU testing included a successful short contact time thermal stage of a few minutes. A more significant decrease in hydrogen requirement results from the conversion of the feed coal with its average composition of CH0.7 to essentially pure carbon at about 800C which otherwise would need an added 1.2 atoms of H to convert them to liquids. This 1.9 H/C savings cuts the hydrogen cost by $10.50 and the product cost to $20/bbl of fuel plus carbon product carbon equal to that in one bbl of fuel which assumes that the carbon has the same value as the oil. Therefore, it was assumed that Carbon products will be 40% of the product slate. The hydrogen formerly found in the coal is recovered when it reports upon the conversion to Carbon Products largely as aromatic distillates that are suitable as part of the fuels product or as chemical products.

DISCUSSION

A reasonable approximation is that the revenue requirements of a co-products plant is the same as the one-product plant. For the one-product plant the revenue requirement equals the typical 4 Bbl/Ton of feed coal at the above reduced price of $20/Bbl made possible by making 0.4 Tons of C-Products/Ton of feed coal giving $80/Ton of feed coal as the required revenue per ton of feed coal. Table 4 gives possible options for pricing of the two co-products that each generate the needed revenue. This shows that the oil product can be priced competitively even with the existing world petroleum prices of $10-14/bbl with the last set of co-product prices shown. The Carbon Product feed price is also realistic since Table 4 shows that with the oil product priced at $10/bbl the required price of C-Product feed is $140/ton of Carbon Product ($0.07/lb.) vs. a carbon fiber manufacturer's estimate that his feed cost is $1.80/lb. for carbon fibers. Table 4 also shows the ability to exercise pricing flexibility, i.e. the capability of the processor to follow the ups and downs in world petroleum prices in order to maximize profitability even as is the case in the pricing of gasolene by the petroleum industry. This compares with $30/bbl oil needed for a single product plant at a 20% ROI. No credit has been taken for the simpler process and reduction in process severity.

CONCLUSIONS

Added R&D will be needed (1) to redefine the conditions required for the two product plant though no dramatic changes are indicated, (2) to demonstrate the integrated process for valuable co-products, (3) to confirm the economics, and (4) to confirm marketing estimates. Ongoing tests by a DOE contractor (CCP) will continue in order to confirm the suitability of the carbon product feeds and carbon products produced. Carbon fiber composites are already common for tennis rackets, for golf clubs, and for aircraft parts. Work on production and marketing of carbon products for automobile and structural applications will be needed. A life cycle study has been reported[(c)] of the use of carbon product composites for automobile manufacture taking into account ease of fabrication, fuel economy, etc to determine the price of carbon fibers at which their use for this application is justified. The study concludes that this price is $5 to $7.50/lb. A major manufacturer has indicated that it already prices carbon fibers at $8/lb. to large users and expects to achieve $5/lb. in the year 2000.

If the proposed added work confirms the above conclusions as to supply-demand for fuels, competitive position of carbon fiber composites for high volume markets, and capability of direct coal liquefaction to supply low cost carbon product feed, a number of important, significant improvements should result. In transportation, use of light weight vehicles manufactured from carbon fiber composites having reduced emissions and lower operating cost will grow. In the fuels area, the coal liquefaction co-product plants will add to domestic fuel resources and create domestic jobs that otherwise would continue their decline. With respect to the future of U.S. coal such co-product plants will speed up utilization of this large domestic energy resource in an environmentally safe manner.

REFERENCES

(a) U.S. D.O.E. and/or contractor estimates, 1997,1998.
(b) U.S.D.O.E. Report DOE/PC/50041-55, Sept, 1985,
(c) A.E.Mascarin & M.M.Brylawski, http://www.rmi.org/hypercars/b_i_w/T95_35.html, 1998

Table 1:PROJECTED RESOURCE BASE CONSUMPTION AND PRICE OF ENERGY THROUGH 2020[1] AND BEYOND[2]

	1996	2000	2005	2010	2015	2020	2040	2060
U.S. Consumption, B/D	18.44	19.62	21.15	22.70	23.65	24.39	----	----
Oil Price, $/B	20.48	19.11	20.19	20.81	21.48	22.32	----	----
Coal Price, $/Ton	27.52	25.80	24.40	23.12	21.76	20.56	----	----
World Product Capability, B/D	75.0	81.0	87.0	93.0	98.0	100.0	55.0	12.0

(1) DOE Energy Information Agency (1998)
(2) DOE Energy Information Agency, as supported by Mitretek (1998)

TABLE 2: CURRENT AND 1982 SINGLE PRODUCT PLANTS VS 1982 CO-PRODUCT PLANTS
(All %'s based on feed coal)

Type Plant:		1982 Single Prod.344b-g	1982 Single Prod., Short Contact,242	Calc'd 1982 Co-prod, Short Contact Time	Current Single Dist. Prod.
	Proc Stage 1				
	Reactor Size	8	2	2	8
	Space Rate, lb/hr,sq ft	40	95	95	40
	Pressure, psi	2400	2400	2400	2400
	Temperature, F	825	825	810	825
	Hydrogen Used, %	1.5	0.7	0.7	3.
	C1/C3 Gas Make,%	4.2	3.3	2.0	4.5
	% C-Prod. Feed or % Resid	5 resid	5 resid	55	5 resid
	Distillables, %	55	28	20	58
	Entire Process				
	Hydrogen Used, %	5	5	2.3	7
	C1/C4 Gas Make, %	7	5	3	7

TABLE 3: WAYS IN WHICH HYDROGEN REQUIREMENT IS REDUCED
(All %'s are % of Feed Coal)

Means of Reducing H2 Requirement	H2 Requirement, Current Single Product Plant	H2 Requirement, Proposed Two Product Plant	Estimated Savings: % H2 on Coal & $/Bbl Equiv.
Reduced "CH3" Gas Make	7.0%	3.0%	0.8% & $1.65/Bbl
H2 Released by "CH.7" Coal Converted to C-Products	0	1.9%	1.9% & $3.20/Bbl
Avoid 1.2 H/C Needed to Convert Above Coal to "CH2" Distillates	0	2.8%	2.8% & $6.00/Bbl
TOTAL SAVINGS			**$10.60/Bbl**

Basis:
(1) Upon the high temperature version of C-Products feed to carbon products essentially all the hydrogen reports as volatized hydro aromatic distillate product.
(2) Estimated 40% of Feed Coal to C-Product Feed

TABLE 4: RESULTANT CO-PRODUCT COSTS

CASE I: MAKE 0.4T. C-PRODUCT+ (0.6)(4 BBL/T) OIL PER TON OF FEED COAL
ASSUME TOTAL PROCESS COST = ($30 - $10 SAVINGS)(4 BBL/T COAL)

Assumed Price of Heavy Oil for C-Product, $/T. C-Product	Resultant Product Oil Cost $/Bbl
100	16.7
50	25.0
75	21.0
140	10.0

Basis: $\frac{0.4 \text{ T. C-Prod} + 2.4 \text{ Bbl Oil}}{\text{T. Coal Feed}}$

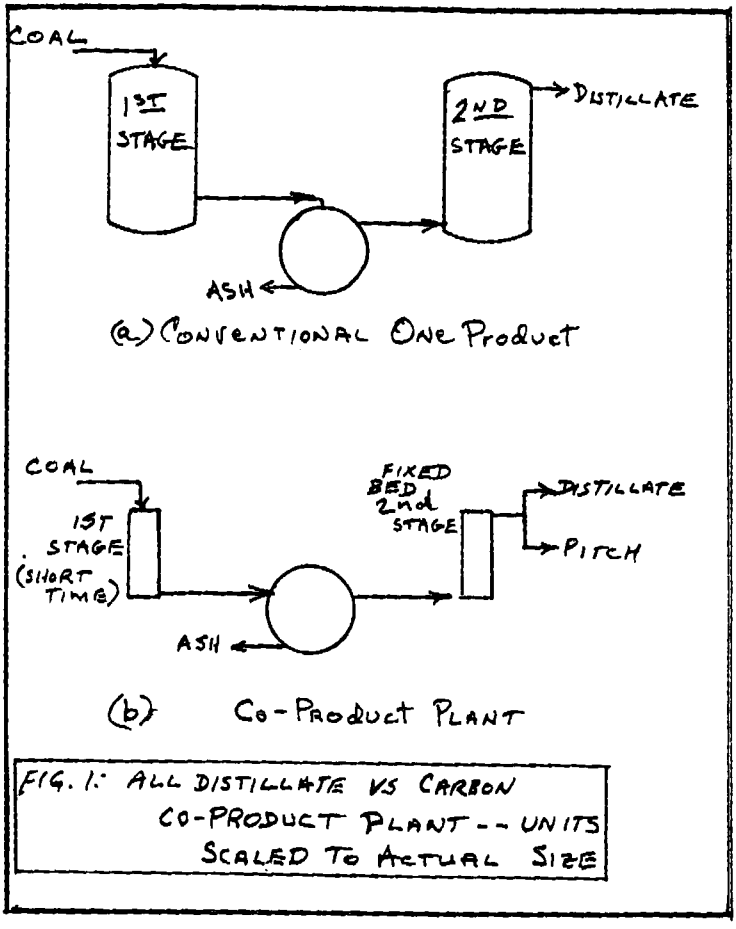

FIG. 1: ALL DISTILLATE VS CARBON CO-PRODUCT PLANT -- UNITS SCALED TO ACTUAL SIZE

ASSESSING CONDENSED AROMATIC COAL MATERIALS AS PRECURSORS FOR HIGH-VALUE CARBON PRODUCTS

M. Mercedes Maroto-Valer[1], Darrell N. Taulbee[2] and Harold H. Schobert[1]

[1]The Energy Institute, The Pennsylvania State University, 405 Academic Activities Bldg, University Park, PA-16802. [2]University of Kentucky - Center for Applied Energy Research, 2540 Research Park Drive, Lexington KY 40511

Keywords: unburned carbon, anthracite, activated carbons.

The increasing role of coal as a source of energy in the 21st century will demand environmental and cost-effective strategies for the use of carbonaceous waste products from coal combustion. Accordingly, this paper demonstrates the ability of unburned carbon from coal combustion waste to generate activated carbons by steam activation. Non-fuel uses of coal will also become more important in the coal industry of the next century. In particular, significant growth potential exists for the production of adsorbent carbons with molecular sieve properties. Anthracites can easily be tailored for this specific purpose due to their inherent fine structure.

INTRODUCTION

The US electric power industry relies heavily on the use of coal as the primary energy source. In 1997, around 90% of the total US coal production was used in coal-fired units to generate over 55% of the total electricity [1]. Furthermore, coal is the most abundant fossil fuel resource in the US, and therefore it will even play an increasing role as a source of energy in the 21st century [2]. However, the use of coal for energy generation faces environmental challenges due to the emissions of pollutants such as NOx and SOx by coal combustion furnaces. Moreover, environmental pressures will only intensify in the next century and to guarantee a key role of coal as energy source, the conventional processes for coal utilization have to be redesigned to comply with clean air regulations. In particular, the implementation of these regulations concerning NOx emissions is being addressed in coal combustion furnaces mainly by a combination of low-NOx burners and catalytic reduction systems. Although low-NOx burner technologies efficiently decrease the emissions level by lowering the temperature of combustion, they also reduce the combustion efficiency, with a corresponding alarming rise in carbonaceous waste product from coal combustion [3]. In 1997, the combustion of 830 million tonnes of coal generated around 75 million tonnes of coal combustion by-products (CCBPs), mainly fly ash containing unburned carbon [4]. Due to the present lack of routes for their effective use, the fate of these products is mainly disposal. However, the increasingly severe regulations on disposal and the limited access to new disposal sites with the subsequent increase in the cost of disposal, will force the coal and energy industry to recycle a larger amount of CCBPs. Consequently, there is a clear need to establish environmental and cost-effective strategies for the use of these carbonaceous waste products from coal combustion.

The carbonaceous residue in fly ash, unburned carbon, is a potential precursor for the production of adsorbent carbons, since it has gone through a devolatilization process while in the combustor, and therefore, only requires to be activated. However, for new precursors to compete effectively with the conventional raw materials like wood, they must have a low cost, low mineral matter content and easily be converted into activated carbons [5]. The unburned carbon in the ash furnishes satisfactorily all these conditions, since it can readily be obtained from the utility industries as a by-product, it can be beneficiated

from the fly ash by commercially available techniques and it has already gone through a devolatilization process in the combustor and, therefore, only requires to be activated. However, no attempt to activate this carbonaceous waste has been conducted thus far.

In addition to the major use of coal as a fuel source, non-fuel uses like production of high-value chemicals and premium carbon products, will also become more important in the coal industry of the next century [2]. Significant growth potential exists for the use of coal as precursor for the production of activated carbons, due to the continuos worldwide growing demand for adsorbent materials. The main reason for this expanding market is the ubiquitous use of activated carbons as adsorbent materials in a broad range of increasing household, medical, industrial, military and scientific applications, that range from gas-phase adsorption in household air conditioning equipment and industrial emissions control, to liquid-phase adsorption for water treatment and even gold recovery. Each application is associated with a specific set of properties of the activated carbon, and precursors that can easily be converted into the required adsorbent materials will excel. This is the case of anthracites, since their fine pore structure makes them excellent raw materials for the production of adsorbent carbons with molecular sieve properties for gas separation in pollution control technologies [6]. However, the use of anthracites as precursors for adsorbent materials is being under-exploited, probably due to the limited number of studies assessing the possible routes for their conversion into activated carbons.

This work addresses the potential use of both unburned carbon from coal combustion and anthracites as precursors for adsorbent carbons. Both materials have highly condensed aromatic structures with a low volatile content. A single step carbonization/activation process was used for the activation of these materials, using steam as the activating agent. The porosity of the resultant activated carbons was characterized by conducting N_2 isotherms at 77K.

EXPERIMENTAL PROCEDURE

Samples A fly ash containing unburned carbon was collected from the mechanical precipitators of unit #3 (70 MW) of the Dale power plant (Eastern Kentucky Power). The sample was screened with a 140 mesh sieve (106 μm), with the 140+ fraction being triboelectrostatically separated to obtain a carbon-enriched sample with a glass content of ~ 10 % volume, as determined by petrography [3]. A detailed description of this unburned carbon sample (UC) is given elsewhere [3]. The Pennsylvania anthracite (A) selected for this study contains 6.8 % ash (db) and the atomic H/C ratio is ~ 0.19. Previous studies conducted by the authors have shown that the particle size of the starting anthracite was the most critical variable that affects the properties of the resultant adsorbent carbon. Accordingly, for this study the anthracite was ground and sieved to obtain a particle size fraction 250-150 μm.

Activation procedure The activation of the samples was carried out in an activation furnace, that consists of a stainless steel tube reactor and a vertical tube furnace, similar to the one used previously by the authors [6]. Small modifications were made in the previous design to improve the flow of steam throughout the reactor and to be able to work with a significant smaller particle size. Typically 3 - 5 g of sample was held isothermally at 850° for periods of 60 (UC-60 and A-60) and 90 (A-90) minutes while flowing steam. A reservoir was used to pump water into the reactor at low flowrates by introducing a slight head pressure of nitrogen. The flowrates used were 0.3 and 1.2 g of water/min for the unburned carbon and anthracite, respectively.

Porosity measurements N_2 adsorption isotherms at 77K were conducted in Quantachrome adsorption apparatus, Autosorb-1 Model ASIT. The BET surface areas (SA) were calculated using the adsorption points at the partial pressures 0.1

- 0.3. For the activated samples, the total pore volume, V_{TOT}, was calculated from the amount of vapor adsorbed at partial pressure 0.95.

RESULTS AND DISCUSSION

Inherent porosity of the raw materials Figure 1 shows the N_2-77K adsorption isotherms for the raw unburned carbon (UC) and anthracite (A) and illustrates the different inherent porosity of these materials. The adsorption isotherm of the unburned carbon (UC) sample is a Type II isotherm according to the classification of Brunauer, Deming, Deming and Teller (BDDT) [7]. This Type II isotherm is typical for nonporous or macroporous adsorbents, on which unrestricted monolayer-multilayer adsorption can occur, and the inflexion point of the isotherm indicates completion of monolayer and the onset of multilayer coverage. Pore size distribution studies have shown that the porosity of this UC sample is mainly due to meso- and macropores, with pore widths typically over 40 nm. In contrast, the adsorption isotherm of the anthracite (A) is Type I (Figure 1), corresponding to a microporous system, as expected due to the well-known fine structure of anthracites. However, this isotherm also presents a tail as saturation pressure is approached, indicating the presence of some macropores.

Table 1 lists the BET surface areas (SA) for the precursors. The unburned carbon sample has a SA of 40 m^2/g, compared to only <1 m^2/g for the anthracite. The reason for the higher SA of the unburned carbon is probably due to the generation of porosity by the combustion process. The extensive and rapid devolatilization that coal undergoes in the combustor, seems to promote the generation of meso- and macropores.

Development of activated carbons from unburned carbon and anthracite All the samples were activated at 850°C for periods of 60 (UC-60 and A-60) and 90 (A-90) minutes. Table 1 lists the solid yields of the activated samples. As expected, when comparing samples with the same activation time, UC-60 and A-60, the UC presents a much higher solid yield than the anthracite, 73 % vs. 59 %, since the UC has already gone through a devolatilization process in the combustor. In fact, elemental analyses conducted in the raw UC have reported an atomic H/C ratio as low as 0.02, indicating the very low content of volatiles and the high degree of condensation of this sample. This makes the UC an attractive precursor for the production of activated carbons, since it presents much higher solid yields than conventional precursors, like wood (volatile content ~ 60%).

Figure 2 shows the N_2-77K adsorption isotherms for the steam activated unburned carbon (UC-60) and anthracites (A-60 and A-90). The three isotherms, regardless of the precursor, are Type I, with the typical concave shape to the P/P_0 axis and approaching a limiting value as the saturation pressure is reached. Although the isotherm of the activated carbon produced from the unburned carbon sample, UC-60, is still Type I, the isotherm does not reach a plateau for high relative pressures. Therefore, although UC-60 has lost the meso- and macroporosity present in the precursor, it has a wider microporosity than the activated samples derived from anthracite. Pore size distribution studies and CO_2 isotherms are being conducted to determine the degree of microporosity for the activated samples.

Table 1 lists the BET SA and total pore volume, V_{TOT}, of the activated carbons generated. As expected from the isotherms (Figure 2), the A-90 has the highest SA and V_{TOT}. When comparing samples activated under similar conditions but derived from different precursors, UC-60 and A-60, the activated carbon generated from the anthracite presents the highest SA and V_{TOT}. Figure 3 illustrates that these differences are not due to the precursors, but to the solid yield. Indeed, extremely good correlations were obtained between the solid yields and both the SA and the V_{TOT}, regardless of the precursor. The effect of the different flowrate of steam used to activated the unburned carbon and the anthracite is being investigated.

The activated carbons generated from the anthracite present SA sigificantly higher than that of previous studies conducted by one of the authors [6]. In fact, the SA of the sample activated after 90 minutes, A-90, presents a SA of 1037 m^2/g, compared to that of 610 m^2/g after six hours of activation. This is probably due to a combination of the lower flowrates (2 g of water / min vs. 12 g of water / min) and smaller particle size (250-150 μm vs. 1-3 mm) used here, resulting in more favourable conditions for the production of activated carbons.

CONCLUSIONS

The work reported here has demonstrated for the first time the ability of unburned carbon from coal combustion waste to generate activated carbons by steam activation with a high solid yield. All the activated carbons investigated present isotherms Type I that are typical for microporous carbons, regardless of the precursor used for their production. Furthermore, the inherent porosity of the precursor does not seem to limit the surface area, neither the total pore volume of the activated carbons. However, these two properties are strongly related to the solid yields. The nature of the precursor does seem to influence the extent of microposity, in the sense that anthracite produced activated carbons with narrower microporosity than the one derived from unburned carbon. The molecular sieve properties of the activated carbons generated from anthracites will be reported.

ACKNOWLEDGMENTS

The authors wish to thank the Consortium for Premium Carbon Products from Coal (CPCPC) at The Pennsylvania State University and the Research Council of the Basque Government for financial support.

LITERATURE CITED

1 Hong, B.D., 1997, Mining Engineering, **50**, 230.
2. Song, C., and Schobert, H.H., 1996, Fuel, **75**, 724.
3. Maroto-Valer, M.M., Taulbee, D.N., and Hower, J.C., 1998, Prepr. Am. Chem. Soc. Div. Fuel Chem., **43**, 1014.
4 Stewart. B., 1998, 15th Annual International Pittsburgh Coal Conference, CD volume, 1-9.
5 Patrick, J.W., 1995, Porosity in carbons, Edward Arnold, London.
6 Gergova, K., Eser, S., and Schobert, H.H., 1993, Energy & Fuels, **7**, 661.
7 Brunauer, S, Deming, L.S., Deming, W.S., and Teller, E., 1940, J. Amer. Chem. Soc., **62**, 1723.

Table 1. Solid yield, BET surface area and total pore volume of the raw precursors and the activated carbons generated from unburned carbon and anthracite [1].

	Activation time / min	Solid yield / % weight	BET S.A. / m^2/g	V_{total} / cm^3/g
UC	-	-	40	-
A	-	-	<1	-
UC-60	60	73	332	0.15
A-60	60	59	613	0.30
A-90	90	33	1037	0.47

[1] The solid yields and surface areas are expressed in ash free basis.

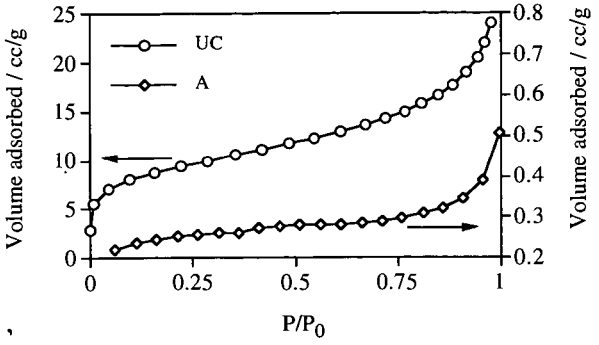

Figure 1 N_2-77K adsorption isotherms for the raw unburned carbon (UC) and anthracite (A).

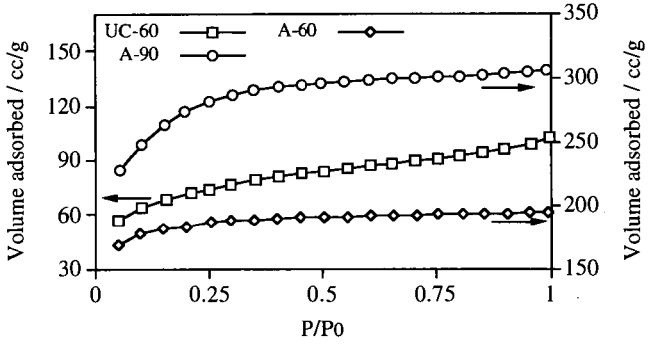

Figure 2 N_2-77K adsorption isotherms for the steam activated unburned carbon (UC-60) and anthracites (A-60 and A-90).

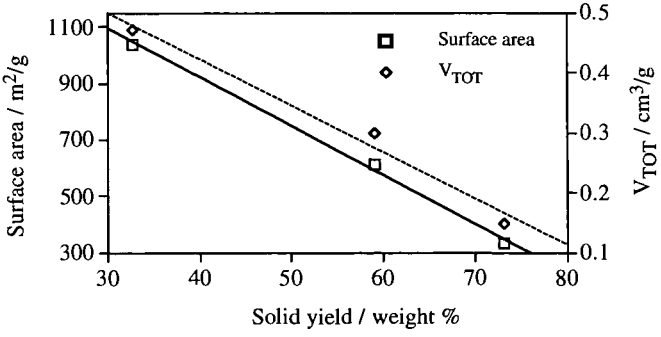

Figure 3 Relationship between solid yields, SA and V_{TOT} for all the activated carbons investigated (UC-60, A-60 and A-90).

CO-COKING: AN ALTERNATIVE PROCESS FOR COAL DERIVED JET FUEL PRODUCTION

Anne E. Fickinger, Mark W. Badger, Gareth D. Mitchell and Harold H. Schobert
The Energy Institute
Coal Utilization Laboratory
The Pennsylvania State University, University Park, PA 16802

Keywords: Coal/resid co-coking, coal derived jet fuels, coke formation.

Introduction

It has been found that coal-derived aviation fuels are more thermally stable than petroleum-derived fuels. This is mainly due to the presence of 2 to 3 ringed aromatic components in the oil fractions, which on further processing yield cycloalkane rich fuels [1,2]. Conventionally, coal-derived fuels were produced via coal liquefaction [3,4]. But due to economic market trends a more viable path to obtain these ringed aromatic components is through co-coking. Co-coking is a thermal process used to upgrade and convert petroleum resid and coal simultaneously. Co-coking involves simulating a delayed coker unit in a refinery while adding coal, so that petroleum resids are upgraded to yield a distribution of products that include oils, gases, and coke. Coal is added to increase oil yields as well as produce the coal-derived aromatic components that make a thermally stable jet fuel.

The delayed coking process involves subjecting a petroleum resid to temperatures of 450 - 500 °C [5,6]. A constant pressure of 10-20 psig within the coke drum is maintained due to the evolution of gaseous products. This process not only produces useful oil products, but also quality coke products depending on the initial feedstock. These conditions produce product yields of 70% liquids, 10% gas, and 20% coke. However, since this process was simulated in batch reactors, the product distribution will vary.

The work presented here represents a continuation of previous studies of co-processing [7].

Experimental

Three high volatile bituminous coals were obtained for the Penn State Coal Sample Bank and Database. The coals were chosen for their extremely high fluidity, as well as their low moisture, and sulfur content. These properties are displayed in Table 1. The samples were ground to a <60 mesh to ensure good contact qualities and then vacuum dried at 110 °C for 2 hours prior to each of the experiments. The petroleum vacuum resid used was a coker feed supplied by BP America.

The reactions were carried out in vertical 25 ml microautoclave reactors with *ca* 6 grams of coker feed and 3 grams of coal (resid/coal ratio of 2:1 by weight) at four temperatures (450, 465, 475, and 500 °C). The reaction length was 2 hours. The reactors were purged with nitrogen to remove any air within the reactors and left at ambient pressure. Once the reaction was complete, the reactors were cooled and the gases that evolved were vented. Any pourable liquid was collected through the stem and later included in the oils (hexane soluble fraction). The products were then removed from the reactor and subjected to a Soxhlet extraction using hexane to remove the oils, toluene to remove the asphaltenes, and finally THF to remove the preasphaltenes. The THF insolubles were then dried in a vacuum oven for 2 hours at 30 °C to remove any excess solvent so the coke product yield could be recorded on a dry weight basis.

The hexane-soluble fractions were subject to analysis by the GC, GC-MS, and the Sim Dis GC. Ultimate analysis was performed on the coke products using a LECO 600 for C, H, and N, and a LECO MAC 400 for proximate analysis to obtain the ash and moisture content to determine the chemical interactions between the coals and the resid. Optical microscopy was also performed to determine how the coal and the resids contributed towards the coke product.

Results and Discussion

Figure 2 shows the GC traces for the four different temperatures for one of the coals used, Powellton coal. By examining this figure the trends described below can be seen. Table 2 shows the percentage yields for the various fractions from co-coking experiments using Powellton, Eagle, and Pittsburgh coal at temperatures between 450 - 500 °C.

The results for the coals and coker feed mixed together at 450 °C, showed high oil yields with relatively high coke yields. However, GC traces showed that the oils contained long-chain paraffins, and not the 2-3 ring aromatics that are precursors to thermally stable jet fuel. The results of the coker feed and the coal at temperatures of 465-475 °C showed an increase in coke production with a decrease in oil yield. GC traces further showed that the oils produced contained the 3-5 ringed aromatic components that could be further processed to desirable precursors. The results of the resid and coal at 500 °C showed a heightened effect of an increase in coke production with a decrease in the oil yield. However, when the GC traces were examined the 1-3 ringed aromatics were the major components, suggesting that the reaction conditions were too severe.

Figure 1 shows the changes in the yield of the solvent fractions for co-coking experiments with Powellton coal. Similar trends for the changes in product yields were observed for the Eagle and Pittsburgh coals. The product yields showed that the coke yield increased with decreasing oil yield. This resulted because the reactors were not vented during the reaction, which caused the volatile gases to build up inside. The higher pressure and sealed environment within the reactor, as well as the longer contact time between the volatile constituents at reaction temperature caused the coke yield to increase to the detriment of the oil yield. This effect was noted previously by Hossain and co-workers [8]. This may be why the yields of the products differ from delayed coking operation yields. Delayed coking is a system that allows the volatiles to be vented off on production, which in turns leads to high oil yields (~70%) and lower coke yields (~20%).

These results indicate that we have a flexibility in our process. Depending on the temperature of operation we can manipulate the product yields and compositions to produce precursors for thermally stable jet fuel. That is, for products with 3-5 ringed aromatics an upgrading/hydrogenation process under severe conditions will produce cycloalkanes in the desired boiling fractions which could be used as thermally stable jet fuels. However, it may be desired that a less severe upgrading process be utilized and therefore a product with 1-3 ringed aromatics would be more advantageous.

Elemental analysis of the coke products has produced some interesting and, as yet, not fully understood results. The general trend noted is that when coal and resid are co-coked, we obtain a product that has a lower H/C ratio (more carbon rich) than when resid is coked alone. This, however, does not unequivocally indicate that the product is of a higher quality. Optical microscopy studies tend to suggest that the presence of the coal changes the way resid coke is formed. Interactions between coal and resid have been noted, which may indicate some dissolution. Initial studies have shown that the optical texture of the cokes produced at 450 °C during co-coking have similar properties of cokes produced from the coking of the resid alone, at temperatures above 475 °C. As to why this is occurring is unclear at present and needs further study.

From the work performed so far in the batch reactor systems, we believe that 465 °C is the best temperature to produce the best quality oil fraction at reasonable yields. Further study will include feed ratio studies, and the effects of reaction length on yields. Alternative feeds, such as decant oil, will also be investigated, with the hope that greater dissolution of the coal will occur while producing different coke products.

References

1. Song,C., Eser, S., Schobert, H.H. and Hatcher, P.G., Energy and Fuels, **7**, 234, (1993).

2. Al, W-C., Song, C., Schobert, H.H. and Aramugam, R., ACS Div. Fuel Chem. Preprints, **37**, 4, 1671, (1992).

3. Song, H., and Hatcher, P.G., ACS Div. Fuel Chem. **37**, 2, 529, (1992).

4. Lai, W-C. and Song, C., Fuel, **74**, 1436, (1995).

5. Speight, J.G. in "The Chemistry and Technology of Petroleum. 2nd Edition", Marcel Dekker Inc., New York, (1991).

6. Gray, M.R. in "Upgrading of Petroleum Residues and Heavy Oils", Marcel Dekker Inc., New York, (1994)

7. Martin, S.C., Tomic, J. and Schobert, H.H., ACS Div. Fuel Chem. **42**, 3, 121, (1997).

8. Hossain, T., Zaman, N., Jahan, S.T., Podder, J. and Rashid, M.A., J. Mech. Eng. Res. Dev. **16**, 47, (1993)

Acknowledgments

The authors would like to express their gratitude to the Department of Defense and Air Force Wright-Patterson Laboratory for the funding of this project under contract F33615-98-D2802 delivery order 0003.

Table 1: Properties of the Coals

	POWELLTON	EAGLE	PITTSBURGH #8
RANK	hVAb	hVAb	hVAb
MOISTURE	6.5	6.8	2.4
ASH	5.0	5.5	10..
%C	87.6	87.3	83.3
%H	5.8	5.6	5.7
%N	1.6	1.6	1.4
%S	0.9	-	1.3
%O	3.9	-	8.4
TEMP. MAX FLUIDITY (C)	448.0	437.0	438.0
FLUIDITY (DDPM)	30000+	30000+	20002

Table 2: Percent yields for the Eagle, Powellton, and Pittsburgh coal at 450, 465, 475, and 500°C

		PERCENT YIELDS						
TEMP (C)	COAL	GAS	OILS	ASPHALTINES	PRE-ASPHALTINES	COKE	TOTAL	LOSSES
450	EAGLE	14.0	24.7	3.5	2.5	42.1	86.8	13.2
	POWELLTON	12.1	32.2	17.2	4.0	37.1	102.5	-2.5
	PITTSBURGH	12.2	19.5	4.3	3.8	44.5	84.4	15.6
465	EAGLE	22.3	13.2	2.7	4.7	50.4	93.3	6.7
	POWELLTON	23.6	12.5	0.7	1.6	51.8	90.1	9.9
	PITTSBURGH	18.0	16.9	1.8	1.0	49.1	86.9	13.1
475	EAGLE	18.3	6.5	8.0	2.3	47.6	82.7	17.3
	POWELLTON	9.1	7.7	0.6	2.4	36.5	56.4	43.6
	PITTSBURGH	24.9	12.5	1.4	4.5	51.2	94.4	5.6
500	EAGLE	17.0	5.4	0.3	4.4	48.5	75.6	24.4
	POWELLTON	28.3	6.7	0.3	2.2	50.5	87.9	12.1
	PITTSBURGH	28.5	6.3	0.5	2.7	50.9	89.0	11.0

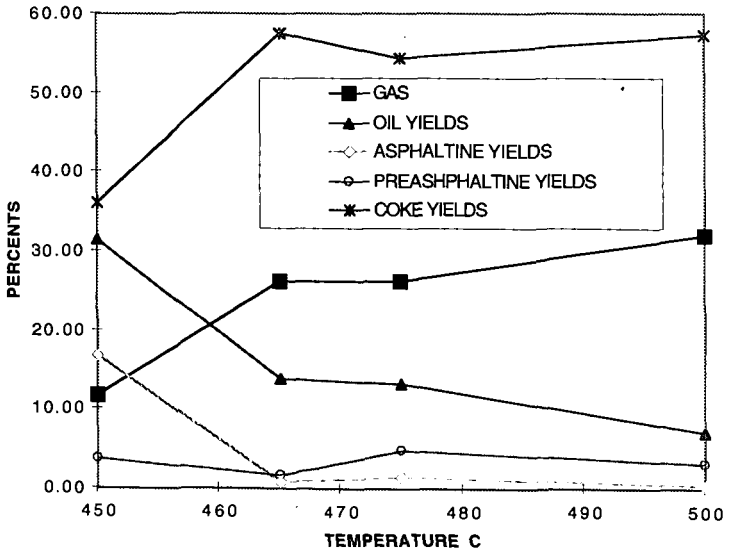

Figure 1: The product yield trends for the Powellton coal at the four temperatures

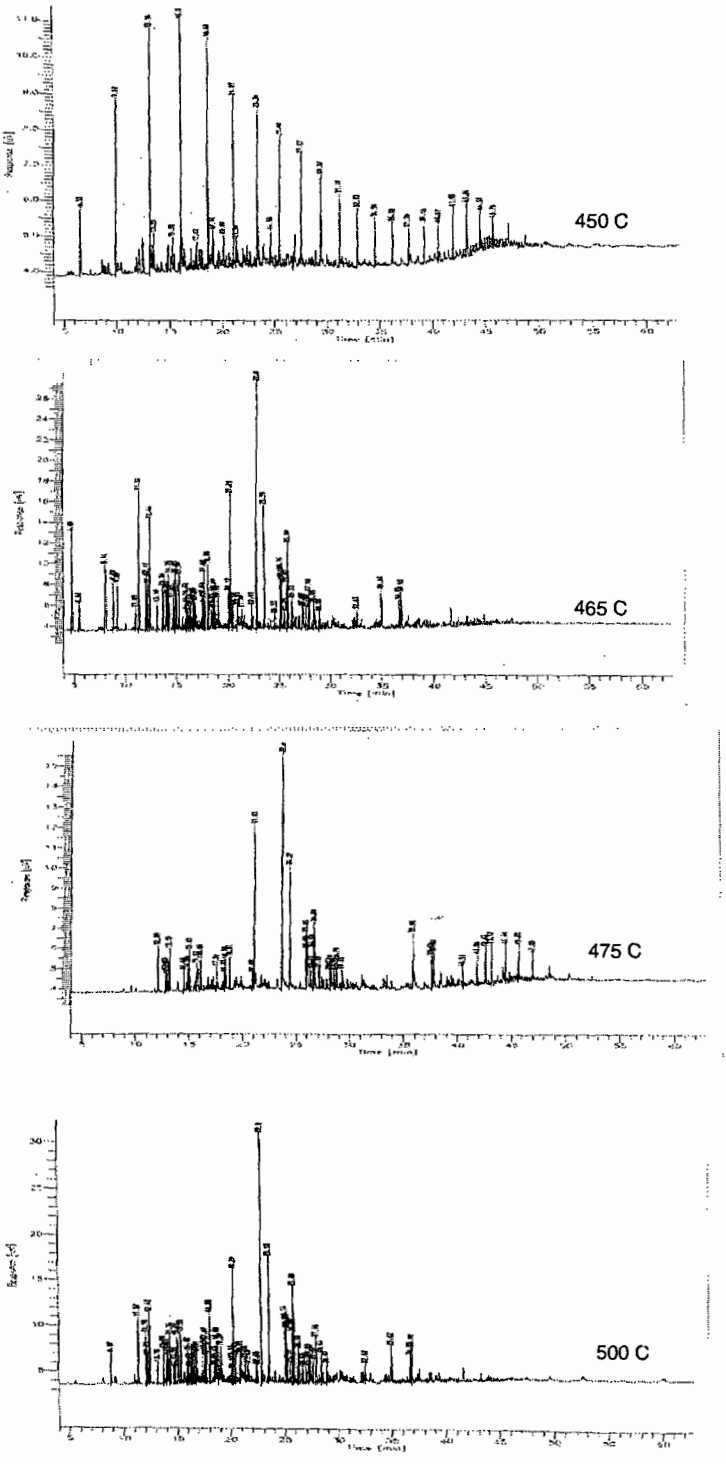

Figure 2: GC Traces for the Powellton coal and coker feed at the four various temperatures [X Axis: time (min) Y Axis: Response (uV)]

ADVANCES IN COAL CLEANING

Ilham Demir, Latif A. Khan, and John M. Lytle
Illinois State Geological Survey, 615 E.Peabody Drive, Champaign, Illinois 61820

Keywords: advanced coal cleaning, flotation, gravity separation

INTRODUCTION

Run-of-mine coal generally has an ash content of 5-40% and a sulfur (S) content of 0.3-8% depending on the geologic conditions and mining technique used. Coal cleaning, therefore, is often required to remove excessive impurities for efficient and environmentally safe utilization of coal. In the US, the coal cleaning is most common at Eastern and Midwestern mines. Over 90% of the 267 US plants operated in 1998 were in eight Eastern and Midwestern states: West Virginia, 70; Kentucky, 56; Pennsylvania, 41; Virginia, 23; Indiana, 16; Illinois, 15; Ohio, 12; and Alabama,11.[1]

Current commercial coal cleaning methods are invariably based on physical separation; chemical and biological methods tend to be too expensive. Typically, density separation is used to clean coarse coal while surface property-based methods are preferred for fine coal cleaning. In the density-based processes, coal particles are added to a liquid medium and then subjected to gravity or centrifugal forces to separate the organic-rich (float) phase from the mineral-rich (sink) phase. Density-based separation is the most common coal cleaning method and is commercially accomplished by the use of jigs, mineral spirals, concentrating tables, hydrocyclones, and heavy media separators. The performance of density-based cleaning circuits is estimated by using laboratory float-sink (F-S) tests. In the surface property-based processes, ground coal is mixed with water and a small amount of collector reagent is added to increase the hydrophobicity of coal surfaces. Subsequently, air bubbles are introduced in the presence of a frother to carry the coal particles to the top of the slurry, separating them from the hydrophilic mineral particles. Commercial surface property-based cleaning is accomplished through froth or column flotation. To estimate the performance of flotation devices, a laboratory test called release analysis is used.[2-5]

Theoretically, the efficiency of physical cleaning should increase as particle size decreases because of the improved liberation of the mineral matter from the coal matrix. Therefore, recent research on advanced coal cleaning has focused on improving fine-coal cleaning. Column flotation devices developed since the 1980s can remove most of the impurities from finely-ground coal.[6-8] Likewise, advanced gravity separators, developed mainly for metal mining industries, were shown in recent years to have a good potential for improving the cleaning of finely-ground coal.[9,10] This paper discusses work on physical fine-coal cleaning conducted at the Illinois State Geological Survey (ISGS) and reviews work conducted elsewhere on the similar subject.

LABORATORY TESTS TO ASSESS FURTHER CLEANABILITY OF ILLINOIS COALS

As-shipped (cleaned) coals from eight coal preparation plants in Illinois were selected to assess the further cleanability of conventionally cleaned coals.[11] The criteria for sample selection were based on the representation of the main producing seams, high and low S coals, high and low ash coals, and different geographic regions of the Illinois coal field. Therefore, the interpretations reported here should apply to most marketed coals from Illinois mines. Release analysis (RA) and F-S test data were generated to estimate the beneficiation of the eight coals, at -60 mesh (<250 μm) particle size and 80%-combustibles recovery.

Froth Floatation Cleanability The RA tests indicated that ash yield and S content of Illinois coals could be reduced substantially beyond conventional cleaning through the use of froth flotation or column flotation. The ash yield was reduced by 24-69% and S content by 4-24% relative to the parent coals (Table 1). The proportion of the total S removed increased with increasing ratio of pyritic to organic S.[11] Both the absolute and relative reduction of ash yield tended to increase with the amount of ash yield in the parent coal.

The RA separation resulted also in significant reductions for the contents of most elements that are classified as hazardous air pollutants or HAPs (Table 1). In some cases, reductions for HAPs approached or exceeded the reductions for ash. Reductions for Mn and P approached or exceeded reductions for ash in almost all cases. A substantial portion of Mn is thought to occur in solid solution in calcite, and P is associated, perhaps primarily, with apatite in coal. Most of the calcite and some of the apatite occur as cleat fillings, nodules, and/or partings[12,13] which are more easily removed during coal cleaning than finely disseminated minerals.

Float-Sink Washability The F-S washability data indicated that density (gravity)-based physical fine-coal cleaning can be quite effective in further reducing ash and S contents of marketed Illinois coals (Table 1). Clean coals having ash yields of 3.6-6.8% can be produced from the eight coals. The ash yields were reduced by 47-75% relative to conventional cleaning. The S content of the eight clean F-S products varied betwecn 0.73% and 3.28%, representing a 21-42% reduction. Comparison of the S data from this study with the data on S forms of feed coals[14] indicated that the S remaining in the clean F-S products is overwhelmingly organic S; most of the inorganic S was

removed during the F-S process.

The clean F-S products had much smaller HAP contents than the conventionally cleaned feed coals, with a few exceptions (Table 1). Reductions of As, Cd, Hg, Mn, and P contents exceeded reductions for ash in almost all cases. Arsenic, Cd, and Hg are associated mostly with sulfide minerals[15] that have high specific gravities and, therefore, respond to gravity separation efficiently. Minerals containing substantial amounts of Mn (calcite) and P (apatite) also showed efficient response to the F-S separation, as well as RA, because, as indicated earlier, these minerals tend to occur as relatively coarse grains in cleat fillings, nodules, or partings. Because As, Cd, F, Hg, Pb, and Se have relatively high atmospheric mobilities during coal combustion[15,16], achieving high removal values for these elements is important from an environmental point of view. Those HAPs that were reduced less than the ash apparently occurred either in organic form or in extremely fine mineral particles disseminated in the organic matter which were not liberated by grinding the coals to the selected particle size. This may be the case for Be, Sb and U in some of the samples. However, the elements that exhibited enrichment or relatively low cleanabilities either have low concentrations in Illinois coals or low atmospheric mobilities during coal combustion[15,16] which would result in low environmental risk associated with their emissions.

In general, the beneficiation of the eight coals through the use of the F-S test was considerably greater than the beneficiation obtained through the RA test (Figure 1). The difference between the F-S and RA results was particularly large for some samples (Table 1). The effectiveness of the F-S separation for the most environmentally critical elements, S and Hg, is particularly important. Because Be tended to stay largely with the organic matter, it was generally enriched more in the F-S products than in the RA products. The comparison of the F-S and RA data suggested that RA can estimate the performance of standard flotation circuits but probably not the performance of advanced gravity separators and some advanced flotation devices. Float-sink tests appear to be more suitable to estimate the ultimate cleanability of coal through the use of advanced physical cleaning.

PILOT SCALE TESTS WITH ISGS FROTH WASHER DEVICE

A froth washer device was developed at the ISGS to improve the performance of both subaeration cells and flotation columns.[17] The ISGS froth washer enables the washing and quick removal of fine contaminants into a separate stream of a flotation circuit. Tests conducted on IBC-112 coal in the Illinois Basin Coal Sample Program indicated that a subaeration cell equipped with the ISGS froth washer removed more ash-forming minerals and S from the coal than a packed column device (Figure 2). The performance of the modified subaeration cell generally approached the ultimate cleanability predicted from F-S tests and the so-called advanced flotation washability analysis (AFW) as defined elsewhere.[17] Using the subaeration cell with the ISGS washer, a second set of tests was performed on a sample of preparation plant fines containing 43.5% ash, 4.2% total S, 2.0% pyritic S, and having a heating value of 7934 Btu/lb. The optimized performance of the subaeration cell with the ISGS washer at a throughput of 50 lb/hr/ft^3 approached that of the AFW process, resulting in 75% ash rejection and 45% pyritic S rejection at 83%-combustibles recovery.

PILOT AND FULL-SCALE TESTS WITH ENHANCED GRAVITY SEPARATORS

It has been reported that gravity-based separation can potentially be superior to surface property-based separation for reducing the pyrite content of coal.[15] Honaker and co-workers[9,10,19-21] evaluated the application of enhanced gravity separation to pilot and full-scale coal cleaning. Using a dense medium Falcon gravity separator, the ash yield and pyritic S content of a 28x325 mesh coal collected from a preparation plant treating Illinois Herrin (No. 6) Coal were reduced from 17.5% to 3.5% and from 0.55% to 0.15%, respectively, while recovering 87.8% of the combustible material.[19] Comparison with AFW data suggested that the dense medium Falcon Concentrator can potentially outperform the best flotation technology available. Pilot scale tests with a Falcon Concentrator, a Knelson Concentrator, and an Altair Jig indicated that they were all effective for cleaning a 28x400 mesh coal sample from the Illinois Springfield (No. 5) Coal.[20] Typically, 80% of the ash and 70% of the total S were rejected at 85% recovery of the combustible material. During full-scale testing with a mass flow rate of 100 t/hr, the Falcon Concentrator efficiently cleaned a refuse pond coal sample.[20] The ash yield was reduced from 22% to 8% for the 28x100 mesh fraction and from 32% to 15 % for the 100x500 mesh fraction, while recovering a little over 80% of the combustible material. Nearly 90% of the pyritic S was rejected, resulting in the reduction of the total S content of both fractions from 7.9% to 2.7% .

OTHER PHYSICAL METHODS FOR ADVANCED COAL CLEANING

Other physical cleaning methods, including selective agglomeration, heavy medium cycloning, and dry separation with electrical and magnetic methods, have been discussed by Couch.[22,23] Selective agglomeration and advanced cycloning have the high probability of commercialization, particularly for reducing S content of coal.[23] In selective agglomeration, the coal is mixed with oil. The oil wets the surface of coal particles and thus causes them to stick together to form agglomerates. The agglomerated coal particles are then separated from the mineral particles that stay in suspension because they do not attract oil to their surfaces. A version of selective agglomeration, called the Otisca T-process, was reported to reduce the ash content of some coals, ground to about 2 μm,

below 1% with a high recovery of the heat content.[24] Conventional cycloning has been used for many years for cleaning relatively coarse coal and considered for fine coal cleaning only in recent years. Coal and heavy medium enters the conical-shape cyclone tangentially near the top. As the cyclone spins around its axis, impurities move downward along the walls and exit through the bottom opening while coal particles move upward near the center and exit from the top. Dry methods that take advantage of the differences between electrical or magnetic properties of minerals and coal particles have not developed enough for commercial applications.

COST OF ADVANCED COAL CLEANING

Progress in fine-coal cleaning has been significant, but the dewatering and material handling stages of the process can be difficult and are expensive. Therefore, the economic and environmental benefits of the final product must justify the cost. Newman et al.[25] estimated the cost of advanced cleaning to be $12/t for run-of-mine coals containing 1-8% S if 90% pyritic S rejection is to be achieved. It is not clear whether dewatering and fine-particle handling costs were included in these estimates. The total cost of advanced cleaning, including dewatering and pelletization (or briquetting), might be $22-27.5/t.[26] One should, however, keep in mind that the product of advanced coal cleaning is a low-ash, low-S, and high-heating value fuel. Therefore, some expenses of the advanced coal cleaning can be offset by (1) reduction in transportation cost per unit of heating value of coal, (2) elimination of milling cost at power plants, and (3) reduced maintenance cost of power plants related to fouling, slagging, and other wear and tear. Furthermore, the pelletization or briquetting costs may be eliminated if the advanced cleaning product is used as a coal-water fuel to replace oil in oil-fired boilers. Transporting coal-water fuels through pipelines would provide further cost-cutting benefits. Although the application of advanced fine-coal cleaning is currently limited, its widespread commercialization may eventually take place, depending on further improvements in technology, supply and demand for different fuels, and future environmental regulations.

CONCLUSIONS

Release analysis (RA) and float-sink (F-S) test data for selected samples suggested that advanced physical cleaning at -60 mesh particle size and 80%-combustibles recovery can potentially reduce the ash yield and S content of Illinois coals up to 75% and 42%, respectively, beyond conventional cleaning. As a result, some of the clean products would have ash yields of <4% and S content of <1%. The F-S process was generally more effective than the RA process for cleaning the samples. The average F-S reductions for HAPs were (in %): As(67), Cd(78), Hg(73) Mn(71), P(66), Co(31), Cr(27), F(39), Ni(25), Pb(50), Sb(20), Se(39), Th(32), and U(8). Beryllium was generally enriched in the clean RA and F-S products. However, elements with relatively low removal or enrichment values would have very little, if any, environmental impact because they either occur in very small quantities in Illinois coals or are fixed largely in coarse ash and slag during coal combustion.

Two advanced cleaning technologies tested on Illinois coals in recent years yielded promising results. The performance of a froth washer device developed at the ISGS to improve the performance of both subaeration cells and flotation columns generally approached the ultimate cleanability predicted from laboratory F-S tests. Pilot and full-scale tests with advanced gravity separators, performed at Southern Illinois University, suggested that such equipment can potentially outperform even the best flotation technology available.

The estimated cost of advanced fine-coal cleaning ranges from $12 to $28 per ton, which is uneconomical under current conditions. However, some expenses of advanced coal cleaning can be offset by reduction in transportation cost, elimination of milling cost at power plants, and reduced maintenance cost of power plants. Widespread commercialization of advanced coal cleaning technologies depends on further improvements in technology, supply and demand for different fuels, and future environmental regulations.

REFERENCES

1. Fiscor S. and Fischer M (1998) U.S. Preparation Plant Census. Coal Age, September 1988, p. 70-76.
2. Dell C. C., Bunyard M. J., Rickelton W.A., and P.A. Young P. A. (1972) Release analysis: a comparison of techniques. Trans. IMM (. C, Mineral Process. Extrac. Metall.) **81**, C89-96.
3. Forrest W. R., Jr. (1990) Processing of Sec High-sulfur Coals using Microbubble Column Flotation. M.S. Thesis, Virginia Polytechnic Institute and State Univ., Blacksburg, VA.
4. Honaker R. Q. and Paul B. C. (1994) A comparison study of column flotation technologies for the cleaning of Illinois coal. Interim Report to the Illinois Clean Coal Institute, Carterville, IL
5. Demir I., Ruch R. R., Harvey R. D., Steele J. D., and Khan S. (1995) Washability of Trace Elements in Product Coals from Illinois Mines. Open File Series 1995-8, Illinois State Geological Survey, Champaign, IL.
6. Yang D. C. (1990) Packed-bed column flotation of fine coal. Part I: laboratory tests and flotation circuit design. Coal Preparation, vol. 8, p19-36.
7. Yoon R-H, Luttrel G. H., Adel G. T., Mankosa M. J. (1990) The application of Microcell column flotation to fine coal cleaning, Presented at Engineering Foundation Conference on Fine Coal Cleaning, Palm Coast, FL, December 2-7, 1990.
8. Kenedy A. (1990) The Jameson flotation cell. Mining Magazine, vol. 163, p. 281-285 .
9. Paul B. C. and Honaker R. Q. (1994) Production of Illinois Base Compliance Coal Using Enhanced

Gravity Separation. Final Technical Report to the Illinois Clean Coal Institute, Carterville, IL.
10. Honaker R. Q., Wang D. and Ho H. (1996) Application of the Falcon Concentrator for fine coal cleaning. Minerals Engineering, vol 9(11), p. 1143-1156.
11. Demir I. (1998) Removal of ash, sulfur, and trace elements of environmental concern from eight selected Illinois coals. Coal Preparation, vol. 19, p. 271-296.
12. Rao C. P. and Gluskoter H. J. (1973) Occurrence and Distribution of Minerals in Illinois Coals. Circular 476, Illinois State Geological Survey, Champaign, IL, 1973.
13. Harvey R. D, R.A. Cahill R. A., Chou C.-L., and Steele J. D. (1983) Mineral Matter and Trace Elements in the Herrin and Springfield Coals, Illinois Basin Coal Field. Contract/Grant Report: 1983-4, Illinois State Geological Survey, Champaign, IL.
14. Demir I, Harvey R. D., Ruch R. R., Damberger H. H., Chaven C., Steele J. D., and Frankie W. T. (1994) Characterization of Available (Marketed) Coals From Illinois Mines. Open File Series 1994-2, Illinois State Geological Survey, Champaign, IL.
15. Demir I, Ruch R. R., Damberger H. H, Harvey R. D., Steele J. D., and Ho K. K. (1998). Environmentally critical elements in channel and cleaned samples of Illinois coals. Fuel, 77: 95-107.
16. Davidson R. M (1996) Trace elements in coal. IEA Coal Research, IECPER/21, London.
17. Khan L. A. and Lytle J. M. (1997) Testing of Improved Froth Washing & Drainage Device for Flotation Machines. Final Technical Report to the Illinois Clean Coal Institute, Carterville, IL
18. Adel G. T., Wang D., and Yoon R. H. (1991) Washability Characterization of fine coal. Proc. 8th Annual International Pittsburgh Coal Conference, 204-209.
19. Honaker R. Q., Rajan B. J., Mohanty M. K., and Sing N. (1998) A Novel High Efficiency Enhanced Gravity Separation Using Dense Medium. Mid-year Technical Report to the Illinois Clean Coal Institute, Carterville, IL
20. Honaker R. Q. and Govindarajan B. (1998) Enhanced gravity concentration: An effective tool for fine coal cleaning. Inside Coal Research, vol. 4(3), p. 2-3, Coal Research Center, Southern Illinois University, Carbondale, IL.
21. Mohanty M. K. and Honaker R. Q. (1998) Evaluation of the Altair centrifugal jig for fine particle separations. Reprint 98-169, SME Annual Meeting, Orlando, Fl.
22. Couch G. R. (1991) Advanced coal cleaning technology. IEA Coal Research, IEACR/44, London.
23. Couch G. R. (1995) Power from coal - where to remove impurities? IEA Coal Research, IEACR/82, London.
24. Keller D. V. and Bury W. M. (1990) The demineralization of coal using selective agglomeration by the T-process. Coal Preparation, vol. 8(1/2), p. 1-17.
25. Newman J., Kanteseria P., and Huttenhain H. (1994) An evaluation of physical coal cleaning plus FGD for coal fired utility applications. In: Proceedings of the 11th International Conference on Coal Utilization and Fuel Systems3/21-3/24/1994, Clearwater, FL, p. 317-327.
26. Smouse S. M. (1994) To clean or not to clean? A technical and economic analysis of cleaning Pittsburgh seam coal. In: Proc. of the Engineering Foundation Conference on the Impact of Coal Fired Power Plants, 6/20-6/25/1993, Solihill, UK. Taylor&Francis, Washington D.C., p. 189-217.

Table 1. Analyses of the eight as-shipped Illinois coals and their clean RA and F-S products at -60 mesh size and 80%-combustibles recovery. All values are on a dry basis.

Feed Lab no.	Feed or Cleaning product	Heating value (Btu/lb)	Ash yield (%)	S (%)	HAP elements (mg/kg) As	Be	Cd	Co	Cr	F	Hg	Mn	Ni	P	Pb	Sb	Se	Th	U
C32778	feed	12709	9.80	1.60	10	2.2	0.60	4.6	12	70	0.04	38	31	87	14	2.2	1.5	1.5	0.9
	RA product	13622	5.63	1.21	5.8	2.6	<0.2	4.0	9.7	57	0.05	13	29	39	8	2.2	1.0	1.3	1.1
	F-S product	13962	4.79	1.19	2.9	4.6	<0.08	3.8	9.4	59	0.01	12	29	39	7	2.2	1.0	1.2	1.3
C32782	feed	12503	11.62	3.90	2.4	<1.0	0.40	1.6	14	78	0.07	55	7	87	<6	0.5	1.9	1.1	1.3
	RA product	13448	8.97	3.65	1.3	1.3	<0.2	1.2	10	66	0.04	18	6	31	4	0.4	1.3	0.9	1.4
	F-S product	13797	5.89	2.99	0.9	2.2	<0.1	1.2	9.7	63	0.02	15	5	28	3	0.4	1.0	0.9	1.4
C32785	feed	12741	9.75	4.17	2.3	1.5	0.40	2.6	17	115	0.07	39	18	131	<5	0.4	3.9	1.3	1.8
	RA product	13538	6.54	4.00	1.6	2.0	<0.3	2.0	12	89	0.07	17	16	35	7	0.4	2.8	1.1	1.8
	F-S product	14029	4.38	3.28	0.7	1.5	0.10	1.8	12	87	0.01	12	14	31	3	0.2	1.9	1.0	1.4
C32815	feed	12422	12.03	3.73	3.0	<1.0	<0.2	2.7	14	88	0.06	61	10	44	12	0.6	2.1	1.7	1.9
	RA product	13538	8.72	3.23	1.8	1.4	<0.3	2.1	13	80	0.05	19	8	17	7	0.5	1.8	1.4	1.9
	F-S product	13933	5.01	2.80	0.9	2.1	<0.09	1.7	11	89	0.02	18	7	13	7	0.4	1.0	1.2	1.9
C32798	feed	12120	16.10	1.05	9.8	1.0	0.90	8.5	19	123	0.06	41	24	87	31	1.0	2.0	3.0	1.0
	RA product	12908	10.59	0.62	8.7	1.9	<0.4	6.5	17	95	0.06	17	19	44	27	0.9	1.9	2.4	0.7
	F-S product	14277	8.80	0.73	4.2	1.7	0.04	5.5	14	51	0.02	11	19	32	14	1.0	1.3	1.8	0.7
C32662	feed	13525	7.00	1.51	14	1.4	<0.3	4.4	10	83	0.08	15	17	175	23	1.0	1.3	1.9	1.9
	RA product	13892	4.58	1.33	9.4	1.9	<0.2	2.8	8.8	65	0.08	8.6	15	100	17	0.9	1.1	1.5	1.8
	F-S product	14143	3.87	1.11	5.2	2.7	<0.07	2.8	7.8	43	0.02	8.0	12	74	14	0.8	0.9	1.2	1.8
C32781	feed	13773	9.71	3.02	4.3	<1.0	0.50	2.7	12	104	0.11	37	11	44	46	1.4	2.5	1.2	2.0
	RA product	13456	7.41	2.86	2.8	1.1	<0.3	1.8	11	63	0.10	18	11	28	28	1.0	1.8	1.1	1.8
	FS product	13915	5.19	2.04	1.4	1.1	<0.09	1.7	9.9	67	0.04	10	8	13	19	1.0	1.3	0.9	1.5
C32793	feed	12402	14.14	1.64	33	1.2	<0.2	5.5	13	124	0.13	39	22	175	36	1.2	1.1	1.8	0.8
	RA product	13947	4.35	1.28	16	1.2	<0.2	4.4	6.0	71	0.09	7.5	16	96	26	1.2	1.0	1.0	0.5
	F-S product	14151	3.59	0.95	6.4	2.0	<0.06	3.7	7.0	38	0.03	8.0	15	57	14	1.1	0.9	0.8	0.8
RA mean %change*		7	-40	-14	-39	32	-26	-25	-19	-26	-9	-63	-13	-54	-24	-11	-21	-20	-9
RA min. %change**		2	-24	-4	-30	0	0	-13	-7	-9	0	-51	0	-41	-13	0	-5	-8	0
RA max.%change**		12	-69	-24	-46	90	-67	-36	-38	-43	-43	-81	-21	-73	-43	-29	-33	-44	-36
F-S mean %change*		10	-55	-28	-67	74	-77	-31	-27	-39	-73	-71	-25	-66	-50	-20	-39	-32	-8
F-S min. %change**		1	-47	-21	-57	0	-55	-17	-18	-16	-64	-60	-6	-55	-39	0	-16	-18	0
F-S max. %change**		18	-75	-42	-75	120	-98	-37	-46	-69	-66	-79	-32	-76	-61	-50	-52	-56	-44

* Mean percentage decrease (negative values) or increase (positive values) in heating value, ash yield, or elemental concentrations for the eight coals. %change for each coal = ((Feed value - Product value)/(Feed value))x100. For values below detection limits, the upper limits were used in the computations.

**Absolute change, regardless of sign.

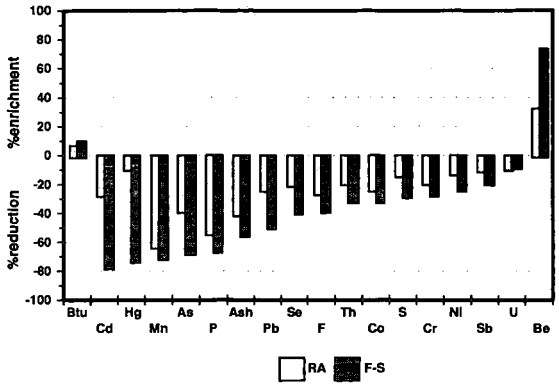

Figure 1. Average changes in heat content (Btu), ash yield, and concentrations of S and HAPs of the eight selected samples of as-shipped Illinois coals as a result of release analysis (RA) and float-sink (F-S) separations at -60 mesh particle size and 80%-combustibles recovery.

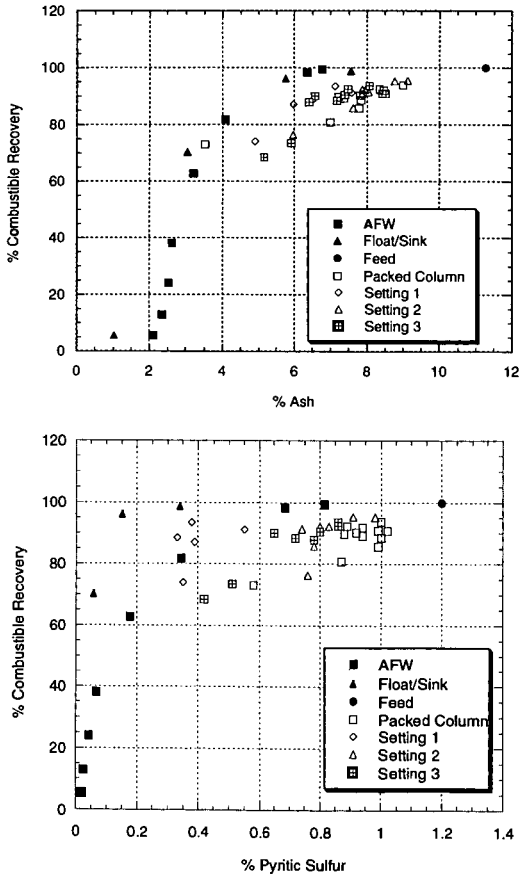

Figure 2. Ash and pyritic S vs. combustible recovery for cleaning IBC-112 ground to 90% -200 mesh using a subaeration cell with the ISGS washer at various settings. For each test, 2 lb/ton kerosene and 2 lb/ton M650 were used.

NEW UPGRADING PROCESS FOR HEAVY OIL USING IRON/ACTIVE CARBON MIXTURE CATALYST

S.Terai, H.Fukuyama, S.Sawamoto, K.Ootsuka
Technology Research Center, Toyo Engineering Corporation
1818 Fujimi,Togo,Mobara,Chiba,297-0017,JAPAN

K.Fujimoto
Department of Applied Chemistry, School of Engineering
The University of Tokyo, Hongo, Bunkyo-ku, Tokyo,113-0033,JAPAN

Key words: hydrocracking, vacuum residue, pyrite/active carbon

Introduction

There are a lot of works and efforts on heavy oil upgrading process. Among them, hydrocracking process converts heavy oil into valuable distillable product minimizing coke formation by using catalyst which may be expensive in some cases and adopting very much high hydrogen pressure which may result in high cost. This paper introduces a mixture of pyrite and active carbon (AC) catalyst which may have advantages over supported metal type in catalyst preparation. The mixture catalyst enabled hydrocracking of vacuum residue (VR) under relatively low hydrogen pressure (7.0-10MPa). The effectiveness of the mixture catalyst on hydrocracking reaction was examined in relation to AC pore structure. The kinetics of reaction using lumping model was also studied to envisage the function of the mixture catalyst.

Experimental

Hydrocracking of VR of which properties are shown in Table 1 was carried out in a one-liter semi-batch magnetically stirred autoclave under constant hydrogen flow rate. Reaction conditions were as follows; VR charge 300g, hydrogen pressure 7.0-10MPa, reaction temperature 415-445°C.

Gaseous products were analyzed by gas chromatography and hydrogen sulfide by detecting tube. The content of naphtha (IBP-171°C), kerosene (171-232°C), gas oil (232-343°C), vacuum gas oil (VGO:343-525°C) and residue (Resid:525°C+) fraction in liquid product were determined by gas chromatography distillation method after separating catalysts and coke by filtration. The amount of coke was determined as toluene insoluble. The hydrocracking conversion was defined as follows; conversion [%] = (100-weight%525°C+ in products)/weight%525°C+ in feed VR.

Results and discussion

Effect of catalyst

The experimental results for various catalyst conditions listed in Table 2 are shown in Figure 1. The coke yield against conversion for each catalyst condition was observed to increase in the order Non-cat.≫Pyrite>Iron/AC≒Pyrite/AC mixture catalyst. In the case of non-catalyst, coke formation began at relatively early stage of conversion and significantly increased in successive reaction. Pyrite could suppress the coke formation only up to the range of 60% conversion. The combination of Iron and AC was examined in order to maximize distillable products with minimal coke formation. Iron supported on AC catalyst showed a good suppression ability of coke formation even through higher conversion level. The mixture of Pyrite and AC also showed the same ability to suppress coke formation as Iron supported on AC catalyst. The usage of mixture catalyst is thought to be advantageous in catalyst preparation

which does not necessitate impregnation with aqueous solution of metal salt, drying, and presulfidation.

Affinity of active carbon with VR

Adsorption tests were conducted to examine the affinity of AC with VR by immersing AC in VR under hydrogen pressure of 10MPa and temperature of 250°C at which cracking was expected not to occur. The quantity of adsorption on AC was defined as weight increase of AC after washing AC with toluene using Soxhlet extraction and vacuum drying. The degree of deasphaltene was calculated as reduction of asphaltene content remained in VR after adsorption. It was observed that AC had affinity with heavier fraction, especially asphaltene.

In order to investigate the relationship between AC pore structure and affinity with asphaltene, the adsorption tests in the same manner as above were carried out differing pore volume and mesopore ratio of AC in the order AC(C)>AC(A)>AC(B). As shown in Figure 2, AC(C) with well grown mesoporous structure exhibited the highest adsorption selectivity to asphaltene.

AC pore structure and Hydrocracking

The influence of AC pore structure on hydrocracking was studied. As shown in Figure 3, it was possible to attain higher conversion with less coke yield with AC which developed more mesoporous structure. From these experimental results, the hydrocracking in the presence of Iron/AC catalyst can be summarized as follows.

- Free radical intermediates are initially generated by thermal cracking of VR.
- Such intermediates are adsorbed on active carbon surface.
- Adsorbed intermediates are hydrogenated and stabilized by Iron and then desorbed from the active carbon surface.
- In the course of this reaction, AC with mesoporous structure provides free radical intermediates with proper sites for adsorption preventing them from polycondensing.

Kinetic study

Kinetic study was carried out to clarify the function and to quantitatively observe activity of catalysts for hydrocracking of VR. Reaction model using lumping species adopted here is illustrated in Figure 4. Residue fraction (525°C+) was classified into saturates (Satu), aromatics (Aroma), resins (Resin) and asphaltenes (Asp) by the method based on ASTM D4124-84 and products were grouped into Lo (Gas, Naphtha, Kerosene, Gas Oil),VGO and Coke. Each reaction path was fitted with experimental data by assuming first-order reaction. The comparison between calculated (lines) and experimental (keys) results for pyrite and pyrite/AC mixture are shown in Figure 5 (A) and (B), respectively. The agreement between calculated and experimental results are fairly good for both cases. The temperature dependence of reaction rate constants for pyrite and pyrite/AC mixture are shown in Figure 6 (A), and (B), respectively. Rate constants for cracking reaction to lighter products (Gas, Naphtha, Kerosene, Gas Oil) and condensation reaction (resins to asphaltenes) of pyrite catalyst were observed to be much sensible to temperature than those of pyrite/AC mixture catalyst. This suggests that pyrite catalyst tends to promote cracking reaction producing relatively lighter products on the one hand, and polycondensation producing asphaltene and finally coke on the other hand. However, pyrite/AC mixture catalyst proceeds reactions keeping middle fractions in products and restricting polycondensation of heavy components such paths from resins to asphaltene and asphaltene to coke. Thus the effectiveness of pyrite/AC mixture catalyst was also verified by this kinetic study.

Conclusions

The pyrite/AC mixture catalyst which is simple in preparation showed excellent effectiveness in hydrocracking of VR with the following results.

- AC with well grown mesoporous structure exhibited the highest adsorption selectivity to asphaltene.
- It was possible to attain higher conversion with less coke yield by using AC which developed more mesoporous structure.
- Kinetic study of reaction by lumping model also verified the effectiveness of pyrite/AC mixture catalyst.
- Hydrocracking was possible under relatively low hydrogen pressure by using mixture catalyst.

Thus pyrite/Active Carbon mixture catalyst was proved to be effective for upgrading of heavy oil with low hydrogen pressure condition.

Acknowledgments

This work has been carried out as a research project of the Petroleum Energy Center with the subsidy of the Ministry of International Trade and Industry, Japan.

Literature

Nakamura,I. and Fujimoto,K., PREPRINTS, Div. of Petro. Chem., ACS, 39(3),1994.

Table 1
Properties and Composition of Vacuum Residue

Feedstock			Middle East Blend VR
Density(15°C)		[g/cm3]	1.0334
Total Sulfur		[wt%]	4.02
Total Nitrogen		[wt%]	0.53
CCR		[wt%]	22.4
Metal	Ni	[wtppm]	53
	V	[wtppm]	180
C/H	C	[wt%]	84.8
	H	[wt%]	10.2

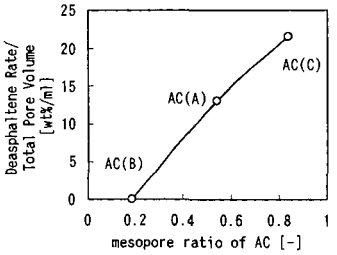

Figure 2 Mesoporous structure and adsorption selectivity of asphaltene

Table 2
Tested Catalysts

Case	Catalyst
1	Non Catalyst
2	Pyrite
3	Iron supported on AC Cat.(Iron/AC)
4	Pyrite/AC Mixture Cat.

AC:Active Carbon

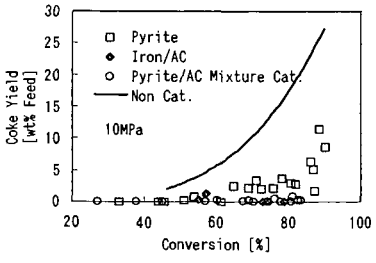

Figure 1 Hydrocracking results with several catalysts

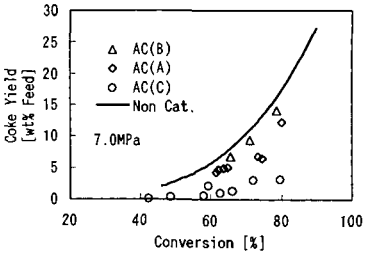

Figure 3 Relationship between porosity of AC and coke yield

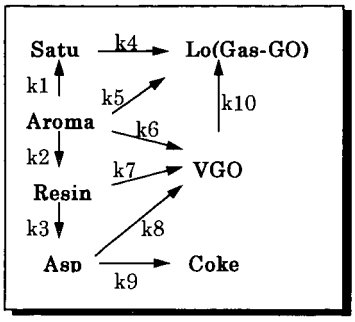

Figure 4 Reaction Model

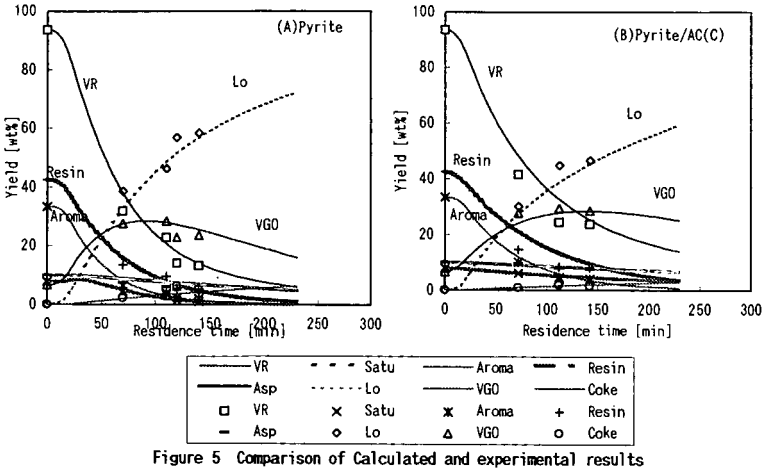

Figure 5 Comparison of Calculated and experimental results

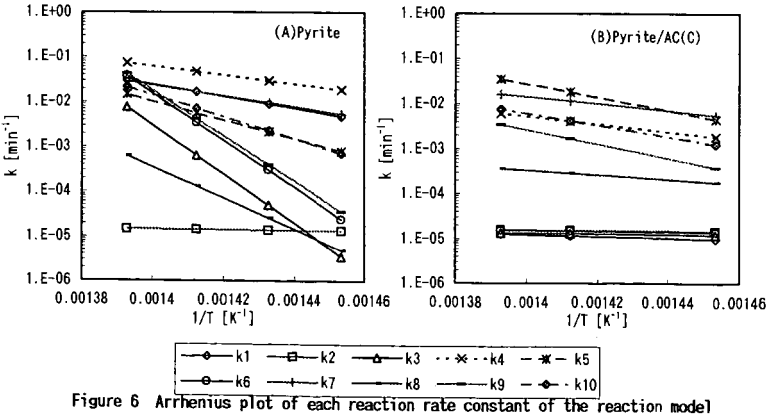

Figure 6 Arrhenius plot of each reaction rate constant of the reaction model

REMOVAL OF VOLATILE METAL CARBONYLS FROM RAW SYNGAS

R. Eijkhoudt, C.J. Smit*, A. J. van Dillen and J. W. Geus
Dept. of Inorganic Chemistry and Heterogeneous Catalysis, Utrecht University, Sorbonnelaan 16, 3584 CA Utrecht, The Netherlands. Email: R.Eijkhoudt@chem.uu.nl
* Shell Research and Technology Centre, Badhuisweg 3, 1031 CM Amsterdam, The Netherlands

Introduction

Industrial processes using carbon monoxide and/or hydrogen obtained from syngas can suffer from metal carbonyls originating from the feedstock used and the piping and reactor system. Nickel tetracarbonyl and iron pentacarbonyl, especially in combination with hydrogen sulfide, cause serious problems during the treatment of raw syngas and subsequent applications, mainly due to thermal and/or chemical carbonyl decomposition. For example, in gas treating processes using a liquid absorbent for the removal of acid gases, such as hydrogen sulfide and carbon dioxide in combination with a Claus plant, pressure build-ups, due to deposition of metal oxides/sulfides can be expected not only in the treating unit, but also throughout the Claus plant, especially on the catalyst bed of the first Claus reactor. In addition, downstream pressure-buildups may occur, as metal is being deposited on catalyst beds in syngas treating, e.g. COS hydrolysis and water gas shift. Furthermore, the active phase in the catalysts can become poisoned or show adversely changing activities and selectivity's due to the deposition of iron/nickel.

Generally, when CO is present in a gas stream as a reactant or (by) product in industrial processes, a suitable absorbent for nickel tetracarbonyl and iron pentacarbonyl often is imperative in order to eliminate or reduce the risk of catalyst poisoning, to extend plant operation life and to reduce the nickel and iron impurities in numerous chemical products originating from syngas.

In the research project described here, several high-surface oxides and zeolitic materials have been studied for their suitability to effectively remove metal carbonyls from raw syngas streams. The properties to be met with these materials are: applicable in a fixed bed, large capacity, regenerability and insensitivity for hydrogen sulfide and water.

Experimental

Absorbents

Several non-bindered zeolites and high-surface metal oxides have been studied for their ability to absorb iron and nickel carbonyls out of hydrogen sulfide and water containing syngas streams. High-surface SiO_2, Al_2O_3, Al_3PO_4, and zeolitic materials including ZSM-5 (MFI), mordenite (MOR), Y (FAU), Beta (BEA), UTD and MCM-41 were used in our experiments. In addition, different samples of faujasite were used, exhibiting a silica alumina ratio (SAR) ranging from 3 to 91. Faujasites with a SAR value higher than 3 had been de-aluminized by steam treating. All zeolitic materials exhibited a total pore volume of about 0.5 ml/g.

The samples were pelletized using a pressure of 1 MPa and subsequently crushed. A sieve fraction of 0.425-0.800 mm was used for absorption experiments. Prior to a measurement, the samples were treated in air for 24 hours at 523 K. Dehydration of the samples took place for 18 hours at 723 K.

Hexamethyldisiloxane (HMDS) was used to modify the hydrophilic character of the alumina and silica samples. This was established through boiling these materials in HMDS for one hour. In addition, the surface of alumina was treated with phosphoric acid in order to study the influence of the surface acidity. This was established through boiling this material in phosphoric acid for one hour.

Absorption experiments

Metal carbonyl absorption experiments were carried out in a fully automated microflow apparatus. In our experiments, simulated syngas was used, consisting of 40 vol.% H_2, 50 vol.% CO and 10 vol.% He. If required, water, hydrogen sulfide, metal carbonyl or a mixture of these components was added.

Prior to use, carbon monoxide was led at room temperature over a carbonyltrap consisting of zeolite Y. Water was introduced into the gas stream by means of a water saturator. Nickel tetracarbonyl was introduced into the gas stream by leading carbon monoxide over a reduced nickel catalyst (Ni/Al_2O_3, 70 wt.%) kept at 243 K. Iron pentacarbonyl was added to the feed by leading a controlled flow of helium through an iron pentacarbonyl saturator kept at 258 K. Helium 5.0, hydrogen 4.5, hydrogen sulfide 2.2 and carbon monoxide 4.7 were purchased from Hoek Loos b.v. Helium, hydrogen and hydrogen sulfide were used without further purification. The total gas flow was set at 100 ml/min, unless stated otherwise, so that an hourly linear space velocity was established of 6000 hr^{-1}. The iron pentacarbonyl and nickel tetracarbonyl partial pressures in the feed were varied between 0 and 30 Pa.

The gas composition upstream and downstream of the absorbent bed was analyzed with a Varian Cary 1E UV Vis spectrophotometer equipped with quartz gas flow cells with a length of 10 cm. The detection limit for iron pentacarbonyl was 0.01 Pa for iron pentacarbonyl, and for nickel tetracarbonyl 0.007 Pa. Furthermore, a Balzers quadrupole mass spectrometer was applied downstream of the bed for determination of the water and hydrogen sulfide partial pressures. 1 ml of absorbent sample (sieve fraction 0.425 to 0.800 mm) was placed in a quartz micro reactor tube (I.D. = 8 mm). If water and / or hydrogen sulfide were present in the gas stream, the absorbent bed was pre-saturated with water and/or hydrogen sulfide before the metal carbonyl was introduced in to the feed. Absorption profiles as a function of time were measured at 298 K. The total amount of metal carbonyl absorbed by the absorbent was calculated by integration of the metal carbonyl concentration difference up and downstream of the absorbent bed.

Absorbent Characterization

Pore size distributions and pore volumina were deduced from nitrogen absorption measurements with a Micromeretics 2000 gas absorption apparatus. The Horvath-Kawazoe model assuming a cylindrical pore geometry was applied.

Results and Discussion

To make a first selection, the suitability of a number of different absorbents was investigated. The influence of the chemical nature and the textural properties of the absorbent on the $Fe(CO)_5$ absorption capacity was examined using high-surface silica, high-surface alumina, zeolite Beta and Faujasite. All samples exhibited surface areas of 400 to 700 m^2/g. Syngas, only containing 20 Pa of iron carbonyl, was led over the absorbent bed. The results are summarized in Figure 1. From these results, it is clear that the zeolitic materials absorb significantly more metal carbonyl than the metal oxides. The absorption capacities of HMDS treated Al_2O_3 and SiO_2 are comparable with the absorption capacities of their unmodified counterparts. Also, the absorption capacity of untreated alumina is comparable with the absorption capacity of phosporic acid treated alumina.

The above findings led us to the conclusion that, when no additional compounds are present in the feed, the specific pore size and specific pore volume is far more important than the chemical nature of the surface for a suitable metal carbonyl absorbent.

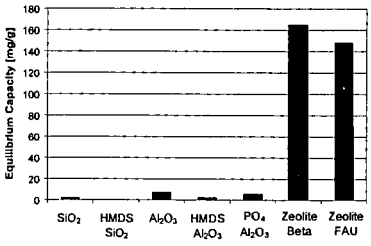

Figure 1: Equilibrium $Fe(CO)_5$ absorption capacities for several types of materials at 298 K. Hexamethyldisiloxane- treated SiO_2 and Al_2O_3 are denoted as HMDS-SiO_2 or HMDS-Al_2O_3, respectively. Al_2O_3 treated with phosphoric acid is denoted as PO_4-Al_2O_3.

Figure 2 displays the iron and nickel absorption capacity per gram of a number of zeolites as a function of pore size. Syngas, only containing 20 Pa of iron carbonyl or 16 Pa of nickel carbonylsulfide was led over the absorbent bed. From Figure 2 it becomes clear that zeolites exhibiting pores with a diameter less than 7 Å absorb only about 1 wt.% iron and nickel carbonyl. This suggests absorption to take place only at the external surface of these zeolite crystals. The kinetic diameter of the metal carbonyl molecules in the gas phase is about 7.4 Å, which is apparently too large to fit into the pore structure.

Zeolite Beta and Faujasite exhibit the largest absorption capacity. The pore (mouth) diameter of these materials is about the same size as the kinetic diameter of iron and nickel carbonyl. UTD and MCM, which have pores with a diameter larger than 8 Å, absorb significantly less. Their absorption capacity is found to be about one-third of the capacities for Beta and Faujasite. These results clearly reflect the

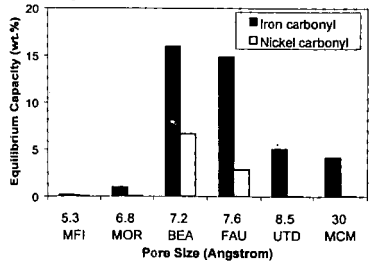

Figure 2: Equilibium absorption capacity at 298 K for Iron pentacarbonyl and Nickel tetracarbonyl as a function of the pore size. The zeolites used in this experiment are ZSM-5 (MFI), Mordenite (MOR), Faujasite (FAU), UTD, and mesoporous MCM-41

influence of the pore diameter on metal carbonyl absorption. For the zeolites tested, the capacity for nickel carbonyl is less than the capacity for iron carbonyl, although the kinetic diameters of iron and nickel carbonyl are about the same. It is beyond the scope of this abstract to go into detail on this issue. For the remainder of this abstract, we confine ourselves to faujasites and absorption of iron pentacarbonyl.

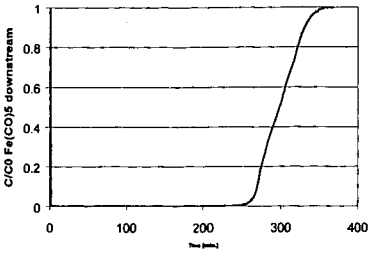

Figure 3: $Fe(CO)_5$ concentration downstream of an absorbent bed consisting of faujasite with a SAR value of 91.

A typical iron carbonyl absorption curve for a faujasite is displayed in Figure 3. Here, the carbonyl concentration downstream of the absorbent bed is plotted as a function of time. Syngas with 20 Pa of iron carbonyl was led over the absorbent bed. This breakthrough curve clearly shows that faujasites are capable of completely removing iron carbonyl out of a dry syngas stream.

Raw syngas contains also noticeable amounts of water and hydrogen sulfide. The question is, whether faujasites preferentially absorb water, hydrogen sulfide or metal carbonyl. Zeolite Y, a faujasite with a SAR value of 2.6, is known for its property to absorb water and, thus, it is used to dry gas streams. Therefore, it is imperative to study the influence of the SAR value on the absorption properties of faujasite for water, hydrogen sulfide and metal carbonyl separately, and in combination.

Syngas, containing both hydrogen sulfide (0.15 vol.%) and water (1.5 vol.%), but no metal carbonyls, was led over an absorbent bed consisting of faujasite with a SAR of 2.6 and 91, respectively. In Figure 4, both the H_2O and H_2S concentrations downstream of the absorbent bed are plotted as a function of time for both faujasites. For the faujasite with a SAR value of 2.6 it shows that initially both water and hydrogen sulfide are absorbed. However, as time progresses, hydrogen sulfide is desorbed from the zeolite and is expelled due to the absorption of water. A subsequently executed temperature-programmed desorption experiment showed only water to be present in the zeolite, the amount of which corresponds to complete pore filling. This result suggests that H_2O exhibits a considerably higher absorption energy than H_2S.
With the faujasite with a SAR value of 91, it turned out that only a small amount of water is absorbed, and no H_2S, since no desorption of H_2S due to absorption of water is measured.

A subsequent temperature-programmed desorption experiment showed that about 2 wt.% water is absorbed, and no hydrogen sulfide. These results demonstrate that from a gas stream containing both water and hydrogen sulfide, water is preferentially absorbed by faujasites.
The amount of water absorbed by the faujasite with a high SAR value, resembles a pore filling of only 4 percent. Therefore, we can conclude that only water might interfere with carbonyl absorption. Of course the extent of interference will be a function of the H_2O partial pressure.
De-aluminized faujasites are good candidates indeed for absorption of metal carbonyl from water and hydrogen sulfide containing gas streams. Additional absorption experiments showed no influence of hydrogen sulfide on the absorption kinetics of iron carbonyl.

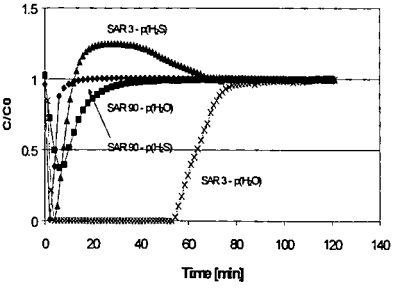

Figure 4: H_2O and H_2S concentrations downstream of the absorbent bed at 298 K, as a function of time onstream for two types of faujasites. The faujasites exhibit a silica alumina ratio of 2.6 and 91, respectively. C_0 is the concentration of H_2O and H_2S, respectively. $c(H_2O)$=1.5 vol.%, $c(H_2S)$=0.15 vol.%.

More information about the influence of water on the metal carbonyl absorption as a function of the SAR we obtained with the following experiments. Syngas, containing 20 Pa of iron carbonyl and either 0, 1.5 or 3 kPa of water, was led over the absorbent bed at 298 K. Figure 5 shows the equilibrium amount of absorbed iron carbonyl as a function of the SAR value, for a number of different H_2O partial pressures.

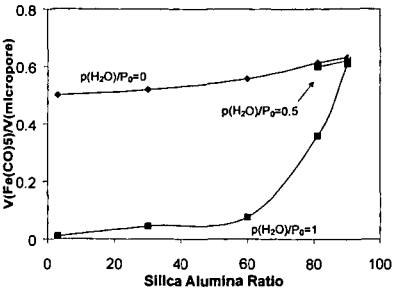

Figure 5: Volume $Fe(CO)_5$ absorbed in faujasite at 298 K, normalized on micro pore volume, as a function of silica alumina ratio and water partial pressure. For pore-filling calculations, it is assumed that $Fe(CO)_5$ absorbed in the micro pores has the same density as the bulk fluid.

From these results we can conclude that at relatively low SAR values, H_2O is preferentially absorbed in faujasites. Therefore, these faujasites exhibit little or no metal carbonyl capacity. However, at increasing SAR values, the influence of water on the amount of iron carbonyl absorbed decreases sharply. Typically, the equilibrium amount of $Fe(CO)_5$ absorbed by a faujasite with a SAR value of 91 is about 21 wt.%, regardless of the presence of water. The amount of water absorbed at $p(H_2O)/P_0=1$ for faujasites with SAR values of 3.6 and 91 is 31 wt.% and 17 wt.%, respectively. Apparently, at an increasing SAR value, the absorption energy of water in the micro pores decreases and metal carbonyl can get in. A high SAR value is therefore of major importance to effective metal carbonyl absorption. In other words, the SAR value is related to the hydrofobicity of the pores, and therefore of importance for lowering of the absorption energy of water. Also, a high SAR value appears to have a positive influence on the metal carbonyl absorption of the faujasites, probably due to textural changes by de-aluminization.

However, it can be expected that the presence of absorbed water for faujasites with a SAR value higher than about 60, obstructs the uptake rate of iron carbonyl to some extent. Lowering of the gas hourly space velocity (GHSV) could neutralize this effect. For the faujasite with a SAR value of 91, we assessed the influence of the GHSV on the iron carbonyl absorption kinetics in the presence of water.

Syngas, containing 3 kPa of water and 20 Pa of iron carbonyl, was led over the absorbent bed at 298 K. In Figure 6 the carbonyl concentration, downstream of the absorbent bed, is plotted as a function of the time for a GHSV of 6000/hr and 1500/hr, respectively. At a GHSV of 6000/hr, iron carbonyl was detected immediately. This was not the case for the dry faujasite at the same GHSV, as can be seen from Figure 3. After a steady state condition had been reached, the metal carbonyl concentration rose from 1.6 to about 2.2 Pa in 230 minutes. Finally, the concentration of metal carbonyl increased sharply, which indicated that the absorbent almost was saturated with iron carbonyl.

Lowering of the gas hourly space velocity from 6000/hr to 1500/hr, resulted in complete removal of iron carbonyl from the gas stream, as is usual for the dry faujasite at a GHSV value of 6000/hr. For both space velocities, the uptake of iron carbonyl remains 21 wt.%, corresponding with a micro pore filling of 65%. The uptake of water remains 17 wt.%.

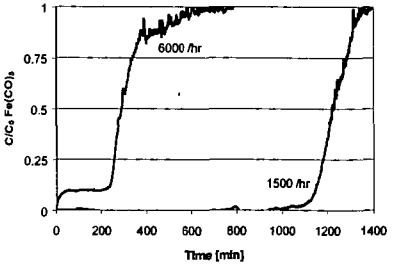

Figure 6: $Fe(CO)_5$ breakthrough curves at 298 K for a faujasite with a SAR value of 91, previously saturated with water. The gas hourly space velocity is varied between 6000 and 1500 /hr.

The results above led us to the conclusion that lowering of the GHSV neutralizes the retarding effect of water on the uptake rate of iron carbonyl. This retarding effect of water can only be explained by assuming that either water is rather easily expelled from the micro pore system of the faujasite due to absorption of iron carbonyl, or water is preferentially absorbed outside the micro pores. The exact nature of the influence of water on carbonyl absorption by de-aluminized faujasites goes beyond the scope of this abstract and will not be discussed here.

Finally, for application in an industrial process, these materials need to be regenerable. Bath [1] and Golden [2] already showed for zeolite Y that gentle heating restores completely the initial absorption capacity. Eijkhoudt et al. [3] showed the same for de-aluminized faujasites.

Conclusions

When carbon monoxide is present in a gas stream as a reactant or (by) product in industrial processes, a suitable absorbent for nickel tetracarbonyl and iron pentacarbonyl often is imperative. Faujasites with a silica alumina ratio of 60 and higher prove to be excellent metal carbonyl absorbents with regenerable capacities up to 21 wt.%, which corresponds to a micro pore filling of 65 %. Under the conditions applied, our experiments show that the metal carbonyl absorption capacity of these faujasites is influenced neither by hydrogen sulfide nor water. However, water retards the uptake rate of metal carbonyl to some extent. This retarding effect is easily neutralized by lowering of the gas hourly space velocity.
Consequently, these absorbents can be used to remove volatile metal carbonyls from raw syngas streams.

Acknowledgements
Shell Research and Technology Centre b.v. for financial support of this research.
Dr. Bonnie Marcus from Zeolyst International, for providing zeolite samples.
Dr. P.J. van den Brink and Dr. E.J. Creyghton from SRTCA Amsterdam for providing samples and for helpful discussions.

1 B. L. Bhatt, *Sep. Sci. and Techn.* 26 (1991), 1559.
2 T.C. Golden, *Ind. Eng. Chem. Res.*, 30 (1991), 502.
3 R. Eijkhoudt, "*Formation and Removal of volatile Metal carbonyls*", thesis, to be published.

SULFUR-RESISTANT BIMETALLIC NOBLE METAL CATALYSTS FOR AROMATIC HYDROGENATION OF DIESEL FUEL

Linjie Hu*, Hong Nie, Lianglong Qu, Guofu Xia, Yahua Shi, Dadong Li

Research Institute of Petroleum Processing, SINOPEC, Beijing 100083, PRC
Phone Number: 010-62315897 X 3862

INTRODUCTION

It is recognized that high aromatic content will lower the cetane number of diesel fuel and contribute significantly to the formation of undesired emissions in exhaust gases. As a result of the stringent environmental regulations, lowering aromatic content in diesel fuel is one of important technologies. Aromatic hydrogenation, especially for monoaromatics, is more difficult than hydrodesulfurization (HDS) and hydrodenitrogenation (HDN) on conventional sulfide catalysts (1). In addition to this, there is thermodynamic equilibrium limitation on aromatic hydrogenation within the normal operating range of hydrorefining. Therefore, the deep hydrodearomatization (HDA) is a formidable task by conventional hydrotreating technology using supported Ni(Co)Mo(W) sulfide catalysts.

Two-stage hydrotreating routes have been recommended to achieve low level of aromatics for its less investment in facilities and lower operating costs (2-5). In a two-stage process, a sulfide catalyst is used in the first stage where the sulfur and nitrogen are brought down, and a sulfur-tolerant noble metal catalyst is used in the second stage for aromatic hydrogenation. The key of the two-stage process is the development of high active noble metal catalyst with fine sulfur-resistance.

It has been generally acknowledged that the sulfur resistance of a noble metal can be enhanced by utilizing an acidic support, such as that of an acidic zeolite (6-14). Literatures on the sulfur resistance of bimetallic catalysts containing noble metals, except for Pt-Pd, are scarce (15). Y-zeolite supported noble metal catalysts, as important industrial catalysts for aromatics hydrogenation, have received increasing attention in recent years (16). Pd-M/Y bimetallic catalysts, where M are non-noble metal elements, were prepared to investigate the effects of the addition of a second metal in this study.

EXPERIMENTAL

70g NH_4Y (Na 1.2%, SiO_2/Al_2O_3=5) was mixed with 30g Al_2O_3, followed by kneading and extrudation, and finally calcined at 600°C for 2h.

The catalyst samples were prepared by incipient wetness impregnation technique. The Y zeolite support was brought in contact with a solution of $Pd(NH_3)_4Cl_2$ in deionized water, followed by drying at 120 for 2h and then calcining at 550 °C for 2h.The palladium-contained Y zeolite contacted with an aqueous solution of $(NH_4)_2CrO_4$, then dried and calcined as before. The Pd-Cr/Y catalyst has been prepared.

The other Pd-M/Y bimetallic catalysts were prepared following the same procedure with Pd-Cr/Y. The second metal precursors used for the preparation of the bimetallic catalysts are listed in Table 1. The metal contents, which were measured by inductively coupled plasma spectroscopy, are also listed in Table 1.

The sulfur resistance of catalyst was tested with a continuous down flow fixed-bed reactor. The reactor was packed with 1.0g catalyst (40~60 mesh) diluted with an inert 40~60 mesh ceramic in a ratio of 1:1. The upper and bottom part was filled with particles of a catalytically inactive ceramic material for preheating and preventing channel effects. The feed, toluene and n-hexane in a volume ratio of 1:1, was mixed with a certain amount of thiophene to prepare a feed of 3000ppm sulfur content. Catalysts were firstly reduced at 300 °C under 600psig of pure hydrogen for 2h. After reduction, the catalytic reactions were carried out with a weight hourly space velosity (WHSV) of $4.0h^{-1}$ and flowing hydrogen (400ml/min), under 600psig. Reaction products were analyzed by an on-line gas chromatography.

RESULTS AND DISCUSSION

The GC analysis results indicate that the main products of toluene hydrogenation on Pd-M/Y catalysts are methylcyclohexane(MCH) and 1,1-dimethyl cycloheptane (DMCH).

Fig.1 and Fig.2 show that hydrogenation activity of Pd-M/Y bimetallic catalysts are remarkably

different from Pd/Y catalyst, though the second metal added was only 0.6%. This indicates that the sulfur resistance of Pd are remarkably affected by the second metal. The sulfur resistance of Y zeolite supported Pd catalyst is improved by Cr and W, but lowered by La, Mn, Mo, Ag.

Fig.3 indicates that the second metal have no effect on the product selectivity of toluene hydrogenation on Pd bimetallic catalysts. The formation of isomer DMCH is related to the acidic properties of catalysts. The isomer selectivity doesn't change with the addition of the second metal. It could be deduced that the second metals have no effects on the acidic properties of Pd catalysts.

It can be observed from Fig.1 and Fig.2 that PdCr/Y and PdW/Y bimetallic catalysts exhibit better sulfur resistance than Pd/Y. This phenomena has not found to be reported yet. Since Y zeolite supported noble metal catalysts is important on industrial aspects, this discovery would have applied prospects for petroleum processing. From the aspects of isomer selectivity of toluene hydrogenation on Pd monometallic and bimetallic catalysts, the change of sulfur resistance of Pd catalysts was not caused by acidic properties. Nowadays, further studies on the mechanism that the second metal affects the sulfur resistance of Pd catalysts are carrying on in our laboratory.

CONCLUSIONS

The second metal has remarkable effects on the sulfur resistance of Y zeolite supported Pd catalysts. Among them, Cr and W improve the sulfur tolerance of Pd catalysts, but La, Mn, Mo and Ag make the sulfur resistance worse. For catalytic hydrogenation of toluene in presence of 3000ppm sulfur in feed on Pd/Y and Pd-M/Y, the second metals(M) have no obvious effects on product selectivity.

ACKNOWLEDGEMENTS

The support of Xiaohong Kang and Group 1508, Research Institute of Petroleum Processing are acknowledged.

Table 1. Summary of Catalyst Preparation and Composition

Catalyst	Precursor of Second metal	Pd content (wt%)	Second metal (wt%)
Pd	-	0.61	0
PdCr	$(NH_4)_2CrO_4$	0.59	0.61
PdW	$(NH_4)_{10}W_{12}O_{41}\cdot 11H_2O$	0.59	0.59
PdLa	$La(NO_3)_3$	0.60	0.60
PdMn	$Mn(NO_3)_2$	0.60	0.60
PdMo	$(NH_4)_2MoO_4$	0.60	0.59
PdAg	$AgNO_3$	0.61	0.61

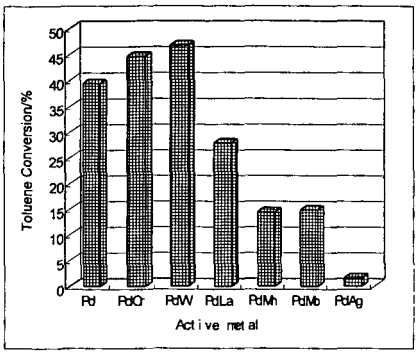

Fig.1 Toluene conversion on Pd bimetallic catalysts(T=280)

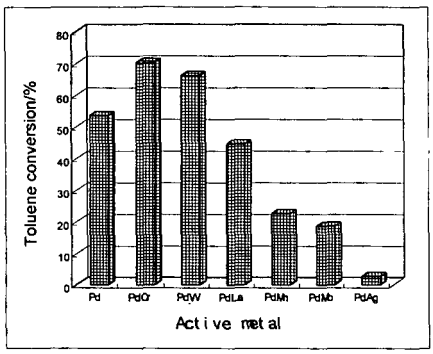

Fig.2 Toluene conversion on Pd bimetallic catalysts(T=300)

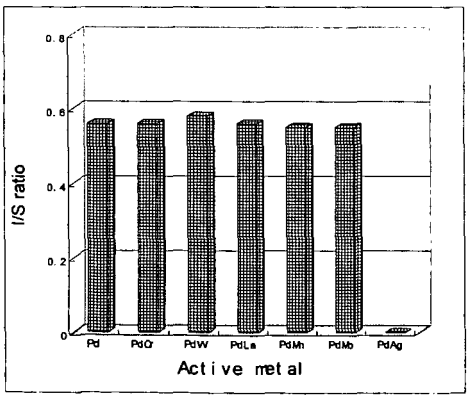

Fig.3 Isomerization selectivity(I/S ratio)
on Pd bimetallic catalysts
T=280°C

LITERATURE CITED

(1) Cooper, B. H., Stanislaus, A. and Nannerup, P. N., Am. Chem. Soc. Div. of Feul Chem. Preprints, 37(1), 41 (1992)
(2) Suchanek, A. J., Karlsson, K., 1993 NPRA Annual Meeting, AM-93-24
(3) Baldassari, M. C., 1994 NPRA Annual Meeting, AM-94-62
(4) Suchanek, A. J., Hamilton, G. L., 1992 NPRA Annual Meeting, AM-92-19
(5) Suchanek, A. J., Hamilton, G. L., 1991 NPRA Annual Meeting, AM-91-35
(6) Gallezot, P., Bergeret, G., Catalyst Deactivation, Dekker, New York, p.263(1987)
(7) Suchanek, A. J., Oil Gas J, May 7, p.109(1990)
(8) Peries, J. P., Billon, A., Hennico, A., Kressmann, S., 1991 NPRA Annual Meeting,
(9) Dalla Betta, R. A., Boudart, M., Proc. 5th Int. Congr. on Catal., North Holland, p.1329(1973)
(10) Homeyer, S. T., Sachtler, W. M. H., Zeolites: Facts, Figures and Future, Elsevier, p.975(1989)
(11) Rabo, J. A., Schomaker, V., Pickert, P. E., Proc. 3rd Int. Congr. on Catal., North Holland, Amsterdam, p.1264(1964)
(12) Chukin, C. D., Proc. 6th Int. Congr. Catal., Chemical Society, London, p.668(1977)
(13) Tri, T. M., Massardier, J., Gallezot, P., Imelik, B., Stud. Surf. Sci. Catal., 5, 279(1980)
(14) Besoukhanova, C., Stud. Surf. Sci. Catal., 6, 201(1980)
(15) Cooper, B. H., Donnis, B. B. L., Appl Catal A: General, 137, 203(1996)
(16) Stanislaus, A., Cooper, B. H., Catal. Rev. Sci. Eng., 36, 75(1994)

OPTIMUM DESIGN OF THE NICKEL CATALYSTS AND MECHANISTIC STUDY FOR CO_2 REFORMING WITH CH_4

Rong-Gang DING Zi-Feng YAN *
State Key Laboratory for Heavy Oil Processing, University of Petroleum, Dongying 257062, P R China

ABSTRACT The possibility of optimizing the composition and the structures of the nickel catalysts and the pretreatment and reaction conditions for carbon dioxide reforming with methane is investigated. The optimum catalyst and the pretreatment and reaction conditions are determined employing the orthogonal and uniform design methods. The optimum nickel catalyst gives promising catalytic performance in terms of activity, selectivity and resistance to coke formation under the pretreatment and reaction conditions. The reaction behaviors and perfect performance of the optimum catalyst are extensively discussed. The properties of the surface carbon intermediates, which are produced by the decomposition of methane, using temperature-programmed desorption, temperature-programmed surface reaction, pulse reaction and on-line quadrupole mass spectroscopy techniques were also investigated. Carbidic C_α, carbonaceous C_β and carbidic clusters C_γ surface carbon species formed by decomposition of methane showed different surface mobility, thermal stability and reactivity. The possible reaction mechanism of carbon dioxide reforming with methane will also be postulated. Methane is firstly decomposed into hydrogen and different surface carbon species, then the adsorbed or gas phase CO_2 reacts with surface carbons to form CO.

KEYWORDS Optimum design, carbon dioxide reforming with methane, mechanism

1. INTRODUCTION

In recent years, catalytic reforming of carbon dioxide with methane to synthesis gas has been received new interest due to its environmental benefits and desired CO/H_2 ratio than steam reforming for the production of hydrocarbons and oxygenated derivatives. Unfortunately, no commercial catalyst is yet available for the reforming of methane with carbon dioxide. Supported noble metals give promising catalytic performance in terms of activity, selectivity and resistance to coke formation.[1-3] Various nickel-based catalysts have been prepared and investigated in the past decades[4-6] with different metal loadings, varieties and quantities of the promoters, and kinds of the supports. But there are few reports comparing the activity and stability of the catalysts with different compositions. No effective method to arrange the catalyst preparation and activity evaluation has yet been proposed. This paper aims at exploring possibility of optimizing the composition of the nickel catalysts and the pretreatment and reaction conditions employing orthogonal design and uniform design methods. There is a limiting amount of fundamental research concerning the reforming of methane with carbon dioxide over nickel-based catalysts. The present study also reports the characterization of the surface carbon intermediates produced in the reforming process and postulation of the reaction mechanism.

2. EXPERIMENTAL

2.1 Catalyst Preparation. A series of nickel-based catalysts were prepared with different supports, promoters and metal contents. La_2O_3, SiO_2, and two kinds of Al_2O_3 are selected as the catalyst supports. Nickel nitrate was loaded on the various supports by the incipient wetness impregnation method, then magnesium nitrate and cerous nitrate were added to the support by the same method. The nickel loading was set from 7.0% to 11.5% (wt%), while each promoter content was kept from 0 to 3% (wt%).

2.2 Catalytic Reaction. The reforming reaction was carried out in a continuous flow quartz fixed-bed reactor (i.d. 6mm) under atmospheric pressure and various reaction temperatures. The composition of reactants/products mixture was analyzed with an on-line SP-3420 gas chromatograph equipped with a TCD and a Porapak QS column.

2.3 Catalyst Characterization. The temperature-programmed experiments are conducted in the quartz fixed-bed reactor following the catalysts pretreatment. The catalysts are treated with oxygen for 30 min, then reduced with H_2 for 1 hr, finally cooled to room temperature and purged with He stream for 30 min.

* To whom correspondence should be addressed. E-mail: zfyan@hdpu.edu.cn

The methane was pulsed continually on the pretreated catalysts using high purity helium as carrier gas at 973 K. Subsequently, a 20 ml/min flow of hydrogen or mixed gas of CO_2/He (1:10) was introduced to flush the reactor continuously to take away the gaseous and physically adsorbed mixture after cooling to room temperature. Then the TPSR was initiated in the hydrogen or mixed gas of CO_2/He at a heating rate of 20 K/min. When the temperature was

increased to 1000 K, the carrier gas was switched again, then H_2 and O_2 were pulsed respectively into the micro-reactor under high temperature. The desorbed products from the metal surface along with the temperature-programmed process were simultaneously detected by on-line ion trap detector (ITD).

TPD experiments were conducted at a constant heating rate (10 K/min), using ultra high purity helium as carrier gas, at a flow rate of 40 ml/min. The reforming reaction was carried out in situ at certain temperature and then the reactor was quickly cooled to room temperature. After purging with He for 30 min, the temperature programming was initiated and the analysis of the desorbed gases was performed with the on-line ITD.

In the TPD process, the helium gas was dried with $Mg(ClO_4)_2$ and deoxygenated with 402 deoxygenating reagent. The residual oxygen that might flow over the catalyst was removed by using liquid nitrogen cold trap before flowing into the reactor. Leak tests on the reaction system were also strictly performed to exclude the possibility of the oxidation of surface carbonaceous species.

3. RESULTS AND DISCUSSION

3.1 Catalyst Optimization. A series of nickel-based catalysts, with various supports, promoters and metal loadings, were prepared by incipient wetness impregnation method according to a certain orthogonal design table. The L_{25} (4^5) orthogonal table is employed to arrange the preparation of catalysts and investigate the interaction between metal and support. In this table, the support-metal strong interaction was considered an important factor. The orthogonal design experimental results for the reforming catalyst are shown as Table 1.

The optimum pretreatment and reaction conditions were determined by a large number of experiments employing the uniform method. Its characteristic and application in the catalytic scientific community will be discussed elsewhere. Catalytic performance tests for all catalysts were carried out under the optimum pretreatment and reaction conditions.

The total molar concentration of CO and H_2 (dry base) is used to evaluate the performance of catalysts. It can be seen that the effect of the factors on the performance of the catalyst is as follows: support > Ni metal loading > MgO addition > CeO_2 addition > interaction between metal and support. It is found that the support shows more influence than metal loading on the performance of catalysts within appropriate metal loading range. It gives evidence that understanding of the nature of support and selection of support may be very important for improving the catalyst.

The weak interaction between metal and support may be attributed to the preparation conditions of the catalysts. In the meantime, MgO and CeO_2 promoter exhibit approximate effect on the activity of catalysts. It can be seen from Table 1 that the OD-5 catalyst is the best reforming catalyst in this experiment. Indeed, it provides 91.3% and 86.9% conversions of CO_2 and CH_4, 86.8% and 89.1% yields of H_2 and CO at 973K, respectively. According to the experimental results, it is deduced that the optimum catalyst constitutes can be described as follows: 8.5 wt% Ni loading supported on Al_2O_3-1 with 3 wt% MgO and 3 wt % CeO_2 added.

The catalyst activity exhibited in Table 1 is the integrative result of the collective effect of metal loading, support, promoter, and interaction between support and metal. It is very difficult to simply compare one catalyst with another in terms of certain factor's influence on the performance of catalyst when the catalyst are prepared and tested according to a orthogonal design method. The orthogonal design considers all factors as an indivisible one and arranges them efficiently to simplify the catalyst screening. For the heavy and complicated catalyst screening, the orthogonal design method may be a desired choice. As a matter of fact, the orthogonal design method has applied to many scientific fields. But to our knowledge less applications of the orthogonal design in catalyst preparation and screening have been reported. In this work, we try to make use of this method to optimize the catalyst and simplify the catalyst screening process. It is convinced of the rapid development of the catalyst orthogonal screening technique in near future.

3.2 Catalyst Characterization.

H_2 TPSR of the catalyst. A great effort was made to detect adsorbed carbonaceous $CH_{x(ad)}$ fragments formed in the decomposition of methane by means of sensitive *in-situ* FT-IR spectroscopy. However, no adsorption bands attributable to any vibration modes of carbonaceous $CH_{x(ad)}$ species were identified either by *in-situ* measurements or after a sudden cooling of the sample in a continuous methane flow at 700 K. This means that all the above carbonaceous $CH_{x(ad)}$ species react or decompose too quickly at high temperature, or their surface concentrations are below the detection limit.

However, the presence of surface carbonaceous $CH_{x(ad)}$ species was well manifested by its reaction with hydrogen. After flushing the reactor with pure helium flow (following methane decomposition at a certain temperature) and switching to a hydrogen flow, the hydrogenation of the surface carbonaceous $CH_{x(ad)}$ species was investigated by TPSR technique. Figure 1 showed that the decomposition of methane could result in the formation of at least three kinds of surface

carbon species on supported nickel catalyst. Generally, the carbon deposition is comprised of various forms of carbon species which are different in terms of reactivity. The distribution and features of these carbonaceous species depend sensitively on the nature of transition metals and the conditions of methane adsorption. These carbonaceous species can be described as: completely dehydrogenated carbidic C_α type, partially dehydrogenated CH_x ($1 \le x \le 3$) species, namely C_β type, and carbidic clusters C_γ type formed by the agglomeration and conversion of C_α and C_β species under certain conditions.

A fraction of the surface carbon species, which might be assigned to carbidic C_α (~461 K), was mainly hydrogenated to methane even below 500 K. Simultaneously, a trace of ethane was also produced in addition to methane. It shows that carbidic C_α species is rather active and thermally unstable on nickel surface. The significant amount of surface carbon species was hydrogenated to methane below 600 K and was assigned to partially dehydrogenated C_β (~583 K) species. The majority of the surface carbon was hydrogenated above 800 K and was attributed to carbidic clusters C_γ (~823 K). The formation of less active C_γ species causes the catalyst deactivation.[8] It also indicated that the formation of three kinds of surface carbon species with different structures and properties largely depend on the exposure temperature and duration to methane. When the nickel catalyst was exposed to methane above 723 K, the carbidic C_α species was not detected, and a significant amount of C_β was transformed into the carbidic clusters C_γ. It shows that the carbidic clusters C_γ species might be the precursor of the surface carbon deposition, which may be produced by the interactions between C_α and C_β species and between C_α and C_β themselves.

TPD of used catalyst. The TPD profiles of used Ni/Al_2O_3 catalyst after 8 h of reaction were shown in Figure 2. Compared with CO-TPD profiles over the fresh Ni/Al_2O_3 catalyst, on which two respective CO_2 desorption peaks appear, an additional intense CO_2 peak at ca. 910 K was observed on used catalyst.

The two CO_2 desorption peaks appear on both the TPD of used catalyst and the CO-TPD profiles over the fresh catalyst at ca. 410 K and 570 K. They seem to correspond to the desorbed CO_2 in the form of weakly chemisorbed on different sites on both catalysts. It is interesting to note that a large quantity of CO and CO_2 desorbed at approximately the same temperature from at ca. 800 K, but the increase of CO obviously lagged behind. This indicates that CO might be the secondary product rather than primary one. The interaction of surface carbon with gaseous CO_2 would result in the formation of CO. The obvious hysteresis effect of CO peak with respect to CO_2 peak and the continuous increase of intensity of CO peak are noteworthy. This could be manifested by the mobility of the surface carbon species and the reactivity of the oxygen species on the nickel catalyst. The mobile surface carbon species can attack the neighboring oxygen adatoms and surface oxygen species to form CO or CO_2. It is also possible that the CO_2 desorbed from the catalyst re-adsorbed and then reacted with surface carbonaceous species to produce CO. The carbon species originally produced by methane are believed to be atomic or carbidic carbon. It is known to be a very active and important intermediate in the CO_2 reforming of methane. The interaction between the adsorbed or gaseous CO_2 and surface carbon species can result in the formation of CO. Based on this consideration, the possible reaction processes of CO_2 reforming of methane can be inferred as follows: methane is firstly decomposed into hydrogen and different surface carbon species, then the adsorbed or gas phase CO_2 reacts with surface carbons to form CO.

CO_2 TPSR and pulse reaction of H_2 and O_2. Firstly, TPSR was performed in the mixed gas of CO_2/He (1:10) following CH_4 pulses over reduced Ni/Al_2O_3 catalyst (Figure 3), then the H_2 or O_2 pulse was introduced into the reactor (Figure 4). A fraction of CO_2 adsorbs on the catalyst at about 300 K and desorbs from 600 K in the CO_2/He flow. The equilibrium between the surfaced adsorbed and gaseous CO_2 is responsible for the high CO_2 desorption temperature than that in He flow. The formation and desorption of CO can be observed while surfaced CO_2 begins to desorb greatly. The consumption of CO_2 and formation of CO reach the maximum at elevated temperature of 740 K. The CO_2 TPSR on the Ni catalyst may give a deduction of the pathway of CO_2: firstly adsorbs on the surface of the catalyst, then reacted with neighboring surface carbonaceous species to form CO. This is similar to the inference from the TPD experiment of the used catalyst as Figure 2 showed.

The formation of CH_4 is not detected in the H_2 pulse reaction following CO_2 TPSR at 973 K. It shows that the surface carbonaceous species which can react with CO_2 have used up. This type of surface carbonaceous species is active and can react with not only CO_2 but also with H_2. At the same time, other inertial carbonaceous species may exist on the surface of the catalyst. The O_2 pulse reaction is continually carried out following the CO_2 TPSR and H_2 pulse reaction in order to verify the existence of other carbonaceous species. The appearance of CO_2 corresponding to the O_2 pulses is good evidence for the existence of the other carbonaceous species, which is difficult to react with H_2 or CO_2. The catalyst deactivation may result from the deposited carbon species, which does not react with H_2 or CO_2 but react with O_2 at high temperature.

Figure 1 becomes conscious of the emergence of at least three kinds surface carbonaceous species at lower temperature. When the catalyst was exposed to methane at 973 K, the carbidic C_α species was completely converted into C_β or C_γ species. The partially dehydrogenated C_β

species can react with H_2 or CO_2 to form CH_4 or CO, but the less active carbidic clusters C_γ species can not react with H_2 or CO_2 even at very high temperature. The H_2 and CO_2 TPSR and pulse reaction provide the mutual verification of the existence and property of the surface carbonaceous species. The further investigation towards the properties of the surface carbon species is the key to suppressing the catalyst deactivation and elucidating the mechanism of the reforming reaction.

4. CONCLUSIONS

(1) The orthogonal design method can simplify the catalyst screening process and evaluate the principal effect and its degree of influence on the performance of the catalyst.
(2) Carbidic C_α, carbonaceous C_β and carbidic clusters C_γ surface carbon species formed by decomposition of methane showed different surface mobility, thermal stability and reactivity. C_α and C_β species are active and the carbidic clusters C_γ species might be the precursor of the surface carbon deposition.
(3) The possible reaction processes may be as follows: methane is firstly decomposed into hydrogen and different surface carbon species, then the adsorbed or gas phase CO_2 reacts with surface carbons to form CO.

ACKNOWLEDGEMENTS

Financial supports by the Young Scientists Award Foundation of Shandong Province and Young Scientists Innovation Foundation of China National Petroleum Corporation are gratefully acknowledged.

REFERENCES

(1) Solymosi, F.; Kustan, G.; Erdohelyi, A. *Catal. Lett.* **1991**, *11*, 144.
(2) Vennon, P. D. F.; Green, H. M. *Catal. Today* **1992**, *13*, 417.
(3) Richardson, J.T.; Paripatyadar, S.A. *Appl.Catal.* **1990**, *61*, 293.
(4) Gadalla, A.M.; Bower, B. *Chem. Eng. Sci.* **1988**, *43*, 3049.
(5) Yamazaki, O.; Nozaki, T.; Omata, K.; Fujimoto, K. *Chem. Lett.* **1992**, 1953.
(6) Chen, Y. G.; Yamazaki, O.; Tomishige K.; Fujimoto, K. *Catal. Lett.* **1996**, *39*, 92.
(7) Wang, S. B.; Lu, G. Q. *Ind. Eng. Chem. Res.* **1997**, *36*, 5103.
(8) Zhang, Z.; Verykois, X. E. *Catal. Today* **1994**, *21*, 589.

Table 1 Orthogonal design experimental results
(T = 973 K, P = 1atm, CH_4 / CO_2 = 1.05)

factor	A	B	A	B	C	D	$(CO+H_2)$	CH_4	CO_2	H_2	CO
	Ni		MgO		CeO_2		concn.(dry	conv.	Conv.	yield	yield
number	(wt%)	support	(wt%)		(wt%)		mol%)	(%)	(%)	(%)	(%)
1	7.0	Al_2O_3-1	1	0	0		71.2	74.6	79.7	74.0	77.2
2	7.0	Al_2O_3-2	2	1	1		75.8	79.5	85.7	784	82.6
3	7.0	La_2O_3	3	2	2		46.5	48.7	54.6	47.0	51.7
4	7.0	SiO_2	4	3	3		68.1	69.7	77.0	67.9	73.4
5	8.5	Al_2O_3-1	2	2	3		84.8	86.9	91.3	86.8	89.1
6	8.5	Al_2O_3-2	1	3	2		79.2	81.9	89.3	80.3	856
7	8.5	La_2O_3	4	0	1		54.3	57.7	68.7	53.8	63.2
8	8.5	SiO_2	3	1	0		61.4	64.3	71.5	62.4	67.9
9	10	Al_2O_3-1	3	3	1		77.3	79.9	86.8	78.5	83.4
10	10	Al_2O_3-2	4	2	0		66.5	68.7	75.1	67.3	71.9
11	10	La_2O_3	1	1	3		52.4	54.0	61.1	51.9	57.8
12	10	SiO_2	2	0	2		56.3	58.4	61.6	58.3	60.0
13	11.5	Al_2O_3-1	4	1	2		62.3	64.6	73.4	62.0	69.0
14	11.5	Al_2O_3-2	3	0	3		59.3	62.0	69.1	60.0	65.6
15	11.5	La_2O_3	2	3	0		48.9	51.2	59.2	48.6	55.3
16	11.5	SiO_2	1	2	1		49.6	51.6	59.3	49.2	55.5
R			14.9	23.4	3.7	8.1	7.1				
prior level			A_2	B_1	$(A\ B)_2$	C_4	D_4				
factor order			2	1	5	3	4				

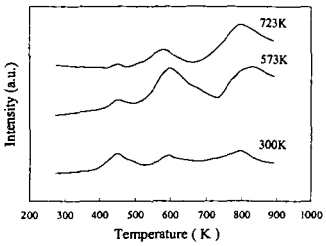

Figure 1. TPSR spectra of CH_4 in H_2 flow on fresh 8wt% Ni/Al_2O_3 at different adsorption temperatures

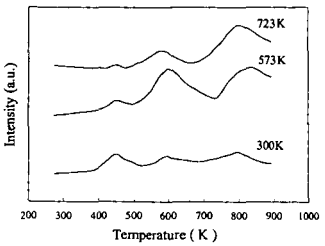

Figure 2. TPD profile over the used 8wt% nickel catalyst supported on alumina

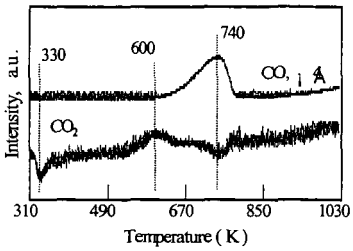

Figure 3. TPSR in CO_2/He (1:10) stream following CH_4 pulse at 973K over reduced Ni/Al_2O_3 catalyst.

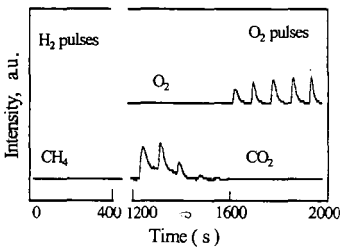

Figure 4. H_2 and O_2 pulses patterns at 973K following CO_2 TPSR over Ni/Al_2O_3 catalyst.

THE MICROWAVE PROMOTED CARBON CATALYZED PRODUCTION OF TERMINAL OLEFINS FROM LONG CHAIN ALKANES AND CARBON-CARBON CLEAVAGE REACTIONS OF ORGANIC MOLECULES

Dennis D. Tanner,[1] Qizhu Ding,[1] Pramod Kandanarachchi[2] and James A. Franz[2]

Contribution from the Department of Chemistry,
University of Alberta, Edmonton, Alberta, T6G 2G2, Canada
and
Pacific Northwest National Laboratory
Richland, WA 99352 USA

Key Words: Carbon-catalyzed, microwave, α-olefins, ethylene, hydrogen production.

ABSTRACT

The selective conversion of saturated linear hydrocarbons at ambient temperature to α-olefins and dihydrogen and other transformations of organic molecules involving the direct scission of carbon-carbon bonds are described. Activated wood charcoals containing trace metals were subjected to microwave radiation in the presence of liquid hydrocarbons at room temperature. Long-chain hydrocarbons were converted with high selectivity to a series of terminal olefins. For example, at less than 30% conversion, n-hexadecane yields n-C_3 to n-C_{14} α-olefins and light gases, predominately ethylene, and dihydrogen. Extensive conversion of linear hydrocarbons leads to substantial yields of α-olefins, diterminal diolefins, and ethylene. Product distributions are consistent with a pathway for olefin formation from linear hydrocarbons at room temperature that does not involve free radical formation. The method is effective for carbon-carbon bond cleavage in and conversion of a wide array of linear and branched hydrocarbon feedstocks to hydrogen, ethylene, and olefins. Saturated organic hydrocarbons containing functional groups (-OH, -CN, $-CO_2H$, $-CO_2CH_3$) undergo carbon-carbon bond scission and olefin formation with substantially intact functional groups. Cyclic alkanes and terpenoid hydrocarbons under ring cleavage, contraction, and ring isomerization reactions. In the presence of small amounts of water, cycloalkanes are converted to cyclic alcohols and ketones. The method makes possible selective chemical transformations involving the direct cleavage of saturated carbon-carbon bonds at room temperature.

INTRODUCTION

The direct cleavage of strong carbon-carbon bonds to effect selective synthesis of lower molecular weight hydrocarbons is a primary goal of research in heterogeneous and homogeneous catalysis. Methods for the selective, direct cleavage of strong carbon-carbon bonds, particularly at ambient temperature and atmospheric pressure, are scarce. Most approaches involve some degree of thermal hydrocracking to effect strong bond scission and structural isomerization, or the involvement of transition metal catalysts capable of activation of a hydrocarbon via oxidative addition of a hydrocarbon C-H bond to a coordinatively unsaturated metal system. Previous work with microwave-activated catalysis has involved creation of high local temperature regimes leading to thermal cracking and reforming involving free radicals, ions, carbenes, atoms and other reactive intermediates. Solution phase microwave promoted chemical transformations have generally dealt with either dielectric heating of the substrate or catalyst,[3] or with reactions carried out using a vapor phase plasma.[4] These approaches using dielectric heating involve the creation of "hot spots" in the catalyst surface that promote chemical transformations through local high temperature regimes.[5] Thus, thermolysis of methane over a glowing microwave catalyst produces ethylene, acetylene, propylene, hydrogen and soot reminiscent of simple thermal pyrolysis.[3d] Under more controlled conditions of low power irradiation, ethylene and acetylene may be prepared from methane and hydrogen with significant selectivity.[5] While previous studies have demonstrated that light organic gases can be converted under plasma initiation conditions, no previous work has explored the utility of microwave activated catalysis in bond-breaking transformations of large organic molecules and functionalized alkanes. Thus, in this work we present results of a study of low-power microwave irradiation of an activated carbon catalyst that leads to carbon-carbon bond cleavage and olefin formation from linear alkanes without formation of characteristic organic pyrolysis products. High yields of olefins and hydrogen result from a range of hydrocarbon precursors and functionalized hydrocarbons. Organic structures are demonstrated to exhibit significant chemical selectivity in carbon-carbon bond scission reactions, in part due to the ability of the liquid organic medium to rapidly quench high energy intermediates.

EXPERIMENTAL

Microwave Conversion of Hexadecane To Olefins. **Hexadecane** (2 g) was mixed with activated charcoal (0.5 g) in a reaction tube and subjected to microwave radiation (20 min) at 60% power

(ca. 30 watts) at 2540 MHz using the apparatus shown in Figure 2. The total volume of the gaseous products were measured by the gas burette, and both gaseous and liquid products were analyzed by GC, GC/IR and GC/MS. Products were identified by comparison of their GC retention times, GC/IR and GC/MS of authentic samples that were available. When the authentic samples were not available, products were identified by their GC/IR and GC/MS which showed similarities to those of authentic homologous compounds. Gaseous and liquid products are shown in Table 1.

Microwave Promoted Reaction of Polyethylene in the Presence of Wood Char. A sample of low density **polyethylene** (2 g) was heated to melt (>130°C) and mixed with activated charcoal (0.5 g) and subjected to microwave radiation for 2 minutes. The products were identified by means of GC, GC/IR and GC/MS and comparison with authentic materials. With extended irradiation, the molten polymer could be completed converted to volatile products consisting primarily of ethylene, along with hydrogen, and minor yields of light olefins and hydrocarbons.

Microwave Promoted Conversion of Diacid Esters. **Dimethyl-1,6-hexanedioic acid ester (Dimethyladipate)**. 0.1g of charcoal and 1 g of substrate were irradiated for 2 hours at 50W. The major products (30% conversion) were methyl acrylate, methyl butenoate, and methyl pentenoate, formed in the ratio 20:5:1. These products composed 85% of the product mixture. Minor products methyl proprionate, methyl butanoate, and methyl pentanoate were formed as 15% of the reaction mixture. Hydrogen was not quantitated in the reaction. These results suggest that dimethyl adipate was cleaved to form methylacrylate with 65% selectivity. **Dimethylmalonate**. 0.15g wood char and 2.5 g substrate were irradiated for two hours. This resulted in less than 4% conversion to gaseous products and less than ca. 1% conversion to liquid products (methanol and methyl acetate). **Diethylsuccinate**. 0.15 g wood char and 2.5 g substrate were irradiated for two hours. About 10% conversion to gaseous products (CO_2, CH_4, C_2H_2, C_2H_4) and 2% conversion to ethanol and ethylacrylate occurred.

Microwave Irradiation of Methyl Palmitate. **Methyl Palmitate** , 1 g and wood char, 0.1 g, were irradiated for 1 hour. Products included gases (C_2H_4, C_2H_2, H_2 and CO_2) accounting for 6% of starting ester and liquids accounting for 14% of the starting ester. The liquid products consisted of a series of terminal olefins, n-$C_3H_7CH{=}CH_2$ through n-$C_{13}H_{27}CH{=}CH_2$, along with a series of corresponding terminal olefins substituted with an ester group, $CH_3O_2C(CH_2)_nCH{=}CH_2$, n=4-12. The esters were each produced in yields comparable to its corresponding simple terminal olefin cleavage pair. This indicates that the ester group remained intact during the carbon-carbon scission reaction.

Microwave Irradiation of Octadecanol. **1-Octadecanol**, 1 g, and pine char, 0.05 g, were irradiated at ca. 50 W for one hour. At ca. 30% conversion, products consist of light gases (ca. 50%), the major component of which is ethylene, and liquids (ca. 50%). The liquid products were composed of a series of terminal olefins and a corresponding series of terminal olefins possessing a terminal hydroxyl group ($C_3 - C_{17}$). The hydroxylated hydrocarbon terminal olefins and hydrocarbon terminal olefins were formed in approximately equal yields.

Microwave Irradiation of Cyclododecane. **Cyclododecane** (damp with water, or dried, by exposure of a solution of hydrocarbon in CH_2Cl_2 to anhydrous $MgSO_4$), 1 g, and white pine char catalyst, 0.05-0.1 g, were warmed to ca. 100 °C to melt the waxy hydrocarbon after which irradiation (ca. 50 W) was carried out for 20 min. Dry cyclododecane underwent ca. 21% conversion in 10 min, yielding gaseous products (11%) and liquid products (10%). The liquid products include ring contraction products (22%), acyclic terminal olefins (56%), and acyclic diterminal olefins (14%). The gaseous products contained hydrogen (16%), methane(4%), ethylene (48%), ethane(2%), acetylene (12%), propylene(8%), butene(3%) and butadiene(7%). Damp cyclododecane gave cyclododecanol (19%) and cyclododecanone (26%) as major products, in addition to hydrocarbon products. In the absence of moisture, the products were as follows: C_{12} Products: 1-dodecene (14%); C_{10} Products: Cyclodecane (21%), 1-methyl-2-propylcyclohexane (2%), n-butylcyclohexane (4%), 1-decene (10%) and 1,9- decadiene(1%); C_9 Products: 1-nonene (4.6%), 1,8-nonadiene; C_8 Products: Cyclooctane (19.5%), 1-octene(7.5%), 1,7-octadiene (2%); C_7 Products: 1-heptene(3%), 1,6-heptadiene (1.6%); C_6 Products, cyclohexane (2%).

RESULTS AND DISCUSSION

Ambient Temperature Conversion of Linear Hydrocarbons. Low power microwave irradiation of liquid hydrocarbons in the presence of a catalyst, activated wood charcoal, leads to the remarkably selective production of α-olefins. In the case of hexadecane, conversion up to ca. 30% leads only to α-olefins and light gases, mainly ethylene. Above 30% conversion, the formation of diterminal diolefins becomes significant, and further conversion of lighter olefins to ethylene occurs. Ultimately, ethylene is the major product from hydrocarbons, with small yields of acetylene from further conversion of ethylene and butadiene. The terminally unsaturated hydrocarbons, C_3-C_{13}, formed from hexadecane are shown in Fig. 1 and Table 1. The gaseous products gave a 47% yield while the liquid products showed a 10% yield, see Table 1. The most notable features of the reaction include (1) the formation of α-olefins from linear alkanes with only trace levels of hydrocarbons, (2) the absence of internal (non-terminal) olefins, and (3) the

absence of alkyl radical termination products (saturated alkanes of higher molecular weight than the parent hydrocarbon). GC analysis of the products of hexadecane reaction and those of other linear hydrocarbons gave no more than trace quantities of simple hydrocarbons and no detectable longer chain ($> C_{16}$) hydrocarbons. Linear alkanes would have been formed in radical-radical termination reactions. Shorter chain fully saturated hydrocarbons would have been formed in radical-radical termination reactions and in abstraction reactions. Finally, some internal (non-terminal) olefins should have formed from disproportionation of secondary alkyl radicals formed in a radical forming initiating process. The absence of these products rules out the buildup of appreciable concentrations of free alkyl radicals as might be expected in a simple pyrolytic free radical mediated bond scission mechanism, at least in the nominally ambient temperature reactions.

Conversion of Polyethylene and More Complex Organic Structures. At the higher temperatures used to melt polyethylene (180 °C), saturated hydrocarbons were formed as minor products in addition to the major products, α-olefins, see Fig. 3. The production of alkanes is consistent with participation of the *functional equivalent* of diradicals or radical pairs resulting in disproportionation leading to the observation of alkane formation.

Conversion of Diesters. Dimethyl adipate, **1**, was found to react much faster than diethylsuccinate, **2**, and dimethyl malonate, **3**, which was nearly inert to the reaction conditions. Dimethyl adipate reacted with about 65% selectivity to give central carbon-carbon bond cleavage yielding methyl acrylate. These observations suggest that surprisingly selective transformations involving cleavage of strong carbon-carbon bonds are made possible by microwave activated catalysis.

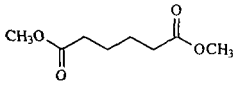

1

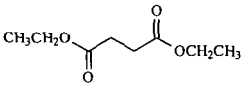

2

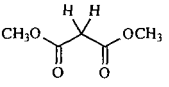

3

Conversion of Cyclic Hydrocarbons. The reaction of cyclododecane, carried out at 100°C, led to ring contraction products cyclodecane and cyclooctane in high yields at short reaction time. This implies that both products are first-generation products, and suggests a path for sequential loss of ethylene units, via the functional equivalent of a diradical pathway, as indicated in Figure 5. This would further seem to suggest that linear alkanes would form alkyl radicals by simple followed by multiple ethylene scission events and a terminating hydrogen atom elimination:

$$CH_3(CH_2CH_2)_x\bullet \rightarrow CH_3(CH_2CH_2)_{x-n}\bullet + n\,C_2H_4 \rightarrow CH_3(CH_2CH_2)_{x-n-1}CH{=}CH_2 + H\bullet$$

Such a scheme would be consistent with the substantial yields of ethylene at low overall conversion of linear hydrocarbons, but it would appear inconsistent with the absence of alkyl free radical products, e.g., the absence of alkane products from abstraction, combination, and disproportionation.

The microwave irradiation of a char catalyst at low power levels is accompanied by the emission of flashes of light. A number of reaction pathways can be proposed for fragmentation of alkanes in the local high temperature plasma regime generated in such a catalyst discharge zone. Among a variety of possibilities, the creation of a coordinatively unsaturated metal site can be envisioned to undergo oxidative insertion into alkanes leading to olefin and dihydrogen formation, see Figure 4.

Catalyst Lifetime. Wood char catalysts exhibited long lifetimes under the conditions of liquid phase hydrocarbon conversion. The wood char catalysts could be used repeatedly by recharging the reactor cell (Fig. 2) with hydrocarbon substrate. The catalyst could be irradiated at low power (ca. 50 W) with no drop in activity after up to eight hours. Thus, the method is suitable for continuous conversion of hydrocarbons and other substrates to olefins and hydrogen.

Summary. The direct cleavage of strong carbon-carbon bonds, leads to a wide variety of potential natural product, biomass, carbohydrate, cyclic and acyclic hydrocarbon bond cleavage reactions, many of which can be envisioned to occur with sufficient chemical selectivity to be of synthetic use. In addition, the present results indicate the potential for use of microwave activated catalysis for the oxidation of hydrocarbons to ketones and alcohols.

ACKNOWLEDGEMENT

JAF and PK acknowledge the support by the Office of Energy Research, Office of Basic Energy Sciences, U.S. Department of Energy, under contract DE AC06 1830 RLO.

REFERENCES

1. Department of Chemistry, University of Alberta, Edmonton, Alberta.
2. Pacific Northwest National Laboratory, Richland, WA.
3. (a) Dayani, R. "Molecular Magic With Microwaves," *Chem. Eng. News*, **1997**, Feb. 10th, *26*.
   (b) von Hippel, A.R. "Dielectric Materials and Applications," MIT Press, Cambridge, MA., USA **1954**.
   (c) Gabriel, C.; Gabriel, S.; Grant, E.H.; Halstead, B.S.J.; Mingos, D.M.P. Dielectric Parameters Relevant to Microwave Dielectric Heating," *Chemical Society Reviews*, **1998**, *27*, 213.
   (d) Majetich, G.; Wheless, K. "Microwave-Enhanced Chemistry," *American Chemical Soc. Publication*, H.M. Kingston and S.J. Haswell, Eds. **1997**, Chapter 8.
4. (a) Beeri, A.; Berman, E.; Vishkautsan, R.; Mazur, Y. *J. Am. Chem. Soc.*, **1986**, *108*, 6413.
   (b) Tanner, D.D.; Zhang, L. *J. Am. Chem. Soc.*, **1994**, *116*, 6683.
   (c) Tanner, D.D.; Kandanarachchi, P.; Das, N.C.; Brausen, M.; Vo, C.T.; Camaioni, D.M.; Franz, J.A. *J. Org. Chem.*, **1998**, *63*, 4587.
   (d) Tanner, D.D.; Zhang, L.; Kandanarachchi, P. *J. Phys. Chem.*, **1996**, *100*, 11319.
5. Mingos, D.M.P.; Whittaker, A.G. *J. Chem. Soc., Dalton Trans.*, **1992**, 2751.
6. For examples of Microwave activated catalysis, see
   (a) A. Revella; Murphy, W.J.; Achia, Biddanda V. "Conversion of C_2+ Hydrocarbons Using Microwave Irradiation", U.S. Pat. 4,975,164 (1990).
   (b) J.K.S. Wan, "Microwave Induced Catalytic Conversion of Methane to Ethylene and Hydrogen",U.S. Pat. 4,574,038 (1986).
   (c) J.K.S. Wan, U.S."Microwave Production of C_2 Hydrocarbons Using a Carbon Catalyst", Pat. 5,472,581 (1995).
   (d) W.J. Murphy, "Conversion of Methane Using Pulsed Microwave Radiation",U.S. Pat. 5,205,912 (1993).
   (e) W.J. Murphy, "Conversion of Hydrocarbons Using Microwave Radiation", U.S. Pat. 5,277,773 (1994).
   (f) W.J. Murphy, D.H. Shaw, "Upgrading of Low Value Hydrocarbons Using A Hydrogen Donor and Microwave Radiation"" U.S. Pat 5,181,998 (1993) and U.S. Pat. 5,328,577 (1994).

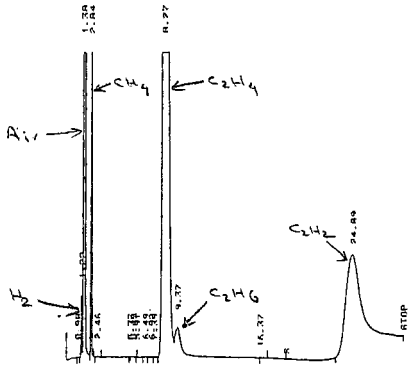

Figure 1a. GLPC Chromatogram of Gaseous Products from the Microwave Irradiation of Hexadecane in the Presence of Wood Char.

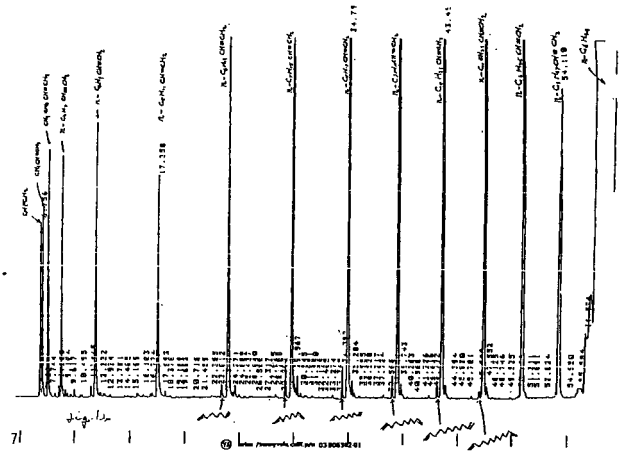

Figure 1b. Glpc Chromatogram of Liquid Products from the Microwave Irradiation of Hexadecane in the Presence of Wood Char.

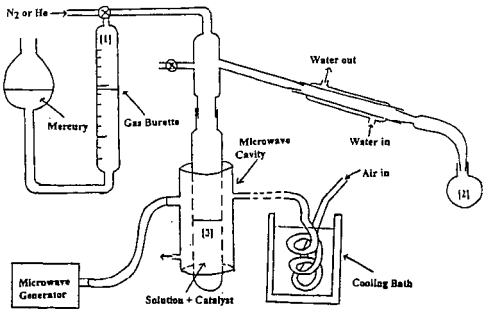

Figure 2. Apparatus for the Microwave Irradiation of Hydrocarbons.

Product	% Yield (Mole basis)
Liquid Products[a], 100-minute reaction	
n-$C_3H_7CH=CH_2$	0.59
n-$C_4H_9CH=CH_2$	1.22
n-$C_5H_{11}CH=CH_2$	1.24
n-$C_6H_{13}CH=CH_2$	3.23
n-$C_7H_{15}CH=CH_2$	14.7
n-$C_8H_{17}CH=CH_2$	17.6
n-$C_9H_{19}CH=CH_2$	14.8
n-$C_{10}H_{21}CH=CH_2$	13.4
n-$C_{11}H_{23}CH=CH_2$	13.2
n-$C_{12}H_{25}CH=CH_2$	13.6
n-$C_{13}H_{27}CH=CH_2$	6.27
Gaseous Products[b]	
H_2	12.0
CH_4	4.83
C_2H_4	40.9
C_2H_6	2.05
C_2H_2	7.12
C_3H_8	16.5
$CH_3CH_2CH=CH_2$	8.16
$CH_2=CHCH=CH_2$	5.79
Others	2.17

[a]Products normalized to 100%. [b]Products normalized to 100%

Table 1. Products from Microwave Irradiation of Hexadecane in the Presence of Wood Char.

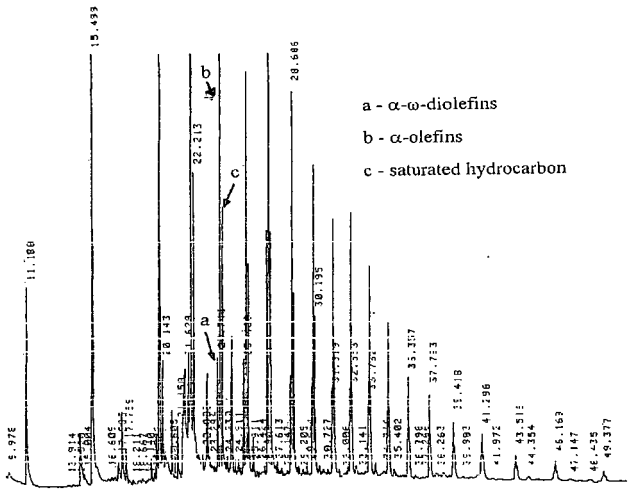

Figure 3. Products Formed from the Catalytic Microwave Oxidative Fragmentation of Polyethylene.

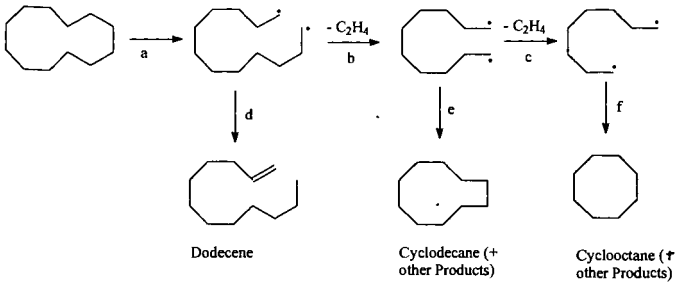

Figure 4. Biradical Mechanism for Hydrocarbon Conversion. Biradical Formation (a) followed by sequential ethylene loss (b,c) with product formation by disproportionation (d) or ring closure (e,f).

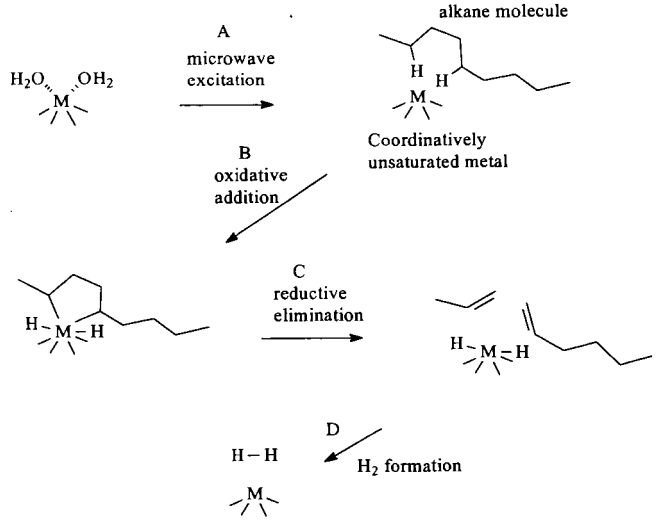

Figure 5. Metal-Centered Catalysis Mechanism for Oxidative Fragmentation of Alkanes.

ENERGY AND EXERGY ANALYSIS OF FCC UNIT

Chun-Min Song, Yong-Shan Tu, Zi-Feng Yan*
State Key Laboratory for Heavy Oil Processing, University of Petroleum, Dongying, 257062, P R CHINA

ABSTRACT The energy and exergy balances were effectively calculated by the three-section model and the two-box method on the basis of field data of the FCC unit. The results show that the net energy consumption of the FCC unit is 2197.60MJ/t. Simultaneously, the efficiency of the exergy of the conversion section is rather poor, and the energy losses of the recovery section are much higher. The losses of the energy and exergy of regenerator are greatest in the conversion section. It means that it is not enough only to reduce the heat losses of the flue gas, the exergy losses of the process is also important to the reduction of the coke formation. In conclusion, the calculations show that conversion and recovery sections have more potential to the reduction of energy consumption. It indicated that the key factors are to reduce the energy consumption of the regenerator, optimize the heat exchanging system and utilize the low temperature heat.

KEYWORDS: catalytic cracking; energy consumption; exergy analysis

1. INTRODUCTION

Catalytic cracking is one of the most important petroleum refining processes. The most significant characteristic of the cracking process is its flexibility in treating the variety of feedstock available from the crude currently being refined, which becomes increasingly important, as refiners are obliged to resort to heavier crude containing refractory or poisonous constituents, due to shortages and to the high price of the more desirable crude. Many technologies are applied to the FCC processes for raising the operating efficiency, innovated decreasing the energy consumption, producing high quality products, and obtaining more remarkable economic benefits. However, the flexibility of the FCC process is negatively weakened by the excessive energy consumption. Thus, the improvement of the efficiency of the energy utilization has been the subject of investigations designed to optimize the fundamental problems in engineering and processes. The great majority of such investigations has been conducted by petroleum companies and held confidential in order to improve the economic benefits. It suggested that the majority of the energy and exergy analysis is purely "applied". Because of the highly "applied" nature of this work in the field, understanding of the various phenomena involved in FCC process is far from complete. In order to understand the effect of energy consumption in FCC process, two kinds of analysis methods of energy and exergy are usually employed in the cracking process.

(1) three-section model[1]. The conversion and transport of energy, technology utilization and energy recovery, i.e., three-sectionm odel of energy analysis is adopted according to the clue of energy utilization and evolution.

(2) two-box method[2]. The gray-box and black-box methods are applied to energy analysis in terms of different systems and equipment involved. The degree of energy utilization of the systems and equipment is available by this method.

The paper aims to study the energy utilization level of the catalytic cracking process employing three-section model and gray-box or black-box methods.

2. EXPERIMENTAL

All field data used in this paper were collected with locale unit. On the basis of field data of the FCC unit, the energy and exergy balances were calculated by the three-section model and the two-box method.

3. ENERGY AND EXERGY BALANCE ANALYSIS

The overall evaluation of the energy consumption according to three-section model is shown in table 1. The net energy consumption and primary energy consumption of the FCC unit amount

* To whom correspondence should be addressed. Email: zfyan@hdpu.edu.cn

to 2197.60 and 2425.43MJ/t, respectively. The conversion and recovery section suffer from high-energy loss and has much potential to improve. The energy and exergy balance analysis is conducted employing gray-box method according to three-section model and the evaluation results of the three-section are shown in table 2[3].

The energy conversion section consists of regenerator (included flue gas energy recovery system), main air blower, gas compressor and pumps. The regenerator suffers great energy and exergy losses with the respective loss coefficient of 21.0% and 41.7%. The energy and exergy analysis of the regenerator is calculated according to the gray-box model and results are shown in table 3. The utilization efficiency and losses of the energy and exergy are evaluated.

The heat exchanger and condenser are made up of the energy recovery section. The cooling energy and exergy are abandoned and puts on the loss item, so only the total cooling energy and exergy are calculated. A portion of energy and exergy of the heat exchanger are lost in the recovery section. The energy and exergy analysis of the heat exchanger is carried out employing black-box model and the results are shown in table 4.

4. DISCUSSION

4.1 Conversion section

It can be seen from table 2 and 3 that the regenerator and recovery system suffer the greatest energy and exergy losses and supply a low energy utilization efficiency of 77.18.The recovery heat energy of the flue gas should be paid attention due to the high energy losses coefficient of 16.80 . Simultaneously the results of the exergy analysis show that the process exergy loss coefficient of 35.16 is much higher than the exhausting flue gas exergy loss coefficient of 6.11 . It means that it is not enough only to reduce the heat losses of the flue gas, the reduction of the exergy losses of the process is more important. The process exergy losses, which consists of the irreversible burning loss of the coke and the heat transfer loss, becomes the weak section of the energy utilization and also the potential aspect to the reduction of energy consumption of the conversion section. The key to reduction of the exergy losses of the regenerative process lies in suppressing coke yield so as to decrease exergy loss of the burning process.

The pressure and heat energy of the flue gas should be recovered in order to improve energy utilization efficiency of the regenerator. The pressure energy of the flue gas can be recovered by the flue gas expander, while the utilization degree of the sensible heat of the flue gas depend on its exhaust temperature. The flue gas expander generated horsepower directly going into the electrical network. In this unit the recovery power ratio (the power ratio of flue gas expander to the air blower) of 73% is lower. The design capacity of the flue gas expander is smaller to partial bypass of flue gas and the heat loss of the flue gas pipelines is greater. Therefore the recovery power ratio can be increased to 114% if pressure energy of flue gas is sufficiently utilized. The expander has a horsepower recovery potential exceeding the requirements of the air blower. In this way, the work recovered by the flue gas expander not only maintains the regular operation of the air blower, but also generate a part of electricity.

The waste heat boiler is used to produce the middle pressure steam of 3.6MPa, and the exhaust temperature of flue gas is at 256, of which energy can be farther recovered. Furthermore, only 65% flue gas flows into the waste heat boiler. It means that 35% of flue gas is exhausted with high temperature of 526. In a word, it is necessary to reduce the direct emission and recover the heat of flue gas more efficiently.

The efficiency of pumps is generally low, 71% of pumps operated with the efficiency below 50%. It indicates that it is worthy to improve the efficiency of the pumps. The application of new type high-efficiency pump or electric machine with frequency converter may be a good choice to improve the drive conversion efficiency. By so doing, electricity energy can be saved.

Although, the power losses of conversion process was lower, but the value high to the other formal energy, hence it cannot be ignored.

4.2 Technology utility section

The total supplied energy of the technology utility section is 2740.76MJ/t, has higher level. Of special is that the proportion of the recovery cycle energy and exergy is low, with 22.5 and 12.7 of the total supplied energy, respectively.

The thermodynamic energy and exergy consumption is that the total supplied energy and exergy transform to the part of the products , with the respective ratio of 19.0 and 27.4. It indicates that the decline of the total supplied energy is also a potential route to improve the energy and exergy consumption.

In technology utility section, exergy losses coefficient of heat dissipated is 3.64 , exergy losses of the process is 18.54 . It means that the reaction and fractionation processes contribute very much to the exergy losses.

The energy utility level of the main fractionation tower has quite influence on the total energy consumption. The exergy loss of the fractionation tower is mostly derived of heat transfer. Therefore heat removal by the top reflux should be minimized while more heat can be removed by hot mid-section reflux and slurry oil reflux if the product quality and yields are ensured. Additionally it is a method to minimize the temperature difference between inlet and outlet tower flows of the reflux.

4.3 Energy recovery section

The ratio of energy and exergy recovery were 54.43 and 45.97, respectively. The cooling energy and exergy losses were 38.39 and 29.56 accordingly in the section supplied energy.

The cooling losses of the whole unit constitutes 35.6 of the net energy consumption and becomes the chief part of the energy consumption. The crux of reducing the cooling(heat rejection) loss rests with the utilization of low temperature heat owing to the most heat below

120 .

The data in table 4 indicate exergy losses coefficient of the heat exchanger network reaches 27.69%. The high temperature difference of heat transfer brings about the great exergy losses. The exergy losses of heat transfer can be inhibited by the optimization of the heat exchanger system.

5. APPROACH OF ENERGY SAVING

The energy conversion and recovery become the weak section of the energy utilization. But technology utility section is core of energy utility. It determines the amount of energy available from recovery and conversion sections. As a result, to minimize the total supplied energy of the technology utility section is the first consideration, subsequently the recovery and conversion sections are considered.

(1) Reducing total supplied energy of the utility section

Introducing advanced technology, optimum catalysts and effective additives are front problems to reducing the total supplied energy of the technology utility section. Besides little heat of steam is utilized in the technology section. The introduction of advanced technical measurements may be a choice to decrease the amount of steam used. For example the dry-gas prelifting technology can not only save energy but also cut down dry gas and coke yield. In addition, appropriate low temperature heat may be used to supply instead of the accompanying steam.

The throttle losses of the exit valve can be reduced through the selection of proper pumps. For the pump with frequent flux change, the variable-frequency electric machine is a good substitute for elevation of pump efficiency and decline of electrical energy.

(2) The optimization of heat exchanger network is an effective way to decrease heat transfer exergy losses and improving the energy recovery ratio. In the first step, the heat exchangers with the temperature difference upwards of 30 s hould be eliminated. Secondly, it is worth while to enhance the heat preservation of high-temperature position. Finally, the integrated utilization of low-temperature heat becomes more and more important with the deepening of the idea of energy savings. A great deal of low-temperature heat supplied with catalytic cracking process can be made use of heating medium of other units or devices, such as preheating water supply and living heating in winter, etc. Next low temperature heat may be considered to upgrading utility, which might face the lower efficiency and higher investment.

(3) The energy utilization efficiency of the regenerator lies on the recovery and utilization of flue gas due to the adoption of the complete combustion technique. Hereby, it is important for the regenerator and energy recovery system to maintain the flue gas expander operates in a perfect performance. In addition, the heat of flue gas should be recovered sufficiently by the waste heat boiler. In a word, it is very significant for the energy saving to maintain the long-cycle, full-loaded, and high-efficient running of the flue gas expander and the waste heat boiler.

6. CONCLUSIONS

The measures of energy saving must be determined in the opinion of energy and exergy balance analysis. For the catalytic cracking unit with the flue gas expander and waste heat boiler, the recommended measurements of energy saving are as follows:

(1) Improving the recovery and utility ratio of the flue gas expander and reducing exhausting temperature of the waste heat boiler. Maintaining the long-cycle, full-loaded, and high-efficient running of the flue gas expander and the waste heat boiler.

(2) Optimizing the heat-exchanging network to reduce temperature difference of heat transfer of the heat exchangers.

(3) Strengthening the integrated utilization of low temperature heat.

ACKNOWLEDGMENTS

We would like to express our gratitude to Rong-Gang Ding for his contributions to write the article.

REFERENCES

[1] Ben Hua. Energy utility analysis and integration of technology processes. Hydrocarbon Processing Press, 1989.p2522 8 8.

[2] Xinyue Xiang. Engineering exergy analysis method. Petroleum Industry Press, 1990.

[3] Anmin Chen. Energy saving method and technique of petrochemical processing. China Petrochemical Press, 1995.

Table 1 the recapitulation statement of energy and exergy analysis using of three-section model

Item		Energy	Exergy
Net energy(exergy) consumption MJ/t		2197.60	2221.96
Primary energy consumption MJ/t		2425.43	
Total supplied energy (exergy) of utilization section MJ/t		2740.76	1455.72
Conversion efficiency		78.30	56.57
Energy utilization efficiency		93.32	77.82
Recovery rate		54.43	45.97
Total ejected energy and exergy MJ/t		1639.57	531.93
Total process exergy losses MJ/t			1255.71
Losses MJ/t :			
	Conversion section	534.42	1067.11
	Utilization section	182.94	322.84
	Recovery section	927.70	396.59

Table 2 The recapitulation statement of gray-box of "three-section" model

Item			energy analysis		exergy analysis	
			Energy MJ/t	Energy loss coefficient %	Exergy MJ/t	Energy loss coefficient %
Energy conversion section	Input	Regenerator	2342.06		2245.29	
		Main air blower	139.42		139.42	
		Gas compressor	42.00		50.42	
		Pump	21.98		21.98	
		Sum	2545.46		2457.11	
	Output	Regenerator	1807.64		1220.02	
		Main air blower	135.39		125.69	
		Gas compressor	39.20		33.38	
		Pump	10.91		10.91	
		Sum	1993.14		1390.00	
	Losses	Regenerator	534.42	21.00	1025.27	41.73
		Main air blower	4.03	0.16	13.73	0.56
		Gas compressor	2.80	0.11	17.04	0.69
		Pump	11.07	0.43	11.07	0.45
		Sum	552.32	21.70	1067.11	43.43
Utilization section	Supplied energy		2740.76		1455.72	
	Thermodynamic energy and exergy consumption		522.09		398.93	
	Exergy Losses	Reactor			135.08	9.28
		Main fractionator			91.42	6.28
		Other units			43.39	2.98
		Sum			269.89	18.54
	Losses of rejection of heat		182.94	6.67	52.95	3.64
	Needed recovery energy		2035.72		733.96	
Recovery section	Recovery cycle		616.63		184.66	
	Recovery output		491.39		152.71	
	Losses	Heat losses	63.77	3.13	19.39	2.64
		Cooling	781.51	38.39	216.96	29.56
		Other	82.42	4.05	5.75	0.78
		Sum	927.70	45.57	242.10	32.98

Exergy losses	Condenser and heat exchanger	124.18	16.92
	Other	30.31	4.13
	Sum	154.49	21.05

Table 3 The results of the regenerator and energy recovery system

Item	Energy MJ/t	Energy loss coefficient	Exergy MJ/t	Exergy loss coefficient
Supplied energy(exergy)	2342.06		2245.29	
Useful energy(exergy)	1807.64		1220.02	
Energy utilization efficiency	77.18			
Exergy utilization efficiency			54.34	
Exhaust flue gas	393.44	16.80	137.22	6.11
CO chemical energy	8.90	0.38	8.90	0.40
Heat losses	127.04	5.42	88.36	3.93
Other	5.04	0.22	1.44	0.06
Process exergy losses			789.35	35.16
Total	534.42	22.82	1025.27	45.66

Table 4 The black-box analysis results of heat exchanger

Energy analysis			Exergy analysis		
Item	Energy MJ/t	Energy loss coefficient	Item	Exergy MJ/t	Exergy loss coefficient
Supplied energy	871.77		Supplied exergy	381.60	
Recovery energy	840.15		Recovery exergy	265.38	
Heat losses	31.62	3.63	Exergy losses of heat	10.55	2.76
			Process exergy losses	105.67	27.69
Total energy losses	31.62	3.63	Total exergy losses	116.22	30.45

ASSOCIATION BEHAVIORS OF COAL-DERIVED MATERIALS IN ORGANIC SOLVENTS

Masashi Iino
Institute for Chemical Reaction Science,
Tohoku University
Katahira, Aoba-ku, Sendai 980-8577, JAPAN

KEYWORDS: Coal-derived material, coal extract, association, organic solvent

INTRODUCTION

Coal-derived materials such as coal extracts and liquefaction products are known to readily associate in organic solvents(1,2). Hydrogen bonds and aromatic π–π interactions are considered to be main associative interactions, though charge transfer and ionic interactions possibly contribute to the associations. Many studies on this topic have been carried out so far, since these association behaviors strongly affect solubility, boiling point, viscosity, and other phisical properties at their bulk or solution state, which are key properties in the operation of coal conversion processes.

This topic is also related to controversial issue in coal structure i.e., covalent crosslinking network or non-covalent (molecular associated) network. Coal swells in an organic solvent and a swollen coal shows elastic behaviors. So, it is sure that coal has a kind of network structure. Although covalently connected crosslinking network structures are often assumed so far, there is no clear evidence for them. Recent works (3-5) suggest that at least for some bituminous coals, non-covalently connected network, i.e., associate structures of coal molecules are a better model than the covalent ones.

Here, association behaviors of coal-derive materials will be reviewed and discussed from solubility, molecular weight, viscosity, surface tension, small angle neutron scattering, and computor simulation, compared with petroleum asphaltenes in solution. Thermodynamics of the solution will also be discussed from sol-gel transition phenomena.

RESULTS AND DISCUSSION

Solubilities.

It is well known that the solubilities of coal-derived materials increase by silylation, i.e., OH $\rightarrow$ $OSiC(CH_3)_3$ or actylation of OH groups. This can be attributed to loss of intermolecular hydrogen bonds among coal molecules. Similarly, the pyridine extraction yields of a high-rank bituminous coal (89.6 carbon %) increases from 5% to 90 % by C-octylation at carbons such as benzylic methylene carbons, probably due to the disruption of the π–π stacking of aromatic rings by the introduction of the large octyl group. (6)

We found (7. 8) that a 1:1 carbon disulfide / *N*-methyl-2-pyrrolidinone (CS_2 / NMP) mixed solvent gave high extraction yields, more than 50 wt%, for several bituminous coals at room temperature. No significant bond cleavage has been observed to occur during the extraction. The extracts obtained, i.e., the mixed solvent soluble fractions, were further fractionated with acetone and pyridine into acetone soluble (AS) fraction, acetone insoluble / pyridine soluble (PS) fraction, and pyridine insoluble (PI) fraction which is a heavier fraction than preasphaltenes. We also have found that 30 – 50 % of PI became insoluble in the extraction mixed solvent, but the solubilities recovered by the re-addition of the separated extract fractions (AS and PS) or the addition of the compounds which have strong interaction with coal molecules, to PI (9, 10). Especially, tetracyanoethylene (TCNE) and tetracyanoquinodimethane (TCNQ) were found to be very effective. The studies on IR spectra of the extract fractions and reversibility of the effect of TCNE addition suggest that the solubility increase is caused by the breaking of noncovalent bonds in associated structures of coal molecules by TCNE, which interact and form new associates with coal molecules which are soluble in the mixed solvent.

Molecular Weight

Hombach(11,12) indicated that usual osmometric methods including VPO is not recommended for molecular weight determinations for complex coal-derived substances, since the van't Hoff equation used for osmotic pressure is not applicable for the substances with polydispersed molecular weights and inhomogeneous chemical structures such as coal asphaltenes. Collins et al.(13) also suggested that there is no accurate method for the molecular weight determinations of coal-derived substances, since coal solutions can not be viewed as a solution of a series of polymer homologues which is a necessary condition for use of osmotic or light-scattering methods. Hombach(12) has reported that a fraction obtained by ultrafiltration (0.2 and 0.035 μm pore filter) in pyridine solution of pyridine extract from a solubilized bituminous coal have very high molecular weights, i.e., 1.59×10^6 using a low-angle laser light-scattering method. Larsen et al.(14) showed that for relatively low molecular weight coal-derived substances mass spectrometry is available, and molecular weights determined by ^{252}Cf plasma desorption mass spectrometry are in good agreement with those obtained by field ionization mass spectrometry and gel permeation chromatography. Asphaltenes from distillation residues of liquefaction products of various coals have 260 - 330 of number-average molecular weight by ^{252}Cf plasma

desorption mass spectrometry.

Lee et al.(15) used VPO as a means for determination of degree of association of coal-derived substances. From the relation between molecular weight and concentration of coal-derived substances in solution, the dissociation constants of dimer, trimer, and higher multimers, and their distribution change with concentration were determined.

Viscosity

Viscosity of coal-derived substances in solution and bulk is related to their associated structures, and in coal liquefaction processes it is important to control high viscosity of coal – solvent mixtures. Bockrath et al.(16) measured the viscosities of preasphaltene, asphaltene (and its acid / neutral and basic components), and oil (pentane soluble) of coal-derived liquids from liquefaction. The viscosity of the mixtures of various compositions of acid / neutral and basic asphaltenes for fixed total asphaltene fraction (30 % asphaltene in oil) was found to be greater than would be expected on the basis of a simple additive relationship, suggesting that hydrogen bonding between acid / neutral with basic asphaltenes increases viscosity. The preasphaltenes, on a weight basis, have approximately twice the effect on viscosity as do the asphaltenes, probably due to their larger molecular weight and functionality in comparison to the asphaltenes. Bockrath et al.(17) also have showed that intermolecular association involving hydrogen bonding is a prime factor for the viscosity increase which occurred with increased asphaltene concentration in a reference solvent. Similarly the importance of hydrogen bonds largely involving phenolic OH in the viscosity increase was suggested.(18) Arganinski and Jones(19,20) also suggest that the influence on the viscosity of coal-derived preasphaltenes and model compounds in THF was the order hydrogen bonding > molecular weight >> degree of aromatic condensation (charge transfer interaction).

Surface Tention

Surface tension is used for analyzing colloidal properties such as micelles formation. We(21) measured the surface tension of *N*-methyl-2-pyrrolidinone (NMP) solution of acetone soluble (AS) and acetone insoluble / pyridine soluble (PS) fractions of the CS_2 / NMP mixed solvent extract of a bituminous coal by the Wilhelmy method. The surface tensions of the solutions freshly prepared by the dilution of the concentrated solution with NMP changed with time, and it took several hours to attain an equilibrium state of lower surface tension. This suggests that the rate of the re-construction to a new association state are very slow. The equilibrium surface tensions of NMP solution of AS decreases with AS concentration and a discontinuity point at some concentration (0.1 – 0.3 g/dL for two different As's) are observed, where the slope in the surface tension - ln c plots changes, suggesting that at this concentration association state abruptly changes, such as the formation of micelles. The discontinuities observed in this study are not so distinct as the case reported for pyridine solution of a petroleum asphaltene by Sheu et al..(22) The discontinuity concentration for the petroleum asphaltene was also found to be about 0.03 g/dL, one order lower than those for the coal extracts, reflecting the difference of micelle structures probably due the difference between chemical structure, molecular weight and shape of both constituents. For PS from the same coal as AS, on the other hand, discontinuity was not observed. Further study is needed to clarify this.

Small-Angle Neutron Scattering

Although small-angle neutron scattering (SANS) studies on the size distribution and shape of petroleum asphaltene associates in solution have been actively carried out, only a few SANS studies on coal-derived substances were reported so far. Cody, Thiyagarajan et al.(23,24) measured SANS of deuteropyridine solutions of pyridine extracts and their O-methylated derivatives. Laser desorption mass spectrometry of the extracts, untreated and methylated, indicates a predominance of relatively low mass materials, with molecular weight of the order 300 and a mass envelope which tails off around a thousand daltons.(23) SANS indicates that the solution structure of the extracts exists as small particles, with radii about 80 Å, and the values of fractal dimension, d (<3) indicates that the small particles further form a randomly assembled, loosely extended aggregates. Considering the molecular weights and radii for the particles, the elemental particles are themselves aggregates of the extract molecules. O-methylation is expected to decrease aggregation and/or make aggregates more loose, since hydrogen-bonding interactions are considered to constitute the dominant associative interparticle interaction. However, the change in the solution state due to O-methylation was found to be slight, and it induces more densed packing of aggregates for the two coals, in which d increases by O-methylation.

SANS data on the CS_2 / NMP mixed solvent extracts in solution by Cody, Thiyagarajan et al.(25) are interesting. The solution of pyridine insoluble / the mixed solvent soluble component, PI in the mixed solvent contains no large aggregates, but the solution of pyridine extract from the same coal, which may be a lighter component than PI, contains large aggregates, though a light component seems less aggregative due to low content of functional groups. Recently we found that addition of 2 wt% of TCNE relative to the amount of PI results in an enortmous change in the SANS behabior, namely, the addition of TCNE reduces the particle (associates) size greatly. This agrees with the enhanced extractability and solubility in CS_2/ NMP mentioned above by the addition of TCNE, considering that the size reduction of the associates of coal molecules makes

themselves more soluble in CS_2 / NMP. This result seems to give a direct evidence for the dissociation of the aggregates of coal molecules by TCNE through its strong interaction ability with coal molecules. However, our recent results (10) shows that some derivatives formed from TCNE may be responsible for the increase in solubility, rather than TCNE itself. So, the mechanism seems more complex than we considered so far. Further detailed study on the effect of TCNE and other additives such as PCP on SANS behaviors of coal extract solutions is needed to clarify the mrchanism for the enhanced extractability and solubility in CS_2/ NMP.

Sol-Gel Transition

To date, no experimental data on sol-gel transition lines are reported on coal related materials. We are trying to address this important gap by direct measurement of sol-gel transition lines of coal related material-solvent mixtures. Our attention is focused upon thermoreversible gelation of coal extracts in organic solvents.

Many earlier studies have approached this problem by investigating rubbery or gelly coal - solvent and extracted coal - solvent systems (26-28) . Based on studies of polymeric gels, it was generally believed that mostly relatively "poor" solvents were capable of gel formation. However, physical-thermoreversible gelation can take place in good solvents due to compound-compound and compound-solvent interactions. This kind of molecular aggregation has been widely observed in polymer-solvent systems, where gels are formed on cooling and disappear on heating. In contrast to the high molecular weight polymers, it has been discovered lately (29) that some lower molecular weight organic compounds (300 - 1000 daltons) can form thermoreversible gels with some organic solvents. Likewise, we have also observed that 2-naphthol (MW = 144 daltons) can form gels with N-methyl-2-pyrrolidinone (NMP). Intuitively speaking, the thermoreversible gelation could be a common feature in organic compound - solvent systems.

In this work we are interested particularly in the thermoreversible gelation in good solvents. Here, we introduce our preliminary approach to make direct measurements to determine the sol-gel transition lines for coal extracts and extract fractions using methods developed for polymer-solvent solutions. So far, no detailed thermodynamic analyses are attempted. In the present program of study we have been using various methods: a standard differential scanning calorimetry, a ball drop method and a thermogravimetric technique. a ball drop method was used to study "gel melting" lines. Experiments were carried out by cooling samples slowly to -30°C and then observing capabilities of solutions to keep 60 mg balls during heating with a rate about 0.5 °C/min. This type of experiment allows us to classify a substance presumably as a "gel" if its network is sufficiently stiff to withstand the 60 mg ball drop due to gravity. Preliminary experimental results using various extracts from Upper Freeport coal will be shown.

Computer Simulation

Computer-aided molecular design (CAMD) has been utilized in the designs of the drugs and new functional materials. Recently, it has been applied to coal.(30-33) Energetically stable three dimensional structure (conformation) of the extract fractions of coal was constructed by computer simulation.(33) The most stable structure in the energy-minimum state for model molecules PS, obtained from the CS_2/ NMP mixed solvent extraction of a bituminous coal was estimated to be an associated structure and the $\pi-\pi$ interactions between aromatic ring systems play a major role to form the association.

REFERENCES

1. Sternberg, H. W., Raymond, R. and Schweighardt, F. K., *Science*, **1975**, 188, 49.
2. Stenberg, V. I., Baltisberger, R.J.,and Patel, K. M. et al., *Coal Science* (ed Gorbarty, M. L.,Larsen, J. W., Wender, I.), Academic Press, *New York*, **1983**, 125-171.
3. Nishioka, M., *Fuel*, **1992**, 71, 941.
4. Cody, G. D., Davis, A.and Hatcher, D. G., *Energy Fuels*, **1993**, 7, 455.
5. Liu, H., Ishizuka, T., Takanohashi, T. and Iino, M., *Energy Fuels*, **1993**, 7, 1108.
6. Miyake, M. and Stock, L.M., *Energy Fuels*, **1988**, 2, 815.
7. Iino, M., Takanohashi T., Ohsuga, H. and Toda, K., *Fuel*, **1988**, 67, 1639.
8. Iino, M., Takanohashi, T., Obara, S., Tsueta, H. and Sanokawa, Y., *Fuel*, **1989**, 68(12), 1588-1593.
9. Sanokawa, Y., Takanohashi, T. and Iino, M., *Fuel*, **1990**, 69, 1577.
10. Iino, M., Kurose, H. Giray, E. S., and Takanohashi, T., *Prepr. Pap. Am. Chem.Soc.,Div. Fuel Chem.* **1998**, 43(3),712-716.
11. Hombach, H.-P., *Fuel*, **1981**, 60, 663.
12. Hombach, H.-P., *Fuel*, **1982**, 61, 215.
13. Collins, C.J., Triolo, R. and Lietzke, M.H., *Fuel*, **1984**, 63, 1202.
14. Larsen, J.W., Lapucha, A.R., Wernett, P.C. and Anderson, W.A., *Energy Fuels*, **1994**, 8, 258.

15. Lee, W.C., Schwager, I. and Yen, T.F., *Prepr. Pap.-Am. Chem. Soc., Div. Fuel Chem.*, **1978**, 23(2), 37.
16. Bockrath, B.C., Lacount, R.B. and Noceti, R.P., *Fuel Process.Technol.*, **1978**, 1, 217.
17. Bockrath, B.C., Lacount, R.B. and Noceti, R.P., *Fuel*, **1980**, 59, 621.
18. Taylor, S.R. and Li, N.C., *Fuel*, **1978**, 57, 117.
19. Jones, M.B. and Argasinski, J.K., *Prepr. Pap.-Am. Chem. Soc., Div. Fuel Chem.*, **1985**, 30(4), 250.
20. Argasinski, J.K. and Jones, M.B., *Prepr. Pap.-Am. Chem. Soc., Div. Fuel Chem.*, **1987**, 32(1), 604.
21. Hayasaka, K., Takanohashi, T. and Iino, M., *Energy Fuels*, **1996**, 10, 262.
22. Sheu, E.Y. and Storm, D.A., *Fuel*, **1994**, 73, 1368
23. Cody, G.D., Thiyagarajan, P., Botto, R.E., Hunt, J.E. and Winans, R.E., *Energy Fuels*, **1994**, 8, 1370
24. Thiyagarajan, P., Cody, G.D., Hunt, J.E. and Winans, R.E., *Prepr. Pap.-Am.Chem. Soc., Div. Fuel Chem.*, **1995**,40(3),397.
25. Cody, G.D., Obeng, M. and Thiyagarajan, P., *Energy Fuels*, **1997**, 11, 495.
26. Hall, P. J., and Larsen, J. W., *Energy Fuels* **1991**, 5, 228.
27. Gody, G. D., and Painter, P. C., *Energy Fuels* **1997**, 11, 1044.
28. Takanohashi, T., Kudo, T., and Iino, M., *Energy Fuels* **1998**, 12, 470.
29. Yasuda, Y., Iishi, E., Inada, H., and Shirota, Y., *Chemistry Letters* **1996**, 575.
30. Carlson, G.A., *Energy Fuels*, **1992**, 6, 771.
31. Faulon, J.L., Hatcher, K.A. P.G., Carlson, G.A. and Wenzel,K.A., *Fuel Process. Technol.*, 34, 277 (1993)
32. Nomura, M., Matsubayashi, K., Ida, T. and Murata, S., *Fuel Process. Technol.*, **1992**, 31, 169
33. Takanohashi, T., Iino, M.. and Nakamura, K. *Energy Fuels*, **1994**, 8, 395

PROBING COAL REACTIVITY BY TIME-RESOLVED SMALL ANGLE X-RAY SCATTERING

R. E. Winans, S. Seifert, and P. Thiyagarajan†
Chemistry Division and †Intense Pulsed Neutron Source Division
Argonne National Laboratory
Argonne, IL 60439

Keywords: Argonne coal swelling, time-resolved small angle neutron scattering

ABSTRACT

The objective of this study is to observe changes in coal structure in situ with small angle X-ray scattering (SAXS) during solvent swelling and during pyrolysis. We have built a SAXS instrument at the Basic Energy Sciences Synchrotron Research Center at the Advanced Photon Source that allows us to obtain scattering patterns in the millisecond time domain. The eight Argonne Premium Coal samples were used in this study. The information that can be derived from these experiments, such as changes in fractal dimensionality and in size and type of porosity, was found to be very rank-dependent. In the swelling experiments, it was noted that for certain coals, structural changes occurred in just a few minutes.

INTRODUCTION

Coal solvent interactions have been studied extensively over the last 25 years. Most coals swell significantly in solvents such as pyridine and this effect has been exploited to study the macromolecular structure of coals (1-8). Typically, the volumetric swell ratio (Q_v) is measured and is defined as the ratio of the swollen volume over the dry volume. Recently, the swelling of individual particles was determined using microscopy combined with video and image analysis (9). Otake and Suuberg studied the temperature dependence of the rate of swelling on some of the Argonne Premium Coal Samples (10). Also, they looked at a larger set of low rank coals (11). They found large differences in the rate of coal swelling with the Illinois No. 6 (APCS 3) being the fastest and the lignite (APCS 8) the slowest. The Upper Freeport (APCS 1) has been studied extensively in part due to its unusually large solubility in the NMP/CS_2 mixed solvent system (12).

Small angle neutron scattering (SANS) has been used to study swollen coals and extracts. For the Pittsburgh coal (APCS 4), it was shown that a rod-like pore structure developed upon swelling in pyridine (13). It has also been shown that pyridine solubles are not truly soluble (14). Finally, the Upper Freeport coal was studied extensively with SANS on both soluble and insoluble fractions for NMP/CS_2 and pyridine (15).

The present study exploits the brilliance of the undulator X-ray source at the Advanced Photon Source to probe, in real time, the structure changes in coal swelling using SAXS. The information derived from the SAXS experiment throws new light on the early stages of structure changes in coal swelling.

EXPERIMENTAL

The eight Argonne Premium Coal Samples were used without modification in this study (16). The SAXS instrument was constructed at ANL and used on the Basic Energy Sciences Synchrotron Radiation Center CAT undulator beamline ID-12 at the Advanced Photon Source (http://www.bessrc.aps.anl/).

Quartz capillaries (1 mm) were used to sample 5 mg of -100 mesh coal. Scattering patterns were obtained on the dry coal, then 10 μl of solvent was added with a syringe such that all the sample was wetted. SAXS data were obtained every minute for one hour with approximately a one minute delay after adding the solvent. Monochromatic X-rays (8.5 - 23.0 keV) are scattered off the sample and collected on a 19 x 19 cm^2 position sensitive two-dimensional gas detector. The scattered intensity has been corrected for absorption, the empty capillary scattering, and instrument background. The differential scattering cross section has been expressed as a function of the scattering vector Q, which is defined as:

$$Q = \frac{4\pi}{\lambda} \sin \theta$$

where λ is the wavelength of the X-rays and θ is the scattering half angle. The value of Q is proportional to the inverse of the length scale ($Å^{-1}$). The instrument was operated with two different sample-to-detector distances, 68.5 cm to obtain data at $0.04 < Q < 0.7$ $Å^{-1}$ and 3740 cm to measure at $0.006 < Q < 0.1$ $Å^{-1}$.

Small Angle X-ray Scattering

A typical two-dimensional plot of the time-resolved data for the swelling of the subbituminous coal (APCS 2) in pyridine is shown in Figure 1. These curves can be analyzed to determine size of features, topology, and changes in total scattering. At small Q in the Guinier region, the radius of gyration (R_g), which is related to the size of the scattering features, can be determined. For example, R_g for spheres can be determined from the slope of I(Q) vs Q^2 in a Q region where $R_g Q \leq 1.0$. Power law slope (fractal dimension) from the data, such as is shown in Figure 1, are used to describe the topology of the system. Finally, the invariant Q_0 is calculated and is proportional to the fluctuation of the electron density in the system. Changes in the invariant are useful in monitoring topological changes in the sample.

$$Q_0 = \int_0^\infty I(Q)\, Q^2\, dQ$$

For example, the invariant goes to zero for a homogeneous system such as a solution of coal molecules that are truly soluble and not aggregated.

RESULTS AND DISCUSSION

This discussion will focus on four of the Argonne coals: lignite, Illinois #6, subbituminous, and Upper Freeport. The slowest swelling coal, lignite (APCS 8), at 25 °C took 230 min. to reach 50% of final swelling (t_{50}) (10), while the Illinois #6 at 24 °C had a t_{50} of 1.7 min. The subbituminous coal was chosen since its swelling rate is of an intermediate value, t_{50}=12.8 min. at 24 °C and its results correlate well with those described in the literature (10). Finally, the Upper Freeport was examined with two solvent systems, pyridine and NMP/CS_2 with very different results between the two solvents.

A set of sixty scattering curves are shown in Figure 1 for the subbituminous coal in pyridine. Initially, there are only small changes, then between 10 and 25 min., the slope and invariant decreased quite rapidly. The change in fractal dimensions is shown in Figure 2 for all four of the coals. It appears that the decrease in the fractal dimension is stopped when the subbituminous coal is fully swollen. Between 10 and 35 min. this data fits an exponential decay with a constant of 0.16 $min.^{-1}$. For short length scales < 30Å, there appears to be an increase in the scattering when the swelling has finished. After the macromolecular structure has expanded, changes at the molecular level can be discerned.

The swelling of Illinois #6 was very rapid, therefore, the changes seen with time in the SAXS data must be due to a molecular aggregation that started after 20 min. However, this new configuration was not stable and slowly rearranged between 30 and 60 min. This was seen much better in the changes of the power law slope as shown in Figure 2. This unusual phenomenon was reproducible and appeared limited to the Illinois coal.

At room temperature, no changes in either the invariant or power law slope were observed for the lignite coal. However, the experiment was repeated at 50 °C, where $T_{50} \approx 25$ min. At low Q, the power law slope decreased, but this change was much smaller than those observed for the other coals. These higher temperature experiments need to be run at high Q to see if changes on a smaller length scale is occurring. In addition, acid treated lignite will be studied. There is considerable organic acid-mineral interactions in lignite.

The Upper Freeport mv bituminous coal does not swell as well as other coals, $Q_v = 1.3$ (12), while all the other lower rank coals swell with $Q_v \geq 2.0$. In NMP/CS_2, the ratio was not measured on the raw coal since it is very soluble (12). In pyridine, a rapid increase in the invariant occurred and then it remained constant after approximately 10 min. (see Figure 3). While the invariant in NMP/CS_2 starts at about the same value and does increase, the magnitude of the increase is much less, and after 10 min., it starts to decrease. Pyridine must decrease the surface area in the coal possibly by dissolution followed by re-aggregation. We know from SANS that pyridine solutions are actually aggregates (14). It is interesting that while NMP/CS_2 is a good extraction solvent for the Upper Freeport, it does not appear to greatly change the 3D structure on the length scales studied here.

CONCLUSIONS

Structure changes in initial solvent swelling are observed in the time-resolved SAXS data from the coals. With high rank coals in pyridine, there is a rapid breakup of the solid structure, followed by a re-aggregation that produces constant scattering. With NMP/CS_2, the effect is much smaller and the scattering decreases with time. For the subbituminous coal, the scattering increases immediately, probably forming a new pore structure with rod-like features.

ACKNOWLEDGMENTS

This work was performed under the auspices of the Office of Basic Energy Sciences, Division of Chemical Sciences and Division of Materials Sciences, U.S. Department of Energy, under contract number W-31-109-ENG-38. The support of the BESSRC staff is appreciated, especially Jennifer Linton and Mark Beno.

REFERENCES

1. Larsen, J. W.; Shawver, S. *Energy Fuels* **1990**, *4*, 74.
2. Cody, G. D.; Eser, S.; Hatcher, P.; Davis, A.; Sobkowiak, M.; Shenoy, S.; Painter, P.C. *Energy Fuels* **1992**, *6*, 716.
3. Hall, P. J.; Larsen, J. W. *Energy Fuels* **1993**, *7*, 47.
4. Suuberg, E. M.; Otake, Y.; Yun, Y.; Deevi, S. C. *Energy Fuels* **1993**, *7*, 384.
5. Yang, X.; Larsen, J. W.; Silbernagel, B. G. *Energy Fuels* **1993**, *7*, 439.
6. Ndaji, F. E.; Thomas, K. M. *Fuel* **1993**, *72*, 1525.
7. Aida, T.; Nawa, Y.; Shiotani, Y.; Yoshihara, M.; Yonezawa, T. *Conf. Proc. - Int. Conf. Coal Sci., 7th* **1993**, *2*, 445.
8. Larsen, J. W.; Gurevich, I.; Glass, A. S.; Stevenson, D. S. *Energy Fuels* **1996**, *10*, 1269.
9. Gao, H.; Artok, L.; Kidena, K.; Murata, S.; Miura, M.; Nomura, M. *Energy Fuels* **1998**, *12*, 881.
10. Otake, Y.; Suuberg, E. M. *Energy Fuels* **1997**, *11*, 1155.
11. Otake, Y.; Suuberg, E. M. *Fuel* **1998**, *77*, 901.
12. Takanohashi, T.; Iino, M.; Nishioka, M. *Energy Fuels* **1995**, *9*, 788.
13. Winans, R. E.; Thiyagarajan, P. *Energy Fuels* **1988**, *2*, 356.
14. Cody, G. D.; Thiyagarajan, P.; Botto, R. E.; Hunt, J. E., Winans, R. E. *Energy Fuels* **1994**, *8*, 1370.
15. Cody, G. D.; Obeng, M.; Thiyagarajan, P. *Energy Fuels* **1997**, *11*, 495.
16. Vorres, K. S. *Energy Fuels* **1990**, *4*, 420.

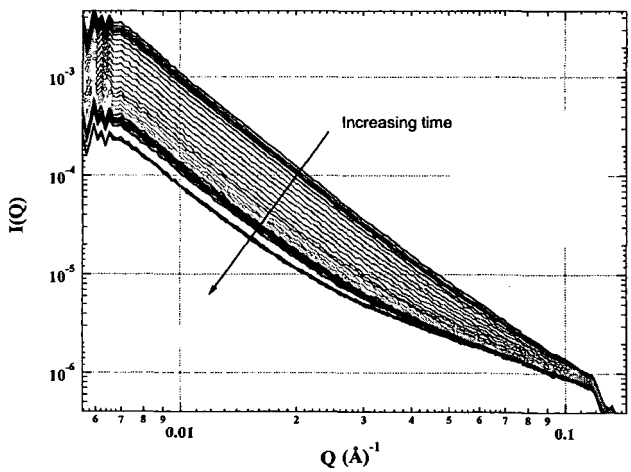

Figure 1. SAXS of the subbituminous coal (APCS 2) in pyridine from 1 to 60 minutes.

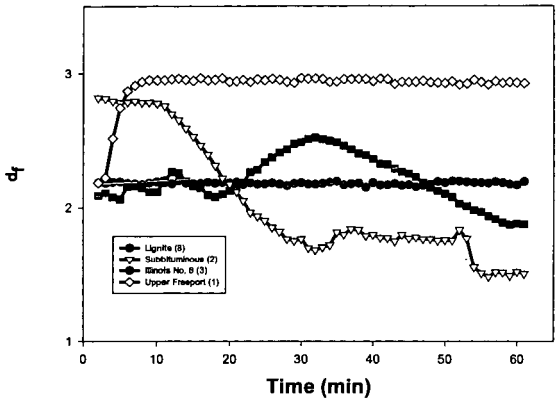

Figure 2. Power law slopes (fractal dimensions) for coal swelling in pyridine at low Q, as a function of solvent contact time.

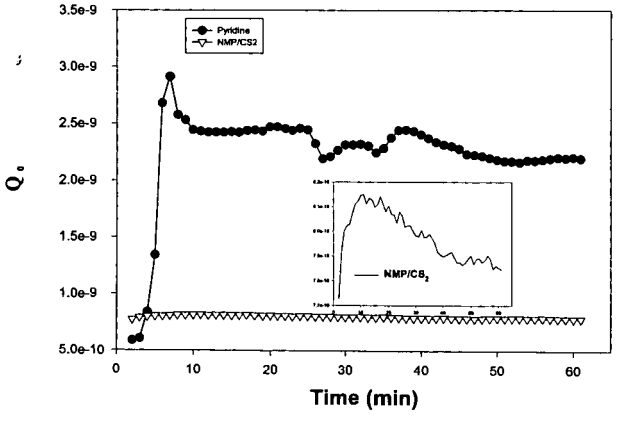

Figure 3. Invariant change with swelling in pyridine and NMP/CS_2 for the Upper Freeport coal. The inset is an exploded view in Q_0 for the NMP/CS_2 data.

MODELING PYROLYSIS BEHAVIOR FOR INTERNATIONAL COALS

M.A. Serio, M.A. Wójtowicz, S. Charpenay, Y. Chen, D.G. Hamblen, P.R. Solomon
Advanced Fuel Research, Inc.
87 Church Street, East Hartford, CT 06108-3742

Keywords: Coal Pyrolysis, Modeling, Coal Type

INTRODUCTION

Pyrolysis (devolatilization) is the initial step in most coal conversion processes, accounting for up to 60% of the initial weight loss from the coal. It is also the process that is most dependent on the organic properties of the coal, and is important because of its influence on the subsequent conversion process. The modeling of coal pyrolysis has progressed from simple, single equation kinetic models for overall weight loss to fairly complex "network" models. These models approximate coal as a polymeric structure and provide more detailed predictions of pyrolysis behavior than is possible with the simpler models. Professor Eric Suuberg has been involved for many years in the study of coal devolatilization modeling, pyrolysis kinetics, tar formation and vaporization, crosslinking reactions, network structure, thermochemistry of pyrolysis reactions, and char gasification and combustion reactivity [1-14]. All of the network model development efforts have greatly benefited from this body of work.

A total of three network coal devolatilization models have been developed, [15-19], which have various capabilities for predicting coal thermal decomposition under practical conditions. These coal devolatilization models are: (1) the Functional Group – Depolymerization, Vaporization, Crosslinking (FG-DVC) model [15-17], (2) the Chemical Percolation Devolatilization (CPD) model [18]; and the FLASHCHAIN model [19]. A common feature of the original versions of these models is that they required a large set of data inputs, including kinetic parameters, coal composition files, and additional parameters describing the coal polymeric structure. These input data could be generated on the basis of experimental measurements for each coal of interest, although this limited predictions to coals that had been studied. Alternatively, some investigators have tried to correlate the devolatilization properties to the coal types using simpler models. For instance, Ko *et al.* [20] and Neavel *et al.* [21] have developed methods for predicting the upper bound of tar yields, X_{tar}, from coal elemental compositions. Recently, successful efforts were made to retain the predictive capabilities of the network models, but with the ability to use ultimate analysis or comparable data to generate the input files. Niksa has developed a correlation method for the FLASHCHAIN model which predicts volatile yields in pyrolysis from ultimate analysis data [22-24]. A similar approach was used by Zhao *et al.* [25] to correlate the input parameter files for the FG-DVC model, while Fletcher and coworkers have used NMR data to correlate input parameters for their CPD model [26].

This paper briefly describes the historical development of one of the network models, the FG-DVC model [15-17], and how its development was influenced by the work of Professor Eric Suuberg. FG-DVC is a network coal devolatilization model which can predict, in addition to the tar and total volatile yields, the yields of individual gas species, the tar molecular weight distribution, and the char fluidity. It has also been coupled with a char reactivity model which incorporates the effect of thermally induced annealing on char reactivity. This model was primarily validated using data for North American coals and is now being extended to a range of international coals. This paper also discusses the progress of these efforts, along with the status and future prospects for coal devolatilization modeling activities in various parts of the world.

BACKGROUND ON FG-DVC MODEL

Coal has a very complicated organic structure, which is essentially a mixture of an aromatic matrix, side chain components, and some loose fragments. The thermal decomposition of the coal structure involves many parallel and competitive processes. In modeling these processes, FG-DVC uses two submodels. The FG model simulates the thermal evolution of various functional groups and the DVC model predicts the depolymerization, vaporization and crosslinking processes occurring in the coal polymer network. In the FG submodel, the gas evolution from functional group precursors is modeled with parallel first order reactions and a distributed activation energy (DAE) formulation is used to reflect the diversity of coal structures. In his doctoral thesis work at Massachusetts Institute of Technology [1,2,9] and in his academic work at the Carnegie-Mellon University [3,4,7], Prof. Suuberg and his colleagues pioneered the development of pyrolysis models which track individual species from coal using DAE kinetic models. These methods were adapted by researchers at Advanced Fuel Research, Inc. (AFR) for coal and related materials in the development of the FG-DVC model. More recently, Professor

Suuberg collaborated with AFR on a major review of pyrolysis experiments, kinetic rates and mechanisms, which summarized the progress in these areas and attempted to resolve the remaining controversies in the choices of kinetic rates and models [14].

The thermal evolution of the coal polymer matrix is modeled with a network model [16], which consists of nodes and the connections between them. The nodes represent the polymer clusters and there are two types of connections between them, i.e., weak and strong bonds and initial crosslinks. At elevated temperatures, there is a competition between bond breaking and crosslinking reactions, and the properties of the network are fully determined by these two competing processes through percolation theory calculations [27]. In the case of coal, cross-linking in the DVC subroutine is computed by assuming that this event is correlated with CO_2 and CH_4 evolutions predicted in the FG subroutine. The yield of rapidly released CO_2 (which is related to coal rank and weathering) is the factor that controls the thermosetting or thermoplastic behavior of coals, an observation that was first made by Suuberg and coworkers [5]. For coals which exhibit thermoplastic behavior, the fluidity is assumed to be limited by the cross-linking associated with the evolution of methyl groups [15-17].

The most important property of the network is the molecular weight distribution of the clusters. The heavy molecules remain in the condensed phase to become char, while the light ones evaporate to become tar. The model originally used the tar vapor pressure law of Unger and Suuberg [7], which was later modified by Suuberg *et al.* [4], and more recently improved by Fletcher *et al.* [26]. The tar rate is further limited by internal transport, which is assumed to be controlled by the evolution rate of gas species and the light tar [15]. This mechanism enables the model to predict the pressure variation of the tar yields.

A char reactivity model was developed as a submodel of FG-DVC [28]. The reactivity model can predict intrinsic reactivity based on correlations with char hydrogen content, coal oxygen content, and coal mineral content. A random pore model and a volumetric model are used for high rank and low rank coals, respectively, in order to predict variations of intrinsic reactivity with burnoff. In the pore diffusion regime, the model uses the Thiele modulus to calculate the reaction rate as a function of the intrinsic rate and char structural properties. The model includes the effects of thermal annealing on reducing the intrinsic char reactivity and also benefits from the work of Suuberg in this area [13].

The FG-DVC model was validated for the eight Argonne Premium coals [29] using measurements of pyrolysis kinetics from TG-FTIR analysis, solvent extraction and solvent swelling to measure extractables and the initial crosslink density, Gieseler plastometer experiments to measure fluidity, pyrolysis-FIMS to measure the tar molecular weight distribution, and ultimate analysis to determine the elemental compositions (C, H, N, S, O) [17]. The large number of experimental inputs allowed the development of a model which can make detailed predictions of coal devolatilization under various conditions of temperature, pressure, and heating rate.

A correlation method was subsequently developed which allows the FG-DVC model to be used for untested coals by providing an interpolation between the input files of known coals based on the coal elemental analysis [25]. The interpolation mesh is composed of nine coals: six from the Argonne Premium Coal Sample Program, and three from the Penn State Sample Bank (PSOC 1474, PSOC 1448, and PSOC 1521). Extensive experimental studies were carried out on these reference coals and the model input parameters are well established. With this scheme, any of the FG-DVC input parameters can be interpolated for an untested coal when its elemental composition is known.

RECENT DEVELOPMENTS IN MODELING OF COAL DEVOLATILIZATION

There are several recent developments and remaining challenges in the area of modeling coal devolatilization. Because of the globalization of coal markets, there is growing interest in predicting the pyrolysis behavior for a wide variety of coals from all over the world. Recent work at AFR has extended the range of FG-DVC model application to include South American, Japanese, Australian, South African, Indonesian, European, and Chinese coals [30]. Niksa has developed his FLASHCHAIN model to be applicable for a wide range of coal types [22-24]. This model has been recently incorporated into the EPRI NO_x-LOI predictor. In this expert system, the FLASHCHAIN model provides the underlying basis for predicting NO_x formation and unburned carbon formation (LOI) in a power plant by calibration against a known coal [31]. Since the partitioning of nitrogen species in pyrolysis has an important influence on NO_x formation in combustion, this aspect of devolatilization modeling has recently received increased attention [31-33].

For the same reasons, there has been increased interest in the incorporation of network devolatilization models into Comprehensive Fluid Dynamic (CFD) codes. Until recently, all of the commercial CFD codes incorporated relatively simple coal devolatilization models. The FG-DVC model has been integrated with research CFD codes, such as the Brigham Young University (BYU) PCGC-2 code and the DOE MFIX fluidized bed code [34,35]. The CPD model was recently integrated with the commercial FLUENT code [36], and the preliminary integration of FG-DVC with a CFD code has been accomplished at the University of Leeds [37]. AFR has also developed a streamlined version of the FG-DVC model which facilitates the integration process [38]. This version involves running the complete model outside the main CFD code and using it to define a set of coefficients that relate individual product evolution to a reference process (e.g., weight loss) over a prescribed range of conditions. AFR is also exploring artificial neural network (ANN) models for coal devolatilization which may result in another streamlined model [39]. In addition, a larger particle devolatilization version of FG-DVC has been developed for use as a submodel in fixed and fluidized bed systems [40].

Matthews *et al.* [41] have devised a molecular modeling approach to coal devolatilization which appears to be successful in predicting the general features of the mass loss and chemical structural changes for vitrinite samples heated in a drop tube. Work on molecular modeling of coal is also underway in Japan [42,43], although so far it has only been used to predict drying and coal/solvent interactions. Finally, coal devolatilization models are being adapted to predict related phenomena, such as coal liquefaction [44] and coal maturation [45].

CONCLUSIONS

During the past decade, the modeling of coal devolatilization has progressed from simple 1 or 2 step models to relatively complex network models. These models approximate coal as a polymeric structure and have demonstrated good predictive capability for a wide range of coal types and experimental conditions. There are three major network model development efforts, all of which have benefited from Professor Suuberg's work on coal macromolecular structure, crosslinking behavior, modeling of pyrolysis kinetics, tar vaporization behavior, and the effects of pyrolysis on intrinsic char reactivity.

ACKNOWLEDGEMENTS

In addition to the authors, the work at Advanced Fuel Research, Inc. (AFR) has involved several individuals who are named in references [15-17,28,30,33-35,38-40,44,45]. Professor Eric Suuberg of Brown University consulted on many aspects of the model development effort. Professor Philip Best of the University of Connecticut also made important contributions. The support of the FG-DVC model development work by the U.S. Department of Energy, National Science Foundation, and the Department of Agriculture is gratefully acknowledged.

REFERENCES

1 Suuberg, E.M., Peters, W.A., and Howard, J.B., *Ind. Eng. Chem. Process Des.*, Dev. 17, 37-46 (1978).
2 Suuberg, E.M., Peters, W.A., and Howard, J.B., *17th Symp. (Int.) on Combustion*, p. 117, The Comb. Inst., Pittsburgh, Pa (1979).
3 Unger, P.E., and Suuberg, E.M., Fuel, 63, 606 (1984).
4 Suuberg, E.M., Unger, P.E., and Lilly, W.D., Fuel, 64, 956 (1985)
5 Suuberg, E.M., Lee, D. and Larsen, J.W., Fuel, 64, 1668 (1985).
6 Suuberg, E.M., Unger, P.E., and Larsen, J.W., Energy Fuels, 1, 305 (1987).
7 Unger, P.E. and Suuberg, E.M., *18th Symp.(Int.) on Combustion*, p. 1203, The Comb. Inst., Pittsburgh, PA (1981).
8 Suuberg, E.M., *Chemistry of Coal Conversion*, R. Schlosberg (Ed.), Chapter 4, Plenum (1985).
9 Suuberg, E.M., Peters, W.A., and Howard, J.B., *Thermal Hydrocarbon Chemistry*, ACS Symposium Series, A.G. Oblad, H.G. Davis and R.T. Eddinger (Eds) 183, pp. 239-257, Washington, DC (1979).
10 Suuberg, E.M., "Properties of Tars Produced During Pyrolysis – Significance in Combustion systems," paper presented at Eastern States Section of Combustion Institute, Atlantic City (1982).
11 Suuberg, E.M. *ACS Div. Fuel Chem. Prepr.* 32(3), 51 (1987).
12 Oja, V. and Suuberg, E.M. *Anal. Chem.*, 69, 4619 (1997).
13 Suuberg, E.M. in *Fundamental Issues in Control of Carbon Reactivity*, J. Lahaye and P. Ehrburger, Eds., NATO ASI Series No. 192, p. 269 ff, Kluwer Academic Publishers, Boston, 1991.

14 Solomon, P.R., Serio, M.A., and Suuberg, E.M., "Coal Pyrolysis: Experiments, Kinetic Rates and Mechanisms," *Prog. Energy Combust. Sci.*, Vol 18, pp. 133-220 (1992).
15 Solomon, P. R., Hamblen, D. G., Carangelo, R. M., Serio, M. A., and Deshpande, G. V., *Energy & Fuels*, 2, 405 (1988).
16 Solomon, P. R., Hamblen, D. G., Yu, Z. -Z. and Serio, M. A., *Fuel*, 69, 754 (1990).
17 Solomon, P. R., Hamblen, D. G., Serio, M., A., Yu, Z. -Z. and Charpenay, S. C., *Fuel*, 72, 469 (1993).
18 Grant, D. M., Pugmire, R. J., Fletcher, T. H., and Kerstein, A. R., *Energy & Fuels*, 3, 175 (1989).
19 Niksa, S., *Energy & Fuels*, 5, 647-683 (1991).
20 Ko, G. H., Sanchez, D. M., Peters, W. A. and Howard, J. B., *Twenty-Second Symp. (Intl) on Comb.*, p. 115, The Combustion Institute, Pittsburgh, 1988.
21 Neavel, R. C., Smith, S. E., Hippo, E. J., and Miller, R. N., *Proc. of Intl. Conf. on Coal Sci.*, p.1, Dusseldorf, Sept. 1981.
22 Niksa, S., *Energy & Fuels*, 8, 659-679 (1994).
23 Niksa, S., *Combust. Flame*, 100:384 (1995).
24 Niksa, S., *Energy & Fuels*, 9, 467 (1995).
25 Zhao, Y., Serio, M.A., Bassilakis, R., and Solomon, P.R., *Twenty-Fifth Symposium (Int.) on Combustion*/The Combustion Institute, pp 553-560, (1994).
26 Fletcher, T.H., Kerstein, A.R., Pugmire, R.J., Solum, M.S., and Grant, D.M., *Energy & Fuels*, 6:4, p. 414-431 (1992).
27 Stauffer, D., and Aharony, A., *Introduction to Percolation Theory*, 2nd Edition, Taylor & Francis, London, UK, 1991.
28 Charpenay, S., Serio, M.A. and Solomon, P.R., "The Prediction of Coal Char Reactivity Under Combustion Conditions," *24th Symposium (Int) on Combustion*, The Combustion Institute, Pittsburgh, PA, 1189-1197 (1992).
29 Vorres, K. S., Energy & Fuels, 4(5), 420 (1990).
30 Wójtowicz, M.A., Serio, M.A., and Bassilakis, R., "Pyrolysis yields and kinetics for coal originating in different parts of the world," submitted to the *10th International Conference on Coal Science* , Taiyuan, China, (September 12-17, 1999).
31 Niksa, S., *ACS Div. of Fuel Chem. Preprints*, 43(1), 131 (1998).
32 Perry, S.T., and Fletcher, T.H., *ACS Div. Of Fuel Chem. Preprints*, 43 (1), 141 (1998).
33 Wójtowicz, M. A., Zhao, Y., Serio, M. A., Bassilakis, R., Solomon, P. R. and Nelson, P. F., in *Coal Science: Proceedings of the Eighth International Conference on Coal Science* (J.A. Pajares and J. M. D. Tascon, Eds.), Coal Science and Technology, vol. 24, Elsevier, Amsterdam, 1995, pp. 771-774.
34 Solomon, P.R., Serio, M.A., Hamblen, D.G., Smoot, L.D., Brewster, B.S., Radulovic, P.T., Final Report (Vol. 2) under DOE Contract No. DE-AC21-86MC23075 (October 1986 – September 1993).
35 Solomon, P.R., Serio, M.A., Zhao, Y., Wojtowicz, M.A., Smoot, L.D., Brewster, B.S., Radulovic, P.T., Topical Report under Contract No. DE-AC21-93MC30040.
36 FLUENT ACERC Module User's Guide, Version 1 (October 1996).
37 Jones, J.M., Patterson, P.M., Pourkashanian, M., Rowlands, L. and Williams, A., "An advanced coal model to predict NO_x formation and carbon burn-out in pulverised coal flames," presented at the 14th Annual International Pittsburgh Coal Conference & Workshop, Taiyuan, China, September 23-27, 1997.
38 Zhao, Y., Chen, Y., Hamblen, D.G., and Serio, M.A., *Proceedings of the 9th International Conference on Coal Science*, Essen, Germany (September 7-12, 1997), pp. 645-648.
39 Serio, M.A., Nelson, C.M., Chen, Y., Final Report for NSF Grant DMI-9761057 (October, 1998).
40 Zhao, Y., Serio, M.A. and Solomon, P.R., *26th Symposium (Int.) on Combustion*, The Combustion Institute, Pittsburgh, PA, 3145-3151 (1996).
41 Matthews, J.P., Hatcher, P.G., Scaroni, A.W., *ACS Div. of Fuel Chem. Preprints*, 43(1), 136 (1998).
42 Kumagai, H., Norinaga, K., Hayashi, J.-I., and Chiba, *Proceedings of the 1998 International Symposium on Advanced Energy Technology*, 2-4 February 1998, Sapporo, Japan, pp. 61-68.
43 Takanohashi, T., Iino, M., and Nakamura, K., *Proceedings of the 1998 International Symposium on Advanced Energy Technology*, 204 February 1998, Sapporo, Japan, pp. 77-84.
44 Serio, M.A., Solomon, P.R., Kroo, E., Bassilakis, R., Malhotra, R., and McMillen, D., *Proceedings of the 1991 Int. Conf. on Coal Science*, New Castle, England, Butterworth-Heinemann, Oxford, (1991).
45 Charpenay, S., Serio, M.A., Bassilakis, R., and Solomon, P.R., *Energy and Fuels*, 10(1),26 (1996).

NANOSTRUCTURES IN COAL-DERIVED CARBONS

Robert Hurt, Joseph Calo, Ying Hu
Division of Engineering
Brown University
Providence, RI 02912

INTRODUCTION

Carbon nanostructure, the local spatial arrangement and orientation of graphene layers, affects many important properties of carbon materials, including mechanical strength and modulus [1,2], coefficient of thermal expansion [2], electrical properties [3] and their directional dependencies, pore size distribution [4,5], and reactivity to oxidizing gases [5]. In coal-derived carbons in particular, the nanostructure influences surface area and fine porosity of coal-derived sorbents, coke strength and gas reactivity, and the graphitizibility of anthracites. This paper examines the fundamental mechanisms that determine nanostructure in carbon materials, with special emphasis on coal as the organic precursor. In common with Professor Suuberg's studies of tar vapor pressures, this work involves the physical chemistry of pyrolysis and carbonization.

RESULTS AND DISCUSSION

Figure 1 shows two example nanostructures in flame-derived coal chars. Structure A exhibits long range orientational order with statistical fluctuations (meandering) about the mean orientational vector. This nanostructure is believed to arise through liquid crystal formation during the fluid stage of carbonization. Structure B exhibits only short range orientational order, in the form of recognizable "crystallites". In some carbons these crystallites are oriented completely at random, while in the lignite char sample in Fig. 1B there is some degree of preferential orientation among the crystallites. The following sections discuss the quantitative description of these structures and the mechanisms of their formation.

Quantification of order

HRTEM fringe images allow quantification of nanostructure by digital image analysis [6-8]. The results are best described as semiquantitative, due to the extremely small sample size probed by the electron beam and the difficulty obtaining statistically significant data for correlation to bulk sample properties. The order parameter, $S = 1/2 < 3 \cos\theta - 1 >$ is a measure of long-range anisotropy, where θ is the angle between a single layer (or line in 2D) and the mean orientational vector, and $<>$ denotes an average. If the anisotropy extends over supramicron length scales it can be easily detected by optical microscopy (where it is referred to as coke texture) and quantified as the difference between the minimum and maximum reflectance upon optical stage rotation under polarized light (optical bireflectance).

Determination of the long-range order parameter for the structures in Fig. 1 yields 0.9 for structure A and 0.6 for the structure B. An analysis based on liquid crystal theory has shown that the 0.9 order parameter is consistent with a liquid crystal formation mechanism, while 0.6 is not [8]. The low grade orientational order in the lignite sample is believed to be caused by strain induced alignment during carbonization [8].

Phase behavior of PAH mixtures

The formation of anisotropic carbon via the liquid crystal route can be treated as a problem in liquid / liquid phase equilibrium [9,10]. As molecular weight increases during carbonization, so does aspect ratio of the oligomers formed from the primary aromatic clusters. At a critical aspect ratio, the oligomers undergo a concerted alignment to form the ordered fluid, which upon further molecular weight growth undergoes a glass transition to form a solid carbon. In PAH mixtures, phase separation occurs in which the higher molecular weight components partition preferentially into the liquid crystalline phase, and lower molecular weight components into the isotropic phase. Further polymerization causes the mesophase (LC phase) to grow at the expense of the isotropic phase until one or both phases solidify.

The quantitative description of this phase behavior is complicated by the lack of model compound studies showing this behavior. Indeed, no pure polyaromatic hydrocarbon has ever been observed to form a discotic liquid crystal! A recent analysis suggests that this paradox is a mixture effect [10]. In complex multicomponent PAH mixtures, crystalline solid phases are suppressed and the underlying liquid crystalline phases are revealed. Figure 2 illustrates this effect in a hypothetical binary mixture. In multicomponent calculations, it is possible for a mixture of N nonmesogens to give rise to liquid crystalline phases due to the severe depression of the liquid / solid phases transition temperatures.

The latent liquid crystal forming tendency in PAH increases with increasing molecular weight (for similar structures), and in a complex mixture, the entire molecular weight distribution influences whether or not the liquid crystalline phase appears. Macroscopic

solution thermodynamics can be used to estimate the amount and compositions of the isotropic and anisotropic phases given the overall molecular weight distribution of the melt [10]. This solution thermodynamics approach is not valid in the low molecular weight limit — i.e. it does not give the correct results for solvents with no liquid crystal forming tendency (nonmesogens). Statistical models based on pseudo-potentials for orientation give a useful description of nonmesogen behavior [9], but are difficult to solve in the general multicomponent case involving N mesogens with differing molecular weights and clearing temperatures. More work is needed to develop comprehensive, tractable equilibrium models of mesophase formation.

Role of Fluidity

In low viscosity pitches, mesophase typically appears as Brooks-Taylor mesospheres, which are thermodynamically favored as they possess the minimum mesophase / isotropic interfacial area. The high viscosities in coal carbonization prevent this thermodynamic state from being reached and lead to irregularly-shaped anisotropic domains. Nonfusible material can also limit the growth and coalescence of mesophase by collecting at the boundaries between the mesophase and isotropic phases or between mesophase regions (domains) of different orientation.

At still lower mobility (higher viscosity), the primary formation of carbonaceous mesophase is suppressed, and the resulting carbon has very short range orientational order (5 - 10 nm). Figure 3 shows results of a numerical simulation that addresses the effect of layer mobility on liquid crystal phase transitions [11]. The simulations employ hard lines which rotate and grow in a two-dimensional continuum. At high mobility (rotational frequency) the lines adopt orientational order at a certain length to avoid overlap. At lower mobility, the lines form finite ordered regions in an isotropic matrix, thus mimicking the observed behavior of carbons. Figure 4 plots the order parameter as a function of the dimensionless mobility-to-growth ratio. The numerical model in its simplest form is sufficient to distinguish two important classes of carbon materials: (1) isotropic carbons formed via all-solid-state routes in which molecular mobility is severely limited (e.g. low-rank coals, woody and cellulosic materials, and oxygen-rich thermosetting polymers), and (2) anisotropic carbons formed from precursors that pass through a mobile, liquid-phase intermediate (high-rank bituminous coals, polyvinyl chloride, anthracene, many petroleum and coal-tar pitches).

It is further found that anthracitic order can be adequately represented by simulations in which the layers have a preferred initial direction (non-zero initial order parameter) and non-zero initial length (see Fig. 4). This is justified by TEM and NMR studies of raw anthracites which indicate that significant aromatic cluster development has occurred during coalification. The simulations in Fig. 4 show a gradual, monotonic increase in final order as the mobility increases, so that anthracites produce chars with long-range order intermediate between the high-rank bituminous coals and the low-rank materials. This simulation behavior is consistent with the observed rank trends.

Figure 5a,b show further comparisons between carbonization studies and the simple numerical simulations. Figure 5a shows measurements of optical bireflectance as a function of carbonization temperature for three coals of various rank [12]. These results are given as a function of temperature, rather than time, but are indicative of the solid structures observed during the various stages of carbonization, as they might occur during non-isothermal heat treatment. The lowest rank coal is isotropic it its initially state and remains essentially so during carbonization. The high-rank bituminous coal shows measurable anisotropy it its raw state, but loses this anisotropy at 400 °C, and regains it at slightly higher temperatures. Apparently the increase in mobility on heating allows the structure to relax from a metastable configuration imposed by high lithostatic pressure to a near equilibrium isotropic configuration at 1 bar pressure. As heating continues, molecular weight growth proceeds until the planar structures reach the critical size (aspect ratio) for liquid crystal formation, and a highly ordered state develops. The bireflectance thus passes through a minimum, as seen in Fig. 7 in the curve labeled high-rank bituminous. The anthracite in raw form shows significant anisotropy, which is unaltered up to 600 °C and then slightly enhanced by higher temperature heat treatment. Despite the high degree of initial order, the anthracite does not develop the same degree of order as the high-rank bituminous coal. This is consistent with the observation that many anthracites are nongraphitizable [13].

Finally, Fig. 5b shows time dependent simulation results for three cases representing important classes of coals. The simulations show that: (1) the low rank coal is nearly isotropic and remain so during carbonization, (2) the high rank bituminous coal loses its initial anisotropy, but regains it during the latter stages of carbonization, (3) the anthracite retains and slightly enhances its anisotropy during carbonization. Comparing Figs. 5a and 5b, it is seen that the simple hard-line simulations also mimic these major trends seen in the bireflectance studies. Overall, the concepts of liquid / liquid equilibrium, together with the kinetic effects associated with limited layer mobility can describe the formation of most carbon types. An exception, however, is isotropic coke, whose formation mechanism receives separate consideration in the next section.

Isotropic coke

Many coal chars pass through a fluid state, but solidify to form isotropic chars. The lack of long range order in these materials cannot be explained by low fluidity (high viscosity) — many of them exhibit higher maximum fluidities than coals which form anisotropic chars. A promising explanation for isotropic coke formation is the suppression of liquid crystalline phases by non-planar molecules, or "non-mesogens".

A key requirement for the formation of liquid crystalline phases is a high aspect ratio, L/D, of the rod-like or disk-like constituent molecules. Most functional groups that act as cross-linking agents for aromatic clusters (aryl, ether, sulfide) involve non-linear single bonds. These cross-links produce oligomers of aromatic clusters that can adopt both planar and nonplanar configurations upon bond rotation. Depending on the shape of the aromatic oligomer (influenced by the geometry of the aromatic clusters and side chains) the planar geometries may be stearically hindered, and the nonplanar structure that results may act as a "nonmesogen" and cause a local disruption in the liquid crystalline phase.

The effect of nonmesogens on LC phases has been studied in the canonical case of spherical solutes (L/D = 1) in rod-like mesogens [14]. Phase diagrams for binary mixtures of mesogens and nonmesogens have been derived from a statistical theory based on a pseudo-potential for orientation. Recently, Shishido [9] have applied this statistical theory to explain the suppression of mesophase in pitch by addition of low-molecular weight pitch fractions (which were presumed to be completely nonmesogenic).

Figure 6 presents a qualitative picture of this effect as it may occur during coal carbonization. Assuming a linear relationship between clearing temperature and molecular weight [10], the Bates-Shishido phase diagram can be plotted as MW vs. the mole fraction nonmesogen. The plot also shows two possible carbonization trajectories for a high-rank and low-rank bituminous coal. The trajectories were calculated using the measured elemental composition of the solid carbonizing phase, and assuming that a fixed fraction, F, of the oxygen and sulfur atoms were present as in functional groups that lead to non-planar cross-links. The average number of these non-planar groups per oligomer is:

$$N = F\,(X_{O+S})\,(MW_{oligomer}) / (MW_{mixture})$$

where X_{O+S} is the mole fraction O and S atoms, and $MW_{mixture}$ is the mean atomic weight of the carbonizing melt. The mole fraction nonmesogens is then the probability that a given oligomer contains one or more non-planar links (and thus has an overall nonplanar geometry), which, assuming a Poisson distribution, is given by: 1 - exp(-N).

Trajectories were drawn for various values of F in an attempt to reproduce the experimental fact that Illinois #6 flame chars are isotropic, while Pocahontas #3 chars are anisotropic (except for inertinite-derived material). A value of 0.05 gives reasonable behavior as shown in Fig. 6. Thus if only 5% of the O and S atoms are involved in nonplanar cross-linking structures, liquid crystal formation will be largely suppressed in the low-rank Illinois #6 coal. This is the most promising explanation for the overall trend of isotropic coke formation from many oxygen-rich and sulfur-rich precursors. The full quantitative relation between chemical functionality and mesogenicity is, of course, complex and must be based on functional group analysis rather than simple elemental analysis.

It is evident from this paper that much more work is needed before we have a complete quantitative understanding of the origin and evolution of carbon nanostructures.

REFERENCES

1. Emmerich, F.G. *Carbon* 33 47 (1995).
2. Sato S., Kawamata, K., Kurumuda, A., Kawamota, M., Ishida, R. *Carbon* 26 (4) 465 (1988).
3. Rouzaud, J.N., Oberlin, A. *Carbon* 27 (4) 517 (1989).
4. Oberlin, A., in *Chemistry and Physics of Carbon, Vol. 22*, ed. P. A. Thrower, Marcel Dekker, New York, 1989, pp. 1-143.
5. Rouzaud, J.N., Oberlin, A. Chapt. 17 in *Advanced Methodologies in Coal Characterization*, Elsevier, Amsterdam, 1990.
6. Palotas, A. B., Rainey, L. C., Feldermann, C. J., Sarofim, A. F., and Vander Sande, J. B., *Microsc. Res. Tech.*, 1996, 33, pp. 266-278.
7. Dobb, M. G., Guo, H., and Jonhson, D. J., *Carbon*, 33 1115 (1995).
8. Shim, H.S., Hurt, R.H., Yang, N.Y.C. "A Methodology for Analysis of 002 LF Fringe Images and Its Application to Combustion-Derived Carbons", *Carbon*, in press.
9. Shishido, M., Inomata, H., Arai, K, Saito, S. *Carbon* 35 (6) 797 (1997).
10. Hurt, R.H., Hu, Y. "Thermodynamics of Carbonaceous Mesophase," *Carbon*, in press, 1998.
11. Hu, Y., Calo, J.M., Hurt, R.H., Kerstein, A. "Kinetics of Orientational Order / Disorder Transitions and Their Application to Carbon Material Synthesis," *Modelling and Simultion in Materials Science and Engineering*, in press.
12. Murchison, D.G., Chap. 31 in *Analytical Methods for Coal and Coal Products*, Academic Press, New York, 1978.
13. Blanche, C., Dumas, D., Rouzaud, J.N. Coal Science (Pajares and Tascon Eds.) Elsevier Science, Amsterdam, 1995, p. 43.
14. Humphries, R.L., and Luckhurst, G.R. *Proc. R. Soc. London, A.* 352 41-56 (1976).

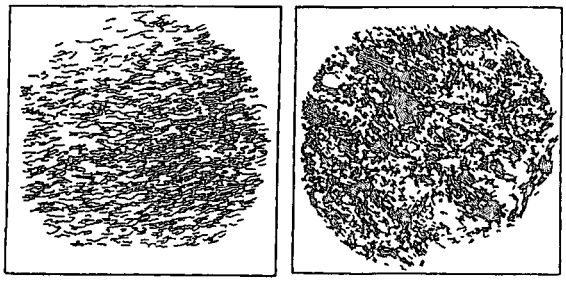

A B

Figure 1. Digitally enhanced high resolution TEM fringe images showing the nanostructures of coal-derived carbons. The lines are graphene layers, imperfect snippets of the graphite lattice, viewed edge-on. A: Pocahontas #3 char; B: lignite char.

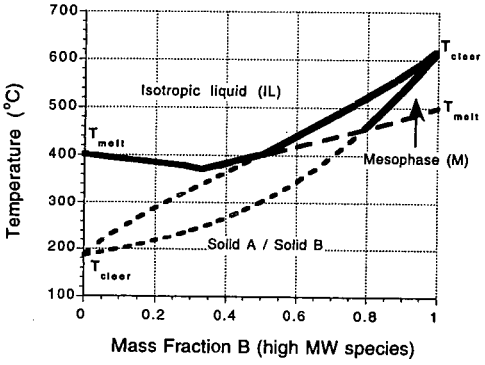

Figure 2. Example binary phase diagram for generic PAH of low and high molecular weight. In the pure state A is nonmesogenic and B is mesogenic.

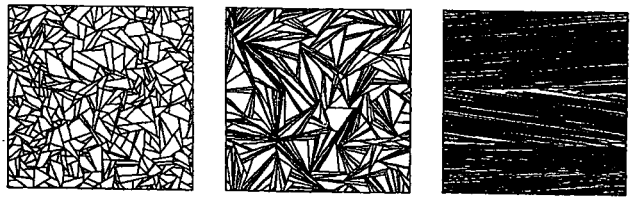

M* = 0 M* = 37 M* = 2,200

Figure 3. Summary of frozen states in hard-line simulations. As mobility/growth ratio, M*, increases, the final structures changes from complete disorder to short range order to a structure in which the ordered length scale is comparable to the size of the simulation box.

Figure 4 Summary of final states in numerical simulations starting from initially random states (isotropic parent materials) and initial ordered states (anisotropic parent materials). Long-range order parameter in the final state vs. dimensionless mobility / growth ratio, M^*. Curve labels show the relation to carbonization processes. Type A carbons: isotropic solids formed through solid-state pyrolysis (e.g from lignites, woody tissue, oxygen-rich polymers); Type B carbons: anisotropic solids formed through liquid phase pyrolysis (pitches, polyaromatic compounds, coking coals); Type C carbons: anisotropic solids formed by solid-state pyrolysis of initially *ordered precursors* (e.g. anthracites).

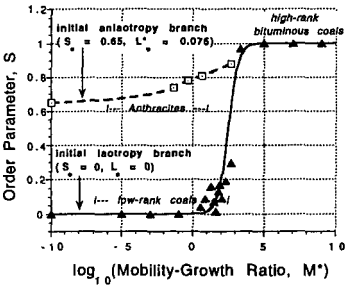

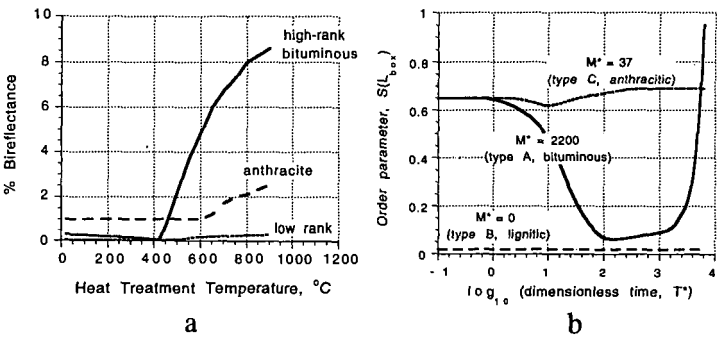

Figure 5. a: Measurements of optical birefectance as a function of carbonization temperature for three important classes of coals from Murchison [12]; b: Time evolution of the long-range nematic order parameter in three simulations representing important classes of carbonization processes.

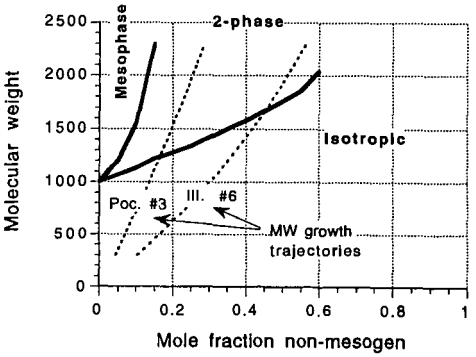

Figure 6 Phase diagram for binary mixture of mesogens and nonmesogens showing possible trajectories describing the carbonization of bituminous coals of different rank. Plot is useful for developing a theory of isotropic coke formation.

THE GASIFICATION REACTIVITY OF CARBONS - NEW DEVELOPMENTS

Eric M. Suuberg
Division of Engineering, Brown University, Providence, RI 02912

Keywords: Coal, carbon, surface area, porosity, gasification, combustion

Introduction

The reactions of chars (or "carbons") with oxidizing gases are among the most important of industrial reactions. Basic to utilization of any solid fuel, and important in processes ranging from activated carbon production to steel-making, they have been extensively studied for more than a century, e.g., 1,2. It is a tribute to the complexity of the processes involved that they have not yet yielded to intensive study, and a quantitatively predictive description of the phenomenon is not yet in hand. The difficulties in developing such a quantitative description are well-known. First, the materials from which the carbons are derived leave an indelible imprint on their character. Second, the temperature history of their preparation also has a significant impact. Modeling the complexity of the relevant pyrolysis processes still represents an imposing challenge (see the presentation by Serio et al. in this symposium). Third, the presence of small amounts of additional elements, serving as catalytic agents, influence both the course of carbon formation and subsequent gasification behavior. Finally, subtle aspects of combined phase and reaction behavior can drive the morphology of the carbons across a wide spectrum of characteristics (see the presentations by Hurt et al. and Winans et al. in this symposium). These morphological differences also play a key role in the subsequent reaction behavior of the carbons, as it is the ability of the oxidizing gases to gain access to the porosity in the carbon which determines some key aspects of the reaction process. Improvements in the quantitative description of these phenomena will require experimental examination of all of these processes at a greater level of detail. No single study will be able to provide all of the pieces, and progress will continue to be achieved through many fundamental examinations of various aspects of the processes. In this presentation, a key focal point will be the question of how porosity develops during gasification processes, and what this tells us about several of the above issues.

Patterns of Porosity Development

One useful new tool in the examination of this question is the use of NO as a model reactant. The reaction rates of carbons with NO are generally intermediate between the rates of carbon with oxygen on the one hand and those with CO_2 or steam on the other hand. Relatively few systematic studies of NO-carbon reactions have been undertaken; activation of carbons in NO is not of known commercial interest and the role of the carbon-NO reaction is of debated significance in practical combustion systems (they appear to clearly be of importance in fluidized beds, but probably of lesser importance in pulverized systems, except perhaps during reburning). Various aspects of the reaction have been recently reviewed[3].

Figure 1 shows that for gasification of a Wyodak coal-derived char in the intrinsic reaction rate regime, the development of *microporosity* follows a qualitatively similar pattern in three oxidizing gases (O_2, CO_2, NO), but there exist quantitative differences between the pattern in CO_2 and in the other gases. Experimental details have been provided elsewhere[4]. Characterization of porosity is here based upon traditional N_2 isotherm-derived quantities, but other adsorptives support the

Figure 1. Wyodak coal char surface area evolution in different oxidizing gases.

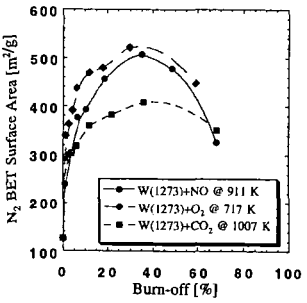

Figure 2. Wyodak coal char mesopore volume evolution in different oxidizing gases

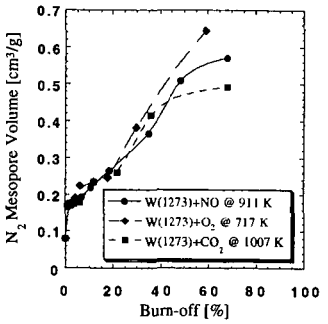

conclusions[4]. The development of *mesoporosity* also follows a very similar pattern in all three gases, even quantitatively up to a certain point, see Figure 2. These results emphasize that some

care is required in selection of data, and criteria, for drawing conclusions regarding the universality (or lack thereof) in a pattern of porosity development.

The so-called random pore models of gasification[5,6] have adopted the viewpoint that there is a single structural parameter which can be used to describe the relationship between conversion (extent of gasification) and porosity in the char. Figure 1 would require viewing this parameter as a a function of both starting material and gaseous environment. Figure 2, however, speaks to the possibility of viewing the structural parameter as a true material constant, at some level of approximation. Existence of a material-specific structural parameter is supported by results such as shown in Figure 3, illustrating development of porosity in a microcrystalline graphite, and Figure 4 showing development of porosity in a char derived from pine wood. Here, the data on porosity are shown as adsorption isotherms. Again, gasification conditions were selected so as to give comparable (apparently intrinsic) rates in all gases.

Figure 3. N_2 isotherms for graphite gasified in three gases (open points- desorption).

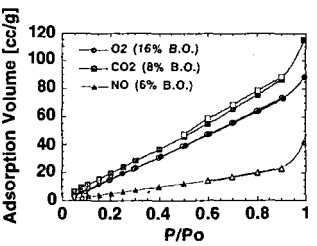

Figure 4. N_2 isotherms for pine char reacted in three gases (adsorption isotherms).

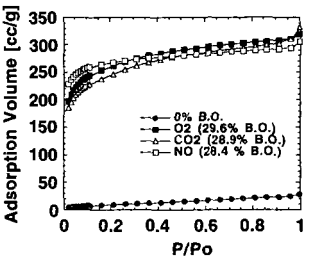

These two cases represent extremes of behavior observed in many other materials. The graphite sample starts with virtually no porosity (the isotherm is at the bottom of the figure) and develops only fairly large-scale porosity (meso- and macroporosity), consistent with pitting of the surface. This is seen in Figure 3 as an increase in slope of the isotherms in the mid- to high- range of P/Po, and this slope increases with burn-off. On the other hand, the char derived from pine shows a dramatic upward shift with burn-off of the isotherms in the low P/Po range, indicating opening of microporosity. There are only modest change in meso- and macroporosity. The isotherms for the Wyodak material described in Figures 1 and 2 can be viewed as a composite of these two behaviors, consistent with the development of both types of pores.

It is clear from the above that the nature of activation is, to a first approximation, a property of the material and not of the reactant gas. The great importance of starting material is well known to those concerned with activated carbons. The reasons for these differences in porosity development patterns are not, however, entirely understood in all cases. It is fairly certain that the graphite cannot develop microporosity because of the locus and nature of the attack on its surface - the oxidizing gases are known to attack edge atoms, dislocations, etc., and this can only happen where the gases have access to such sites on the external surface. The pine char has a highly disordered structure to begin with, and a great deal of porosity, providing reactant gases access to its interior. Some of the dramatic increase in micropore volume in Figure 4 is an artifact of the well-known problem of activated diffusion of nitrogen at the low temperatures of measurement of the isotherms, but a large part is not, and there appears to be true development of both microporosity (and some mesoporosity). Does this require penetration of the reactant gases on the micropore size scale, as has been often suggested? It is unclear at the present time.

There can be no doubt that catalysis can play an important role in influencing the course of the observed processes. Figures 5 and 6 illustrate the mesopore size distributions observed after gasification of the Wyodak char in its original and demineralized states. The pore size distributions were calculated using the Barrett-Joyner-Halenda (BJH) method, corrected for micropore volumes[7]. This type of calculation is often criticized on various theoretical grounds, but the qualitative conclusions are very clear. The original Wyodak char, which is known to contain an abundance of catalytic mineral matter, develops very similar mesoporosity in all three gases (consistent with Figure 2). After demineralization, there is little mesoporosity development over the same range of burn-off. It is believed that it is the catalyst particles which in some manner dictate the development of the mesoporosity in the original sample, a conclusion consistent with the limited literature on this topic[8].

The above results notwithstanding, the results of Figure 1 show, as does much of the literature on activation of carbons, that the development of porosity during reaction of carbons in different gases can show distinct patterns, even if the reaction rates are closely matched, e.g., ref. 8. The results of Figures 3 through 6 appear to directly contradict a conclusion that CO_2 and O_2 will necessarily

Figure 5. Pore size distributions for Wyodak char gasified in three gases.

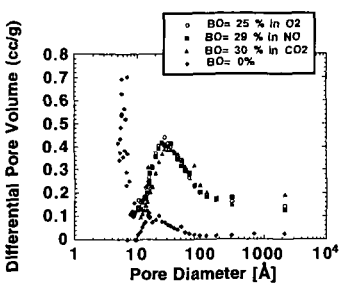

Figure 6. Pore size distributions for demineralized Wyodak char gasified in NO and CO_2.

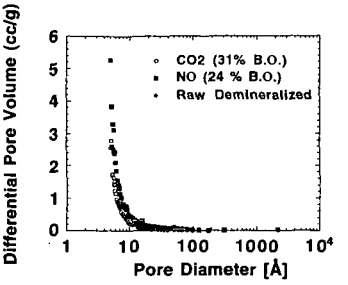

involve a very different pattern[8], but it is important to note that sometimes differences emerge only at higher burn-offs. Again, the reasons for the initial similarity and subsequent divergence are not yet understood. What does appear to be clear is that the differences are not an artifact of the choice of adsorptive used for examining porosity - both nitrogen and CO_2 isotherms offer similar conclusions. The other conclusion which may be drawn is that the simple, empirical porosity development models cannot yet handle this issue.

Annealing

In the gasification and combustion literature, there is a well-established pattern of decrease in reactivity with increase in heat treatment temperature[9-19]. This phenomenon has often been termed annealing, on the basis that heat treatment "heals" the surface, removing the imperfections that constitute the main active sites. We have empirically modeled the process as involving an extension of high-temperature pyrolysis phenomena. The activation energy distributions characteristic of pyrolytic release of hydrogen merge with the activation energy distributions characteristic of graphitization. The distributed activation energy approach has been quite successful in predicting the changes in reactivity with heat treatment[12,20].

What has remained unclear is what physical factors are most important in determining the change in reactivity with heat treatment. Is the phenomenon tied to the gradual perfecting of aromatic structure, associated with the growth of condensed aromatic structures? Success has been achieved in correlating reactivity with hydrogen remaining in the structure[21]. Or is the loss of active sites mainly attributable to a loss of surface area with heat treatment? Both factors are sure to contribute to differing extents in different situations. In some cases, loss of catalyst or catalyst dispersion has also been cited.

The simple picture of reactivity loss with heat treatment is further complicated by several recent findings. First, there is the observation that annealing does not proceed at the same rate with respect to NO reactivity as it does with respect to oxygen reactivity[3]. In the case of NO, the annealing of a phenolic char could be entirely explained on the basis of surface area changes, whereas in the case of oxygen, there was an effect beyond surface area change involved. Another issue which has received attention recently is "memory loss" in gasification. As gasification conversion increases, differences in reactivity attributable to differences in heat treatment tend to disappear[11,22]. The effect has been attributed to selective burn-off of less ordered material early in the process, leaving behind increasingly similar more ordered and less reactive residues as conversion increases. What occurs is, however, not so clear when data on active site concentration variations with burn-off are considered. Figure 7 shows these trends in a phenolic resin char, in which active surface area (ASA) was determined by oxygen chemisorption[23]. As burn-off increased, the more highly heat treated char approached the less highly heat treated char in both total surface area (TSA) and ASA. Meanwhile, the 573 K oxygen gasification reactivities of the samples slowly approached one another, in the usual fashion. What this means is that by one measure of structure and reactivity, the highly heat treated sample is becoming more reactive with burn-off. By the other measure, the less heat treated sample is declining in reactivity, while the more highly heat treated is remaining more or less the same. Clearly these results call into question the assay of ASA by oxygen chemisorption, and its significance with respect to high temperature gasification rates. But these results also suggest that the penetration of porosity by the oxygen reactant may be quite different in different reaction regimes; in the low temperature chemisorption regime, the oxygen reaches different porosity than in the higher temperature regime. This is, in fact, the basis of an exciting new carbon activation process being developed by AFR, Inc.[24].

Figure 8 shows that the more highly heat treated char develops a larger porosity than does the less heat treated char (again relying on a BJH-type pore size distribution analysis). The N_2 surface areas of these two samples are within about 15% of each other. Thus it seems possible that the

Figure 7. Reactivity and ASA variation in phenolic resin chars heat treated for 2 hours at indicated temperatures.

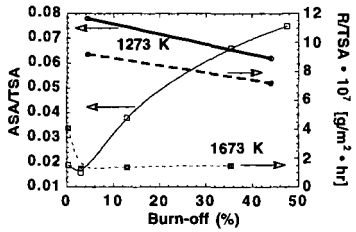

Figure 8. Pore size distributions for chars of Fig. 7, after approx. 20% burn-off in oxygen.

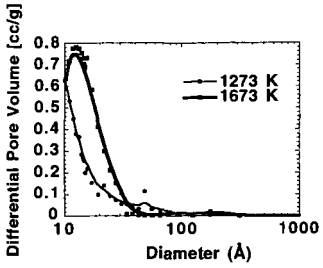

very different ASA behaviors are a consequence of the creation of more large porosity, in the case of the 1673 K char, and may not really be a good indicator of truly available ASA at high temperatures.

Surface Area and Reactivity

It has been recognized for quite some time that the rate of gasification of a carbon should in some way be related to its surface area. The above data and discussion have perhaps already raised concerns regarding how difficult it might be to assess the correct surface areas. Historically, two main methods have been employed for measuring the areas. One involves the use of nitrogen isotherms and the BET equation, and the other involves use of carbon dioxide isotherms and some form of the Dubinin-Radushkevich equation. The relative merits of both methods have been debated for some time. While it is true that activated diffusion barriers are sometimes a problem for N_2 adsorption at liquid nitrogen temperatures, the importance of this issue has perhaps been overplayed. Carbon dioxide is, on the other hand, often unable to interrogate the larger micropores[7]. It has thus been recommended that a combination of both probes be used to avoid drawing false conclusions[7]. We have recently examined a number of adsorptives on the same chars, and concluded that there was no particular advantage to use of carbon dioxide over nitrogen[4].

Reactivity data for the Wyodak chars are shown in Figure 9, again using the three main oxidizing gases of this study. All of these data show an increase in reactivity per mass of remaining carbon, with burn-off (note that the behavior in this case was only tracked to 70% burn-off). The question of whether the reactivities could be normalized by surface areas was then examined. Figure 10 shows the results of normalization by BET surface areas. The only special feature of this normalization is that the reactivity at 1% burn-off was taken as the reference, in order to avoid

Figure 9. Reactivity of Wyodak char in different oxidizing gases.

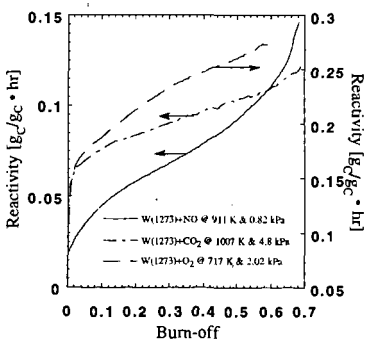

Figure 10. Normalized reactivities of Wyodak char.

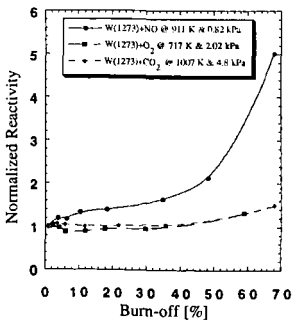

issues related to severe activated diffusion limitations leading to apparently low BET areas at near zero burn-off. Thus if surface area truly normalizes reactivity, a horizontal line should be obtained at unity. Such is very nearly the case in oxygen and in carbon dioxide, but not in NO. Still, caution must be exercise in concluding that reactive gases can reach all of the available micropore surface areas in the cases of oxygen and carbon dioxide. It was suggested in connection with Fig. 5 that the main locus of reaction may be catalyst particles. In such a case, an apparent correlation of reactivity with surface area may be indirect; catalyst area may correlate with micropore area for some reason. In any case, a correlation with surface area might actually only be a correlation with numbers of micropores, and reactants may be unable to use any more than the mouths of the micropores. Suggestions that micropores might not be fully utilized in reaction are numerous[5,16,25,26].

The case of NO reactivity was particularly interesting. In the case of this reactant, the normalization appeared to be poor. Examined more closely, the curve for NO does, however, show a period of relatively constant reactivity per unit of surface area. This has been taken to indicate that the normalization reactivity per unit area (at 1% burn-off) was actually too low, in this case by about 50%, since the period of constant reactivity occurs at a normalized value of about 1.5 . This in turn indicates that the microporosity initially present was not all available for reaction, and was only opened up by 10% burn-off. Beyond 40% burn-off, the curve begins to rise sharply once again. This is further indication that the original normalization was based upon the wrong (too high) surface area. Only as the microporosity is opened up (becomes wider) does NO gain greater access to the surface. This was verified by sharp changes in the pore size distributions in this range of burn-offs. Thus, the use of BET or DR surface areas to normalize reactivities is of little fundamental significance, and should be approached with great caution.

Summary

Results have been obtained for a wide range of carbons, which suggest that the development of porosity is most strongly dependent upon the nature of the starting material. Gasification environment can play a role in porosity development, as may the presence of catalysts. Annealing of the carbon influences its porosity and therefore, accessibility of reactant gases. Surface areas for reaction of gases with carbons are a useful concept, but the methods presently used to normalize reactivities must be viewed as essentially empirical. There is evidence to suggest that micropore surfaces are not available for reaction.

Acknowledgment

The important contributions of former graduate students are most gratefully acknowledged, in particular, those of Indrek Aarna, Marek Wójtowicz and Hsisheng Teng. The financial support of the NSF, under grant BES- 9523794, is also gratefully acknowledged.

References

1. Walker, P.L., Jr.; Rusinko, F., Jr.; Austin, L.G. *Adv. Cat.* **1959**, *XI*, 133.
2. Essenhigh, R.H. in *Chemistry of Coal Utilization, Second Supplementary Volume*, M. Elliott, Ed., Chap. 19, Wiley, 1981.
3. Aarna, I.; Suuberg, E.M. *Fuel*, **1997**, *76*, 475.
4. Aarna, I.; Suuberg, E.M. *27th Symp. (Int.) on Comb.*, in press, 1998.
5. Gavalas, G.R. *AIChEJ*, **1980**, *26*, 577.
6. Bhatia, S.K.; Perlmutter, D.D. *AIChEJ*, **1980**, *26*, 379.
7. Rodríguez-Reinoso, F.; Linares-Solano, A., in *Chemistry and Physics of Carbon, Vol. 21*, P. A. Thrower, Ed., p. 1, Dekker, New York, 1989.
8. Rodriguez-Reinoso, F.in *Fundamental Issues in Control of Carbon Gasification Reactivity*, J. Lahaye, P. Ehrburger, Eds. p. 533 , Kluwer Academic, Dordrecht, 1991.
9. van Heek, K.H.; Mühlen, H.J. *Fuel*, **1985**, *64*, 1405.
10. Duval, X. *Ann. de Chem., 12th Ser.*, **1955**, *10*, 58.
11. Senneca, O.; Russo, P.; Salatino, P.; Masi, S. *Carbon*, **1997**, *35*, 141.
12. Suuberg, E.M. in *Fundamental Issues in Control of Carbon Gasification Reactivity*, J. Lahaye, P. Ehrburger, Eds. p. 269, Kluwer Academic, Dordrecht, 1991.
13. Serio, M. A.; Solomon, P.R.; Bassilakis, R.; Suuberg, E.M. *ACS Div. Fuel Chem. Prepr.* **1989**, *34(1)*, 9.
14. Beeley, T.; Crelling, J.; Gibbins, J.; Hurt, R.; Lunden, M.; Man, C.; Williamson, J.; Yang, N. *26th Symp (Int.) on Comb.* p. 3103, The Combustion Institute, Pittsburgh, 1996.
15. Jenkins, R.G.; Nandi, S.P.; Walker, P.L., Jr. *Fuel*, **1973**, *52*, 288.
16. Radovic, L.R.; Walker, P.L., Jr.; Jenknis, R.G. *Fuel*, **1982**, *62*, 849.
17. Gale, T.K.; Bartholomew, C.H.; Fletcher, T.H. *Energy Fuels*, **1996**, *10*, 766.
18. Kasaoka, S.; Sakata, Y.; Shimada, M. *Fuel*, **1987**, *66*, 697.
19. Sahu, R.; Levendis, Y.; Flagan, R.; Gavalas, G. *Fuel*, **1988**, *67*, 275.
20. Hurt, R.H.; Sun, J.K.; Lunden, M. *Comb. Flame*, **1998**, *113*, 181.
21. Charpenay, S.; Serio, M.A.; Solomon, P.R. *24th Symp (Int.) on Comb.* p. 1189, The Combustion Institute, Pittsburgh, 1992.
22. Anxustegi, M.M.; Calo, J.M.; Hurt, R.H.; Shim, H. S. *Proc. Eurocarbon '98*, p. 675, GFEC, 1998.
23. Suuberg, E.M.; Wójtowicz, M.; Calo, J.M. *Carbon*, **1989**, 27, 431.
24. Wójtowicz, M.; Markowitz, B.L.; Simons, G.; Serio, M.A. *ACS Div. Fuel Chem. Prepr.* **1998**, *43*, 585.
25. Hurt, R.H.; Sarofim, A.F.; Longwell, J. *Fuel*, **1991**, *70*, 1079.
26. Dutta, S.; Wen, C.Y.; Belt, R.J. *Ind. Eng. Chem. Proc. Des. Dev.* **1977**, *16*, 20.

EFFECTS OF CHLORINE IN COAL ON BOILER SUPERHEATER/REHEATER CORROSION

M.-I.M. Chou and J.M. Lytle
Illinois State Geological Survey
Champaign, IL 61801

S. C. Kung
McDermott Technology Inc.
1562 Beeson St., Alliance, OH 44601

K.K. Ho
Illinois Clean Coal Institute
Carterville, IL 62918

Keywords: chlorine, coal, corrosion

Abstract
Many British studies have correlated superheater/reheater corrosion in pulverized coal boilers with the total chlorine (Cl) content in coals, which has led many US boiler manufacturers to set their maximum recommended Cl level at 0.3%. However, Cl-related boiler corrosion has not been reported by US utilities burning high-Cl Illinois coals. Other factors, such as boiler parameters, have been studied for their effect on corrosion rate. This study measured the rate of corrosion caused by two high-Cl coals (British and Illinois) and one low-Cl Illinois coal under identical pilot-scale combustion conditions for a duration which would give reliable comparisons. The results showed no correlation between coal Cl content and rate of corrosion, but showed a correlation between the rate of corrosion and the metal temperature used. These data could provide a basis for lifting the limit of burning high chlorine Illinois coals in the utility boilers.

Introduction
Many British studies have correlated accelerated fireside corrosion of heat exchanger tubes in utility boilers with the high-Cl content in coal (Raask, 1963; Reid, 1971; Meadowcroft and Manning, 1983). Their correlations implied that the corrosion rate of boiler tubes increased proportionally with increasing Cl concentration in the coal. Based on these correlations, US boiler manufacturers and utility operators consider coals containing more than 0.3% Cl to be potentially corrosive and have set guidelines on the Cl content (<0.3%) of coal to be used in their boilers. These guidelines were based primarily on extrapolation British coal data to predict the probable corrosion behavior of US coals. The guidelines on the Cl level have discouraged the burning of high-Cl Illinois Basin coals in utility boilers.

A survey conducted jointly by Electric Power Research Institute and Illinois Clean Coal Institute during 1992 (Doane et al., 1994; Wright et al., 1994) indicated that some US utilities have decades of experience burning high-Cl coals in pulverized coal (PC) fired boilers. Although fireside corrosion problems have been reported, none of them could be directly related to the presence of Cl in coal. This contradiction with published data suggested that the role of Cl in coal on boiler-tube corrosion was not fully understood. It is possible that the level of Cl in coal is not as harmful as predicted, or the corrosivity of high-Cl Illinois coal is less severe than that of British coal, or other coal properties such as sulfur and potentially volatile alkali metals in coals are possibly associated with boiler corrosion (Chou et al. 1998). The differences in boiler design and operation between US and UK utilities, such as boiler superheater/reheater temperatures, might also have attributed to this discrepancy.

This study focuses on how the corrosivity of a high-Cl Illinois coal compares with that of a British coal with a similar Cl content at superheater/reheater temperatures. Three pilot-scale combustion tests were conducted . The rates of corrosion caused by two high-Cl coals (British and Illinois) and a low-Cl baseline Illinois coal were measured under identical combustion conditions for a duration which would give a reliable comparison. The corrosion tests used Alloy 304SS which is a frequently used material at the hottest superheater section of both US and UK utility boilers. The corrosivity data from a temperature range including two specific metal temperatures, 1100°F and 1200°F were determined. The cooler metal temperature is common in the US boilers and the hotter temperature is common in the UK boilers.

Experimental
Coal samples - During sample acquisition, the available high-Cl British coals from the British Coal

Corporation Coal Research Establishment (CRE) coal sample bank were obtained for screening analysis (CRE, 1993). One of the coals obtained had a chlorine content (~0.4%) comparable to that of the high-Cl Illinois coal chosen. This British coal is also currently the most mined coal. A 20-ton lot of the British coal, therefore, was purchased from RJB Mining in Great Britain and shipped to the US for the combustion test. To form a basis for assessing the corrosion effect of the two high-Cl coals, a low-Cl Illinois coal was included in the combustion tests. Splits of the 20-ton lots of the three coals were analyzed for chlorine, sulfur, and ash content using the ASTM methods (1994).

Pilot scale combustion test - A refractory-lined, stoker-fired Fireside Corrosion Test Facility at McDermott Technologies, Inc. in Alliance, Ohio was used to burn the coal. A variable-speed screw feeder supplied the coal to the bottom of the stoker combustion chamber. A forced draft fan provided the primary air that entered the furnace through tuyers surrounding the burner. Penetrations right above the combustion chamber were used to accommodate the corrosion probes. Two sets of probes were used to approximate US and UK boiler tube wall temperatures. One set was regulated to include the temperature of 1200°F (649°C) which is common in UK boilers, and the other set was regulated to include the temperature of 1100°F (593°C) which is common in US boilers. A frequently used commercial alloy at the hottest superheater section of utility boilers was used to fabricate the corrosion probes. The ASTM designation of this alloy is SA213-T304 (304SS). The nominal composition of 304SS is given in Table 1. The essential features of the test matrix are given in Table 2.

High-temperature corrosion probe designation -Tube samples of the alloy in a dimension of 1" in outside diameter by 0.94" in length were fabricated and placed in series (Figure 1). The ends of each tube segment were shaped to extrude and concave chamfers at 10° and 45°, respectively. The chamfers allowed multiple segments to be assembled on the corrosion probe with an air-tight seal. A mechanical force was applied to the ends of the probes so that a tight fit could be achieved. Duplicate samples of the alloy were included in the corrosion probes. Type-K thermocouples were attached to one of the tube samples through the inner surface of the probes. The thermocouple junctions were positioned in EDM-drilled holes inside the samples facing the flue gas. Room-temperature compressed air was used to cool the corrosion probes and maintain the metal temperatures. Flow rate of the cooling air was regulated automatically by a controller that responded to the set points of the probe temperatures.

Corrosion rate measurements - The initial weight and initial outer diameter of each tube sample were measured. In addition, the wall thicknesses were carefully measured around the perimeter of each sample at eight points. The points were identified as 12:00, 1:30, 3:00, 4:30, 6:00, 7:30, 9:00, and 10:30 positions, with the 12:00 position being the leading edge facing the flue gas (Figure 2). After fireside corrosion exposure was completed, it was found that metal wastage on the inner surface of the tube samples were negligible, so only outside diameters of the tube samples were measured. All measurements were made in the middle section of the tube samples.

After the corrosion exposure, one of the duplicate samples was chemically cleaned. The chemical cleaning removed the coal ash deposit and scale formed on the sample surfaces during the exposure. After the cleaning, the final weight was again measured. Based on the total weight changes and initial surface areas, the average corrosion rates of the alloy were calculated. The wall thicknesses of the chemically cleaned samples were also measured at the same positions mentioned above. As a result, the corrosion wastage of the tube samples could be determined, which were subsequently used to calculate the local corrosion rates. The corrosion rates for the two high-Cl coals were extrapolated from the 1000-hour test result and reported as mils per year (mpy). Because of equipment difficulty during the low-Cl coal test, the sample was only combusted for 813 hours. The data, however, were again extrapolated and reported in mpy for comparisons with the other coals.

Cross sectional examination - A cross-section was prepared metallograpically from one of the alloy samples after the corrosion exposure. The sample was mounted in Bakelite, cut, and polished dry to preserve any water-soluble compounds that might exist on the alloy surfaces. The ash and scale layers of the sample from each test were examined under an optical microscope and a scanning electron microscope (SEM) equipped with energy dispersive X-ray (EDX) analytical capability. The remaining metal thicknesses of the samples were also determined using a Nikon Microscope at the eight positions as described before.

Results and Discussion

Chemical composition of the three coal samples - Splits of the 20-ton lots of the three coals were analyzed for chlorine, sulfur, and ash content (Table 3). The two high-Cl coals contained medium-

sulfur contents; whereas, the low-Cl Illinois coal contained high-sulfur content. Also, the as-shipped Illinois high-Cl coals had much less ash than did the British high-Cl coal.

Pilot Scale Combustion - Rate of Corrosion

Three long-term, pilot-scale combustion tests were conducted using SA213-T304 (304SS) to evaluate boiler corrosion produced at two specific boiler wall temperatures. The corrosion rate was most pronounced at the 1:30, 3:00, 9:00, and 10:30 positions; in other words 30 to 90° from the leading edge (Figure 2). These measurements were extrapolated to the amount of corrosion in one year or mils per year (mpy).

High-Cl Illinois coal - In general, the corrosion rates at the leading edge (12:00 position) were less than those measured at 30 to 90° away from the leading edge. For example, the corrosion rate of 304SS at 1100°F at the 12:00 position was approximately 40 mpy (not shown), while the greatest corrosion rate between 30 to 90° positions was greater than 100 mpy (shown in Figure 3). Such variation was consistent with the general observation of superheater corrosion in the field. The changes for the corrosion rate with respect to metal temperature at the positions between 30 to 90° are shown in Figure 3. The corrosion rate of 304SS within the temperature range analyzed appeared to show an earlier stage of a bell-shape relationship. It showed increases with increasing metal temperature; and the increases in the corrosion rate were quite significant. For example, the corrosion rate was approximately 120 mpy at 1100°F, and about 260 mpy at 1200°F.

High-Cl British coal - Similarly, the corrosion occurring on the probes at the 30 to 90° locations was more severe than that at the leading edge. The changes of corrosion rate at the positions between 30 to 90° locations with respect to increasing metal temperature are shown in Figure 4. The corrosion rate, similar to what was seen in the test for the high-Cl Illinois coal, increased consistently with increasing metal temperature; and the increases in the corrosion rate were quite significant. The corrosion rate was about 190 mpy at 1100°F, and about 267 mpy at 1200°F

Low-Cl Illinois coal - As usual, the corrosion occurring on the probes at the 30 to 90° locations was more severe than at the leading edge. The changes of corrosion rate between the 30 to 90° positions with respect to increasing metal temperature are shown in Figure 5. Similar to the tests of high-Cl coals, the corrosion rate increased consistently with increasing metal temperature, and the increases in the corrosion rate were quite significant. The corrosion rate was about 120 mpy at 1100°F; and about 250 mpy at 1200°F.

In general, the data showed no correlation between the rate of corrosion and the chlorine content in coal. The results showed a correlation between the rate of corrosion and the metal temperature used. Within the range of the metal temperatures used, a greater corrosion rate was observed at the higher metal temperature. In addition, the corrosion rates observed for the British coal appeared to be slightly greater than those of the two Illinois coals.

Summary and Conclusions

The results of pilot-scale combustion tests showed no correlation between the coal Cl content and rate of corrosion, but showed a correlation of the rate of corrosion with the metal temperature used. The corrosion rate was increased with an increase in the metal temperature during the combustion for all three coals. These data suggested that the different field history of the corrosivity caused by burning high-Cl Illinois coal and high-Cl British coal might have been the result of different superheater/reheater metal temperatures used in the US and UK utility boilers. These data could provide a basis for lifting the limit of burning high chlorine Illinois coals in the utility boilers

Acknowledgment & disclaimer

This study was supported, in part, by grants made possible by U.S. Department of Energy (DOE) Cooperative Agreement Number DEFC22-PC92521, the Illinois Coal Development Board (ICDB), and the Illinois Clean Coal Institute (ICCI). Neither the authors nor any of the subcontractors, nor the U.S. DOE, ISGS, ICDB, ICCI, nor any person acting on behalf of either assumes any liabilities with respect to the use of, or damages resulting from the use of, any information disclosed in this paper. The authors wish to thank Dr. Murray Abbott of CONSOL Inc. Dr. Nigel Paterson of the British Coal Corporation, and Ms. Lisa Duffy and Mr. Charles Smith of Freeman Energy Co. for providing coal samples.

References

ASTM Book of Standards, Vol 5.05 Gaseous Fuels; Coal and Coke, D2361, D3177, D3173, D3174 and D3685, American Standard Testing Materials, 1994.

Chou, M.-I., J.M. Lytle, J.A. Bruinius, S.M. Kung, and K.K. Ho. 1998. Effects of Chlorine in Coal on Boiler Corrosion. Final Report to the Illinois Coal Development Board, Illinois Clean Coal Institute. September1, 1996 - March 31, 1998.

CRE, The CRE Sample Bank: Users Handbook, Gloucestershire, UK, 1993.

Doane E.P., J.A.L. Campbell, and M.F. Abbott, Combustion of High-Chlorine Illinois Basin Coals in Utility Boilers, Proceedings: The Effect of Coal Quality on Power Plants, Fourth International Conference, EPRI, August 1994.

Meadowcroft D.B.and M.I. Manning, Corrosion Resistant Materials for Coal Corrosion Systems, Applied Science Publishers LTD, Essex England, 1983.

Raask, E. in the Mechanism of corrosion by fuel impurities, Butterworths, London, 1963, pp.145-154.

Reid, W.T., External Corrosion and Deposits in Boilers and Gas Turbines, American Elsevier Publishing Company, Inc., New York, pp.138-142, 1971.

Wright, I.G., A.K. Mehta, and K.K. Ho, Survey of the Effects of Coal Chlorine Levels on Fireside Corrosion in Pulverized Coal-Fired Boiler, in postprints of second annual EPRI conference on Effects of Coal Quality on Power Plants, August 17-19, 1994.

Table 1. Partial composition of 304SS superheater alloy in wt%

Element	C	Mn	P	S	Si	Ni	Cr
%	≤0.08	≤2.0	≤0.04	≤0.03	≤0.75	8-11	18-20

The balance of the alloy is Fe.

Table 2. Test matrix for pilot scale stoker boiler combustion

Test	Coal Sample	Metal temperature*
A	High-Cl IL coal	1100°F
B	High-Cl IL coal	1200°F
C	High-Cl British Coal	1100°F
D	High-Cl British Coal	1200°F
E	Low-Cl IL Coal	1100°F
F	Low-Cl IL Coal	1200°F

* Actually, the rate of corrosions were measured for four temperatures within a range from1000 to 1200°F.

Table 3. Total chlorine, total sulfur, and ash content of the three coals.

wt % dry coal basis	High-Cl IL Coal	High-Cl British Coal	Low-Cl IL Coal
Total Chlorine	0.44	0.46	0.14
Total Sulfur	1.22	1.32	4.48
Ash	7.90	23.56	9.38

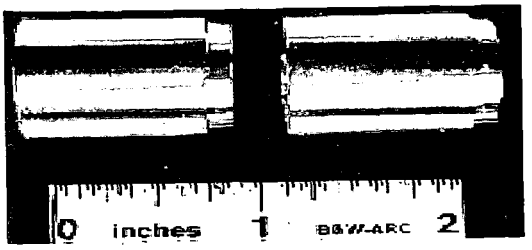

Figure 1: Arrangement of the chamfered tube segments on the corrosion probe

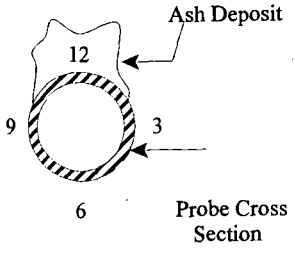

Figure 2. Illustration of the probe cross section, the leading edge (12:00 position), and the 30° to 90° area away from the leading edge for corrosion rate measurement

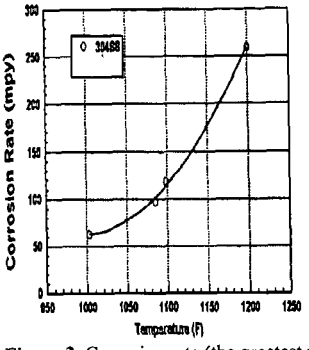

Figure 3. Corrosion rate (the greatest value) versus temperature at the positions between 30° and 90° for the test burning the high-Cl Illinois coal.

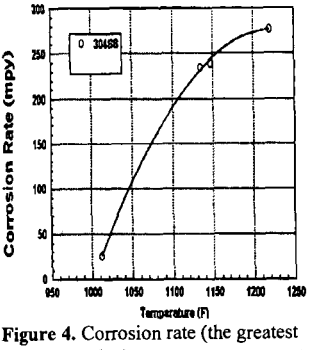

Figure 4. Corrosion rate (the greatest value) versus temperature at the positions between 30° and 90° for the test burning the high-Cl British coal.

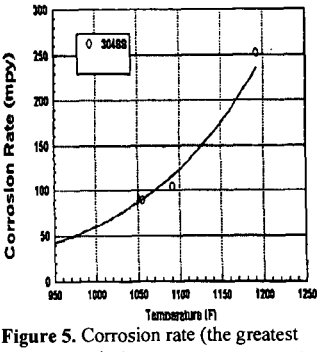

Figure 5. Corrosion rate (the greatest value) versus temperature at the positions between 30° and 90° for the test burning the low-Cl Illinois coal.

QUANTITATIVE EVALUATION OF SULFUR TYPES IN MIDDLE DISTILLATES

Y. Briker, P. Rahimi, A. Iacchelli, Z. Ring and C. Fairbridge
National Centre for Upgrading Technology, 1Oil Patch Drive,Suite A202, DEVON, Alberta T9G 1A8, Canada
R. Malhotra
SRI International, 333 Ravanswood Avenue, Menlo Park, CA 94025

KEYWORDS: sulphur determination in fuels, field ionization mass spectrometry, hydrocarbon type analysis

ABSTRACT

The utilization of fossil fuels in the transportation sector is changing. Due to increasing environmental constrains it is anticipated that changes in transportation fuel specification will be required. It will be necessary to improve diesel fuel quality to address the problems of emission from diesel powered vehicles. A trend in the transportation fuel production indicates an increase of the proportion of diesel fuel produced from oil sands and heavy crude oil. The relatively poor ignition quality of this middle distillate puts pressure on the petroleum industry to produce fuel that is more environmentally clean and yet economically feasible. In the future, knowing which of fuels' physical and chemical properties influence engine exhaust emissions will become very important. Currently, there are several mass spectrometry techniques that can determine the hydrocarbon type composition of diesel fuels. This paper will discuss the results of hydrocarbon type analyses obtained for middle distillate sample by using HVLREI GC-MSD (high voltage low resolution electron impact mass spectrometry) and GC-FIMS (Field Ionization Mass Spectrometry). Comparison of aromatic sulfur types, such as di- and benzothiophenes, calculated by mass spectrometry methods and by GC-FID/SCD (Sulfur Chemiluminescent Detector) will be discussed.

INTRODUCTION

There are few standardized methods available based on high voltage low resolution electron impact mass spectrometry to perform detailed analyses of complex petroleum mixtures. For fractions boiling in the naphtha range, the ASTM 2789 method is used. For hydrocarbon distillates boiling above the naphtha range, prior chromatographic separation is usually required in order to avoid interference between saturate and aromatic types. The saturate fraction can be analyzed by the ASTM 2786 methods and the aromatic fraction, by the ASTM 3239 method for petroleum fractions boiling within the range from 205 to 540 °C. For fractions boiling within the diesel range (177 to 343°C),the ASTM 2425 method is applied. The Robinson method offers a one-step analysis that does not require the separation into saturate and aromatic fractions. The method, developed by C. J. Robinson in 1971(1), covers the full boiling range and resolves up to 4 saturate and 21 aromatic compound types including 3 thiophenoaromatic types (assuming no olefins are present in the sample).

There is also a GC-FIMS method that identifies the composition of liquid fuel by compound type (z-values) and molecular size (2). The method, developed at SRI, is based on replacing the electron-impact ionizer of an HP GC-MSD system with the SRI volcano-style field ionizer. For most compounds, field ionization produces only the molecular ion. Analysis by FIMS expresses the data as z-series tables giving the composition by compound type (z-values) and molecular size (number of carbon atoms).

This work is a continuation of the GC-FIMS application for compositional analysis of transportation fuels (3). We analyzed light cycle oil (LCO) by GC-MSD and by GC-FIMS for hydrocarbon type composition and found some pronounced differences, especially in the saturate types. The distribution of aromatic types was identical. In order to evaluate the methods, we analyzed one of the samples by GC/FID/SCD(sulfur chemiluminescence detector) in order to quantify the thiophenoaromatic types present in the sample. We compared these results with those obtained by mass spectrometry methods.

EXPERIMENTAL

Initially, the fuel sample was analyzed by GC-MSD and the hydrocarbon types were calculated using the Robinson method. The sample was then separated into saturate, aromatic and polar fractions using a liquid chromatographic procedure, which was a modified ASTM D2007 method (4). The saturate and aromatic fractions were analyzed separately by both, GC-MSD and by GC-FIMS. The aromatic fraction composition was calculated by ASTM D3239, and the saturate fraction composition was calculated by ASTM D2786. The computer programs for calculation of hydrocarbon types were written by R. Teeter (5) based on modification of the original methods and supplied by PSMASPEC, USA.

For GC-MSD runs, a Hewlett Packard GC-MS with HP 5972 MSD, HP 7673 GC/SFC injector and HP 5890 GC was used. The column was a 30m x 0.25mm x 0.25μm High

Resolution GC Column J122-5532 DB-5MS. The oven was held at 35°C for 3 min and was then heated at 10°C/min to 280°C. The MSD temperature was 280°C. The cool on-column injection technique was employed with helium as the carrier gas at a constant flow rate of 1.2 ml/min.

For the GC-FIMS runs, a 30-m x 0.25mm x 0.25µm HP1-MS non-bonded column was used. The injection (0.2µl; 19:1 split) was made with the oven at 45°C. The oven was heated at 17°C/min to 300°C. Sulphur determination was performed using Hewlett Packard gas chromatograph HP6890 series equipped with cool on-column injector and nonaliter adapter, FID/SCD detector (Sulphur Chemiluminescence Detector) SIEVERS 355. The HP 19091Z-213, HP-1 Methyl siloxane (30.0m x 320.00µm x 1.00µm) column with the injection volume of 0.5µl was used. The total sulphur content was calculated by using the response factor determined from running the sulphur standard with the known sulphur concentration. For aromatic sulfur speciation, the standards benzothiophene and dibenzothiophene were analyzed. Knowing the retention time for both compounds, the baseline integration was performed separately for benzothiophenes and dibenzothiophenes on the sample chromatogram. Then, each of the sulfur groups was calculated knowing the response factor and assuming the average molecular weight 190 Da for benzothiophenes and 220 Da for dibenzothiophenes. The calculated result was confirmed with the result obtained by using the standard method for sulfur determination such as: ASTM D4294 (Sulfur in Petroleum Products by Energy-Dispersive X-Ray Fluorescence Spectroscopy).

RESULTS AND DISCUSSION

HYDROCARBON TYPES

The GC-MSD and GC-FIMS results are presented in Table1. The results for separated fractions are presented together with the Robinson results for the total sample. The hydrocarbon type composition of fuels analyzed by GC-FIMS is usually presented as a z-series. All the numbers in a z-table (Table 2) are given as sums of the weight fractions from C_1 to C_{20} for z-numbers from -2 to -14. The elemental formula of any hydrocarbon can be generally expressed as C_nH_{2n+z}, where z is a measure of the unsaturation index. All acyclic alkanes have the general formula of C_nH_{2n+2} (i.e., z-value of +2), and monocyclic alkanes have the general formula of C_nH_{2n} (i.e., a z-value of 0). The z-value decreases by 2 for every degree of unsaturation (ring or double bond). Since the fractions were analyzed separately, it was possible to identify all the saturate types and some of the aromatic types without any interference.

In Table 1, each saturate type in the GC-FIMS column corresponds to a z-series number given in Table 2 for the saturate fraction. It is quite noticeable that the saturate region mainly covers the intensities in z series from +2 to –4, that is from paraffins to tricyclic alkanes. The aromatic region covers mainly the intensities in z series from –6 to –14 corresponding to alkylbenzenes up to naphthocycloalkanes. Some of the peaks detected with z <-6 in the saturate fraction could be attributed to some aromatic impurities due an incomplete separation. The numbers in Table 1 suggest that in this case those impurities are negligible. For the aromatic fraction, the masses detected in the saturate region are also minor and could be due to a small amount of saturates, such as tricycloalkanes, that are left behind after saturate separation and later coeluted with the aromatics.

In Table 1, there are three columns for the results from GC-FIMS analysis. The first column is a direct translation of a z-table into hydrocarbon types. First, comparison of the aromatic types obtained by GC-MSD and FIMS suggested that there was a difference in the polyaromatic types. FIMS showed results about 10% higher for the total mono- and diaromatics. The difference in alkylbenzenes was 11%, in naphthalenes, 17%. Tri- and tetraaromatics were not calculated by FIMS, while they were 9.0% and 2.9% by ASTM D3239. These differences could be explained by the fact that because of the limited number of samples analyzed by GC-FIMS, the response factors for various series have not yet been optimized. Furthermore, at this stage of development, FIMS only calculates the hydrocarbon types for lighter material.

However, by analyzing the SICs (single ion chromatograms) from the GC-FIMS analysis of LCO, compounds such as fluorenes (z-16), phenanthrenes (z-18), phenanthrocycloalkanes (z-20) and pyrenes (z-22) were found in the spectra. In order to avoid a discrepancy between the actual spectra and the results of a z-table, it was assumed that the amount of phenanthrenes, fluorenes and pyrenes calculated by FIMS would be very close to the ones calculated by other MS methods. According to data in Table 1, there was no significant difference between the aromatic types obtained by ASTM D3239 and the Robinson method. The aromatic compounds tend not to fragment too much when analyzed by both techniques and there is reason to believe that the analysis by FIMS would produce a similar distribution. The amount assumed for phenanthrenes was 9.0%, for fluorenes , 5.0%, and for pyrenes, 3.0% (average from ASTM3239 and Robinson results). Recalculated results are presented in the second column of FIMS analysis (Table 1). Now the comparison was much better with the results from other GC-MS methods with the exception of alkylbenzenes and naphthalenes. These are the groups that overlap with the aromatic sulfur types.

In order to compare two different MS methods, we had to compare results for all hydrocarbon types. When the Robinson and ASTM 2786 methods were compared, the total

amount of cycloparaffins was in a good agreement, however, there were differences within the cycloparaffinic types and between straight chain paraffins. The values for normal paraffins and polycycloparaffins calculated by ASTM 2786 were higher than the corresponding values calculated by the Robinson method while the order was reversed for monocycloparaffins. For samples where the saturates content is high and cycloparaffin content is high, these differences could be much more profound. There is a method, INT 101 (6), that overcomes the discrepancies of the Robinson method, however it still does not answer the question of true saturates distributions. Comparison of saturates distribution measured by the GC-FIMS and GC-MSD also could not answer this question.

If field ionization produced only the molecular ions, then it could be assumed that the results obtained by GC-FIMS would reflect the true distributions. Consequently, the results in Table 1, obtained by the electron impact GC-MSD, especially for the cycloparaffins, would be greatly underestimated. However, at this point the results obtained by FIMS for the saturate fraction do not quite reflect the compound distribution. The isoparaffins tend to fragment and do not produce the molecular ion. They can not be accounted for in the calculation and therefore lower the amount of the calculated total paraffins. It will be our future task to determine the proper response factors for various paraffin mixtures and adjust the calculation. At this point the methods could be evaluated based on aromatics distribution. We looked particularly at the aromatic sulfur distribution and compared it with the results determined by another method rather then mass spectrometry.

As mentioned before, the aromatics distributions for the sample were identical except for the overlapping species in FIMS results. The numbers with the asterisk (Table 1) present the sums of intensities for a particular z-series that have interference within the series, such as alkylbenzenes with benzothiophenes and naphthalenes with dibenzothiophenes. We were able to calculate the values for benzothiophenes and dibenzothiophenes. The calculation was performed by setting the separate time windows for the sulfur and the hydrocarbon types. It was possible since the two species were separated by GC prior to being analyzed by FIMS.

The nominal mass of dibenzothiophene is 184 Da, which is the same as that of a C_4-naphthalene. Figure 1 shows the selected ion chromatograms (SICs) for m/z 184, 198, 212, 226, 240 and 254 extracted from the TIC of MD2-aromatics. The C_4-naphthalenes (m/z 184) elute between 9.4 and 10.6 min. The cluster of peaks due to C_4-naphthalenes is followed by a strong peak at 10.8 min., which is due to dibenzothiophene. The control run of dibenzothiophene is shown in Figure 2. The SIC of mass 198 in Figure 1 shows a similar pattern as that found for m/z 184. Here, the alkylnaphthalenes are between 9.2 and 11.2 min., and the isomeric methyldibenzothiophenes are between 11.3 and 12.4 min. The pattern is repeated for the SICs of other masses up to mass 268. Integration was performed for the dibenzothiophene portion of the SIC for every extracted mass. The integrated area was related to the total area of the SIC. The ratio then was multiplied by a corresponding mass percent taken from a z-table in order to calculate the dibenzothiophene portion (assuming the response factors being the same for both compound types). The same exercise was performed for benzothiophenes (the SICs for m/z 134, 148, 162, 176, 190 and 204 were extracted). The integration was done for benzothiophenes with m/z up to 232.

LCO was analyzed also by another technique, GC/SCD (gas chromatograph/ sulfur chemiluminescence detector). The GC/SCD chromatogram of this run is presented in Figure 3(a). The chromatograms of benzothiophene (retention time 19.520 min.) and dibenzothiophene (retention time 32.686 min.) standards are presented in Figures 3(b) and 3(c) respectively. The total sulfur was calculated using the total area and the factor as was explained earlier. The sulfur obtained by this method was 1.38wt.%. This number was verified by the ASTM 4294 method (Dispersive x-Ray Fluorescence Spectroscopy) which reported sulfur of 1.45wt.%. Knowing the retention time for benzothiophene and dibenzothiophene, part of the chromatogram was integrated between 19.52 and the beginning of peak at 32.686 min. for benzothiophenes, and between start of peak at 32.686min to the end for dibenzothiophenes. The calculation was performed according to a procedure described above. The results of sulfur determination are summerized in Table 3.

Total sulfur determined by GC/SCD was in a good agreement with the result from ASTM 4294. The result obtained by the GC- FIMS was the closest to the SCD result, especially in terms of distribution between di- and benzothiophenes. This comparison favors the GC-FIMS method for calculation of other hydrocarbon types in fuels with a high degree of accuracy provided that the response factors for the paraffins would be adjusted.

CONCLUSION

The results presented in this paper demonstrate the ability of various GC-MS methods to provide rapid and detailed group-type analysis of middle distillates. Analysis of data from each method suggests a discrepancy, particularly for saturates distribution, between the Robinson method for unseparated sample and between ASTM D2786 and ASTM D3239 for separated fractions. The difference was even greater when these results were compared with GC-FIMS

results. Comparison of di- and benzothiophenes content in one of the samples calculated by different methods indicates that analysis by GC-FIMS may offer more reliable distribution of hydrocarbon types compared to the other two methods, provided that the results would be corrected for the isoparaffins fragmentation. The GC-FIMS combination allowed the overlapping species in the same z-series to be separated by time and thus accurately calculated. By creating separate time windows for the GC-separated species and determining their response factors it could be possible to analyze the samples having a full boiling range without prior separation.

REFERENCES

1. C. J. Robinson, *Anal. Chem.*, **1971**, 43, 1425.
2. R. Malhotra, M. J. Coggiola, S.E. Young, C.A. Spindt, "*Analysis of Transportation Fuels", AM Chem. Soc., Div. Petr. Chem., Preprints*, **1996**, 41(4), 652.
3. R. Malhotra, M. J. Coggiola, S.E. Young, S. Hsu Chang, J.Dechert, Exxon, P. M. Rahimi, Y. Briker, "*Rapid Detailed Analysis of Diesel Fuels by GC-FIMS*", AM Chem. Soc., Div. Petr. Chem., Preprints, **1998**.
4. Y, Briker, P.Rahimi, N.Mclean, A. Iacccelli, Z. Ring, and C. Fairbridge, "*Process Modeling: Development of a Procedure for the Distribution of GC-MS Hydrocarbon Type Characterization by Boiling Point*", NCUT Report 98-09.
5. Richard M. Teeter, "*Software for calculation of hydrocarbon types*", PCMASPEC, 1925 Cactus Court, #2, Walnut Creek, CA 94595-2505, USA.
6. C. Pachego and M. Hazos, INTEVEP, S.A., "*Aromatic and Saturate Analysis by Low Resolution Mass Spectrometry*", AM Chem. Soc., Div. Petr. Chem., Preprints, August 23-28, 1992.

Table 1 – Comparison of hydrocarbon type analyses results for Light Cycle Oil by different GC-MS methods

Hydrocarbon CnH2n+Z	Z No.	Robinson Total	ASTM 2786 Saturates	ASTM 3239 Aromat.	GC-FIMS Saturates	GC-FIMS Aromat.1	GC-FIMS Aromat.2	GC-FIMS Aromat.3
SATURATES		**21.90**	**22.70**		**22.70**			
Paraffins	2	11.90	12.40		5.96			
Cycloparaffins		**10.00**	**10.30**		**16.74**			
Monocycloparaffins	0	6.40	4.10		7.92			
Dicycloparaffins	-2	3.60	2.50		1.76			
Polycycloparaffins	-4	0.00	3.70		7.06			
AROMATICS		**78.10**		**73.70**		**73.70**	**73.70**	**73.70**
Monoaromatics		**21.50**		**20.40**		**29.70***	**22.90***	**19.60**
Alkylbenzenes	-6	9.50		8.60		21.10*	16.20*	12.90
Benzocycloalkanes	-8	9.70		9.60		7.10	5.50	5.50
Benzodicycloalkanes	-10	2.30		2.20		1.50	1.20	1.20
Diaromatics		**35.20**		**33.40**		**44.00**	**38.80***	**32.30**
Naphthalenes	-12	21.20		21.30		38.80*	29.80*	23.30
Naphthocycloalkanes	-14	7.60		6.80		5.20	4.00	4.00
Fluorenes	-16	6.30		5.30		0.00	5.00	5.00
Triaromatics		**10.70**		**9.00**		**0.00**	**9.00**	**9.00**
Phenanthrenes	-18	9.10		7.80		0.00	7.80	7.80
Phenanthrocycloalkanes	-20	1.60		1.20		0.00	1.20	1.20
Tetraaromatics		**3.30**		**2.90**		**0.00**	**3.00**	**3.00**
Pyrenes/Benzofluorenes	-22	2.70		2.60		0.00	3.00	3.00
Chrysenes	-24	0.50		0.30		0.00	0.00	0.00
Pentaaromatics		**0.00**		**0.20**		**0.00**	**0.00**	**0.00**
Chrysocycloalkanes	-26	0.00		0.20		0.00	0.00	0.00
Benzpyrenes/Perylenes	-28	0.00		0.00		0.00	0.00	0.00
Dibenzanthracenes	-30	0.00		0.00		0.00	0.00	0.00
Unidentified		**0.00**		**0.00**		**0.00**	**0.00**	**0.00**
CnH2n-32/CnH2n-46	-32	0.00		0.00		0.00	0.00	0.00
CnH2n-36/CnH2n-26S	-36	0.00		0.00		0.00	0.00	0.00
CnH2n-38/CnH2n-28S	-38	0.00		0.00		0.00	0.00	0.00
CnH2n-42/CnH2n-32S	-42	0.00		0.00		0.00	0.00	0.00
CnH2n-44/CnH2n-34S	-44	0.00		0.00		0.00	0.00	0.00
Aromatic Sulfur		**7.50**		**7.80**		**0.00**	**0.00**	**9.80**
Benzothiophenes	-10S	3.40		3.60		0.00	0.00	3.30
Dibenzothiophenes	-16S	3.90		4.00		0.00	0.00	6.50
Benzonaphthothiophenes	-22S	0.20		0.20		0.00	0.00	0.00

Arom.1- Original data from z-table
Arom.2- Data adjusted for polyaromatics
Arom.3- Data adjusted for aromatic sulfur

Table 2 - FIMS results for saturate and aromatic fractions of LCO by z-series

Sample ID	2	0	-2	-4	-6	-8	-10	-12	-14	
Aromatics(%of Ar.)	0.02	0.08	0.05	0.12	28.65	9.61	2.03	52.72	6.72	100.00
Aromatics(%of Total)	0.01	0.05	0.04	0.09	21.10	7.07	1.50	38.84	5.00	73.70
Aromatics(%of Ar.)*	0.01	0.06	0.04	0.09	22.06	7.40	1.57	40.60	5.17	77.00
Aromatics(%of Total)*	0.01	0.03	0.03	0.06	16.25	5.45	1.16	29.91	3.80	56.70
Saturates(%of Sat.)	26.28	34.92	7.82	24.04	0.42	2.89	3.34	0.35	0.16	100.24
Saturates(%of Total)	5.96	7.92	1.76	5.45	0.10	0.64	0.75	0.08	0.04	22.70

* - Results are recalculated for the presence of fluorenes, phenanthrenes and pyrenes

Table 3 – Aromatic sulfur types determined by different methods

Aromatic sulfur types Wt.% of total	ASTM 4294	GC-SCD	GC-FIMS	GC-MS ASTM D3239	GC-MS Robinson
Benzothiophenes	-	2.7	3.3	3.6	3.4
Dibenzothiophenes	-	6.0	6.5	4.0	3.9
Naphthobenzothiophenes	-	N/D	N/D	0.2	0.2
Total aromatic sulfur	-	8.7	9.8	7.8	7.5
Total sulfur	1.45	1.38	1.50	1.19	1.14

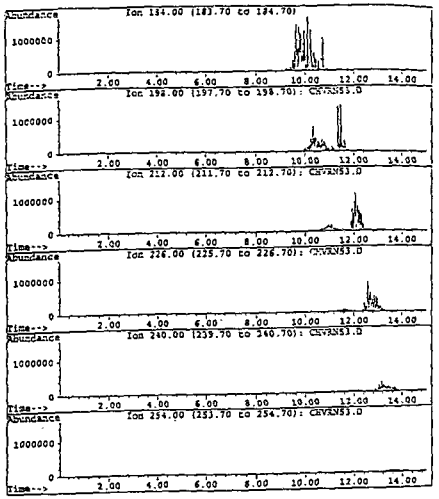

Figure 1. Selected Ion Chromatogram of m/z 184,198,212,226,240,254 Extracted from GC-FIMS analysis of LCO

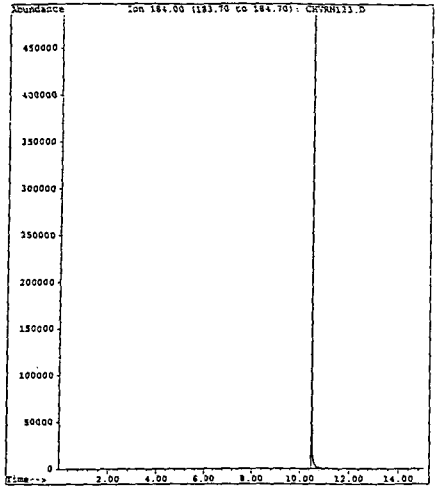

Figure 2. Selected Ion Chromatogram of m/z 184 extracted from GC-FIMS Analysis of dibenzothiophene

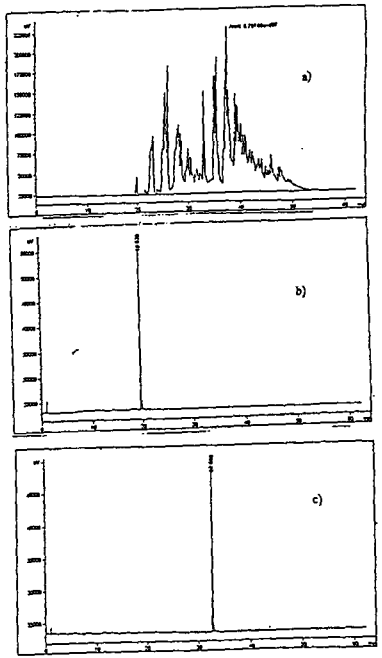

Figure 3. GC-FID/SCD chromatogram of LCO
a) GC-FID/SCD chromatogram of the total sample
b) GC-FID/SCD chromatogram of benzothiophene
c) GC-FID/SCD chromatogram of dibenzothiophene

BENCH SCALE CO-PYROLYSIS OF A LOW RANK COAL AND A PETROLEUM RESIDUE

I.Suelves, R.Moliner and M.J.Lázaro
Instituto de Carboquímica (CSIC). María de Luna, 12. 50015 Zaragoza (Spain)

INTRODUCTION

During coal pyrolysis, both degradation processes that create free radicals and crosslinking reactions, happen simultaneously. To increase the liquid yields obtained from coal pyrolysis radical stabilisation should be promoted and crosslinking reactions should be decreased[1-3]. However, coal hydrogen content is not high enough to promote this radical stabilisation and so that, hydrogen should be provided from other sources. One of the most promising ways of increasing the hydrogen content is provide it from hydrocarbon materials, specially hydrocarbon wastes that can be co-pyrolyzed with coal[4-7]. This way two benefits are expected: first coal may enhance the conversion of the hydrocarbon material and beside this the presence of the waste would improve the quality of the products obtained from coal. Petroleum residue is a very interesting material that observes the main characteristics needed to be used in this type of processes: hydrogen content, aliphatic nature, etc. However, there are few references in literature on this subject because the most important works on co-utilization of coal and petroleum residues are related with catalytic coprocessing reactions, using high hydrogen pressures. In our previous works at analytical scale we have shown that there is a synergetic effect for the production of some interesting compounds like light olefins and BTX when coal and petroleum residue are co-pyrolyzed[8,9]. Therefore at this scale, secondary reaetions were disfavoured and there was no possibility of stabilising mass balances or evaluating the influence of co-pyrolysis on char formation. For that reasons, the main objectives of this work are: (i) to evaluate the interactions between coal and petroleum residue during co-pyrolysis at bench scale and (ii) to study the influence of the experimental conditions on char formation.

EXPERIMENTAL

Different experimental series were carried out, each of them dedicated to the study of the influence of temperature, pressure and petroleum residue mass ratio on the mixture behaviour. Temperatures used were 600, 650 and 700ºC; pressures, 0.1, 0.5 and 1MPa and mass ratio (Coal/PR) 70/30 and 50/50.

Materials

Samca coal (Teruel, Spain) and a petroleum vacuum residue (PR) have been used in this work. Samca is a subbituminous coal with high volatile content and with high sulphur and oxygen content. The petroleum residue proceeds from the distillation of different crudes and has been submitted by REPSOL (Puertollano, Spain). The main characteristics of these materials have been described in our previous works [8,9].

Experimental installation

Bench scale pyrolysis unit used in this work has been shown elsewhere[10]. In summary it consists of an oven heated reactor with two different parts; the bottom of the reactor, where pyrolysis happens, is filled with a ceramic rings bed. The sample is feeded from the upper part and falls into the reactor by gravity. When the sample is introduced, the reactor has reached the pressure and temperature conditions of the pyrolysis run. Pyrolysis products are recovered from the bottom of the reactor sweeped by a nitrogen stream. They are cooled in a Peltier effect cooler. Liquids are collected in a liquid-cyclone and gases are collected in a gas sampling bag which volume is measured after each run.

Sample preparation

First coal and PR were pyrolyzed alone and then as a mixture. Preparation of the mixtures was as follows: PR was first solved in THF and then coal was added. The mixtures were subsequently sonicated. After 15 minutes, THF was evaporated by heating under vacuum. The dried samples were grounded to <0.2 mm. A cryogenic grounding technique was used in order to increase the grindibility of the sample and to improve the homogeneity of the mixtures. Samples of around 10g were used in each run

Analytical Methods

The ponderal yields of char and liquids were determined by direct weight whereas gas global-yields were calculated from the sum of the individual yields of each of the components obtained by gas-chromatography. A run was considered as a valid one if the ponderal yield sum of all recovered products was higher than 95%. Global results were normalised to 100% in order to facilitate comparison between runs.

Gases were analysed by gas chromatography using three separate analytical methods: a packed column of Molecularsieve 13X with nitrogen as carrier gas and TCD detection for hydrogen; two packed columns: Molecularsieve 13X and Porapak with helium as carrier and TCD

detection for permanent gases; an alumina capillar column with helium as carrier and FID detection for C_1-C_6 hydrocarbons. Hydrocarbons chromatographied between n-pentane and n-hexane were accounted for together as C_5. In the same way, compounds chromatographied between n-hexane and benzene were accounted for as C_6.Quantification of gas components was carried out by means of standard gas mixtures.

Liquids were formed by the organic phase, tar and water. The separation of tar and water was very difficult, so that they were weighed all together. Liquids were analysed by GC/MS. All compounds present in liquids were identified by using a computerised library of mass spectra. Tri and tetramethylbenzenes were accounted for as "alkyl-benzene" and all the compounds chromatographied between naphthalene and phenanthrene were accounted for as "2-3 rings". Quantitative composition of liquids was determined by the internal standard method using octane as the internal standard.

RESULTS AND DISCUSSION

If there is no interaction between the components of the mixture, the yields obtained in the co-pyrolysis (experimental values) should be equal to the sum of yields obtained in the pyrolysis of the individual components (theoretical values). In this way, by comparing experimental and theoretical values, the existence of a synergetic effect in the yields of the most interesting pyrolysis products and the influence of the experimental conditions have been evaluated. First the evolution of the char, liquid and gases yields as a whole was studied and after that, the yields of the most interesting gaseous products and the evolution of the liquid fraction was evaluated.

Evolution of synergism with temperature

The 70/30 mixture was copyrolyzed at 600, 650 and 700ºC. At 600ºC the experimental char yield is higher than the theoretical one and there is an experimental decrease on liquid and gases production compared with the theoretical one. Analysing the evolution of the individual products only a higher experimental yield is observed for CO_2, SH_2 and methane. This fact can be related with the enhancing of cross-linking reactions that favour the evolution of this kind of gases as a by-product of char formation[11,12]. At 700ºC although there is a better liquid production than working at 600ºC and even the experimental yields of some interesting gaseous products are higher than the theoretical ones, the experimental char production is also very high.

Figure 1 show the comparison between the experimental and theoretical yields obtained working at 650ºC. It can be observed from this figure that the theoretical and experimental char yields are almost equal and that the experimental liquids yield increase in detriment of the gases one after the co-pyrolysis of the mixture. The comparison between the experimental and theoretical yields of the individual components of the gas fraction shows that there is a decrease in the experimental yield of carbon oxides and SH_2 and that on the other hand, the experimental yields for light olefins: ethylene, propylene and C_4 olefins are higher than the theoretical ones and so that, a favourable synergetic effect is observed. At 650ºC there is also an important synergetic effect for the production of all aromatic compounds, specially for benzene derivatives.

During pyrolysis of hydrocarbon nature materials[1,13] two types of reactions are suggested: first degradative processes that produce small radicals and then recombinative reactions were this small radicals take part. When secondary reactions happen via Diels-Alder, aromatic compounds are obtained. This seems to be a good explanation for 70/30 mixture behaviour: first PR is degraded and due to its high aliphatic fraction[1] it leads to a great ethylene and other light olefins production. Then the ethylene radical reacts in gas phase with the small radicals obtained from coal and so that, BTX experimental production increases. In summary it can be concluded that the main objectives of this work are achieved, working with mixtures in a mass ratio of 70/30 at 0.1MPa and 650ºC.

Evolution of synergism with pressure

All runs studying the evolution of yields with pressure were carried out at 650ºC. The good results obtained working at atmospheric pressure and 650ºC do not occur when pressure increases. There are no important differences between working at 0.5 or 1MPa. Figure 2 shows the comparison between the theoretical and the experimental yields obtained at 1MPa. The experimental char yield is higher than the theoretical one, in detriment of gases and liquids yields. The evolution of the individual components of the gas phase shows that there is no synergetic effect for any of the interesting compounds. Moreover this, working at high pressure the liquid fraction could not be evaluated. The liquids obtained have very high water content and solid suspensions and for that reason they could not be chromatographied. So, increasing pressure seems to disfavour gas phase reactions, probably because intraparticle reactions that lead to an increase on char yield[14] are enhanced.

Evolution of synergism with petroleum ratio in the mixture

Figure 3 shows the comparison between the theoretical and the experimental yields obtained for the 50/50 mixture working at 0.1MPa and 650ºC. It can be observed an important increase in the experimental char yield comparing with the theoretical values which contrast with the similar experimental and theoretical values obtained for the 70/30 mixture. There is also a slight

experimental increase for the production of CO_2, SH_2, methane and ethylene but the most important fact that should be taken into account is the bad results obtained for the liquid fraction. The only synergetic effect happens for the higher weight aromatic compounds. For benzene, toluene, xylene and alkyl-benzenes, the theoretical yields are higher than the experimental ones. From these results it can be concluded that the increase in the petroleum residue ratio in the mixture disfavours tar forming reactions while enhances char formation. One of the suggested explanations for the behaviour of the 50/50 mixture is that although PR degradation occurs, when PR mass ratio in the mixture increases, the formed radicals can not react with the radicals emerging from coal and this way secondary reactions in gas phase that lead to the BTX formation are not allowed, and only intraparticle reactions that increase char formation are enhanced. A more detailed study of these processes and probably the analysis of the nature of chars obtained would provide enough information to consolidate the present explanation.

REFERENCES

1. Ofosu-Asante K., Stock L.M, Zabransky R.F. (1989). Fuel. Vol.68, 567-572.
2. Hayashi J., Kawakami T., Taniguchi T., Kusakabe K., Morooka S. (1993). Energy&Fuels, 7, 1118-1122.
3. Miura K., Mae K., Asaoka S., Hashimoto K.(1991). Energy&Fuels, 5, 340-346.
4. Fontana A., Braekman-Danheux C., Laurent P. (1995). "Coal Science and Technology 24".(Elsevier. J.A. Pajares, J.M.D. Tascón Eds.) pp 1089-1092.
5. Laurent P., Braekman-Danheux C., Fontana A., Lecharlier M. (1997). ICCS 97. Vol II. (Ziegler et al Eds.), 837-840.
6. Palmer S.R., Hippo E.J., Tandon D., Blankenship M. (1995). "Coal Science and Technology 24".(Elsevier. J.A. Pajares, J.M.D. Tascón Eds.) 29-33.
7. Klose W., Stuke V. (1993). Fuel Processing Technology, 36, 283-289.
8. Moliner R., Suelves I., Lázaro M.J. (1998). Energy&Fuels. Vol.12, N°5, 963-968.
9. Suelves I., Lázaro M.J., Moliner R.(1997) ICCS 97. Vol. II 745-748 (Ziegler et al Eds.)
10. Moliner R., Lázaro M., Suelves I. (1997). Energy&Fuels. Vol.11, N°6, 1165-1170.
11. Ibarra J.V., Cervero I.,García M., Moliner R.(1990). Fuel Processing Technology, 24, 19-25.
12. Suuberg E.M., Lee D., Larsen J.W.(1985). Fuel. Vol.64, 1668-1671.
13. Moliner R. (1995). Final Report Project CECA 7220-EC/763.
14. Moliner R., Ibarra J.V., Lázaro M.J. (1994). Fuel. Vol.73, n°7, 1214-1220.

Figure 1. Experimental and theoretical yields: Samca/RP (70/30). P=0.1MPa. T=650ºC.
A) Mass balance

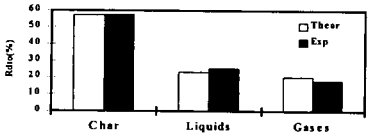

B) Gases

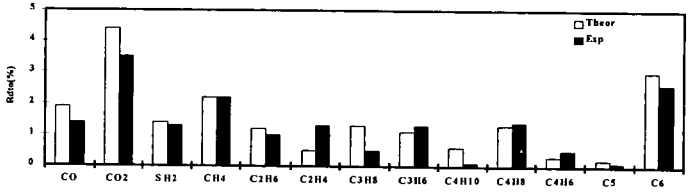

C) Liquids

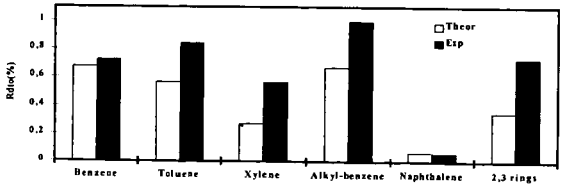

Figure 2. Experimental and theoretical yields: Samca/RP (70/30). P=1MPa. T=650°C.
A) Mass balance

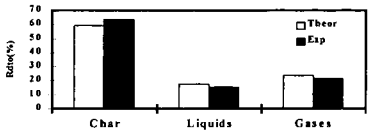

B) Gases

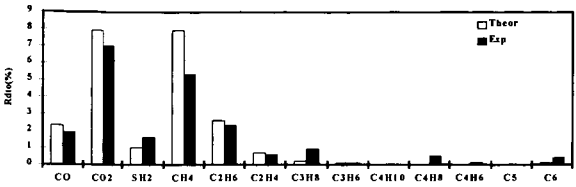

Figure 3. Experimental and theoretical yields: Samca/RP (50/50). P=0.1MPa. T=650°C.
A) Mass balance

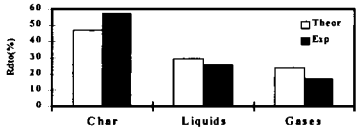

B) Gases

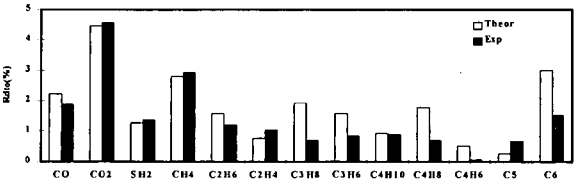

C) Liquids

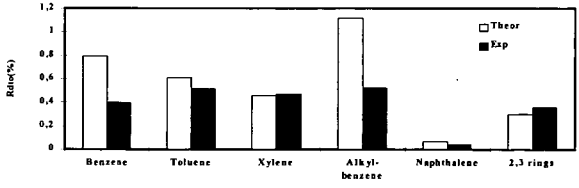

THERMAL CRACKING PROPERTY OF MARLIM VACUUM RESIDUE

Teruo Kondo[1], Shinya Sato[1], Akimitsu Matsumura[1], Ikuo Saito[1]
Albertino Machdo de Carvlho[2], Wladimr Ferraz de Souza[2]

[1]National Institute for Resources and Environment
16-3 Onogawa, Tsukuba, Ibaraki, 305-8569 Japan

[2]PETROBRAS Research and Development Center
Cidade Universitaria Quadra 7 s/n CEP 21949-900
Rio de Janeiro, Brazil

Keywords : Marlim residue, Thermal cracking, coking, asphaltene structure

INTRODUCTION

The world-wide demand for transportation fuels and light fraction oils is expected to increase steadily, while the world supply crude has become rather heavier. Therefore, development of the upgrading technology of heavy oils is very important. However, upgrading of heavy oils is generally very difficult because of serious problems such as coke formation and catalyst deactivation. These problems are mainly caused by asphaltene in heavier oil. In catalytic hydrocracking of heavy oils, asphaltenes are known to be the most refractory. It is profitable for the progress of upgrading of heavy oils such as vacuum residue to understand the reaction behavior of asphaltene cracking. Many investigators provide ample information about pathways, kinetics and coke formation mechanism in the thermal cracking of asphaltenes or residues[1-9]. The purpose of this study is to clarify thermal cracking behavior of Brazilian Marlim vacuum residue, its asphaltene and deasphalted oil. Marlim crude is Brazil off-shore of large scale reservoir and a typical heavy oil. The vacuum residue in Marlim crude is as many as 30-33% and has high asphaltene contents.

EXPERIMENTAL

Feed materials used in this study were Marlim vacuum residue(MLVR) and the asphaltene (MLVR-AS) and the deasphalted oil (MLVR-DAO) obtained from MLVR. MLVR-AS was precipitated with excess of n-heptane (40:1), stirred for 24 hours and separated with a centrifuge. Finally, the asphaltene was dried under vacuum at 50°C, for 24 hours. MLVR-DAO was obtained from n-heptane solubles by removing n-heptane with evaporator.

A 110 ml batch autoclave with magnetic stirrer was used in the thermal cracking. An autoclave was loaded with 3 g of feed and 15 g of decalin as solvent and pressurized to 1 MPa of nitrogen gas and heated up to the reaction temperature(400-440°C) at 10°C/min. After holding at reaction temperature for the desired time(0-90 min), the autoclave was cooled down to room temperature and gases were vented off and analyzed by gas chromatography. The reaction products in the autoclave were separated into the oil and the solid products by suction filtration.The solid product was extracted with toluene using ultra sonic. Toluene insoluble material in the solid product was defined as coke.

^{1}H and ^{13}C NMR were measured using JEOL Lamda 500. The conceptual structure model of asphaltene samples were deduced from the structural parameters obtained from NMR, elemental analyses and average molecular weight with the proposed by Sato's method[10].

RESULTS AND DISCUSSION

The properties of three Marlim samples (MLVR, MLVR-DAO and MLVR-AS) and Arabian Light vacuum residue asphaltene (ALVR-AS) are shown in Table 1. Nitrogen content of MLVR-AS is about twice of DAO and nitrogen is concentrated in the asphaltene fraction. On the other hand, sulfur contents of asphaltene and deasphalted oil are almost the same. On the comparison between MLVR-AS and ALVR-AS, nitrogen content of MLVR-AS is higher than ALVR-AS, but the content of sulfur and vanadium is lower than ALVR-AS. H/C atomic ratios and fa of MLVR-AS is similar to ALVR-AS.

Coking property of MLVR, MLVR-DAO and MLVR-AS are shown in Figure 1. Coke yield from MLVR-AS increased rapidly from 410°C of cracking temperature. In contrast, the coke formation from DAO did not take place even 420°C. But asphaltene were observed to form in the product oil after thermal cracking of MLVR-DAO. The coke yield from MLVR corresponded to the total amount of coke generated from asphaltene fraction and maltene fraction in MLVR. Asphaltene fraction are easily caused the coke formation during the thermal cracking.

Figure 2 shows the relationship between the reaction time and the coke yield in thermal cracking of MLVR-AS at the various temperatures. When cracking temperature was 410°C, The coke formation was not observed until 30 min of the reaction time and seemed to have an induction period. On the other hand, at higher temperature (430, 440°C), coke was formed rapidly at high rate without an induction period. This tendency was observed in thermal cracking of ALVR-AS[11].

Gas yield from MLVR-AS cracking is shown in Table 2. H_2 and hydrocarbon gases increased with an increase of reaction severity (temperature and time). It seems that coking of asphaltene progresses attended with dehydrogenation and dealkylation. A small amount of CO and CO_2 were observed in the generated gases. CO_2 yield was almost constant regardless of the reaction conditions. CO_2 formation suggests asphaltene molecule has carboxylic functionality and decarboxylation is finished at the initial stage of the reaction.

The composition and structure of original asphaltene were changed with thermal cracking. Elemental analyses and molecular weight and NMR spectra of reacted asphaltene were measured. The H/C atomic ratios and molecular weight of reacted asphaltenes decreased with an increase of the cracking temperature (Figure 3). Especially, the molecular weight of reacted asphaltene decreased rapidly with an increase of the reaction severity. Structural parameters of original asphaltene (MLVR-AS) and reacted asphaltene are shown in Table 3.

Figure 4 shows the conceptual model structure of original asphaltene and reacted asphaltene at 400, 430 and 440°C of the cracking temperature. As shown in this picture (figure 4), at low cracking temperature(400°C), asphaltene decomposition occurs through the cleavage of bridge chain which connects the cluster unit structure in asphaltene molecule. At higher temperature, in addition to the cleavage of bridge chain, dealkylation of alkyl substitutes connected to fused ring and dehydrogenation of naphthenic ring are found to be occurred. The reacted asphaltene obtained at 440°C was almost composed of fused aromatic ring.

CONCLUSION

This work was carried out to investigate the thermal cracking behavior of Barazilan Marlim vacuum residue.

1. Marlim vacuum residue has relatively high CCR , asphaltenes and nitrogen. Nitrogen compounds are concentrated in the asphaltene fraction. The asphaltene from VR has high aromaticity.
2. Coking reaction of the asphaltene was caused rapidly from 410°C. For deasphalted oil from VR, the formation of coke was not observed even at the temperature of 420°C.
3. Molecular weight and H/C atomic ratios of reacted asphaltene decreased with an increase of the cracking temperature. Asphaltene reacted at higher temperature shows highly aromatic structure with a little alkyl substitutes.

ACKNOWLEDGMENT

This work was supported by ITIT program of Agency of Industrial and Science Technology, MITI , Japan.

REFERENCES

1) Savage P.E., Klein M. T., Kukas S. G., Energy & Fuels, **2,** 619(1988)
2) Moschopedis S. E., Parkash S., Speight J. G., Fuel, **57** , 431(1978)
3) Truth D. M., Yasar M., Neurock M., Nigam A., Klein M. T., Kukes S. G., Fuel Sci. Tech. Int., **10,** (7), 1161(1992)
4) Del Bianco A., Panariti N., Anelli M., Beltrame P. L., Carniti P., Fuel, 72, 75 (1993)
5) Yasar M., Truth D. M., Klein M. T., Prepr. ACS., Div. Fuel Chem., **37**, (4),1878 (1992)
6) Wiehe I. A., Ind. Eng. Chem. Res., **32**, 2447(1993)
7) Kawai H., Kumata F., Prepr. ACS., Div. Pet. Chem., **42**, (2), 406(1997)
8) Shengha L., Chenguang L., Guohe Q., Wnejie L., Yajie Z., Prepr. ACS., Div. Pet. Chem., **42,** (2), 411(1997)
9) Karacan O., Kok M. V., Energy & Fuels, **11**, 385(1997)
10) Sato S ., Sekiyu Gakkaishi, **40,** (1), 46(1996)
11) Kondo T., Sato S., Matsumura A., Saito I., Proceedings of JECAT' 97, 335(1997)

Table 1 Properties of Marlim Vacuum Residues

	MLVR	MLVR-DAO	MLVR-AS	ALVR-AS*
C (wt%)	86.66	86.59	87.12	83.94
H(wt%)	10.17	10.88	8.62	7.86
N(wt%)	0.98	0.72	1.49	0.95
S(wt%)	0.90	0.88	1.04	6.72
H/C (atm)	1.40	1.50	1.18	1.12
V(ppm)	82	43	230	466
Ni(ppm)	59	33	160	128
n-C7 IS(wt%)	21.4			
C.C.R.(wt%)	22.8	15.7		
fa	0.30	0.26	0.45	0.42

* ALVR-AS : Arabian Light Asphaltene

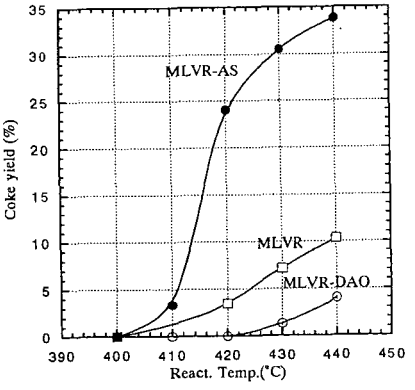

Figure 1. Coking property of Marlim vacuum residues

N2 :1MPa, Feed/DH=3/15wt, React. time : 60 min

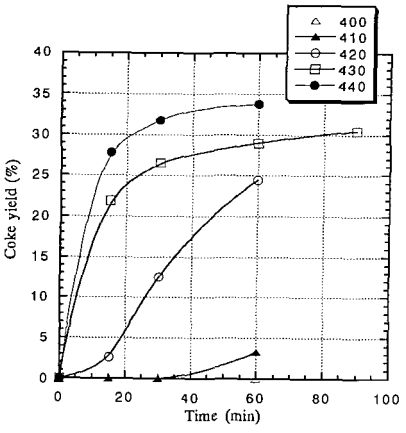

Fugure 2. Effect of reaction time on coke formation of MLVR-AS thermal cracking

Table 2 Reaction conditions and gas distribution from MLVR-AS thermal cracking

Conditions		Yield (wt%/AS)		Gas mmol/g AS × 100						
Temp.(°C)	Time(min)	Coke	Gases	H_2	CH_4	C_2H_6	C_3H_8	$C_2H_4+C_3H_6$	CO	CO_2
440	15	27.8	2.6	44	62	15.0	7.7	7.0	4.0	1.8
	30	31.8	3.3	63	83	19.7	10.0	8.0	4.0	1.8
	60	33.8	4.4	113	123	28.3	13.7	9.4	4.3	2.0
430	15	21.9	2.0	27	50	10.7	5.3	5.0	3.3	2.0
	30	26.5	2.4	42	62	14.3	6.7	4.0	4.0	2.0
	60	29.7	3.3	71	86	20.2	9.7	8.0	4.3	2.0
420	15	2.6	1.1	20	28	6.0	2.7	1.3	3.0	1.8
	30	12.7	1.4	31	36	7.7	3.3	2.0	3.3	1.7
	60	24.4	2.1	86	56	12.0	5.7	2.7	3.3	1.9
410	15	0.0	0.7	14	19	4.0	1.7	1.4	2.3	1.8
	30	0.0	0.8	12	18	3.7	1.7	1.4	2.7	1.8
	60	3.3	1.1	27	30	6.0	2.3	1.3	3.0	1.8
400	15	0.0	0.3	3	7	1.3	0.6	0.0	1.7	1.6
	30	0.0	0.5	9	11	2.3	1.0	0.8	1.6	1.6
	60	0.0	0.7	14	18	3.7	1.3	1.0	2.0	1.8

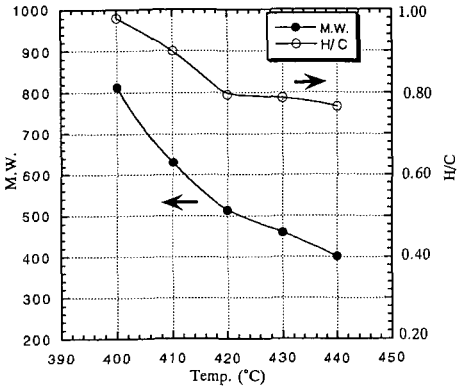

Figure 3. Effect of cracking temperature on molecular weight and H/C of reacted asphaltene

N2 : 1Mpa, MLVR-AS/DH=3/15wt, React. time 60 min

Table 3 Structural Parameters of MLVR-AS and reacted asphaltene

Parameter	MLVR-AS	Cracking temp. (°C)		
		400	430	440
H/C	1.19	1.03	0.79	0.76
M.W	1730	813	459	401
fa	0.45	0.55	0.66	0.88
Ct	128	61	35	31
Ht	152	63	28	24
Car	58	34	24	24
Har	16	10	9	9
H_α	26	15	6	6
H_β	83	28	10	6
H_γ	27	11	3	3
M	3.0	1.5	1.0	1.0
Rt	24.0	13.0	10.0	8.0
Ra	15.0	9.0	6.0	7.0
Rn	9.0	4.0	4.0	1.0
Cap	34.0	19.0	14.0	12.0
Ctr	81.0	43.0	33.0	27.0
N	9.2	4.5	1.0	2.0
l	5.2	3.9	2.0	2.0

Ct : Number of total carbon
Ht : Number of total hydrogen
Car : Number of aromatic carbon
Har : Number of aromatic hydrogen
H α : Number of hydrogen α to aromatic rings
H β : Number of hydrogen β to aromatic rings
H γ : Number of hydrogen γ to aromatic rings
M : Number of fused ring units
Rt : Number of total rings
Ra : Number of aromatic rings
Rn : Number of naphthenic rings
Cap : Number of peripheral carbon of aromatic rings
Ctr : Number of total carbon of fused rings
N : Number of paraffinic chain
l : Average chain length

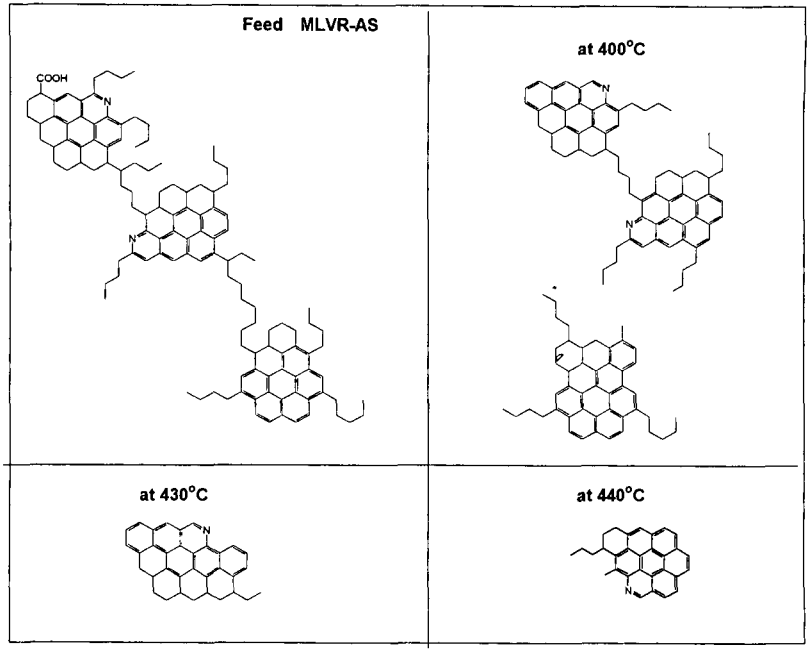

Figure 4. Strucutural Change of MLVR-AS in Thermal Cracking

INDUSTRIAL GAS TURBINE FUEL SURVEY-BASIC PROPERTIES

Bruce Rising
Siemens Westinghouse Power Corporation
4400 Alafaya Trail
Orlando, Florida 32826-2399

Keywords: Fuel, Gas Turbine, Emissions

ABSTRACT

In the last few decades, the quality of industrial feedstocks to refineries has continued to decline. Here in the United States many of the large remaining petroleum reserves are high in aromatics and sulfur content, while at the same time environmental standards call for lower sulfur in all fuel classes, and reduced aromatics in the large volumes of gasoline produced. These competing requirements force refineries to upgrade the feedstocks more aggressively in order to comply with the stricter environmental standards. This is particularly true of feedstocks coming from the west coast, or the Alaskan North Slopes. The impact of these lower quality feedstocks is expected to impact the quality of the final products available.

To ascertain the general quality of industrial fuels used in gas turbines, a survey of liquid fuels was undertaken. The purpose of the fuel survey was to characterize the properties of both domestic and international fuel supplies using a battery of test methods. This information would be used in estimating the fuel performance in an industrial gas turbine. Fuel properties of key interest were sulfur content, boiling point distribution, chemical constituents, ash content, and smoke point.

The survey required fuel samples from both domestic and international sources. Samples of fuel were taken from multi-product pipelines, bulk terminals, on-site storage facilities, and vendor supplied stocks. The bulk of the testing techniques employed were based on standardized ASTM methodologies. The scope of testing was greatly expanded beyond the normal fuel qualifications employed for industrial fuel characterization.

Results showed confirmation of the US EPA's regulatory efforts to reduce fuel sulfur levels to less than 0.05 wt%. However, there was not a significant difference between the sulfur levels of the higher grades of No. 1 type fuels (kerosine blends) and that of the more widely available No. 2 grade distillates.

The No. 2 grade distillates available in the US also showed a higher aromatics content than equivalent grades selected from international sources. This appears to be due to refinery processes in the US that are designed to optimize the gasoline yield from the refinery, resulting in higher aromatics content in some distillate streams.

INTRODUCTION

An industrial fuel survey was undertaken to understand potential changes in the quality of fuels available in the commercial markets. Of specific interest were fuel properties that might result in less than ideal performance when used in industrial gas turbine applications.

Historically, gas turbines have been well known for the ability to effectively use fuels of wide ranging characteristics and properties. Where reciprocating engines are impacted by the ignition quality of the fuel, or require a specific vapor pressure to burn, gas turbines do not typically exhibit sensitivity to fuel ignition properties. From an operating point of view, as long as the fuel can reach the fuel nozzle, and atomize properly, the only significant characteristic of concern is the presence of metals. Metals in the fuel, particularly alkaline and alkaline-earth elements are especially aggressive in their attack of hot metal surfaces. Therefore the metals content is often very tightly specified and controlled.

Advance turbines designed for low NO_x emissions have unique fuel hardware designs. Conventional designs consist of a pressure atomizing orifice type nozzle. The design is very forgiving, as well as easily manufactured and easy to repair. However, stricter environmental requirements have forced fuel system designers to develop improved atomization and mixing to reduce emissions, with an emphasis on NO_x. In some cases, the newer designs may impose more stringent requirements on the fuel. Determining a relationship between fuel properties and a system design was one of the long term goals.

METHODS

Standard ASTM[1] test methods were used extensively to evaluate fuel properties for this test program. No new methods were developed specifically to support these efforts. Other techniques which were also used include GC analysis of the fuel hydrocarbon structures.

Fuel samples were collected from various sources, placed in teflon bottles, and then shipped by overnight courier to the laboratories for analysis. Sample chemical analysis was usually completed within seven days after collection.

RESULTS

The test results are summarized by fuel grade (or type). In general, there were three grades of fuels identified:

1) No. 1/Jet A/Kerosene, but not including JP-5 grades
2) No. 2 distillate (including No. 2 fuel oil and diesel oils)
3) Gas-oils. Fuels similar to No. 2 based on ASTM classification, but with a wider distillation range, typically an endpoint that is greater than 700°F.

In addition, a reference highway No. 2 diesel fuel was used as a benchmark. This fuel sample was found to maintain relatively consistent analytical chemical properties from source-to-source, and from year-to-year.

The first comparison made is to summarize all of the fuels on a single chart, showing their boiling point range as a function of the percentage of the fuel distilled. From this chart, it is possible to clearly distinguish the specific grades of fuels just described. At the bottom of the chart lies a cluster for the No. 1 grade fuels. These are the kero-jet grades, widely available within the United States, but not the first fuel of choice for industrial applications because of the higher costs often associated with this transportation grade fuel.

The next cluster on the chart shows the No. 2 grade fuels. These fuels comply with the ASTM requirement that 90% of the fuel must be distilled at temperatures less than 640°F. In close proximity to the No. 2 grade fuels are the gas-oils, with a unique boiling point distribution. The gas-oils are identified primarily by the higher final boiling point which is exhibited on the right hand side of the figure.

Fuel Sulfur Analysis

Here in the United States, fuel is often hydro-treated to reduce the fuel sulfur levels. EPA requirements in the US have established diesel fuel sulfur maximums of 0.05 wt% (500 ppmw)[2], with gasoline sulfur requirements even lower. With declining feedstock quality, it is a requirement to upgrade the fuel using hydro-treatment, a process which lowers the product sulfur content. Table 1 summarizes the average sulfur levels encountered from fuel samples taken from both domestic and international sources.

Boiling Point

The data in Figure 1 show the clear delineation between the three types of fuels tested in this program. (Table 2 summarizes the endpoint analysis extracted from that data.) This figure shows that the end points on the gas-oils, samples collected from overseas sources, are distinctly different from comparable No. 2 grade fuels available in the United States.

Based on field test data, the effect of the higher end points for the gas-oil type fuels is expected to result in a higher smoke/particulate emissions than a lower boiling point fuel. A rule-of-thumb has been to require fuels with an end point that is less than 700°F in order to minimize the formation of a visible smoke plume, particularly at reduced loads.

Hydrocarbon Types

Hydrocarbon types were evaluated by two different methods: ASTM D 5291 and by chromatography. The general hydrocarbon classifications of interest are aromatics, olefins, and saturates determined using ASTM D 5291. The results of the analysis are summarized Table 3.

These are the results of 15 samples tested. The bulk of the US fuel samples exhibit saturates which are less than the average value shown in (70% for the average US values). All of the international fuel samples, with one exception, have higher saturate levels than the average shown in Table 3. A similar statement could be made for the aromatics, except that in this case, the lower aromatics tend to be clustered with the international fuel types (and the Jet A kerosines), while the higher aromatics are centered among the domestic grades of fuel (28.5%).

This appears to be consistent with the processing technologies associated with US refineries, and the limitations on aromatic hydrocarbons in the gasoline pool. Here in the US feedstocks are extensively upgraded to increase gasoline yields. This results in blending with Light Cycle Oil at the refinery that can produce very high concentrations of aromatics in the distillate streams. In addition, there are limits on the maximum aromatics content in the gasoline streams This requires that the excess aromatic components be re-distributed, and the distillate stocks targeted for stationary applications is the most convenient outlet.

For highway diesel and aviation kerosine applications aromatics more tightly controlled maintain cetane levels (for diesel fuels) and to meet aromatic specifications (for aviation applications). However, in the distillate heating oil market, there is no specific aromatic or cetane requirement for these fuels. Thus there would be a tendency to let the higher aromatic contents collect in this refinery stream.

In overseas markets there is still continued use of straight run distillates in large quantities. Also, Cetane improvers are not as widely used outside the United States. So the refinery stream for the distillates reflects a higher saturates and lower aromatics content than in the US.

Chromatography was used to further distinguish the chemical constituents that make up the fuel products. These are summarized in Figure 2. These results also show that the international grades clearly show lower aromatics, and higher paraffinic content that domestic US blends. Also, a high grade No. 2 highway diesel fuel is shown on the chart.

Ash Content

As expected, all samples tested showed ash contents that were reported at levels at or near the detection limits. The detection limits for ash using ASTM D 482 is reported to be 0.001 wt%; however, lower levels of detection are possible by using larger fuel sample volumes. In this program this was done to achieve the minimum detection levels reasonably achievable. The industry average of all fuel samples is 0.0015 wt% (15 ppmw). The significance of accurate ash measurement will be discussed in the next section.

Property Comparison: No. 1 and No. 2 Grades

Other relevant fuel properties were determined in addition to those described in previous section. A summary of those results is provided in Table 4.

DISCUSSION

The results show that US blends of both No. 1 and No. 2 fuels with sulfur levels consistent with the mandated US EPA requirements of 0.05 wt% maximum. While the average value shown in the table is slightly higher than that required by the EPA, the mean value is substantially influenced by a single sample which has a fuel sulfur level of 0.155 wt%. Removing this sample from the database lowers the average value to less than 0.043 wt%, meeting the US EPA requirements for fuel sulfur.

No. 1 Fuel

Results of the No. 1 fuel survey show excellent low sulfur characteristics. However, these fuels are substantially Jet A grade fuels (API gravity greater than 37 and 90% point is less than 540°F). Interestingly the No. 1 fuels show a broader boiling point range (exhibit a higher standard deviation) than the domestic No. 2 fuels. This is of virtually no impact with regard to fuel performance, although initial expectations were that the No. 2 fuel would likely exhibit the greater dispersion of the two fuel types.

International Fuel Grades

There is a clear trend toward the use of wider boiling point fuels in markets outside the United States and Canada. This was first observed by the author from fuel survey's conducted in Europe in the early 1990's. Higher end points were frequently found for distillate oils sold into the industrial/consumer markets. These fuels often did not meet the specific requirements established by the ASTM for No. 2 grade fuel (ASTM D396, D2880 or D375). The general performance of these fuels is expected to be similar to those of No. 2 grade fuels. However, there are some distinct differences to be expected. One of the most evident would be the production of a visible smoke plume. This phenomena has been associated with the liquid fuels exhibiting an endpoint that is 700°F or higher. This endpoint is reached or exceeded for most fuels similar to No. 2 distillate that are available in the international markets (Europe, Asia, South America).

In Germany, two grades of this fuel are available for general consumption. They are classified as IGO (Industrial Gas Oil) and AGO (Automotive Gas Oil). The AGO cut exhibits a lower endpoint, and less smoking tendency, than the IGO product. The features associated with AGO (reduced final boiling point) produce a less visible exhaust plume when burned in power applications.

ENVIRONMENTAL IMPACT

Certain fuel properties clearly affect their environmental performance. Fuel bound sulfur and nitrogen are the two of the most important. However, test results in this program have shown that both the domestic and international fuels exhibit very low sulfur levels, and would produce SO_2 emissions that would be difficult to measure during exhaust emission testing.

Not so clear is the impact of other fuel qualities, such as aromatics content, smoke point, and ash. These specific fuel properties, as well as others, can impact the formation of smoke, particulates, and a visible plume. Distinguishing particulates between carbon/organic and inorganic (or ash) components is difficult to predict. However the inorganic ash component is the easiest of the two to estimate. The laboratory results from ASTM D 482 are assumed to represent the same ash constituents that would be released into the environment. For a large industrial gas turbine, using 100,000 lb/hr of liquid fuel consumption, a test analysis with detection limits of 0.01 wt% would produce an expected particulate emission rate of 10 lb/hr (0.0077 lb/MMBtu, HHV basis), based solely on the ash constituents. There is no straightforward mechanism for estimating the additional particulates due to the carbon/organic fraction. But evidence from field tests clear shows that fuels with final boiling points in excess of 700°F can, under the proper set of conditions, produce a visible plume.

Based on the test results from this program, using the same conditions just described would result in particulate emissions due to the ash content of the fuel at approximately 1.5 lb/hr (0.00077 lb/MMBtu, HHV basis). This level of particulates would produce no visible plume, and would be extremely difficult to measure using standardized test methods.

CONCLUSION

Fuel sulfur levels within the United States reflect the impact of federal legislation mandating sulfur reductions to less than 0.05 wt% (500 ppmw). Only in one instance was a fuel for gas turbine applications identified with a sulfur content greater than this.

US fuels are substantially dominated by higher aromatics and lower saturate contents than comparable non-domestic grades of fuels (excluding the Jet A kerosine grades). The higher aromatic contents may result in greater particulate emission, or possibly a visible smoke plume. International samples show trends of higher saturates and lower aromatics, somewhat similar to the general hydrocarbon information identified for Jet A grades of fuel.

Ash contents of all fuel samples tested were very close to the detection limits of the test method. An average value of 15 ppmw was reported.

These results, as well as additional test parameters being considered, will eventually be used to develop more useful and effective fuel specifications for industrial gas turbine applications.

ACKNOWLEDGMENTS

This work could not have been completed without the help of Phil and Nader Sorurbakhsh of Texas Oil Tech Laboratories, in Houston, Texas.

REFERENCES

[1] ASTM 100 Barr Harbor Drive, West Conshohocken, Pa. 19428

[2] US EPA 40 CFR 80.29. Beginning 1 Oct 93 sulfur is limited to 0.05 wt% for highway diesel.

[3] "A Comparison of Low and High Sulfur Middle Distillate Fuels in the United States", J. Andrew Waynick, 215th ACS National Meeting, Dallas, TX. March 29, 1998

Table 1 Measured Fuel Sulfur Levels (ASTM D4294)

Fuel Type	Average	Minimum	Maximum	Standard Deviation
No. 1	0.0207	0.003	0.0322	0.0119
No. 2	0.0535	0.025	0.155	0.035
Amoco Fuel Analysis (1994)[3]				
Low Sulfur Diesel	0.0296			0.0092
High Sulfur Diesel	0.2082			0.0902

Table 2 Boiling point distribution

	End Point		50% Point		90% Point	
	Average, °F	SD	Average, °F	SD	Average, °F	SD
No. 1	540.8	17.1	424.7	12.8	493.4	15.8
No. 2	657.1	7.8	511.4	11.7	607.6	7.3
Gas Oil	693.6	23.5	538.9	8.7	647.9	21.4

Table 3. Fuel classification by hydrocarbon types (ASTM D 5291)

	Hydrocarbon Analysis by Volume % (All Fuels Tested)			
	Olefins	Aromatics	Saturates	Smoke Point
Average	1.13	23.06	75.80	18
Standard Deviation	0.472	6.982	7.127	3.0
Maximum	2.3	35.8	84.92	23
Minimum	0.39	14.2	62.4	12

Table 4 General fuel properties

	No. 1/Kerosene	No. 2 Distillates
Flash Point, °F	144	160
Pour Point, °F	-59	-8
Kinematic Viscosity @ 104°F (cSt)	2.08	3.03
Specific Gravity	0.82	0.854
LHV, Btu/lb	18,526	18,327
HHV, Btu/lb	19,747	19,446
Carbon Content, wt%	86.22	86.71
Hydrogen Content, wt%	13.57	13.05
Oxygen Content, wt%	0.16	0.13
Nitrogen Content, wt%	0.0078	0.018
Sulfur Content, wt%	0.0322	0.0535

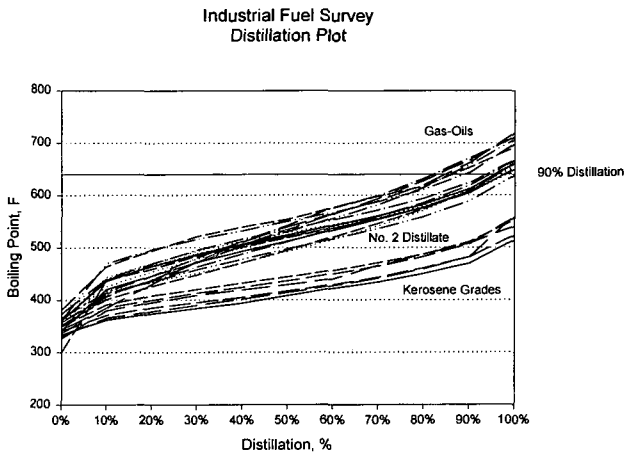

Figure 1. - Boiling Point Distribution for Three Fuel Grades

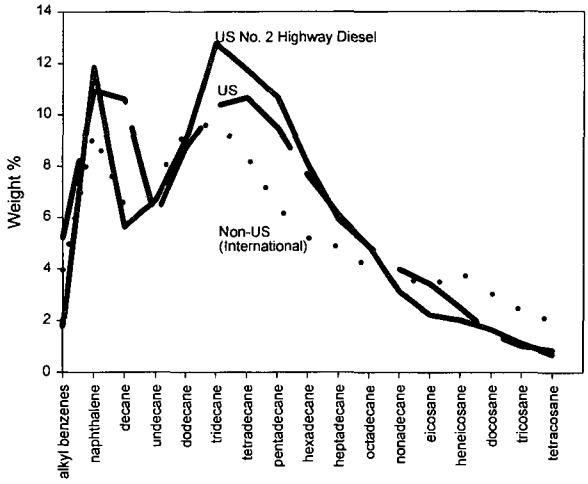

Figure 2. - Fuel Chromatography Analysis.

SUPPRESSION OF PYROLYTIC DEGRADATION OF N-ALKANES IN JET FUELS BY HYDROGEN-DONORS

John M. Andrésen, James J. Strohm, Michael M. Coleman and Chunshan Song*
Applied Catalysis in Energy Laboratory, The Energy Institute
The Pennsylvania State University, University Park, PA 16802.

KEYWORDS: Pyrolysis, thermal stability, aviation jet fuels.

ABSTRACT

The pyrolytic degradation of alkanes in jet fuels can be extensively reduced by adding suitable hydrogen donors, that suppress the formation of free radicals. Accordingly, this paper characterizes the chemical interactions between n-tetradecane and the hydrogen donors benzyl alcohol and 1,2,3,4-tetrahydro-1-naphthol. The hydrogen donors produced the expected overall enhancement on the liquid yields and reduced cracking of the n-tetradecane. The observed suppression of pyrolytic degradation was strongly related to a reduction in the alkane products adding benzyl alcohol, but the 1,2,3,4-tetrahydro-1-naphthol indicated an initial decrease in the alkenes.

INTRODUCTION

The use of hydrogen donors to suppress pyrolytic degradation of jet fuels (1-3), is a potential route to reach the JP-900 thermal stability requirement set up by the US Air Force (4). Since the fuel also functions as the main coolant for the different electronic and system components of the aircraft, the fuel temperatures may increase up to 480°C (900°F) and thermal stability to obtain reduced solid deposition is a key element in this research (5). The pyrolytic conversion of alkanes, typically found in petroleum derived jet fuels, is generally considered to involve the formation of free radicals (6). The propagation of these reactive intermediates results in a broad distribution of smaller alkane and alkene units, and triggers the aromatization of the liquid, which leads to undesirable solid depositions. As a solution, the free radicals can be halted right after the initiation step by the use of hydrogen donors (1-3). However, the chemistry involved in inhibiting free radical reactants during thermal degradation of fuels is not fully understood. This is addressed in this study, where the suppression of reactive intermediates between the n-alkane, n-tetradecane, and the hydrogen donors benzyl alcohol and 1,2,3,4-tetrahydro-1-naphthol, has been characterized.

EXPERIMENTAL

The compounds used were n-tetradecane (TD, Aldrich 99%), benzyl alcohol (BA, Aldrich 99.8%) and 1,2,3,4-tetrahydro-1-naphthol (THNol, Acros 97%). Stressing of TD alone or in different mixtures with BA or THNol were performed for 30 minutes in a fludized sandbath at 425, 450 and 475°C. A detailed description of the experimental setup and analytical determination of the product distribution using GC and GC/MS, has been reported elsewhere (1, 5).

RESULTS AND DISCUSSION

The liquid yields for the n-tetradecane (TD) stressed alone at 425, 450 and 475°C and its mixture with 0.5, 1, 3 and 5 mole% benzyl alcohol (BA) and 1,2,3,4-tetrahydro-1-naphthol, are plotted in Figure 1. The amount of gaseous products is scarce at 425°C, yielding only around 2 wt%. However, adding 0.5 mole% of either BA or THNol resulted in a marked increase in the liquids (Figure 1). At 450°C, the liquid yields are still high and the same initial rise in remaining liquid is observed with the addition of only 0.5 to 1 mole% of hydrogen donors. Rising the temperature to 475°C resulted in a significant decrease in the liquid yields. Still, the more dramatic enhancement in the liquid yields was observed after the

addition of 1 mole% of the hydrogen donors. When comparing the increase in liquid yields at the three temperatures for TD alone and with 1 mole% addition of BA or THNol, there is a significantly rise from around 1-2% at 425°C to 4-6% at 475°C, as an effect of hydrogen donors. Scheme 1 presents in a simplified manner the role of the hydrogen donors in the thermal stabilization of the fuel. The n-tetradecane is cracked due to the influence of heat into two primary radicals. The additive can cap a radical at this stage, preventing the propagation of the reaction and leaving a n-alkane product. However, if the radical is not stopped, it will abstract a hydrogen from another TD molecule. This may leave a primary radical on the TD, which yield a n-tetradecane upon stabilization. More likely, a secondary radical will be formed. Through β-scission, the secondary radical will yield a 1-alkene and a primary radical product. The extent of this cyclic process can be monitored through the concentration of 1-alkenes (in bold). The primary radical capture has been reported in the literature to be the main target for benzyl alcohol (3). However, the ability of hydrogen donors to aim specially at secondary radicals has not been described.

The ability of the hydrogen donor to capture any of the radicals will hinder the propagation reaction, resulting in an increased ratio of remaining TD in the liquid product, when compared to that initially used. Figure 2 compares this relationship for n-tetradecane at the three temperatures 425, 450 and 475°C with the addition of 0.5 to 5 mole% of THNol. Clearly, as the temperature is increased, the TD remaining over that initially is decreasing for the TD stressed alone, from about 85 mole% at 425°C to around 30 mole% at 475°C. At the three different temperatures, there is a sharp initial rise in the TD remaining content with the addition of only 0.5 to 1 mole% of THNol, similar to that found for the liquid yields. However, as the temperature becomes more elevated, a further slow increase is also observed for the addition of THNol up to 5 mole%. For BA, a similar temperature and concentration dependence was found, in accordance with that previous reported for BA at 450°C (3).

The n-alkane and 1-alkene product distributions for the series of THNol addition at 450°C are shown in Figures 3 and 4, respectively. With the addition of 0.5 mole% THNol, there is a decrease in both the alkane and alkene gaseous products (C1 to C3) in accordance with the observed increase in liquid yield (Figure 1). However, for C4 and higher there is a marked decrease in the 1-alkene products (Figure 4), when adding only 0.5 mole% THNol. The n-alkanes from C4 and higher for the TD alone and with 0.5 mole% THNol show a similar product distribution. Referring back to Scheme 1, the THNol seems to target the secondary radicals at this low concentration. Increasing the THNol concentration appears to enhance the ability of the THNol to target primary radicals as well, resulting in a steady decrease of n-alkane products (Figure 3), as the 1-alkene concentration is decreasing at a lower rate. The selective targeting of secondary radicals has also been indicated from the GC analysis of the liquid products from TD/THNol mixtures at 475°C. Figure 5 shows the ratio of the 1-alkene peak area over that of the corresponding n-alkane for TD alone and with 0.5 mole% THNol and BA addition. There is a clear reduction in the alkene/alkane ratio for the THNol mixture, supporting the finding that THNol is targeting secondary radicals at low concentrations. In addition, Figure 5 shows that BA is mainly targeting the primary radicals at 475°C, as illustrated by the relative decrease in the n-alkane peaks in comparison to that of the 1-alkenes. The different reaction mechanisms for the different hydrogen donors may result in synergistic effects from mixing small amount of both stabilizers, where each has the task of capping different radicals.

CONCLUSIONS

The most significant effect of benzyl alcohol (BA) and 1,2,3,4-tetrahydro-1-naphthol (THNol) on the stabilization of n-tetradecane takes place with the addition of 1 mole%. THNol appears to target secondary radicals to a greater extent than BA at low concentrations of the hydrogen donors.

ACKNOWLEDGMENTS

The authors wish to thank the U.S. Air Force Wright Laboratory, the U.S. DOE / Federal Energy Technology Center for their support. We also thank Prof. Harold H. Schobert for his support and helpful discussion.

REFERENCES

(1) Song, C., Lai, W.-C. and Schobert, H.H., Ind. Eng. Chem. Res., 1994, **33**, 548-557.
(2) Coleman, M.M., Sobkowiak, M., Fearnley, S.P. and Song, C., Prep. Am. Chem. Soc.- Div. Petro. Chem., 1998, **43(3)**, 353-356.
(3) Venkataraman, A., Song, C. and Coleman, M.M., Prep. Am. Chem. Soc.- Div. Petro. Chem., 1998, **43(3)**, 364-367.
(4) Edwards, T., Prep. Am. Chem. Soc.- Div. Petro. Chem., 1996, **41(2)**, 481-487.
(5) Andrésen, J.M., Strohm, J.J. and Song, C., ACS Petroleum Chemistry Division preprints, 43(3), 412-414 (1998).
(6) Song, C., Lai, W.-C. and Schobert, H.H., Ind. Eng. Chem. Res., 1994, **33**, 534-547.

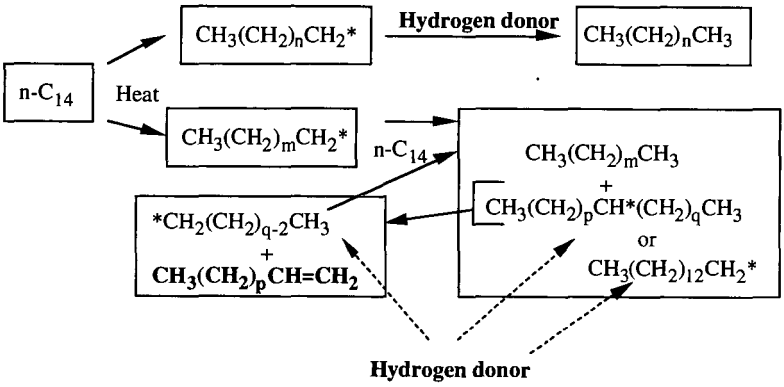

Scheme 1. General concept of the role of the hydrogen donors in stabilizing the n-alkanes leading to suppression of pyrolytic degradation.

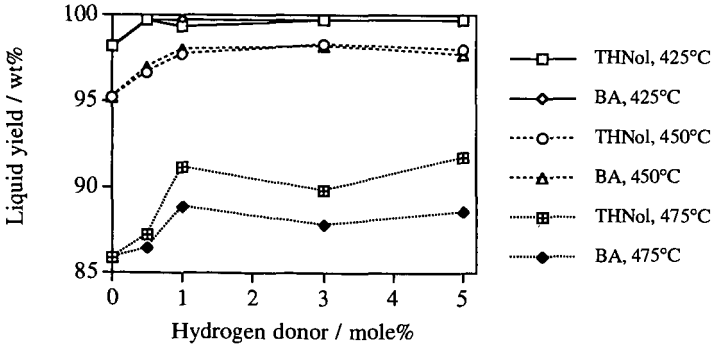

Figure 1. The changes in liquid yields with addition of the hydrogen donors benzyl alcohol and 1,2,3,4-tetrahydro-1-naphthol in the range of 0.5 to 5 mole% at 425, 450 and 475°C.

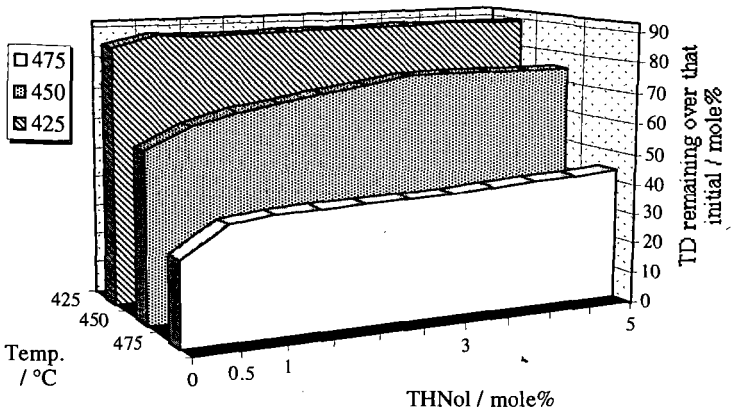

Figure 2. Comparison of remaining n-tetradecane content over its initial concentration for different mixtures with 1,2,3,4-tetrahydro-1-naphthol, stressed at 425, 450 and 475°C for 30 minutes.

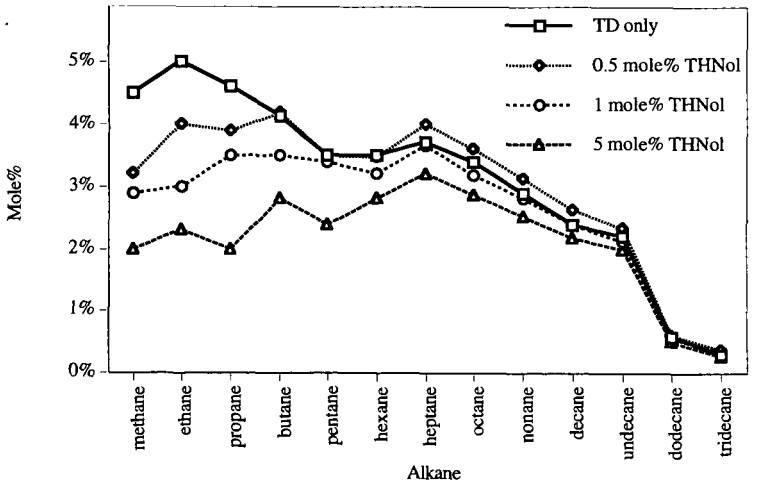

Figure 3. Variation in the n-alkane distribution for pure n-tetradecane and its 0.5, 1 and 5 mole% mixture with 1,2,3,4-tetrahydro-1-naphthol stressed at 450°C for 30 minutes.

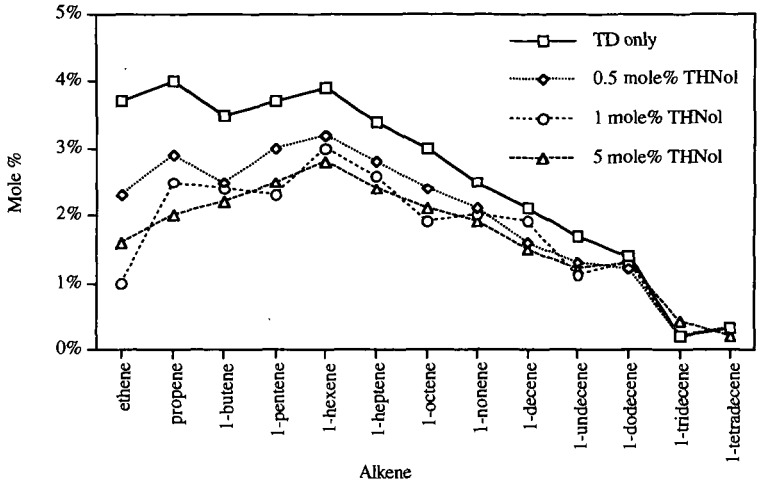

Figure 4. Variation in the 1-alkene distribution for pure n-tetradecane and its 0.5, 1 and 5 mole% mixture with 1,2,3,4-tetrahydro-1-naphthol stressed at 450°C for 30 minutes.

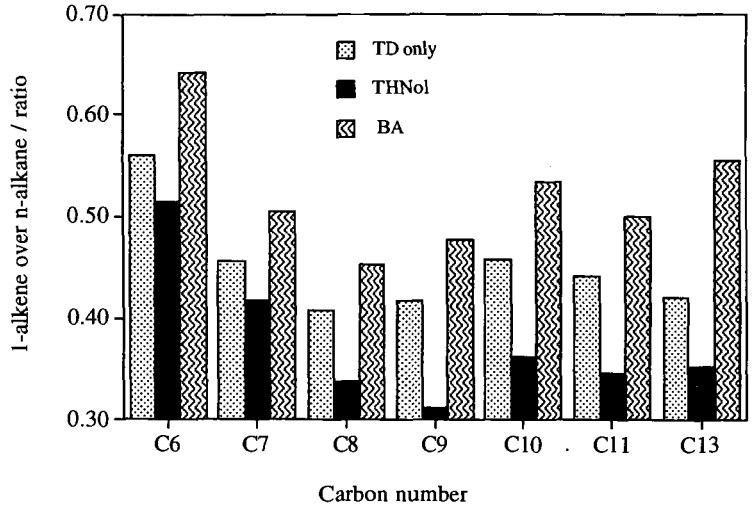

Figure 5. Ratio of the 1-alkene peak area over that of the corresponding alkane for TD alone and with 0.5 mole% THNol and BA addition at 475°C stressed for 30 minutes.

CHEMICAL INTERACTIONS BETWEEN LINEAR AND CYCLIC ALKANES DURING PYROLYTIC DEGRADATION OF JET FUELS

John M. Andrésen, James J. Strohm and Chunshan Song*
Applied Catalysis in Energy Laboratory, The Energy Institute and
Department of Energy and Geo-Environmental Engineering,
The Pennsylvania State University, University Park, PA 16802.

KEYWORDS: Pyrolysis, thermal stability, aviation jet fuels.

ABSTRACT

Potential jet fuels derived from hydrogenation of liquids from coal and petroleum fractions, are rich in both cycloalkanes and long-chain alkanes. Their thermal interactions have been studied using decahydronaphthalene and n-tetradecane as model compounds. Chemical interactions were indicated in the pyrolytic regime by the decrease in gaseous products with increasing addition of decahydronaphthalene to the n-alkane. The improved thermal stability of the n-tetradecane was mainly attributed to the ability of the cycloalkane to capture free radicals from the cracking of the n-alkane.

INTRODUCTION

There is an increasing demand of improved thermal stability of jet fuels for high Mach flights, as illustrated by the JP-900 requirement of the Air Force (1). However, the present aviation jet fuels do not meet these criteria, due to their high content of alkanes in the range C_7-C_{17}, which readily lead to thermal degradation (2). The JP-900 goal has been approached by jet fuels derived from coal liquids (3). Coal derived jet fuels differ substantially from those generally obtained from petroleum in their high content of cyclo-alkanes and a relatively lower concentration of linear alkanes. This chemical distinction is one of the main reasons why coal derived fuels show greater thermal stability in the pyrolytic regime than those of petroleum origin (4). Cyclo-alkanes alone show a great chemical stability in the pyrolytic regime (5). However, due to economical concerns, other potential routes to obtain cyclo-alkane rich fuels are considered, including hydrogenation of aromatic petroleum fractions or by blending of coal and petroleum derived fuels (4). These fuels will still present a relatively high content of long-chain linear alkanes. Earlier tests in batch reactors have shown reduced solid depositions in petroleum fuels at 450°C with addition of decahydronaphthalene (6). This suggests a synergistic effect between the linear and the cyclic alkanes at elevated temperature. Accordingly, this study addresses the chemical interactions between cyclo-alkanes and n-alkanes typical for coal and petroleum derived fuels, where decahydronaphthalene was used as a cyclic model compound, while n-tetradecane represented the linear alkanes.

EXPERIMENTAL

The compounds used were n-tetradecane (TD, Aldrich 99%) and decahydronaphthalene (DHN, Aldrich 98%, a mixture of 46 mole% cis- and 54 mole% trans-decahydronaphthalene). Stressing of TD alone or in 5 or 30 mole% mixtures with DHN were performed for 2 hours in a fludized sandbath at 425, 450 and 475°C. A detailed description of the experimental setup and analytical determination of the product distribution using GC and GC/MS, has been reported elsewhere (4).

RESULTS AND DISCUSSION

Figure 1 compares the gas, liquid and solid yields on a weight basis for pure n-tetradecane (TD) and the mixtures of 5 and 30 mole% decahydronaphthalene (DHN) in TD stressed for 2 hours under an initial pressure of 100 psi N_2 at the

temperatures 425°C (a) and 475°C (b). The development of solids at both temperatures shows the same trend, where the pure TD has a higher value than those observed for both the mixtures. This is especially the case at 475°C, where the pure TD deposited nearly 5 wt% solids compared with around 3 wt% for the mixtures. The liquid residue is in addition lower for the pure TD than for the mixtures (Figure 1). Even at temperatures as low as 425°C, the liquid yield increased from around 82 wt% for TD alone to 97 wt% with only 5 mole% DHN added. Assuming that virtually all the DHN stays in the liquid product (based on evidence discussed later), this corresponds to a relative decrease in the gaseous product from the TD of (18-3.2)/18 = 80%. Similar data was obtained at 450°C. This clearly indicates that DHN prevents gas and solid formation when compared with TD alone. Figure 2 shows that this thermal enhancement is closely related to the reduced cracking of the TD, where the GC traces of the liquid product distribution for TD alone (top) and its mixture with 30 mole% DHN (bottom) stressed at 425°C, are plotted. A great reduction in the cracking products is obtained, where their distribution is shifted towards longer alkanes and 1-alkenes.

Tables 1 to 3 list the total reaction products based on the initial amount at 425, 450 and 475°C for the pure TD and its 5 and 30 mole% DHN mixtures, respectively. With increasing DHN addition, there is a decrease in the amount of linear or branched alkanes at all temperatures, which is also the case for alkenes. The cyclo-alkanes, on the other hand, become more important at higher temperatures, but there is no clear relation to the DHN concentration. Some small amount of alkylated DHN, such as n-butyl-decalin, are also included in these values. In further studies at shorter stressing time (30 minutes), where secondary reactions are expected to be low, a significant amount of ethyl- to dodecyl- substituted decahydronaphthalenes were detected in the liquid products. However, at the relatively long stressing times used here, these intermediates have generally been converted into hydroaromatics (tetralin, alkylated tetralin and indanes) or completely dehydrogenated into naphthalenes (7). However, the increased addition of DHN markedly reduces the development of benzenes, where at 475°C, TD alone produced 23 mole%, while the mixture with 30 mole% DHN only gave 16 mole% benzenes.

The fraction of TD remaining over the initial amount is compared in Figure 3 for the pure TD and its mixtures with 5 and 30 mole% DHN at 425, 450 and 475°C. At 425°C, the increasing content of DHN significantly prevents the thermal decomposition of the TD, where with no DHN added only 40 mole% TD remains compared to nearly 80 mole% for the 30 mole% DHN mixture. Even though this trend is decreasing when the temperature becomes more elevated, there is still a significant rise in the TD content obtained at 450°C with only 5 mole% DHN. After 2 hours stressing at 475°C, the TD has almost vanished and the stabilization effect of the DHN is most likely affecting shorter linear alkanes based on the enhancement in the liquid yield and suppression of solid deposition (Figure 1). Figure 4 compares the remaining DHN over its initial concentration for the 5 and 30 mole% mixtures at 425, 450 and 475°C. Around 90-100 mole% remains up to 450°C followed by a sudden drop at 475°C to around 30-45 mole%. The values are higher for the 5 mole% DHN mixture, as an estimated value of 0.5 % in the calculations gives 0.5/5=10% error in this values (see error bar). The small reduction in DHN concentration at 425 and 450°C is related to stabilization of free radicals via alkylation of the DHN, as discussed earlier. This suggests that DHN at high contents is a benign prohibitor of thermal decomposition of TD up to 450°, due to its own thermal stability.

At increasing temperatures, the benzenes and naphthalenes concentrations are increasing for TD stressed alone and its 5 and 30 mole% DHN mixtures (Tables 1 to 3). The mixtures with DHN are expected to contain a certain amount of naphthalenes due to the dehydrogenation process it experiences during the chemical interaction with the free radical products from the cracking of the TD. Therefore, the total content of naphthalenes must be considered on the basis of the consumed content of DHN. Figure 5 compares the content of naphthalene, where the consumed content of DHN is subtracted, at 450 and 475°C for the pure

TD and its 5 and 30 mole% DHN mixtures. Although resulting in higher overall concentrations of naphthalenes (Tables 1 to 3), Figure 5 illustrates that the naphthalene developed is decreasingly resulting from thermal decomposition of TD as the addition of DHN is increased. This again supports the previous findings that the DHN in mixture with TD prevents thermal decomposition of the n-alkane by suppressing its decomposition into small alkanes and the production of naphthalenes or more condensed aromatic products.

CONCLUSIONS

Tetradecane (TD) has been stressed alone and in mixtures with 5 and 30 mole% decahydronaphthalene (DHN) at 425, 450 and 475°C. A significant decrease in the solid deposition and increase in liquid yields were observed at all temperatures with the addition of DHN. Further, the content of TD remaining was greatly enhanced at temperatures up to 450°C, but was not significant at 475°C due to the thermal decomposition of DHN itself.

ACKNOWLEDGMENTS

The authors wish to thank the U.S. Air Force Wright Laboratory, the U.S. DOE / Federal Energy Technology Center for their support. We also thank Prof. Harold H. Schobert for his support and helpful discussion.

REFERENCES

(1) Edwards, T., Prep. Am. Chem. Soc.-Div. Petro. Chem., 1996, **41(2)**, 481.
(2) Song, C., Lai, W.-C. and Schobert, H.H., Ind. Eng. Chem. Res., 1994, **33**, 534.
(3) Song, C., Eser, S., Schobert, H.H. and Hatcher, P.G., 1993, Energy & Fuels, **7**, 234.
(4) Andrésen, J.M., Strohm, J.J. and Song, C, Prep. Am. Chem. Soc.-Div. Petro. Chem., 1998, **43(3)**, 412.
(5) Lai, W.C. and Song C., Fuel, 1995, **74**, 1436.
(6) Song, C., Lai, W.-C. and Schobert, H.H., Prep. Am. Chem. Soc.-Div. Fuel Chem., 1992, **37(4)**, 1655.
(7) Song, C. and Lai, W.-C., Prep. Am. Chem. Soc.-Div. Petro. Chem., 1998, **43(3)**,462.

Table 1: Distribution of the total reaction products based on the initial amount at 425, 450 and 475°C for the pure TD.

Products / mole%	425°C	450°C	475°C
Alkanes C_{14}^-	22.1	31.6	11.7
Alkanes C_{14}^+	1.8	6.5	<0.1
Cyclo-alkanes	5.1	7.6	7.5
Alkenes	11.7	3.4	1.0
Hydro-aromatics	<0.1	1.8	2.7
Benzenes	<0.1	11.5	23.0
Naphthalene	<0.1	0.9	6.7

Table 2: Distribution of the total reaction products based on the initial amount at 425, 450 and 475°C for the 5 mole% DHN in TD mixture.

Products / mole%	425°C	450°C	475°C
Alkanes C_{14}^-	20.3	27.4	13.1
Alkanes C_{14}^+	7.2	0.6	0.1
Cyclo-alkanes	7.8	8.1	9.5
Alkenes	8.9	1.9	1.3
Hydro-aromatics	<0.1	1.0	3.0
Benzenes	0.1	7.6	21.2
Naphthalene	<0.1	1.8	4.8

Table 3: Distribution of the total reaction products based on the initial amount at 425, 450 and 475°C for the 30 mole% DHN in TD mixture.

Products / mole%	425°C	450°C	475°C
Alkanes C_{14}^-	4.8	15.2	3.6
Alkanes C_{14}^+	1.0	0.5	<0.1
Cyclo-alkanes	3.2	8.0	6.5
Alkenes	2.4	2.2	1.7
Hydro-aromatics	<0.1	3.4	4.4
Benzenes	0.1	7.1	16.0
Naphthalene	<0.1	3.1	14.2

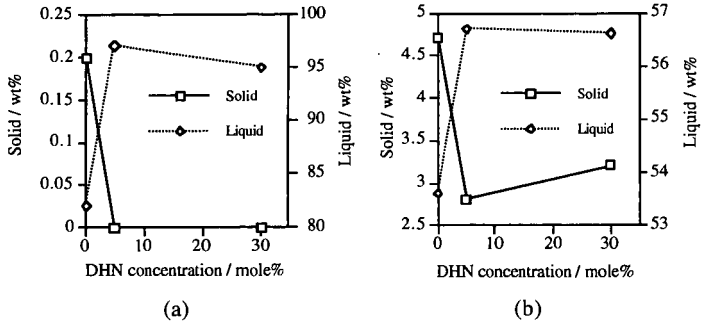

Figure 1. Comparison of liquid and solid yields for pure TD and its mixtures with 5 and 30 mole% DHN stressed for 2 hours under an initial pressure of 100 psi N_2 at the temperatures: (a) 425°C and (b)475°C.

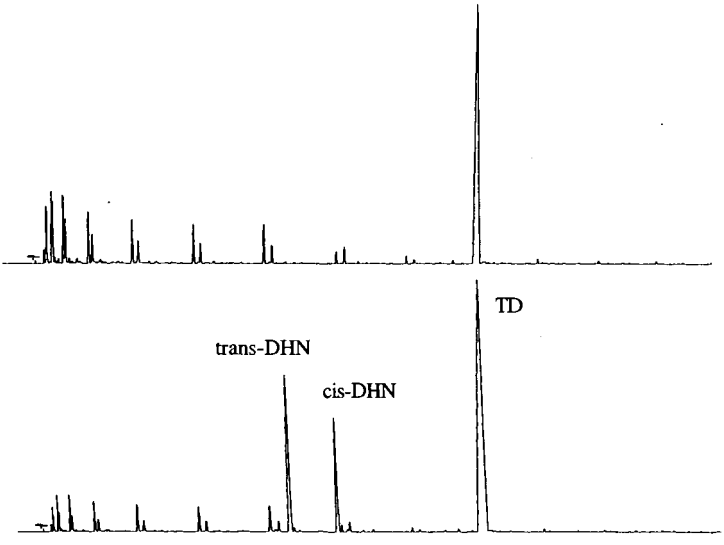

Figure 2. The GC traces of the liquid product distribution for TD alone (top) and its mixture with 30 mole% DHN (bottom) stressed at 425°C.

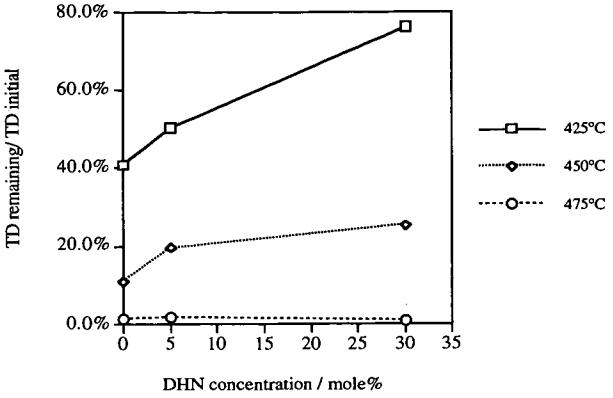

Figure 3. The fraction of TD remaining over its initial concentration for TD alone and its mixtures with 5 and 30 mole% DHN at 425, 450 and 475°C.

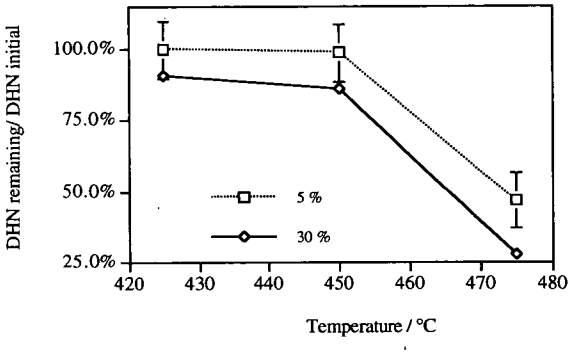

Figure 4. Comparison of the remaining DHN over its initial concentration for the 5 and 30 mole% mixtures with TD at 425, 450 and 475°C.

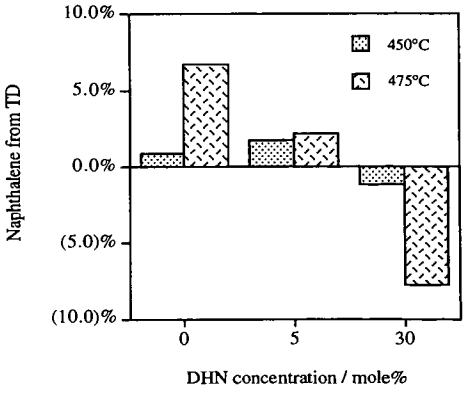

Figure 5. Comparison of the content of naphthalenes where the consumed content of DHN is subtracted at 450 and 475°C for the pure TD and the 5 and 30 mole% DHN in TD mixtures.